



# The Journal of Gemmology

Volume 38 / No. 3 / 2022



Emerald from  
Chitral, Pakistan

Turquoise from  
Xinjiang, China

Emerald Jewels from  
St Peter's Archabbey

# SSEF

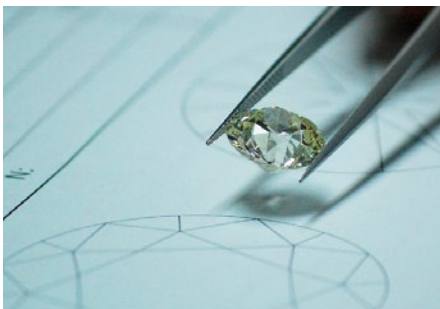
SCHWEIZERISCHES GEMMOLOGISCHES INSTITUT  
SWISS GEMMOLOGICAL INSTITUTE  
INSTITUT SUISSE DE GEMMOLOGIE



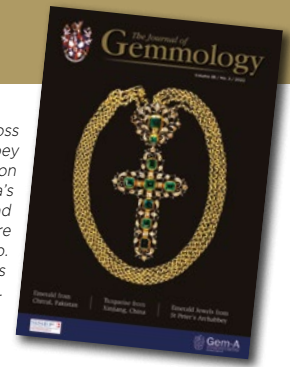
ORIGIN DETERMINATION · TREATMENT DETECTION

DIAMOND GRADING · PEARL TESTING

EDUCATION · RESEARCH



THE SCIENCE OF GEMSTONE TESTING™



**Cover photo:** This emerald-bearing pectoral cross (12.5 x 5.8 cm) was donated to St Peter's Archabbey in Salzburg, Austria, in 1786. Although oral tradition has assumed the emeralds came from Austria's Habachtal deposit, microscopic examination and portable EDXRF chemical analysis indicate they are from Colombia, as described in the article on pp. 272-283 of this issue. Courtesy of St Peter's Archabbey, Salzburg; photo by N. Urban.

## COLUMNS

### What's New 213

Yehuda Diamond Detectors | De Beers' 2021 Sustainability Report | Gemmological Society of Japan 2022 Annual Meeting Abstracts | JNA's Lab-Grown Diamond Special Issue | Lab-Grown Diamond Consumer Segments | Platinum Jewellery Business Review 2022 | Santa Fe Symposium Proceedings 2022 | World Silver Survey 2022 | Branko Gems' Diamond Academies | GemGenève Seminar Presentations | Masterpiece London: Collecting Natural Treasures from the Mineral Kingdom

### Gem Notes 216

Emerald with Bertrandite-Phlogopite Veins Resembling Fracture Fillings | Cinnabar Inclusions in Ethiopian Opal | Violet Spinel with Strong Green Fluorescence | New Finds at the Tourmaline King Mine, Pala, California, USA | A New Amber Imitation: Amber-Epoxy Composite | Transparent Optical Ceramic as a Gem Material? | Record-Breaking Laboratory-Grown CVD Diamonds | Mica-Coated Emerald Imitations from Zambia | Ring with Flat-Cut Synthetic Moissanite | Black Synthetic Moissanite Coloured by a Pleochroic Mechanism | Green-coated Topaz Coloured by Cobalt

219



Photo by C. Williams

## ARTICLES

### Emerald from the Chitral Region, Pakistan: A New Deposit 234

By Carina Silke Hanser, Bilal Gul, Tobias Häger and Roman Botcharnikov

### Gemmological Characteristics of Turquoise from Hami, Xinjiang, China 254

By Yanhan Wu, Quanli Chen, Yan Li, Min Cao, Zuwei Yin, Haitao Wang and Xianyu Liu

### Origin of Emeralds in a Late-Eighteenth-Century Pectoral Cross and Ring from St Peter's Archabbey, Salzburg, Austria 272

By Karl Schmetzer and H. Albert Gilg

222



Photo by Orasa Weldon

255

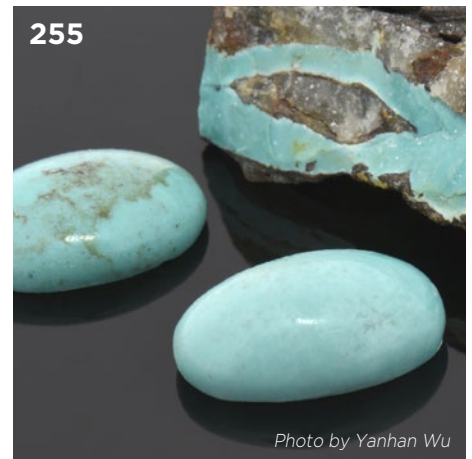


Photo by Yanhan Wu

### Conferences 284

AGA Las Vegas Conference | 23rd General Meeting of the International Mineralogical Association

### Gem-A Notices 288 New Media 292

### Learning Opportunities 290 Literature of Interest 300

The Journal is published by Gem-A in collaboration with SSEF and with the support of AGL.



# The Journal of Gemmology

## EDITORIAL STAFF

Editor-in-Chief  
**Brendan M. Laurs**  
brendan.laurs@gem-a.com

Executive Editor  
Alan D. Hart

Editorial Assistant  
**Carol M. Stockton**

Editor Emeritus  
**Roger R. Harding**

## ASSOCIATE EDITORS

**Ahmadjan Abduriyim**  
Tokyo Gem Science LLC,  
Tokyo, Japan

**Raquel Alonso-Perez**  
Harvard University,  
Cambridge, Massachusetts,  
USA

**Edward Boehm**  
RareSource, Chattanooga,  
Tennessee, USA

**Maggie Campbell Pedersen**  
Organic Gems, London

**Alan T. Collins**  
King's College London

**Alessandra Costanzo**  
National University of  
Ireland Galway

**John L. Emmett**  
Crystal Chemistry, Brush  
Prairie, Washington, USA

**Emmanuel Fritsch**  
University of Nantes,  
France

**Rui Galopim de Carvalho**  
PortugalGemas Academy,  
Lisbon, Portugal

**Al Gilbertson**  
Gemological Institute  
of America, Carlsbad,  
California

**Lee A. Groat**  
University of British  
Columbia, Vancouver,  
Canada

**Thomas Hainschwang**  
GGTL Laboratories,  
Balzers, Liechtenstein

**Henry A. Hänni**  
GemExpert, Basel,  
Switzerland

**Jeff W. Harris**  
University of Glasgow

**Alan D. Hart**  
Gem-A, London

**Ulrich Henn**  
German Gemmological  
Association, Idar-Oberstein

**Jaroslav Hyršl**  
Prague, Czech Republic

**Brian Jackson**  
National Museums  
Scotland, Edinburgh

**Mary L. Johnson**  
Mary Johnson Consulting,  
San Diego, California, USA

**Stefanos Karampelas**  
Laboratoire Français de  
Gemmologie, Paris, France

**Lore Kiefert**  
Dr. Lore Kiefert Gemmology  
Consulting, Heidelberg,  
Germany

**Hiroshi Kitawaki**  
Central Gem Laboratory,  
Tokyo, Japan

**Michael S. Krzemnicki**  
Swiss Gemmological  
Institute SSEF, Basel

**Shane F. McClure**  
Gemological Institute  
of America, Carlsbad,  
California

**Jack M. Ogden**  
London

**Federico Pezzotta**  
Natural History Museum  
of Milan, Italy

**Jeffrey E. Post**  
Smithsonian Institution,  
Washington DC, USA

**George R. Rossman**  
California Institute of  
Technology, Pasadena,  
USA

**Karl Schmetzer**  
Petershausen, Germany

**Dietmar Schwarz**  
Bellerophon Gemlab,  
Bangkok, Thailand

**Menahem Sevdermish**  
Gemewizard Ltd, Ramat  
Gan, Israel

**Andy H. Shen**  
China University of  
Geosciences, Wuhan

**Guanghai Shi**  
China University of  
Geosciences, Beijing

**James E. Shigley**  
Gemological Institute  
of America, Carlsbad,  
California

**Christopher P. Smith**  
American Gemological  
Laboratories Inc.,  
New York, New York

**Elisabeth Strack**  
Gemnologisches Institut  
Hamburg, Germany

**Tay Thy Sun**  
Far East Gemological  
Laboratory, Singapore

**Frederick 'Lin' Sutherland**  
Port Macquarie, New  
South Wales, Australia

**Pornsawat Wathanakul**  
Kasetsart University,  
Bangkok

**Chris M. Welbourn**  
Reading, Berkshire

**Bear Williams**  
Stone Group Laboratories  
LLC, Jefferson City,  
Missouri, USA

**J. C. (Hanco) Zwaan**  
National Museum of  
Natural History 'Naturalis',  
Leiden, The Netherlands



**Gem-A**  
THE GEMMOLOGICAL ASSOCIATION  
OF GREAT BRITAIN

21 Ely Place  
London EC1N 6TD  
UK

t: +44 (0)20 7404 3334  
f: +44 (0)20 7404 8843  
e: [information@gem-a.com](mailto:information@gem-a.com)  
w: <https://gem-a.com>

Registered Charity No. 1109555  
A company limited by guarantee and  
registered in England No. 1945780  
Registered office: Palladium House,  
1-4 Argyll Street, London W1F 7LD

## PRESIDENT

Maggie Campbell Pedersen

## VICE PRESIDENTS

David J. Callaghan  
Alan T. Collins

## HONORARY FELLOWS

Gaetano Cavalieri  
Andrew Cody  
Terrence S. Coldham  
Richard Drucker  
Emmanuel Fritsch

## HONORARY DIAMOND MEMBER

Martin Rapaport

## CHIEF EXECUTIVE OFFICER

Alan D. Hart

## COUNCIL

Justine L. Carmody – Chair  
Nevin Bayoumi-Stefanovic  
Louise Goldring  
Joanna Hardy  
Philip Sadler  
Christopher P. Smith

## BRANCH CHAIRMEN

Midlands – Louise Ludlam-Snook  
North East – Mark W. Houghton  
North West – Liz Bailey

## COVERED BY THE FOLLOWING ABSTRACTING AND INDEXING SERVICES:

Clarivate Analytics' (formerly Thomson Reuters/ISI) Science Citation Index Expanded (in the Web of Science), Journal Citation Reports (Science Edition) and Current Contents (Physical, Chemical and Earth Sciences); Elsevier's Scopus; Australian Research Council's Excellence in Research for Australia (ERA) Journal List; China National Knowledge Infrastructure (CNKI Scholar); EBSCO's Academic Search Ultimate; ProQuest (Cambridge Scientific Abstracts); GeoRef; CrossRef; Chemical Abstracts (CA Plus); Mineralogical Abstracts; Index Copernicus ICI Journals Master List; Gale Academic OneFile; British Library Document Supply Service; and Copyright Clearance Center's RightFind application.

Science Citation Index  
Expanded

Web of Science



## CONTENT SUBMISSION

The Editor-in-Chief is glad to consider original articles, news items, conference reports, announcements and calendar entries on subjects of gemmological interest for publication in *The Journal of Gemmology*. A guide to the various sections and the preparation of manuscripts is given at <https://gem-a.com/membership/journal-of-gemmology/submissions>, or contact the Editor-in-Chief.

## SUBSCRIPTIONS

Gem-A members receive *The Journal* as part of their membership package, full details of which are given at <https://gem-a.com/membership>. Laboratories, libraries, museums and similar institutions may become direct subscribers to *The Journal*; download the form from *The Journal's* home page.

## ADVERTISING

Enquiries about advertising in *The Journal* should be directed to [advertising@gem-a.com](mailto:advertising@gem-a.com). For more information, see <https://gem-a.com/news-publications/media-pack-2021>.

## COPYRIGHT AND REPRINT PERMISSION

For full details of copyright and reprint permission contact the Editor-in-Chief. *The Journal of Gemmology* is published quarterly by Gem-A, The Gemmological Association of Great Britain. Any opinions expressed in *The Journal* are understood to be the views of the contributors and not necessarily of the publisher.

## DESIGN & PRODUCTION

Zest Design, London. [www.zest-uk.com](http://www.zest-uk.com)

## PRINTER

Paragon Leycol, London, <https://www.dg3leycol.com>



© 2022 Gem-A (The Gemmological Association of Great Britain)  
ISSN 1355-4565 (Print), ISSN 2632-1718 (Online)

# What's New

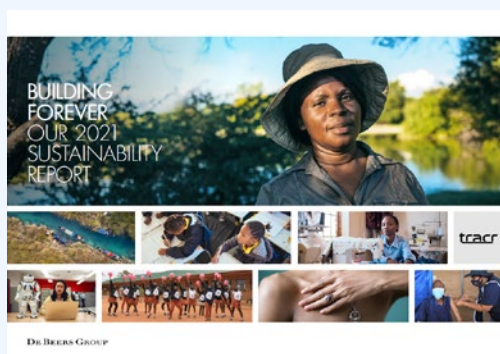
## INSTRUMENTATION

### Yehuda Diamond Detectors

The latest generation of Yehuda's Sherlock Holmes diamond detector, version 4.0 (<https://www.yehuda.com/sh-4-0>), was released in January 2022. This model uses the same detection method as its 2.0 predecessor (see *The Journal*, Vol. 36, No. 5, 2019, p. 393) to detect CVD- and HPHT-grown diamonds, and can check up to 27 rings or 250 carats of loose diamonds simultaneously. A monthly subscription provides cloud-based storage for about 1,000 test results, software updates and maintenance. For those looking for a smaller, more portable version, Yehuda now offers a Sherlock sidekick: Dr. Watson (<https://www.yehuda.com/dr-watson>). This instrument uses the same detection method and has most of the same features, with the ability to check up to six rings or 50 carats of loose diamonds simultaneously.



## NEWS AND PUBLICATIONS



### De Beers' 2021 Sustainability Report

Released 31 May 2022, *Building Forever: Our 2021 Sustainability Report* is a detailed overview of progress achieved in the year since the De Beers Group announced its 12 sustainability goals for 2030. Progress has included increased capacity of their diamond traceability blockchain platform, initial marketing of ethically sourced artisanal and small-scale-mined diamonds, reduction of energy use (with the goal to be carbon neutral by 2030), support for community development in Africa and promotion of diversity among diamond jewellery entrepreneurs.

For a detailed summary, and to download the 174-page report, visit <https://www.debeersgroup.com/media/company-news/2022/de-beers-group-reports-on-progress-towards-achieving-2030-sustainability-goals>.

### Gemmological Society of Japan 2022 Annual Meeting Abstracts

Abstracts of 'special lectures' presented during the online June 2022 Annual Meeting of the Gemmological Society of Japan are available at [https://www.jstage.jst.go.jp/browse/gsj/44/0/\\_contents/-char/en](https://www.jstage.jst.go.jp/browse/gsj/44/0/_contents/-char/en). The 17 abstracts cover a variety of topics (in Japanese with English summaries), including akoya cultured pearls, pearl identification using UV fluorescence, optical defects of

diamond, synthetic diamond, 'pink jade', talc resembling chrysocolla, zoning in opal, determining geographic origin of ruby and Paraíba tourmaline, and more. Also available are abstracts from previous GSJ conferences.

**Abstract of Papers Presented at Annual Meeting of the Gemmological Society of Japan**

## JNA's Lab-Grown Diamond Special Issue

In mid-2022, JNA released a special issue (in English and Chinese) on lab-grown diamonds that mainly focuses on their marketing by various producers. Brief articles cover sustainability, grading, jewellery design and market acceptance. Download the issue at <https://tinyurl.com/9s4ymvxp>.



### Lab-Grown Diamond Consumer Segments

In August 2022, USA-based market-research group The MVEye released its most recent report, *The MVEye's Core 3.5 LGD Consumer Segment*. It presents results related to core consumer segments driving the growth of lab-grown diamonds (i.e. those currently making purchases, self-educating and likely to purchase in the future). They indicate a willingness to pay a premium for custom-designed jewellery and 'concierge experiences' in both digital and in-person shopping sites. To purchase the report, visit <https://www.themveye.com/download-premium-report.php?report=14>.



## Platinum Jewellery Business Review 2022



Platinum Guild International has released its 44-page *Platinum Jewellery Business Review – 2021 Results Summary and Outlook*, with infographics organised by country (Japan, China, India and the USA) that illustrate retail sales developments for platinum jewellery. Projections for 2022 envision continued strong growth, returning to pre-pandemic levels. To download this review, as well as detailed quarterly reports for 2018–2021 and the first quarter of 2022, visit <https://platinumguild.com/research-publications/platinum-jewellery-business-review>.

## Santa Fe Symposium Proceedings 2022

Full papers covering presentations at the 2022 Santa Fe Symposium are now available online at <https://tinyurl.com/567tth54>. Held 22–25 May, this was



the 34th and final Santa Fe Symposium. The primary focus of this long-running conference (held annually in New Mexico, USA) is on jewellery manufacturing, but some of the presentations are also of interest to those in the gem trade. Topics include lab-grown diamond, digital jewellery manufacturing, the Birmingham School of Jewellery, blockchain technology and more. Proceedings from previous symposia are also available online for the years 1987 and 2000–2019.

## World Silver Survey 2022

The Silver Institute in collaboration with Metals Focus released this infographic report in April 2022 at <https://www.silverinstitute.org/wp-content/uploads/2022/04/Metals-FocusWWS2022Launch.pdf>. Since the steep rise in the price of silver in August 2020, the metal has maintained a value mostly above USD22/ounce, with dips primarily reflecting inflation in the USA. Production of silver from mining rose significantly as the industry recovered from COVID-19, contributing to a 5% growth in global supply. The top four silver fabricators (excluding coin and bar) in 2021 were China, the USA, India and Japan. India far leads the rest of the world in jewellery gains. Global supply for 2022 is predicted to hit a six-year high, up 3%, with global demand projected to rise more than 5%.



## OTHER RESOURCES

### Branko Gems' Diamond Academies



In June 2022, Branko Gems (Vancouver, British Columbia, Canada) released its Intermediate and Advanced Diamond Academies. The Intermediate Diamond Academy consists of two parts: (1) a documentary movie on 'Laboratory-Grown Diamonds – From Factories to Markets' that summarises presentations by 19 international experts given in ten webinars from October to March 2020, and (2) four lectures covering pink diamonds, diamond treatments and portable

instruments for the screening and identification of diamond. The Advanced Diamond Academy consists of seven recordings of lectures based on the book *Diamonds: Natural, Treated & Laboratory-Grown* (see *The Journal*, Vol. 38, No. 2, 2022, pp. 201–202). The lectures cover the principles of instrumentation used for diamond identification, optical spectroscopy of natural and lab-grown diamonds, Chinese synthetic diamonds, colour-treatment of natural and lab-grown diamonds, screening and identification using portable instruments, testing by spectroscopy and fluorescence imaging, and case studies from the CGL Canadian Gemlab. To purchase the Academies as downloadable files or on a USB drive, visit <https://www.brankogems.com/shop/product-category/advanced-diamond-academy>.

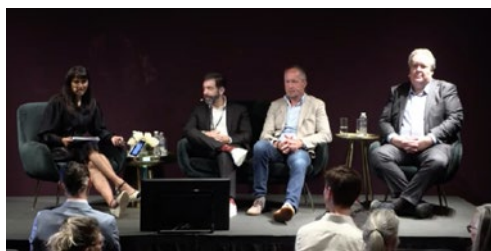
instruments for the screening and identification of diamond. The Advanced Diamond Academy consists of seven recordings of lectures based on the book *Diamonds: Natural, Treated & Laboratory-Grown* (see *The Journal*, Vol. 38, No. 2, 2022, pp. 201–202). The lectures cover the principles of instrumentation used for diamond identification, optical spectroscopy of natural and lab-grown diamonds, Chinese synthetic diamonds, colour-treatment of natural and lab-grown diamonds, screening and identification using portable instruments, testing by spectroscopy and fluorescence imaging, and case studies from the CGL Canadian Gemlab. To purchase the Academies as downloadable files or on a USB drive, visit <https://www.brankogems.com/shop/product-category/advanced-diamond-academy>.

### GemGenève Seminar Presentations

Twelve 'Live Talks' from the May 2022 GemGenève show in Geneva, Switzerland, are now available online as recorded videos. The presentations are each about one hour long and cover a range of jewellery and gem topics, including enhancing the value of 'jewellery heritage', glyptic arts (engraving, cutting, carving, etc.—in English and French), enamel, modern design trends, colour in gemmology (in French), African gems, history of necklaces and more. To access the talks, register at <https://digital.gemgeneve.com/live-talks>.



## MISCELLANEOUS



### Masterpiece London: Collecting Natural Treasures from the Mineral Kingdom

This year's Masterpiece London Art Fair (30 June–6 July 2022) included a panel presentation on mineral and gem collecting for the first time. Panel speakers included Daniel Trinchillo (Fine Minerals International, Edison, New Jersey, USA), Alan Hart (Gem-A, London) and Joel Bartsch (Houston Museum of Natural Science, Texas, USA).

The context of this event at an art fair represents a broadening of interest in gem and mineral collecting. Video and audio recordings of the one-hour discussion are available at <https://www.masterpiecefair.com/event-detail/110>.

**What's New** provides announcements of new instruments/technology, publications, online resources and more. Inclusion in What's New does not imply recommendation or endorsement by Gem-A. Entries were prepared by Carol M. Stockton unless otherwise noted.

# Gem Notes

## COLOURED STONES

### Emerald with Bertrandite-Phlogopite Veins Resembling Fracture Fillings

Recently, the American Gemological Laboratories received an emerald ring for identification and enhancement reporting. Visual observation showed a system of interconnected surface-reaching fissures with possible infillings, which appear whitish in Figure 1.

Microscopic observation revealed the presence of fissures penetrating deep into the stone that appeared to be filled by some type of material (Figure 2). To our surprise, Fourier-transform infrared (FTIR) spectroscopy of the fractured areas did not show the presence of any oil, resin or other filler material that we usually observe in clarity-enhanced emeralds. Therefore, we decided to investigate further using Raman micro-spectroscopy.

Viewing the sample with the reflected light of the Raman microscope more precisely revealed this complex system of fissures. Variations in grey tones differentiated the emerald host (the lightest-appearing areas) from darker veined areas and even darker lines along well-demarcated fissures (Figure 3a). Raman analysis of several spots (Figure 3b) showed the veined areas were composed of bertrandite (one of the most important ores of beryllium; see Lederer *et al.* 2016), while the accompanying fissures contained phlogopite.

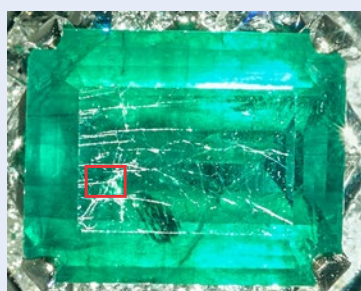


**Figure 1:** The examined emerald (10.02 × 7.93 × 4.38 mm) shows a network of fissures on its surface. Fibre-optic lighting was oriented to accentuate their visibility.

The area studied using Raman micro-spectroscopy is marked by the rectangle. Photo by Alex Mercado.



**Figure 2:** One of the fissures in the emerald in Figure 1 is seen here in darkfield illumination with the gemmological microscope. Photomicrograph by Christopher P. Smith; magnified 30×.

Two of the six Raman point analyses of the veined areas gave a slightly better match for eckermannite (a rare sodic amphibole; see Oberti *et al.* 2015) than bertrandite. However, a comparison to reference spectra for eckermannite and bertrandite in the RRUFF database revealed the latter was actually a better fit. In terms of geological processes, the association of emerald with bertrandite has been previously documented (Barton & Young 2002), while the only reported occurrence of eckermannite is together with jadeite (Colombo *et al.* 2000; Harlow & Sorensen 2001). We therefore ruled out the presence of eckermannite in the veined areas of the sample, and consider bertrandite to have formed as an alteration product of the emerald.

The presence of phlogopite along the fissures is not surprising, since this mineral is commonly associated with emerald in schist-type deposits (Giuliani *et al.* 2019). Phlogopite has been observed not only as a host-rock constituent (in phlogopite reaction zones) surrounding emeralds, but also as inclusions or along fractures within the emeralds at both microscopic and macroscopic scales (Araújo Neto *et al.* 2019).



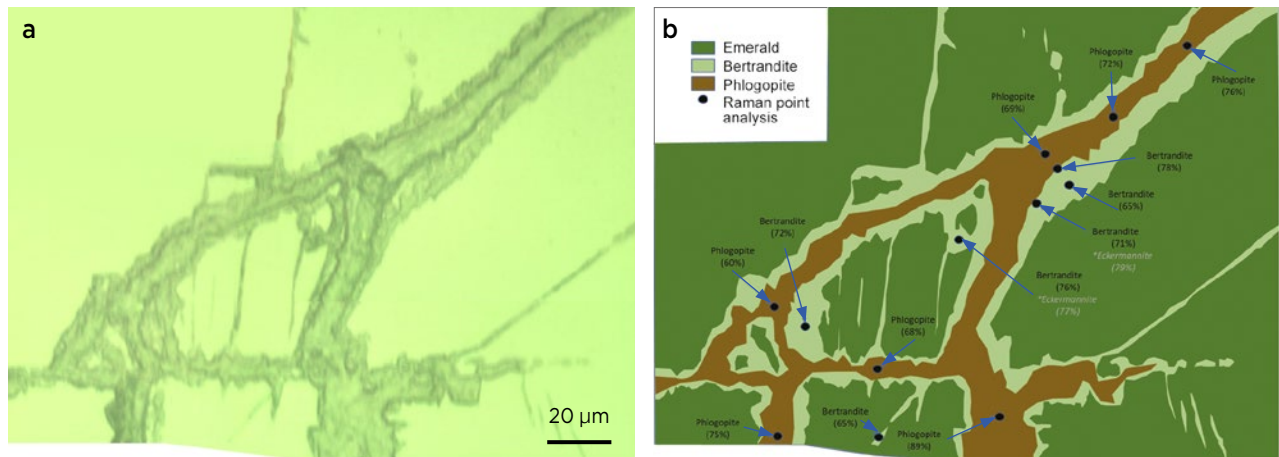


**Figure 3:** (a) This reflected-light image of the studied area of the emerald, as seen with the Raman microscope, shows tonal variations corresponding to different domains that are present. (b) A mineral map of this area depicts the relationship among the various phases: the emerald host, a bertrandite-bearing alteration zone and a fissure network filled by phlogopite. In parentheses are the ‘match percentages’ obtained for each Raman analysis point. Photomicrograph and diagram by R. Zellagui.

Based on our observations, we propose that after the emerald crystallised, a late-stage fluid entered the fissures and induced an alteration halo by transforming the emerald host into the bertrandite-bearing assemblage, and this was accompanied by the formation of phlogopite along the open fissures. The use of both reflected light at high magnification and Raman micro-spectroscopy

were necessary for differentiating the various mineral phases present and their spatial and temporal relationships in the studied emerald.

Dr Riadh Zellagui ([riadh@aglgemlab.com](mailto:riadh@aglgemlab.com))  
American Gemological Laboratories  
New York, New York, USA

## References

- Araújo Neto, J.F. de, Barreto, S. de B., Carrino, T.A., Müller, A. & Santos, L.C.M. de L. 2019. Mineralogical and gemological characterization of emerald crystals from Paraná deposit, NE Brazil: A study of mineral chemistry, absorption and reflectance spectroscopy and thermal analysis. *Brazilian Journal of Geology*, **49**(3), article e20190014 (15 pp.), <https://doi.org/10.1590/2317-4889201920190014>.
- Barton, M.D. & Young, S. 2002. Non-pegmatitic deposits of beryllium: Mineralogy, geology, phase equilibria and origin. In: Grew, E.S. (ed) *Beryllium*. Mineralogical Society of America, Washington DC, USA, 591–692, <https://doi.org/10.1515/9781501508844-015>.
- Colombo, F., Rinaudo, C. & Trossarelli, C. 2000. The mineralogical composition of maw-sit-sit from Myanmar. *Journal of Gemmology*, **27**(2), 87–92, <https://doi.org/10.15506/JoG.2000.27.2.87>.
- Giuliani, G., Groat, L.A., Marshall, D., Fallick, A.E. & Branquet, Y. 2019. Emerald deposits: A review and enhanced classification. *Minerals*, **9**(2), article 105 (63 pp.), <https://doi.org/10.3390/min9020105>.
- Harlow, G.E. & Sorensen, S.S. 2001. Jade: Occurrence and metasomatic origin. *Australian Gemmologist*, **21**(1), 7–11.
- Lederer, G.W., Foley, N.K., Jaskula, B.W. & Ayuso, R.A. 2016. *Beryllium—A Critical Mineral Commodity—Resources, Production, and Supply Chain*. U.S. Geological Survey, Reston, Virginia, USA, 4 pp.
- Oberti, R., Boiocchi, M., Hawthorne, F.C., Ball, N.A. & Harlow, G.E. 2015. Eckermannite revised: The new holotype from the jade mine tract, Myanmar—Crystal structure, mineral data, and hints on the reasons for the rarity of eckermannite. *American Mineralogist*, **100**(4), 909–914, <https://doi.org/10.2138/am-2015-5132>.

## Cinnabar Inclusions in Ethiopian Opal

The authors recently examined a 15.8 ct Ethiopian opal (Figure 4) that contained numerous red dendritic particles that each measured up to 70–100 μm in diameter (Figure 5). The Ethiopian origin of the opal was confirmed by its physical properties (slight hydrophane

character and rounded columnar structure) and its chemical composition (high Ba concentration; Rondeau *et al.* 2010). The inclusions were identified by Raman micro-spectroscopy as cinnabar (HgS). Energy-dispersive X-ray fluorescence (EDXRF) chemical analyses of



**Figure 4:** This 15.8 ct opal from Ethiopia was examined for this report. Photo by C. Caplan.

the top surface of the sample confirmed the presence of Hg and S. Cinnabar and opal are associated in numerous localities, particularly in the western USA (Knopf 1915; Gettens *et al.* 1972; <https://www.mindat.org/min-3004.html>). However, cinnabar is only rarely mentioned as inclusions in opal (see, e.g., Gaillou 2015). Also known is an opalised or silicified cinnabar material known as myrickite, in which the high concentration of cinnabar inclusions induces an intense orange or red colour (Manutchehr-Danai 2009; Melero *et al.* 2019).

To the authors' knowledge, this is the first time that cinnabar inclusions have been documented in opal from Ethiopia. Their dendritic habit suggests relatively fast growth, whereas magnetite inclusions reported in Ethiopian opal have a well-formed octahedral habit (Rondeau *et al.* 2010), suggesting slow growth. This points to a vast domain of parameters possible (at least in terms of growth rate and chemistry) for the formation of inclusions in Ethiopian opal, which perhaps reflects the expansive region over which those deposits occur.

Féodor Blumentritt<sup>1</sup> ([feodor.blumentritt@ggtl-lab.org](mailto:feodor.blumentritt@ggtl-lab.org)),  
Candice Caplan<sup>1</sup>, Emmanuel Fritsch FGA<sup>2</sup>  
and Franck Notari<sup>1</sup>

<sup>1</sup>GGTL Laboratories Switzerland, Geneva, Switzerland  
<sup>2</sup>IMN-CNRS and University of Nantes, France

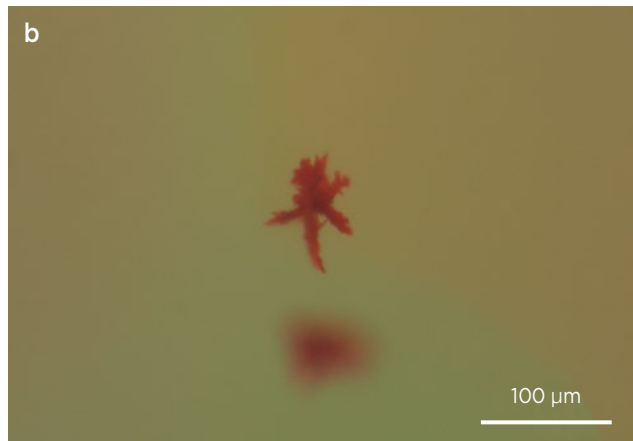
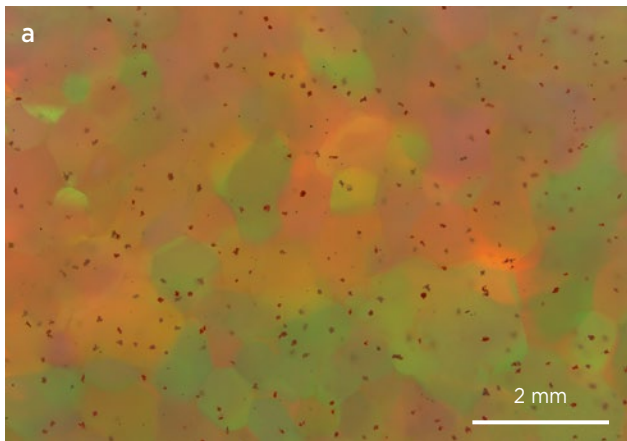


**Figure 5:** (a) The opal contains red cinnabar inclusions across the top surface of the cabochon. (b) A closer look at one of these inclusions shows its dendritic form. Photomicrographs by F. Notari.

## References

- Gaillou, E. 2015. An overview of gem opals: From the geology to color and microstructure. *Thirteenth Annual Sinkankas Symposium—Opal*, Carlsbad, California, USA, 18 April, 10–19.
- Gettens, R.J., Feller, R.L. & Chase, W.T. 1972. Vermilion and cinnabar. *Studies in Conservation*, **17**(2), 45–69, <https://doi.org/10.2307/1505572>.
- Knopf, A. 1915. Some cinnabar deposits in western Nevada. *Contributions to Economic Geology, 1915. Part I. Metals and Nonmetals Except Fuels*, U.S. Geological Survey Bulletin 620, 59–68, <https://pubs.usgs.gov/bul/0620d/report.pdf>.
- Manutchehr-Danai, M. 2009. *Dictionary of Gems and Gemology*. Springer, Berlin and Heidelberg, Germany, 1,037 pp., <https://doi.org/10.1007/978-3-540-72816-0>.

Melero, D., Lobato, B., López-Antón, M.A. & Martínez-Tarazona, M.R. 2019. Identification of mercury species in minerals with different matrices and impurities by thermal desorption technique. *Environmental Science and Pollution Research*, **26**(11), 10867–10874, <https://doi.org/10.1007/s11356-019-04245-8>.

Rondeau, B., Fritsch, E., Mazzero, F., Gauthier, J.-P., Cenki-Tok, B., Bekele, E. & Gaillou, E. 2010. Play-of-color opal from Wegel Tena, Wollo Province, Ethiopia. *Gems & Gemology*, **46**(2), 90–105, <https://doi.org/10.5741/gems.46.2.90>.

## Violet Spinel with Strong Green Fluorescence

Recently submitted to Stone Group Laboratories by gem dealer John Bachman was a 3.73 ct marquise-cut spinel showing light violet ('lilac') colouration (Figure 6a). It was cut from a rough parcel that he had acquired more than 30 years ago from Okkampitiya, Sri Lanka. Of note was its strong, bright bluish green fluorescence to long-wave UV excitation (Figure 6b), since most gem spinel is either inert (due to the presence of Fe) or fluoresces red (due to Cr or Co).

The stone's identity as spinel was confirmed by Raman analysis using a Magilabs GemmoRaman-532SG instrument. Its RI was 1.713 and hydrostatic SG was 3.56. The relatively low RI eliminated the possibility of it being a Verneuil-grown (flame-fusion) synthetic spinel. Between crossed polarisers, anomalous extinction was seen rolling across the stone while it was rotated. Only a very faint magnetic susceptibility was detected using the float method. The stone was eye-clean, and microscopic examination revealed only one small 'fingerprint' and some surface features: a 'natural' on the girdle and what appeared to be a surface-reaching fissure or stress crack.

EDXRF spectroscopy was performed with an Amptek X123-SDD spectrometer (Figure 7). Although significant Fe was present, Mn was also found in an unusually high concentration for spinel. Also detected were Zn, Ni and Ga. The presence of Ga confirmed the natural origin of this stone (which the unusual fluorescence had initially

called into doubt).

Ultraviolet-visible-near infrared (UV-Vis-NIR) spectroscopy (Figure 8) with a Magilabs GemmoSphere unit revealed absorption features resembling those recorded by Kammerling & Fritsch (1991) for a similar-coloured lilac spinel that showed somewhat weaker green fluorescence. Most prominent were absorption peaks at 555, 576 and 620 nm related to  $\text{Co}^{2+}$  (cf. Belley & Palke 2021). (Although no Co was found with EDXRF analysis, this element is often below the detection limit of our instrument and is frequently masked by or merged with the  $K\alpha$  or  $K\beta$  peaks of adjacent elements.) The absorption spectrum also showed Fe-related peaks in the 375–478 nm range, and a sharp, distinct peak at 427 nm attributed to  $\text{Mn}^{2+}$  (cf. Schmetzer *et al.* 1989). We infer that the presence of  $\text{Fe}^{2+}$  and  $\text{Fe}^{3+}$  with traces of  $\text{Co}^{2+}$  in tetrahedral coordination is responsible for the lilac (violet) body colour of this spinel.

To compare the green fluorescence of this stone to a spinel showing more common red luminescence, fluorescence spectroscopy was performed with a Magilabs EXA spectrometer (Figure 9). The emission peak of the lilac spinel's green fluorescence was centred at about 510 nm. By contrast, the red spinel's red fluorescence produced a series of luminescence peaks that were centred around 700 nm. Green fluorescence in spinel is attributed to tetrahedral  $\text{Mn}^{2+}$  (Kammerling & Fritsch 1991; Sehgal &



**Figure 6:** (a) This 'lilac' spinel from Sri Lanka weighs 3.73 ct and measures 12.64 × 7.22 × 6.52 mm. (b) Viewed under long-wave (369 nm LED) UV radiation, the spinel emits an unusual strong bluish green luminescence. Photos by C. Williams.

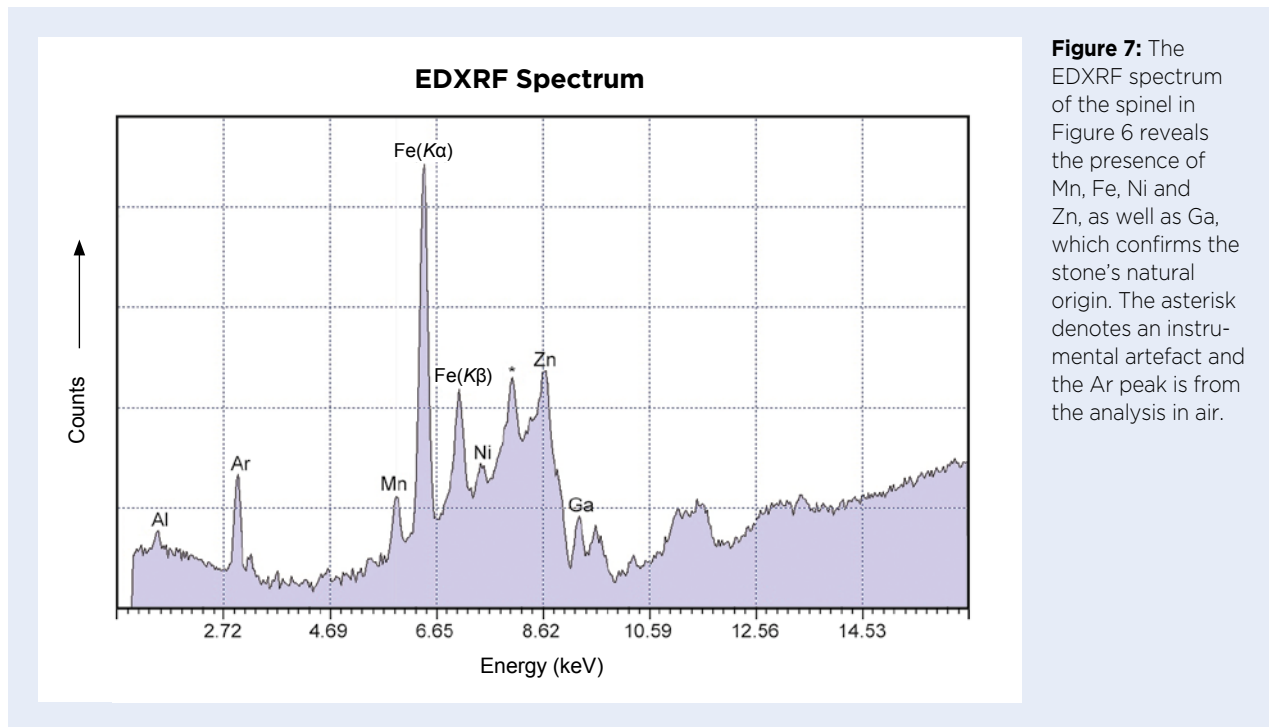


**Figure 7:** The EDXRF spectrum of the spinel in Figure 6 reveals the presence of Mn, Fe, Ni and Zn, as well as Ga, which confirms the stone's natural origin. The asterisk denotes an instrumental artefact and the Ar peak is from the analysis in air.

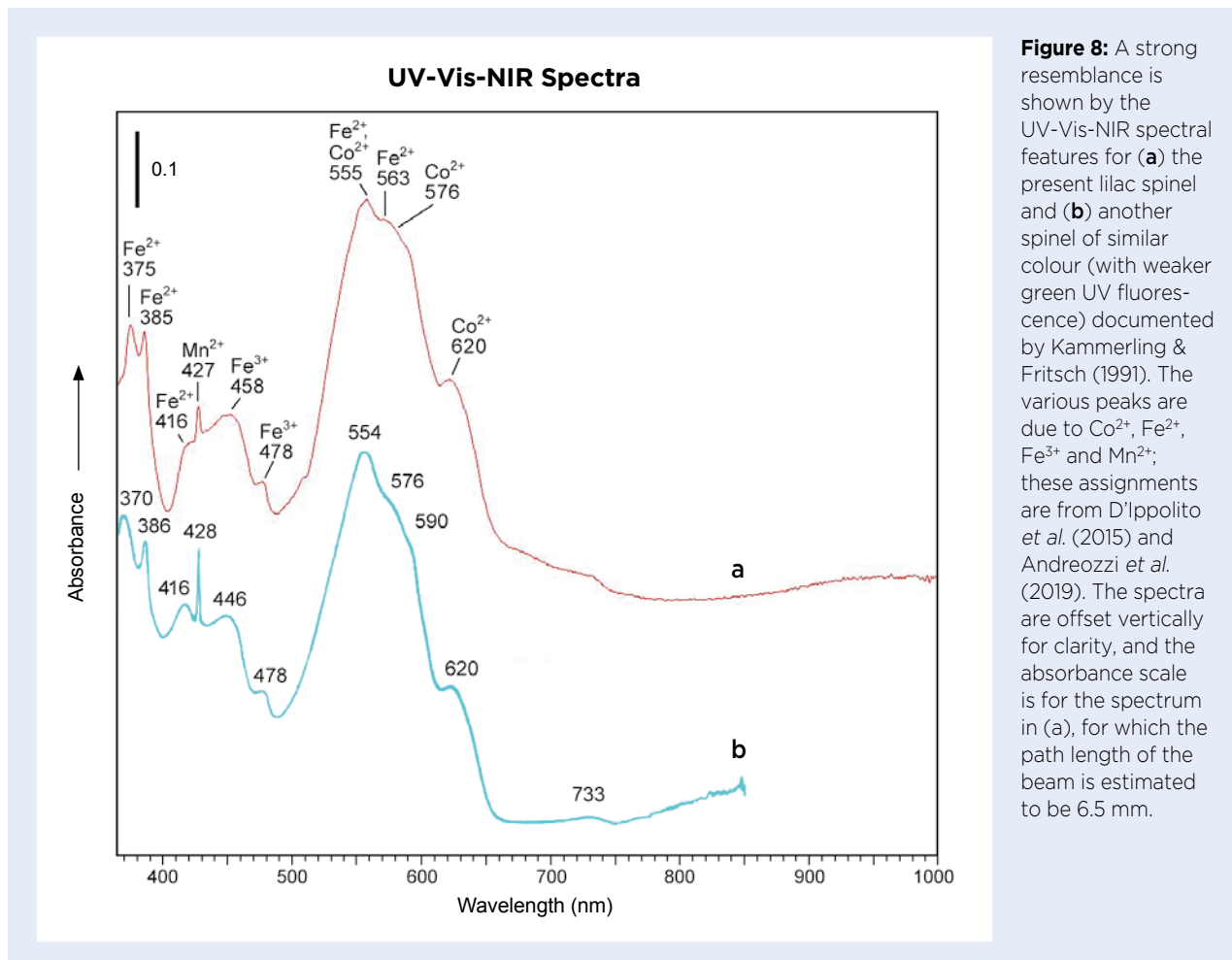


**Figure 8:** A strong resemblance is shown by the UV-Vis-NIR spectral features for (a) the present lilac spinel and (b) another spinel of similar colour (with weaker green UV fluorescence) documented by Kammerling & Fritsch (1991). The various peaks are due to Co<sup>2+</sup>, Fe<sup>2+</sup>, Fe<sup>3+</sup> and Mn<sup>2+</sup>; these assignments are from D'Ippolito *et al.* (2015) and Andreozzi *et al.* (2019). The spectra are offset vertically for clarity, and the absorbance scale is for the spectrum in (a), for which the path length of the beam is estimated to be 6.5 mm.

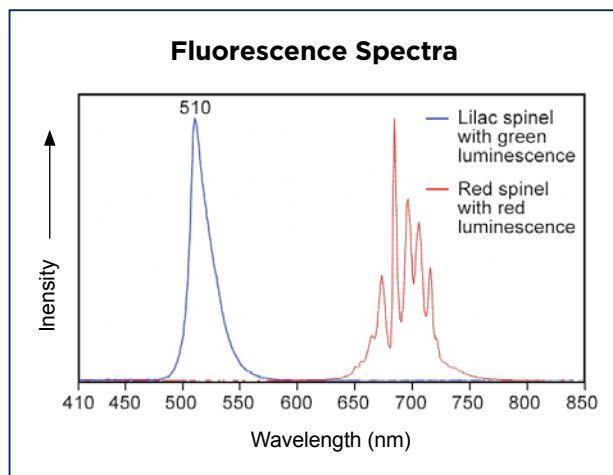


**Figure 9:** Fluorescence spectra of the lilac spinel and a typical red spinel are significantly different. The peak at 510 nm corresponds to the lilac spinel's strong bluish green luminescence, whereas the red-fluorescing spinel displays a series of peaks around 700 nm.

Girma 2016). The unusually strong green fluorescence of the present lilac spinel is due to its enriched Mn content, apparently combined with relatively low Fe as compared to the stone documented by Kammerling & Fritsch (1991).

*Cara Williams FGA and Bear Williams FGA  
(info@stonegrouplabs.com)  
Stone Group Laboratories  
Jefferson City, Missouri, USA*

## References

- Andreozzi, G.B., D'Ippolito, V., Skogby, H., Hålenius, U. & Bosi, F. 2019. Color mechanisms in spinel: A multi-analytical investigation of natural crystals with a wide range of coloration. *Physics and Chemistry of Minerals*, **46**(4), 343–360, <https://doi.org/10.1007/s00269-018-1007-5>.
- Belley, P. & Palke, A. 2021. Purple gem spinel from Vietnam and Afghanistan: Comparison of trace element chemistry, cause of color, and inclusions. *Gems & Gemology*, **57**(3), 228–238, <https://doi.org/10.5741/gems.57.3.228>.
- D'Ippolito, V., Andreozzi, G.B., Hålenius, U., Skogby, H., Hametner, K. & Günther, D. 2015. Color mechanisms in spinel: Cobalt and iron interplay for the blue color. *Physics and Chemistry of Minerals*, **42**(6), 431–439, <https://doi.org/10.1007/s00269-015-0734-0>.
- Kammerling, R.C. & Fritsch, E. 1991. Gem Trade Lab Notes: Spinel, with unusual green fluorescence. *Gems & Gemology*, **27**(2), 112–113.
- Schmetzer, K., Haxel, C. & Amthauer, G. 1989. Colour of natural spinels, gahnospinel and gahnites. *Neues Jahrbuch für Mineralogie, Abhandlungen*, **160**(2), 159–180.
- Sehgal, A. & Girma, D. 2016. Lab Notes: Unusual yellowish green spinel. *Gems & Gemology*, **52**(2), 194–195.

## New Finds at the Tourmaline King Mine, Pala, California, USA

The Pala District in San Diego County, California, USA, is famous for producing high-quality tourmaline, morganite, kunzite and other gem and mineral commodities from various pegmatite mines such as the Stewart, Tourmaline Queen, Tourmaline King and Pala Chief (Jahns & Wright 1951). Recent work at one of these mines, the Tourmaline King, has produced the first significant finds of tourmaline and morganite from this deposit in more than 100 years.

The Tourmaline King has a relatively long history and, according to Jahns & Wright (1951, p. 55):

The mine was opened by F. B. Schuyler of San Diego in 1903, and during the early years of its operation yielded much gem tourmaline of exceptional quality. It was later purchased by R. M. Wilke of Palo Alto, who carried on a very thorough program of exploration but obtained only small returns.

According to Bill Larson (Pala International, Fallbrook, California), most of the initial production took place during 1903–1909—particularly from one very large gem-bearing pocket that was discovered in 1904—and then operations ceased after the death of the Chinese Dowager Empress who had been purchasing most of the carving-grade pink tourmaline from this and other mines in southern California. Subsequent work at the Tourmaline King by R. M. Wilke mostly took place in 1919–1922, via a lower adit that ultimately had to be abandoned due to the collapse of the tunnel in a shear zone. The mine then lay dormant for decades, while being occasionally visited by gem and mineral collectors who screened the tailings. In 2002, the mine was purchased by Gary and Sheila Martin, who partnered with Scott Ritchie to prepare for future underground exploration. They have worked the deposit intermittently since the early 2010s, with most activity taking place since 2017 by Ritchie and miner Kiel Snyder,



**Figure 10:** These gem tourmaline crystals (30.0–34.3 mm long) were recently recovered from the historically important Tourmaline King mine in Pala, California, USA. Photo by Orasa Weldon.

after they gained unimpeded access to the property and began using Bill Larson's mining equipment that was formerly employed at the Mountain Lily mine.

By 2020 they had tunnelled nearly 60 m to bypass the shear zone that stopped Wilke's advance, and in the following two years they penetrated another 60+ m before they encountered signs of pocket mineralisation. Eventually, on 12 January 2022, at a depth of 145 m, a pocket was found that measured 46 × 38 × 38 cm and contained 'pastel pink' tourmaline as loose single crystals and on a matrix of smoky quartz and cleavelandite feldspar. Some of the tourmalines were quite large, weighing up to 1 kg. Numerous gem pencils were also recovered (e.g. Figure 10), as well as several well-crystallised morganite specimens. Photos of the mining activities and the gem pocket are available on Pala International's website at <https://mailchi.mp/palaminerals/long-live-the-king-pala-news-tucson-2022>. In total, approximately 50 kg of gem and specimen material were recovered from the so-called Pastel Pocket. Some of the pieces showed distinct chatoyancy, and several cabochons of cat's-eye



**Figure 11:** Some of the tourmaline from the new production at the Tourmaline King mine displays chatoyancy, as shown by this 37.7 g crystal and these cabochons (2.33–9.18 ct) that were cut by Meg Berry (Megagem, Fallbrook, California). Photo by Orasa Weldon.

tourmaline have been cut that range from 0.94 to 9.18 ct (e.g. Figure 11). The chatoyancy is due to abundant fine growth tubes oriented parallel to the *c*-axis.

The production from the Tourmaline King mine is being sold by Pala International, and the first specimens were offered at the Tucson gem and mineral shows in February 2022. Additional pieces will become available as they are cleaned and prepared for display. Further mining has continued to yield some small vugs containing tourmaline (of darker pink colour) as well as morganite, providing encouragement for more finds in the future. Most recently, in August 2022, a vug containing green tourmaline was found, and a clean 17 ct stone was faceted.

Brendan M. Laurs FGA

## Reference

- Jahns, R.H. & Wright, L.A. 1951. *Gem- and Lithium-bearing Pegmatites of the Pala District, San Diego, California*. Special Report 7-A, Division of Mines, State of California, San Francisco, California, USA, 72 pp.

## SYNTHETICS AND SIMULANTS

### A New Amber Imitation: Amber-Epoxy Composite

Amber is very popular in the Taiwanese market, and amber-related gem enhancements and imitations are constantly evolving. Plastic, copal and pressed amber are the most common imitations of natural amber. Recently, a string of translucent dark brown beads (Figure 12) was submitted to the Taiwan Union Lab of Gem Research (TULAB) as natural amber, but it proved to consist of a new imitation.

The spot RI of the beads was about 1.54–1.53, which is consistent with that of amber. Initial microscopic observations showed that these beads had a vaguely granular structure, but they did not quite resemble the

typical appearance of pressed amber. Under long-wave UV radiation, the fluorescence pattern of the beads showed an uneven blue appearance with angular boundaries consistent with an aggregate of blocky pieces cemented together with some kind of bonding material (Figure 13). Different areas of the beads were analysed by Raman spectroscopy (785 nm laser excitation) and compared with data reported in the literature (Brody *et al.* 2001; Chike *et al.* 2016). The results revealed that the blocky particles were composed of amber fragments and the bonding material was epoxy resin (Figure 14).

Due to the amount of bonding material present, we identified these beads as a composite material made of amber fragments with brown epoxy resin. Although visual observation and RI measurements might not be enough to distinguish this material from natural (pressed) amber, long-wave UV fluorescence and Raman spectroscopy are effective for identifying such imitations.

*Shu-Hong Lin (service@tulab.com.tw)*  
*Institute of Earth Sciences*  
*National Taiwan Ocean University*  
*and TULAB, Taipei*

*Tsung-Ying Yang, Kai-Yun Huang and Yu-Shan Chou*  
*TULAB, Taipei*



**Figure 12:** These beads were submitted to TULAB as natural amber. Photo by Tsung-Ying Yang.



**Figure 13:** Long-wave UV fluorescence of the beads is unevenly blue, and they appear to consist of blocky pieces cemented together with a bonding material. Photo by Yu-Shan Chou.

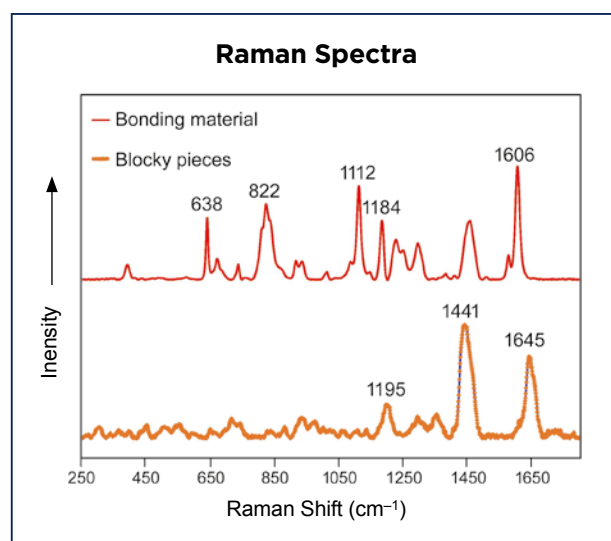


**Figure 14:** The Raman spectra of the beads reveals that the blocky pieces are amber and the filler material is an epoxy resin. The spectra are offset vertically for clarity, and are baseline-corrected and normalised.

## References

Brody, R.H., Edwards, H.G.M. & Pollard, A.M. 2001. A study of amber and copal samples using FT-Raman spectroscopy. *Spectrochimica Acta Part A: Molecular and Biomolecular Spectroscopy*, **57**(6), 1325–1338, [https://doi.org/10.1016/s1386-1425\(01\)00387-0](https://doi.org/10.1016/s1386-1425(01)00387-0).

Chike, K.E., Myrick, M.L., Lyon, R.E. & Angel, S.M. 2016. Raman and near-infrared studies of an epoxy resin. *Applied Spectroscopy*, **47**(10), 1631–1635, <https://doi.org/10.1366/0003702934334714>.

## Transparent Optical Ceramic as a Gem Material?



**Figure 15:** This orange gem (approximately 14 × 12 mm) set in a custom-made mounting was identified as a BaZrO<sub>3</sub>-type ceramic material. Photo by B. Williams.

A rectangular, emerald-cut, orange gem set in a custom-made gold ring (Figure 15), which had previously passed through several hands with various conflicting identifications, was recently submitted to Stone Group Laboratories. The item had been inherited by the owner

and its history was unknown. Upon initial testing, the reasons for its problematic identification became apparent, as its gemmological properties did not readily match any familiar gem material.

The gem measured 13.81 × ~11.8 × 6.41 mm and displayed a vivid orange colour. It was singly refractive with an RI of 1.67. Specific gravity measurements were not possible due to the mounting, and we were not given permission to unset the gem. It was inert to long- and short-wave UV radiation, and under the Chelsea Colour Filter it appeared reddish orange. No magnetic susceptibility was detected. Polariscopes readings were weak, partly due to the obstruction caused by the setting, although there appeared to be a subtle blink that occurred four times during a 360° rotation, indicating a possible crystalline structure. Microscopic observation with up to 30× magnification revealed no internal features.

UV-Vis-NIR spectroscopy with a Magilabs GemmoSphere unit revealed general absorption in the blue region with no notable peaks. Raman spectroscopy with a Magilabs GemmoRaman-532SG unit yielded a distinct spectrum (Figure 16), but we could not find a match

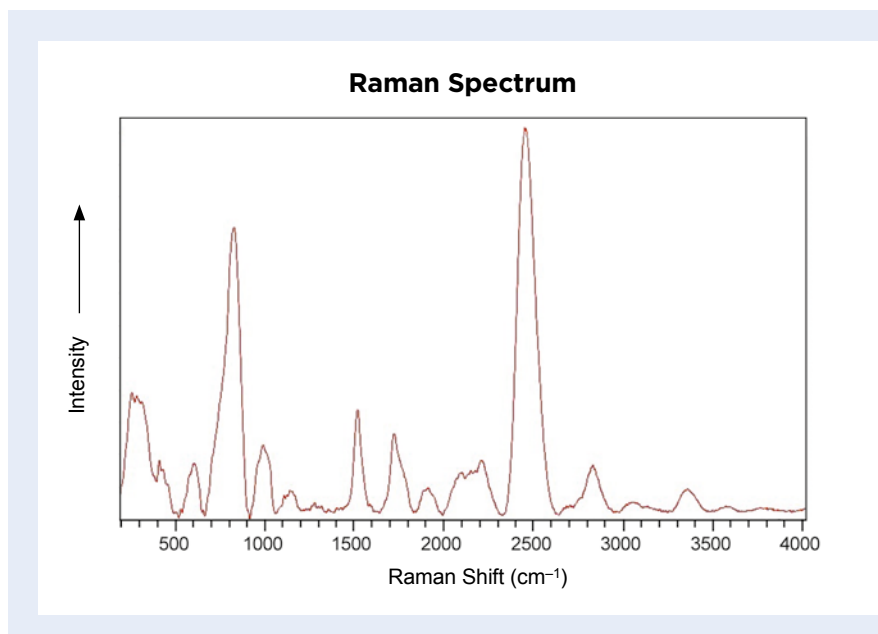


**Figure 16:** Raman spectroscopy of the orange gem does not match any reference spectrum in publicly available databases.



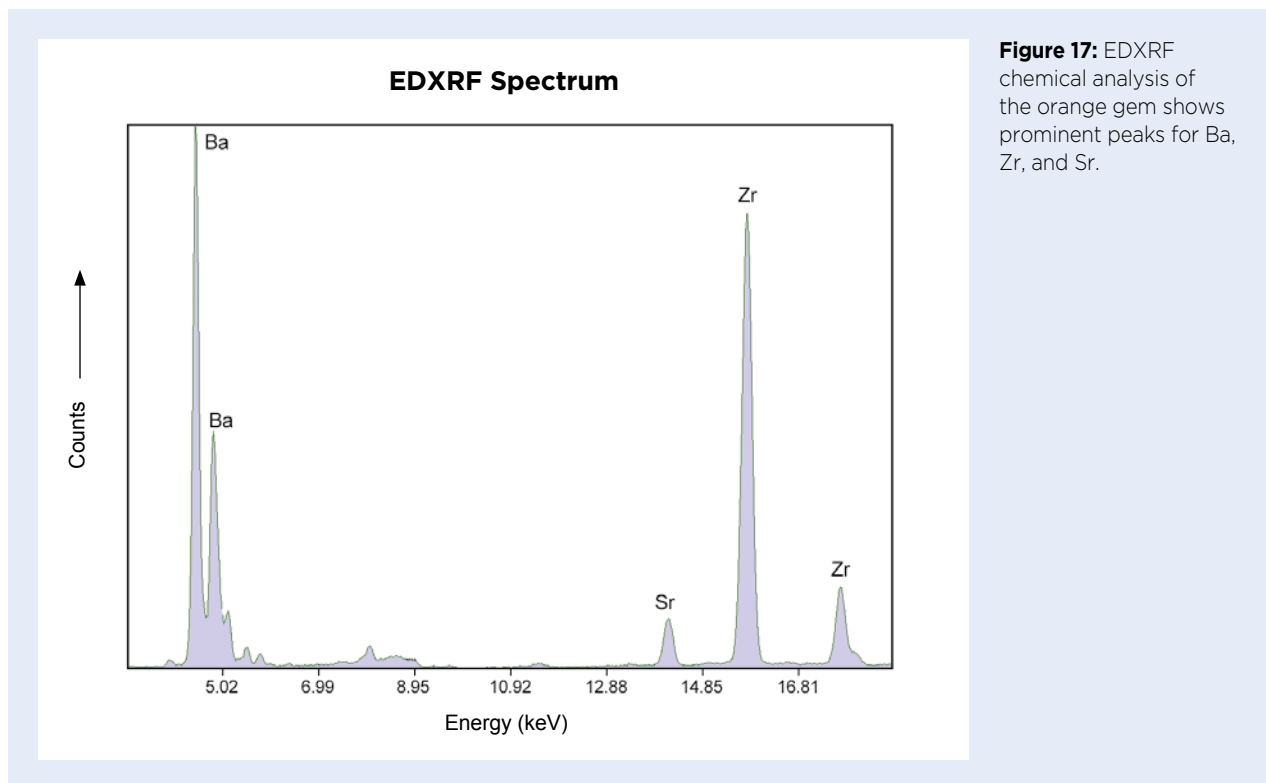


**Figure 17:** EDXRF chemical analysis of the orange gem shows prominent peaks for Ba, Zr, and Sr.

in the GemmoRaman or RRUFF databases. The latter database, in particular, consists exclusively of natural minerals. Likewise, the infrared spectrum, obtained with a Magilabs GemmoFtir spectrometer, was also inconclusive for identification. EDXRF chemical analysis with an Amptek X123-SDD spectrometer revealed significant amounts of both Ba and Zr, with minor Sr (Figure 17).

The composition and overall nature of this sample are consistent with some artificial BaZrO<sub>3</sub>-type glass-like ceramics with perovskite structure (cf. Bhalla *et al.* 2000; Benabdallah *et al.* 2014; Xiao *et al.* 2020). Based

on a process of elimination, this is the most likely identification of this sample. A conclusive identification was not possible without further research and comparison samples of ceramics with perovskite-type structure of a similar color and composition. Transparent optical ceramics have been used for various industrial applications due to their thermal and electrical conductivity, and it is surprising to encounter such material used as a gem.

Cara Williams FGA and  
Bear Williams FGA

## References

- Benabdallah, F., Veber, P., Prakasam, M., Viraphong, O., Shimamura, K. & Maglione, M. 2014. Continuous cross-over from ferroelectric to relaxor state and piezoelectric properties of BaTiO<sub>3</sub>-BaZrO<sub>3</sub>-CaTiO<sub>3</sub> single crystals. *Journal of Applied Physics*, **115**(14), article 144102 (8 pp.), <https://doi.org/10.1063/1.4870933>.
- Bhalla, A.S., Guo, R. & Roy, R. 2000. The perovskite structure—A review of its role in ceramic science and technology. *Materials Research Innovations*, **4**(1), 3–26, <https://doi.org/10.1007/s100190000062>.
- Xiao, Z., Yu, S., Li, Y., Ruan, S., Kong, L.B., Huang, Q., Huang, Z., Zhou, K. *et al.* 2020. Materials development and potential applications of transparent ceramics: A review. *Materials Science and Engineering R: Reports*, **139**, article 100518 (66 pp.), <https://doi.org/10.1016/j.mser.2019.100518>.

## Record-Breaking 20 and 30 ct Laboratory-Grown CVD Diamonds

In May 2022, laboratory-grown diamonds of record-breaking sizes were submitted to the International Gemological Institute (IGI). Produced using the chemical

vapor deposition (CVD) technique, the 30.18 and 20.24 ct gems (Figure 18) were analysed and graded by IGI just five days apart. Also graded at approximately the

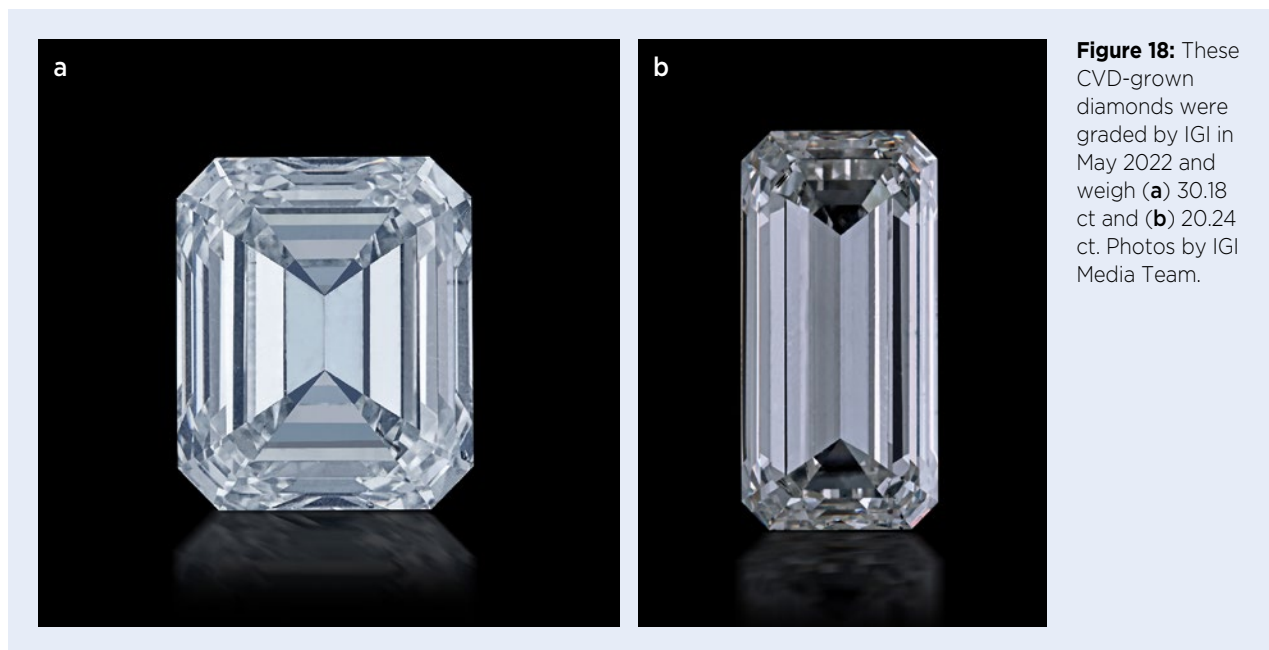


**Figure 18:** These CVD-grown diamonds were graded by IGI in May 2022 and weigh (a) 30.18 ct and (b) 20.24 ct. Photos by IGI Media Team.

same time was a 27.27 ct CVD-grown diamond, but its details cannot be released at this time per client confidentiality wishes. The 30.18 ct lab-grown diamond was named 'Pride of India' by its producer (Ethereal Green Diamond LLP, Mumbai, India). The 20.24 ct lab-grown diamond was named 'Shivaya' by its producer (Greenlab Diamonds LLP, Surat, India), as one of a trio of 15+ ct CVD-grown diamonds named in honour of the mantra *Om Namah Shivaya*, an ancient meditative expression. The other two in the trio weighed 27.27 ct (as mentioned above) and 15.16 ct (see <https://tinyurl.com/4u9jpnxb>).

The 30.18 ct emerald-cut sample measured  $18.85 \times 15.85 \times 9.71$  mm, with a 72% table facet and total depth of 66.4%. It had VS<sub>2</sub> clarity, H color and Excellent polish and symmetry. IGI was told the rough material from which it was fashioned took approximately four weeks to grow. The 20.24 ct emerald-cut sample measured  $22.17 \times 10.93 \times 7.26$  mm, with a 65% table facet and total depth of 61.3%. It had SI<sub>2</sub> clarity, H color and Excellent polish and symmetry.

Microscopic examination showed graphitic growth remnants in both of the lab-grown diamonds. In the 30.18 sample these graphitic particles that were comparable to pinpoint, cloud and crystal inclusions seen in naturally formed diamonds. The 20.24 ct gem had a series of grade-setting (SI<sub>2</sub>) feathers in its crown and pavilion, along with graphitic particles that were also comparable to pinpoint, cloud and crystal inclusions.

FTIR spectroscopy confirmed that both of the lab-grown diamonds were type IIa. In addition, for both gems photoluminescence (PL) spectroscopy showed

features consistent with those of CVD-grown diamonds that have been subjected to post-growth HPHT treatment to make them more colourless (Figure 19). With 514 nm laser excitation, an intense PL peak at 552 nm identified the material as diamond. Interestingly, there was no 637 nm peak (due to the NV<sup>-</sup> centre) recorded in the PL spectra of either lab-grown diamond. In addition, there was no doublet at 596/597 nm, which is commonly recorded in as-grown CVD lab-grown diamonds but is removed by post-growth HPHT treatment (Wang *et al.* 2012). The doublet at approximately 737 nm due to SiV<sup>-</sup> defects is typical for diamond growth with the CVD process (D'Haenens-Johansson *et al.* 2011).

DiamondView imaging of both samples showed green fluorescence (Figure 20a, b) and faint green phosphorescence under high-energy ultra-short-wave UV radiation, which is consistent with post-growth treatment (cf. Wang *et al.* 2012). The images also revealed banding associated with disruptions in the growth process, characteristic of CVD growth. For comparison, DiamondView imaging of as-grown (with no further treatment) CVD diamond typically shows orange-to-pink fluorescence (e.g. Figure 20c).

The large sizes and high qualities of these lab-grown diamonds demonstrate continued improvements in the growth process for the CVD technique. Previously, the largest CVD-grown diamond documented in the literature weighed 16.41 ct (Wang *et al.* 2022).

John Pollard ([John.Pollard@igi.org](mailto:John.Pollard@igi.org)),  
Dr Nikhil Alfred and Steven Rees  
IGI Worldwide

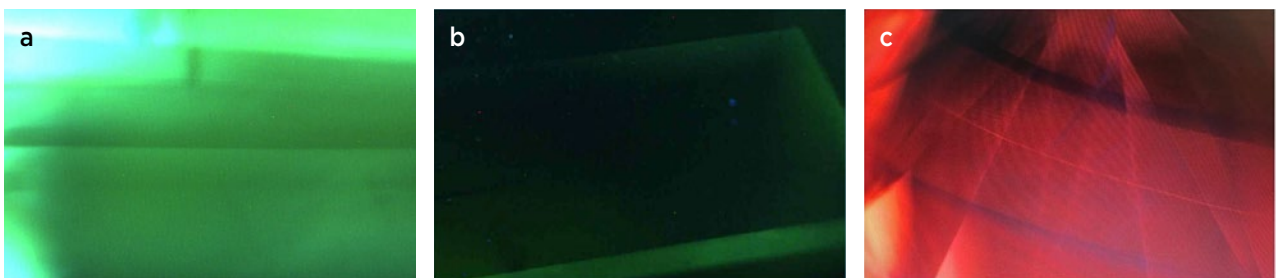
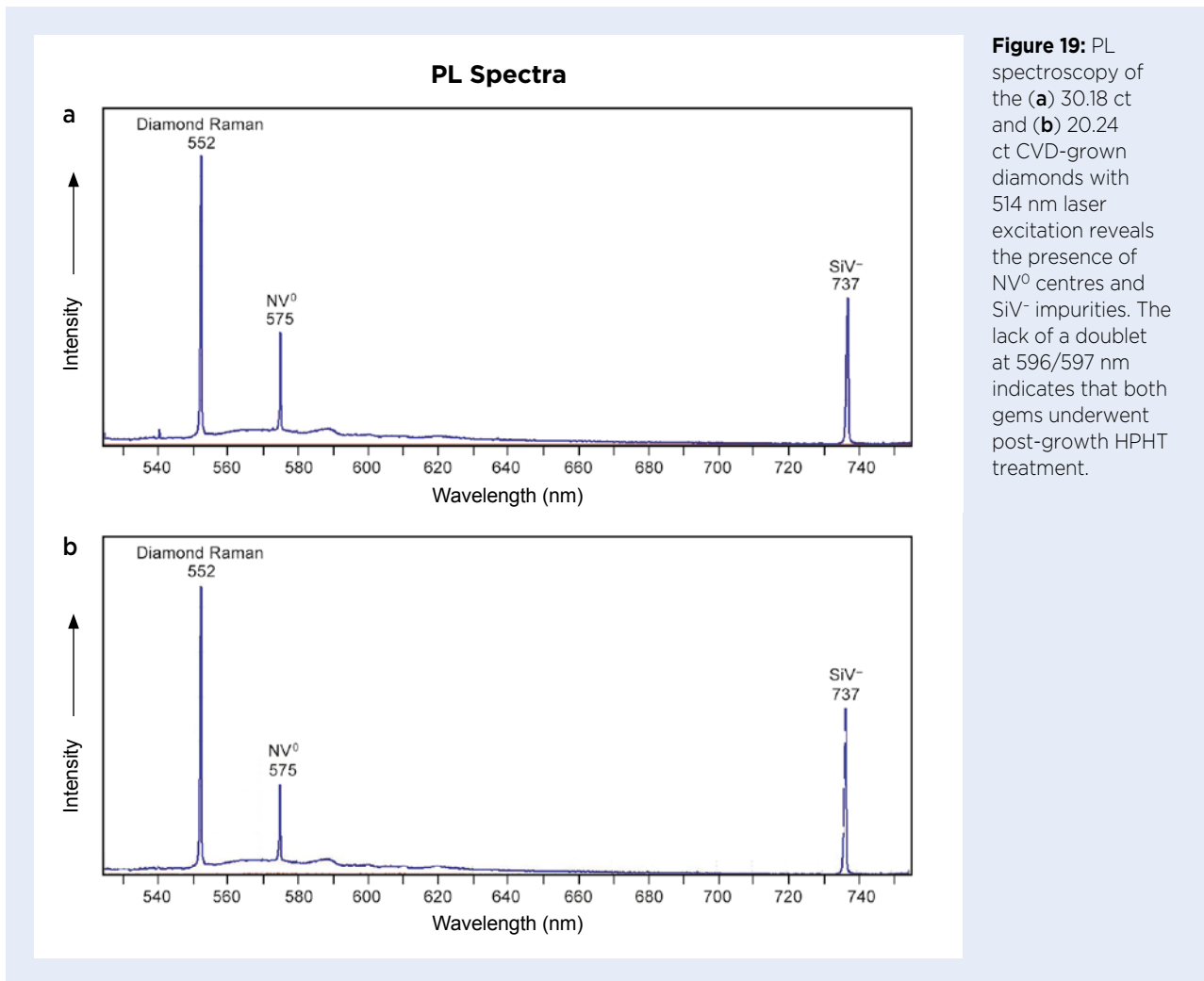


**Figure 20:** Both the 30.18 and 20.24 ct CVD-grown diamonds (a and b, respectively) emit green fluorescence in the DiamondView, indicative of post-growth HPHT treatment. Parallel growth banding is also seen, particularly in the larger sample. (c) By comparison, as-grown CVD diamonds typically show orange-to-pink fluorescence in the DiamondView. The banding results from interruptions in the CVD growth process. Images by N. Alfred.

## References

- D'Haenens-Johansson, U.F.S., Edmonds, A.M., Green, B.L., Newton, M.E., Davies, G., Martineau, P.M., Khan, R.U.A. & Twitchen, D.J. 2011. Optical properties of the neutral silicon split-vacancy center in diamond. *Physical Review B*, **84**, article no. 245208 (14 pp.), <https://doi.org/10.1103/physrevb.84.245208>.
- Wang, W., D'Haenens-Johansson, U.F.S., Johnson, P., Moe, K.S., Emerson, E., Newton, M.E. & Moses, T.M. 2012. CVD synthetic diamonds from Gemesis Corp. *Gems & Gemology*, **48**(2), 80–97, <https://doi.org/10.5741/gems.48.2.80>.
- Wang, W., Persaud, S. & Myagkaya, E. 2022. Lab Notes: New record size for CVD laboratory-grown diamond. *Gems & Gemology*, **58**(1), 54–56.

## Mica-Coated Emerald Imitations from Zambia

Imitations have been used for a very long time, and are usually made with a lower-value material of the same colour as the gem it is supposed to simulate (Karampelas *et al.* 2020). In some cases they are made by combining natural and synthetic materials, as described for a specimen composed of fragments of natural and synthetic (Verneuil) ruby held together by glue and coated with mica (Scarratt 1984). More often, however, such imitations are made to resemble emerald—especially the mica-coated material commonly originating from East Africa (Scarratt 1984).

During a visit to Zambia in March 2022, author AA encountered local dealers selling what appeared to be rough emeralds of various sizes on the streets of the capital city Lusaka. The specimens looked like typical emerald crystals coated in mica. She purchased some samples for faceting, but later in the laboratory we found two of them actually consisted of manufactured imitations (Figure 21).

The two specimens measured 21.0 × 15.8 × 15.2 mm and 19.8 × 23.5 × 16.8 mm. The larger one fell apart when we first handled it, revealing an interior cavity and two metal plates (Figure 22). The interior surface of the cavity was mostly coated with an amorphous material containing gas bubbles (Figure 23).

The smaller, unbroken sample had a hydrostatic SG of 2.80, which is somewhat similar to that of emerald (2.65–2.78). But the larger, broken sample had a much greater SG value of 3.74, consistent with the presence of the metal plates. The metal pieces were evidently added to give the sample greater ‘heft’.

To determine the chemical composition of the metal plates in the broken sample, we performed EDXRF spectroscopy with an Olympus Delta Classic Plus



**Figure 21:** These two specimens (10.80 and 6.15 g) were sold in Zambia as rough emeralds. Photo by J. Štubňa.

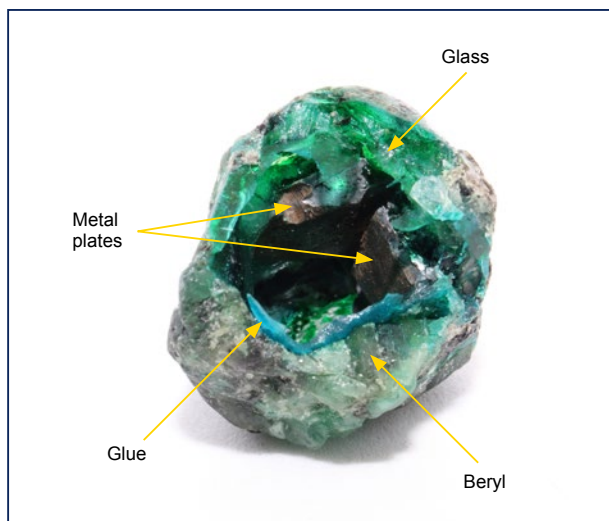


**Figure 22:** The larger sample inadvertently broke during handling, revealing a central cavity containing two metal plates. Photo by J. Štubňa.

handheld unit (configured for analysing metal alloys). The analyses revealed an alloy composed of Pb (82.6–88.6 wt. %), Sb (5.7–6.7 wt. %), Ga (4.2–4.4 wt. %) and Fe (5.6–6.9 wt. %).

With Raman spectroscopy, we found that both of the imitations consisted of beryl (pale green), quartz (colourless) and glass (green and colourless). These materials were held together by a greenish blue glue, which fluoresced blue to long- and short-wave UV radiation (Figure 24). The specimens showed no reaction (appearing green) when viewed with the Chelsea Colour Filter.



**Figure 23:** Viewed with a microscope, the internal surface of the cavity in Figure 22 shows an amorphous material with gas bubbles, which proved to be glass. The green colour of the glass was restricted to its surface. Also visible are areas of greenish blue glue (seen mostly on the lower right). Photo-micrograph in transmitted light by J. Štubňa; magnified 7.5×.

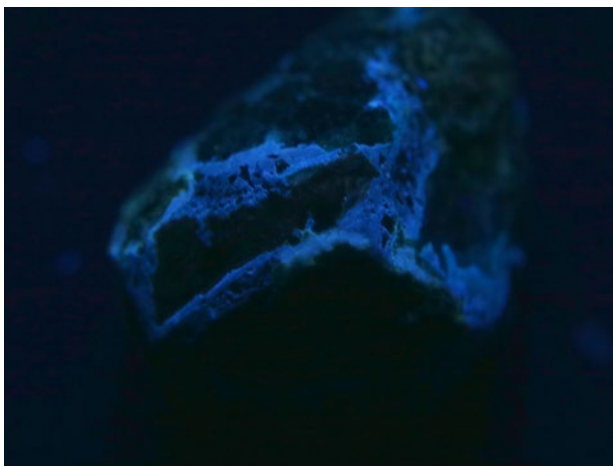


**Figure 24:** Blue luminescence to long-wave (365 nm) UV radiation reveals the presence of glue, as seen here for the 6.15 g sample. Photo by J. Štubňa.

A repeat visit to Zambia later in 2022 showed that such specimens are still routinely offered by rough dealers, sometimes in sizes of hundreds of carats. This

is a reminder that buyers must always be watchful when purchasing samples on the street from unknown sellers. When in doubt, observing specimens with UV radiation can be helpful for identifying such imitations.

*Dr Ján Štubňa (janstubna@gmail.com)  
Gemmological Laboratory, Constantine the  
Philosopher University in Nitra, Slovakia*

*Alžbeta Andrášiová  
Atelier GemmaAnima, Slovakia*

## References

Karampelas, S., Kiefert, L., Bersani, D. & Vandenabeele, P. 2020. *Gems and Gemmology: An Introduction for Archaeologists, Art-Historians and Conservators*. Springer Nature Switzerland AG, Cham, Switzerland, 112 pp., <https://doi.org/10.1007/978-3-030-35449-7>.

Scarratt, K. 1984. Notes from the laboratory. *Journal of Gemmology*, **19**(2), 98–124, <https://doi.org/10.15506/JoG.1984.19.2.98>.

## Ring with Flat-Cut Synthetic Moissanite

Recently, the authors had the opportunity to investigate an interesting gold-plated silver ring with a flat, colourless centre stone surrounded by smaller colourless rose cuts (Figure 25). The ring was submitted for testing since all the gems had tested as ‘diamond’ with a standard diamond tester that used thermal and electrical conductivity, but the owner doubted this result for the centre stone.

Macroscopically, the simple workmanship of the ring attracted attention (Figure 26): The accent stones had only been pressed into the silver, and the centre stone was glued into its mounting. A standard diamond tester indeed identified all the gems as ‘diamond’, and the inclusions in the accent stones (graphite platelets and colourless crystals that are typical of diamond) confirmed this identity. The centre stone, however, had some fissures (again, see Figure 26) but no other inclusions. Therefore, additional tests were carried out.

A polariscope revealed that the centre stone was doubly refractive. It was even possible, using a conoscope, to obtain a uniaxial optic figure (Figure 27). Its RI was determined as approximately 2.951 with a digital reflectometer (Presidium Refractive Index Meter II). A UV-transparency tester (SmartPro Optimum-I) identified the sample as ‘moissanite’. Due

to the higher-than-expected RI reading (which for synthetic moissanite should range from 2.65 to 2.69), Raman spectroscopy was used to confirm the identity of the sample as synthetic moissanite (SiC). In addition,



**Figure 25:** This gold-plated silver ring was submitted to the DSEF German Gem Lab for testing. The centre stone measures approximately 12 × 10 mm; although it is colourless, it appears yellowish here because the ring shank shows through the flat cut. Photo by Q. Wang.



**Figure 26:** A detailed view of the ring shows that the accent stones were simply pushed into the silver, while the centre stone was glued to fix it in place. Photomicrograph by T. Stephan; image width approximately 16 mm.

qualitative chemical analysis by EDXRF spectroscopy showed the expected presence of Si. The relatively high RI can be explained by the cut: the reflectometer measures the amount of light reflected at the surface, but the flat cut caused the backside to simulate a ‘second surface’ that reflected additional light, so the instrument calculated a higher RI.

To the knowledge of the authors, this is the first description of a synthetic moissanite imitating an old-cut diamond. This again shows that the use of a standard diamond tester is sometimes not appropriate for conclusive identification of synthetic moissanite (see Henn 2021). Additional testing with a UV-transparency tester (e.g. Presidium Ari, SmartPro Optimum-I, etc.) is helpful



**Figure 27:** The conoscope reveals the centre stone in the ring to be optically uniaxial, consistent with the authors’ identification of it as synthetic moissanite. Photo by T. Stephan.

for confirming the identification provided by a standard diamond tester.

*Dr Tom Stephan (t.stephan@dgemg.com)  
German Gemmological Association  
Idar-Oberstein, Germany*

*Stefan Müller  
DSEF German Gem Lab  
Idar-Oberstein, Germany*

## Reference

Henn, U. 2021. Gem Notes: Synthetic moissanite testing as ‘diamond’ using diamond testers. *Journal of Gemmology*, 37(8), 778–779, <https://doi.org/10.15506/jog.2021.37.8.778>.

## Black Synthetic Moissanite Coloured by a Pleochroic Mechanism

Synthetic moissanite, or silicon carbide (SiC), has been used in jewellery since the late 1990s (Nassau *et al.* 1997). Various colours of synthetic moissanite result from the incorporation of impurities. However, black-coloured synthetic moissanite, characterised by an opaque appearance, is somewhat different from the other products. The



opacity can result from a very dark green body colour (Nassau 1999; McClure & Moses 2000; Kitawaki 2009) or a densely aggregated texture. The latter can show a fine-grained (Caplan *et al.* 2015) or mosaic appearance (Moe *et al.* 2013) made of light and dark grey regions, with surface-reaching black inclusions visible to the unaided eye or with a standard gemmological microscope.

Recently, the gemmological laboratory of Stuller Inc. examined four black faceted beads (Figure 28) that were presented by the vendor as a ‘new experimental moissanite product’. They ranged from 2.05–2.08 × 1.82

**Figure 28:** These black synthetic moissanite beads (2.05–2.08 × 1.82 to 4.75–4.80 × 4.70 mm) were presented as a ‘new experimental product’. Photo by G. Borenstein.

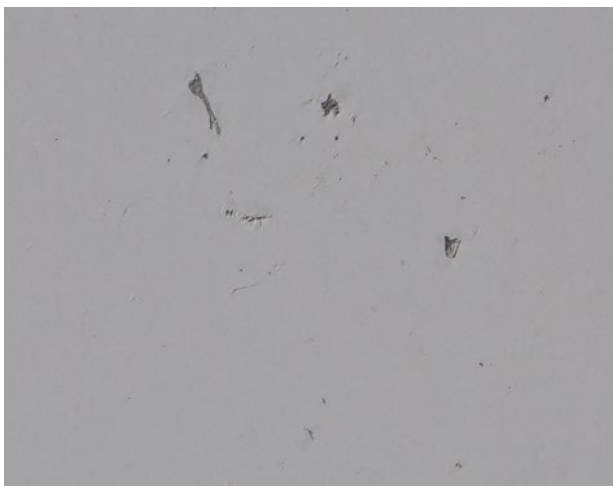


**Figure 29:** At high magnification, no significant granular surface texture of the beads was observed in reflected light. Photomicrograph by John Butler; magnified 200×.

to 4.75–4.80 × 4.70 mm. Raman analysis in several directions using a Magilabs GemmoRaman-532SG unit confirmed the material as the 6H-SiC polymorph of synthetic moissanite, with peaks at 967, 786, 502 and 238 cm<sup>-1</sup> (cf. Kiefert *et al.* 2001).

Observation with a standard gemmological microscope using reflected light showed a smooth black surface. Stronger magnification from a Keyence VHX-7000 digital microscope revealed a uniform surface with almost no indications of a granular texture (Figure 29). Strong transmitted light revealed the material to be transparent, displaying a very dark grey body colour with flashes of reddish orange and blue-green. No inclusions were observed.

As the 6H polytype of synthetic moissanite is anisotropic (hexagonal crystal system), further analysis was carried out to determine the origin of the coloured flashes. Using transmitted light and a polarising filter, the samples were found to be distinctly dichroic with medium-tone reddish orange and blue-green pleochroic colours. One of the beads showed both colours from the same direction, suggesting a growth interference within the material (Figure 30).

The colouration of this black synthetic moissanite is different from that described in previous reports. Both orange and green have been observed before as body colours—and even together in a particoloured sample (Choudhary 2015)—but this combination has never been reported previously as pleochroic colours (cf. Kiefert *et al.* 2001).

These samples' pleochroism and lack of a granular texture suggest a new technique to produce black-coloured synthetic moissanite. In this case, the green component

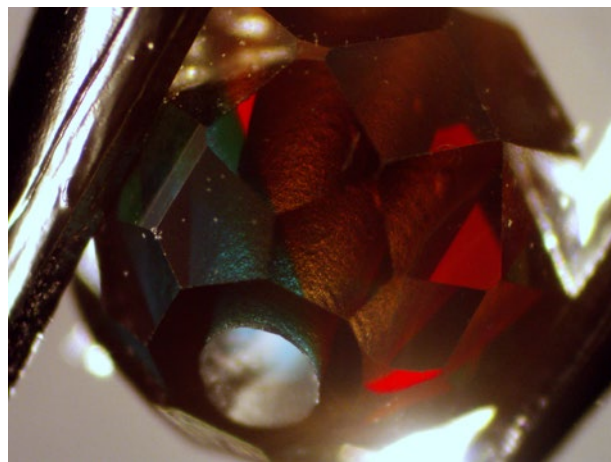


**Figure 30:** Viewed with strong transmitted light and a polarising filter, this black synthetic moissanite bead shows zonal colours, suggesting a growth interference. Photomicrograph by G. Borenstein; magnified 40×.

is not of sufficient darkness to absorb enough light to produce an opaque-like black appearance. Instead, the two pleochroic colours apparently combine to produce the black appearance.

Guy Borenstein FGA (Guy\_Borenstein@stuller.com)  
Stuller Inc. Gemological Laboratory  
Lafayette, Louisiana, USA

## References

- Caplan, C., Hainschwang, T. & Notari, F. 2015. Gem Notes: New large black synthetic moissanite as a black diamond imitation. *Journal of Gemmology*, **34**(5), 399–401.
- Kiefert, L., Schmetzer, K. & Hänni, H.A. 2001. Synthetic moissanite from Russia. *Journal of Gemmology*, **27**(8), 471–481, <https://doi.org/10.15506/JoG.2001.27.8.471>.
- Kitawaki, H. 2009. Lab Alert: Black moissanite. GAAJ-ZENHOKYO Laboratory, 3 February, [https://grjapan.ddo.jp/gaaj\\_report/2009/2009\\_01\\_02-01en.html](https://grjapan.ddo.jp/gaaj_report/2009/2009_01_02-01en.html), accessed 13 August 2022.
- McClure, S.F. & Moses, T. 2000. Lab Notes: Synthetic moissanite: A black diamond substitute. *Gems & Gemology*, **36**(3), 256–257.
- Moe, K.S., Johnson, P. & Lu, R. 2013. Lab Notes: Large synthetic moissanite with silicon carbide polytypes. *Gems & Gemology*, **49**(4), 255–256.
- Nassau, K. 1999. Moissanite: A new synthetic gemstone material. *Journal of Gemmology*, **26**(7), 425–438, <https://doi.org/10.15506/JoG.1999.26.7.425>.
- Nassau, K., McClure, S.F., Elen, S. & Shigley, J.E. 1997. Synthetic moissanite: A new diamond substitute. *Gems & Gemology*, **33**(4), 260–275, <https://doi.org/10.5741/gems.33.4.260>.

## TREATMENTS

### Green-coated Topaz Coloured by Cobalt

Recently, the Laboratoire Français de Gemmologie (LFG) in Paris received a faceted green topaz weighing 5.77 ct and measuring 12.0 × 10.0 × 6.3 mm (Figure 31). Its RIs (1.610–1.620), hydrostatic SG (3.53) and Raman spectrum were consistent with those of topaz. The gem was inert to both long- and short-wave UV radiation. Viewed with a microscope, a thin green coating layer with a spotted surface appearance was observed in reflected light (Figure 32a). In addition, areas where the green coating had chipped off (evidently due to abrasion) could be seen on some of the facet junctions with diffused transmitted light (Figure 32b).

The stone's UV-Vis spectrum highlighted the presence of Co, with a typical absorption around 620 nm (Figure 33). To the authors' knowledge, this is the first time that green colouration due to Co has been confirmed by UV-Vis spectroscopy for coated topaz. The presence of Co was further confirmed by EDXRF analysis. Raman spectroscopy showed only the vibrations associated with topaz and weak photoluminescence bands possibly linked with Co in topaz. No additional Raman bands were present that could be associated with the coating.

Topaz is frequently enhanced or treated to modify its colour using various techniques such as irradiation (Nassau 1985; Ashbaugh & Shigley 1993), coating (especially with Ag, Au or Ti), or diffusion coating

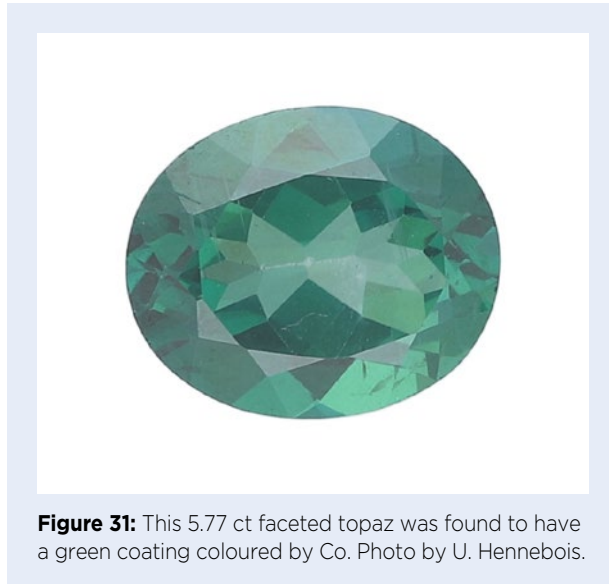


**Figure 31:** This 5.77 ct faceted topaz was found to have a green coating coloured by Co. Photo by U. Hennebois.

(Schmetzer 2006; Befi *et al.* 2006; Gabasch *et al.* 2008). Similar-coloured green-coated topaz has been described previously, but with a more durable Co-bearing coating (Befi *et al.* 2006).

From time to time LFG receives coated gems for identification, but this is the first time that a Co-coloured coated topaz has been analysed by this laboratory.

*Ugo Hennebois, Aurélien Delaunay and  
Dr Stefanos Karampelas (s.karampelas@lfg.paris)  
LFG, Paris, France*



**Figure 32:** (a) The spotted surface appearance of the coating on the green topaz is visible with reflected light. (b) Diffused transmitted light reveals where the coating has been chipped off some facet junctions, mostly likely by abrasion. Photomicrographs by U. Hennebois; image widths 2 mm each.



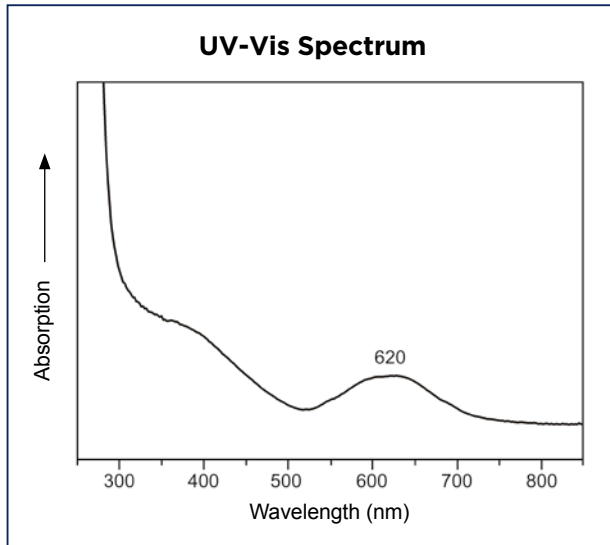


**Figure 33:** The UV-Vis absorption spectrum of the coated topaz reveals absorption centred around 620 nm that is associated with Co.

## References

- Ashbaugh, C.E. & Shigley, J.E. 1993. Reactor-irradiated green topaz. *Gems & Gemology*, **29**(2), 116–121, <https://doi.org/10.5741/gems.29.2.116>.
- Befi, R., Kiefert, L. & Htut, M. 2006. Coated topaz. *Gems & Gemology*, **42**(3), 128–129.
- Gabasch, H., Klauser, F., Bertel, E. & Rauch, T. 2008. Coloring of topaz by coating and diffusion processes: An X-ray photoemission study of what happens beneath the surface. *Gems & Gemology*, **44**(2), 148–154, <https://doi.org/10.5741/gems.44.2.148>.
- Nassau, K. 1985. Altering the color of topaz. *Gems & Gemology*, **21**(1), 26–34, <https://doi.org/10.5741/gems.21.1.26>.
- Schmetzer, K. 2006. Surface coating of gemstones, especially topaz – A review of recent patent literature. *Journal of Gemmology*, **30**(1–2), 83–90, <https://doi.org/10.15506/JoG.2006.30.1.83>.

## Gem-A: over **110 years of experience** in gemmology education

Our FGA and DGA Members are located around the world – join them by studying with Gem-A

**STUDY  
IN ONE  
OF THREE  
WAYS**

At Gem-A HQ  
London



Worldwide at one  
of our ATC's



Online with  
practical lab classes  
in your area



Find out more by contacting: [education@gem-a.com](mailto:education@gem-a.com)

*Creating gemmologists since 1908*



# Emerald from the Chitral Region, Pakistan: A New Deposit

Carina Silke Hanser, Bilal Gul, Tobias Häger and Roman Botcharnikov

**ABSTRACT:** Emeralds from a new deposit in the Chitral District of Pakistan were investigated with polarised UV-Vis-NIR, FTIR and Raman spectroscopy, and their chemical compositions were studied using EPMA and LA-ICP-MS analyses. The results are compared to data from the literature for classical emerald deposits such as those in Colombia and Zambia, as well as the nearby Panjshir region of Afghanistan and others. It was found that the macroscopic appearance and habit of the Chitral specimens are similar to those from Khaltaro (Pakistan), and their spectroscopic characteristics resemble those of schist-hosted deposits (e.g. Zambia). The chemical analyses show high Cs and Li contents (consistent with a pegmatite-related origin), which are greater than the ranges of these elements reported in the literature for emeralds from most other important localities. In 2021, the Chitral deposit produced approximately 130 kg of loose emerald, and greater amounts are expected to be mined in the 2022 season.

*The Journal of Gemmology*, 38(3), 2022, pp. 234–252, <https://doi.org/10.15506/JoG.2022.38.3.234>  
© 2022 Gem-A (The Gemmological Association of Great Britain)

**B**eryl,  $\text{Be}_3\text{Al}_2(\text{Si}_6\text{O}_{18})$ , is a relatively common mineral in rocks with magmatic, hydrothermal and metamorphic genesis. For instance, it occurs in granitic pegmatites, hydrothermal veins and schists (Groat *et al.* 2008). Depending on the geological setting, it is associated with a variety of minerals, such as quartz, calcite, feldspar, garnet and topaz (Nassau & Wood 1968; Viana *et al.* 2002). Common beryl is often colourless to pale yellowish green and translucent (Jehlička *et al.* 2017), but beryl can also occur as colourful, transparent, columnar, gem-quality crystals. With regard to the various beryl varieties—goshenite (colourless), heliodor (yellow), morganite (orange-pink to pink), red beryl (magenta to red), aquamarine (greenish blue to blue), Maxixe beryl (dark blue) and emerald (green)—the last is probably the most well known. Emerald is a popular gem material and has been mined in many countries from decades to hundreds or even thousands of years (Groat *et al.* 2008). Famous deposits for gem-quality material include those in Colombia and Zambia, with those from the

former location typically being the most sought-after (Karampelas *et al.* 2019). However, top-quality emeralds from the Panjshir region in Afghanistan have also been sourced in recent years (Krzemnicki *et al.* 2021).

In 2021, a new emerald deposit was found in the Chitral region of north-western Pakistan, in an area that was unavailable for mining for the past 40 years and had only recently been opened for this purpose by government authorities. Since the deposit contains gem-quality emerald (e.g. Figure 1), it is likely that this beryl will find its way into the gem market in the near future. Therefore, the aim of this study is to characterise this material spectroscopically and chemically, and to compare these emeralds to those from more well-known localities as well as with those found in some other deposits in Pakistan.

## GEOLOGY

### *Regional Setting*

As a result of the collision of the Indian subcontinent with the Asian tectonic plate and the subsequent

orogenesis of the Himalayan mountain belt, Pakistan exhibits a variety of rock types and deformation zones (Figure 2). The Chitral district in the north-western part of the country is characterised by two main formations, the East Hindu Kush block and the western portion of the Karakoram block, which are separated by the Tirich Mir fault zone (Zahid *et al.* 2016). The East Hindu Kush block extends across the border into Afghanistan and consists of metamorphic and igneous rocks. Metamorphism at comparably high temperatures and moderate-to-high pressures, and the influence of CO<sub>2</sub>-poor and low-pH hydrothermal fluids, have been shown to be pronounced in some parts of the East Hindu Kush block (Zahid *et al.* 2016). To the south, the Karakoram block is confined by the Karakoram suture zone (Main Karakoram Thrust) and the adjacent Kohistan arc terrane, followed by the Main Mantle Thrust, also referred to as the Indus suture zone (Kazmi 1989; Zahid *et al.* 2016). This latter unit comprises metamorphic rocks such as blueschist, however, rarer ophiolites (parts of oceanic crust having been thrust onto their continental counterpart) are also present (Kazmi 1989).

A variety of minerals can be found as gem-quality specimens in Pakistan, and the majority of them occur in the north of the country with its marked history of metamorphic and hydrothermal activities (Kazmi 1989). With regard to emerald, well-known deposits are hosted by the Indus suture zone (Kazmi 1989; Lawrence *et al.*

1989), which is sometimes also referred to as ‘the emerald belt’ (Lawrence *et al.* 1989), in which the aforementioned remnants of oceanic crust supply the Cr needed for the formation of this gem variety (Kazmi 1989; Snee *et al.* 1989). These include the emerald occurrences of the Swat District, which were found in 1958 (Kazmi *et al.* 1989; Lawrence *et al.* 1989), and the Mohmand District, discovered in 1966 (Kazmi *et al.* 1989). Lawrence *et al.* (1989) also mentioned unconfirmed reports of further emerald deposits in the Allai Kohistan part of the eastern Indus suture zone. Emeralds have also been found outside the Indus suture zone near Khaltaro, although this deposit is still close to this fault zone (Kazmi *et al.* 1989; Lawrence *et al.* 1989; Snee *et al.* 1989). Compared to the other emerald localities in Pakistan, samples from Khaltaro are generally larger in size and lighter in colour (Kazmi *et al.* 1989). Furthermore, they are associated with pegmatitic and hydrothermal veins intruding amphibolite bodies instead of metamorphosed ophiolite-related melanges (Lawrence *et al.* 1989; Laurs *et al.* 1996).

### *Emerald Mining Area*

The newly discovered emerald deposit in the Chitral District is located in the far north-west of Pakistan. Thus, it also lies outside of the Indus suture zone, and at a greater distance from it than Khaltaro (Figure 2). The nearest town is Besti, which is located about 10 km from the mining area. Rocks of the Chitral District mainly

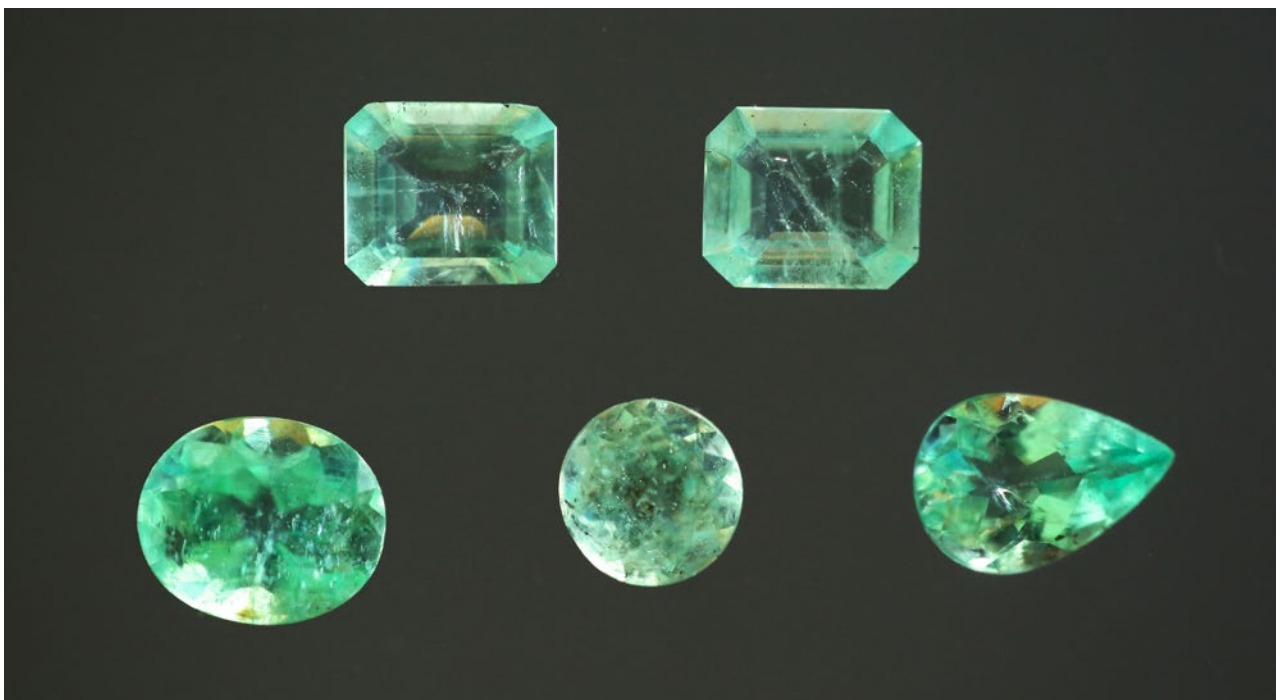
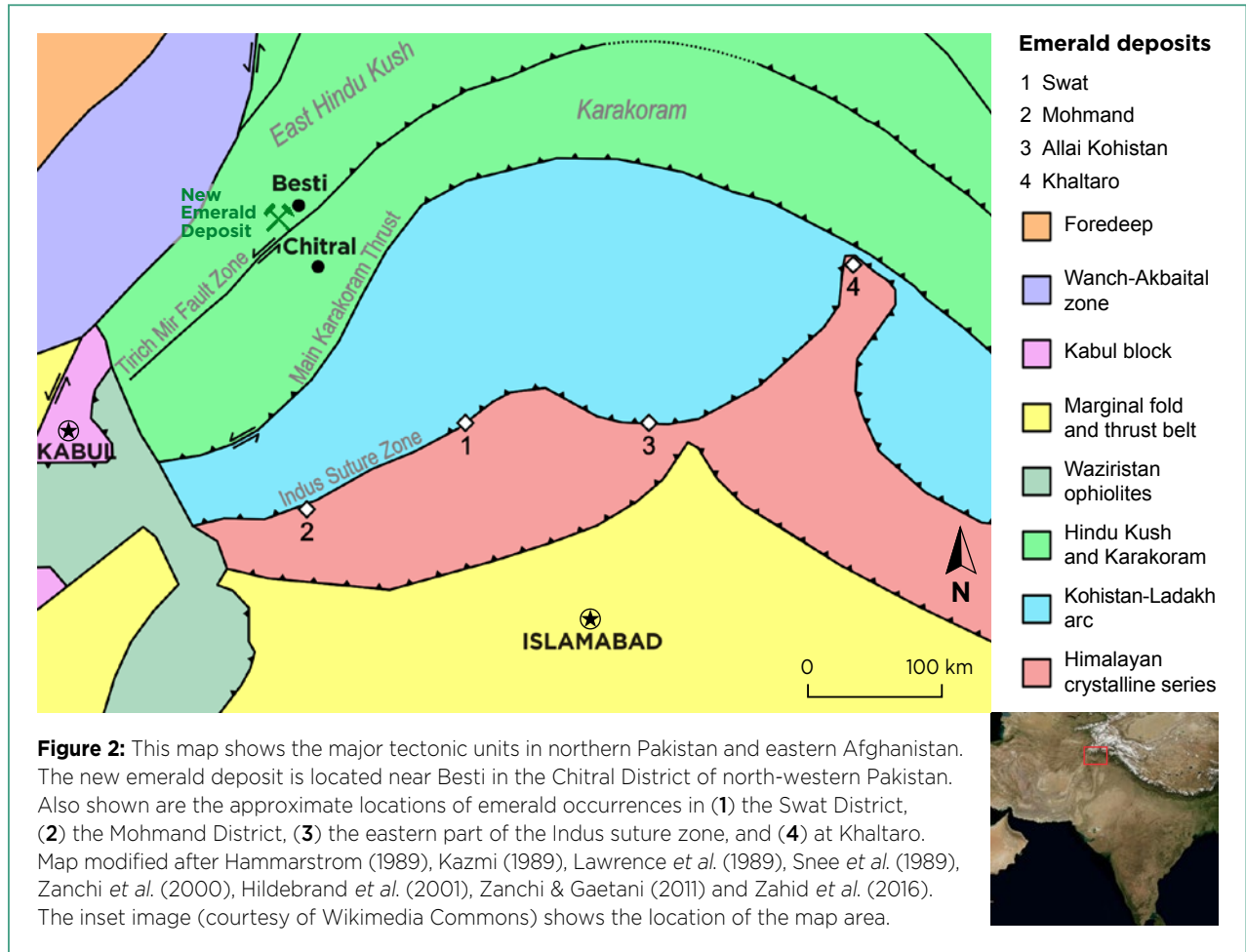


**Figure 1:** Five faceted (and oiled) emeralds (0.42–0.74 ct) were cut from some of the rough material from Chitral, Pakistan, obtained by the authors. The rectangular stones measure 6 × 5 mm. Photo by T. Häger.



consist of the Jurassic Arkari Formation. It comprises metapelites, which include, amongst others, quartzites, phyllites and various types of schists. Similar to the Khaltaro amphibolites, these were intruded by partly pegmatitic leucogranite plutons and dykes (Khan 1986; Laurs *et al.* 1996; Zahid *et al.* 2016). The rocks hosting the deposit are metamorphic in origin with different degrees of weathering overprint. Mafic and ultramafic rocks, especially peridotites and serpentinites, occur in the Tirich boundary zone, which runs along the Tirich Mir fault zone (Zanchi *et al.* 2000). This zone is located only a few kilometres from the mining site and might have supplied Cr for the genesis of the emeralds. However, Cr might also have come from mica-bearing schists in the mining area. Since there is very little detailed geological literature on this part of Pakistan, the likely source of Cr can only be speculated, and further investigations are necessary to identify it.

Figures 3 and 4 show the mining site and the area surrounding it. The region is situated in an elevated, rocky and hardly accessible terrain within the Hindu Kush Mountains at approximately 4,500 m above sea level, not far below glacial altitude. A narrow, provisional, unpaved

road leads to the mining camp, about 200 m below and 400 m from the mining site (Figure 5). While access to the mine is already difficult in the summer months, the area is fully inaccessible in winter time, since the already bad infrastructure is further worsened by snow and very low temperatures. Therefore, the deposit can only be worked during a period of four to five months a year.

In 2021, a section of the deposit about 10 × 1.5 × 5 m was excavated manually and, partially, with the aid of explosives. Around 3,000 kg of emerald-bearing ore were extracted, from which 130 kg of loose emeralds were obtained. Some of them reached several centimetres in length and weighed more than 300 g (e.g. Figure 6). Faceted Chitral emeralds typically range from light to medium green and are translucent to transparent (e.g. Figure 7).

The high altitude and the associated low concentration of oxygen makes manual work difficult for the miners. Therefore, in mid-2022 the narrow road was extended from the camp to the mining site to allow transport of electrical and hydraulic equipment there. This will facilitate the excavation of the deposit, which is expected to yield about 500 kg of loose emerald material in 2022.



**Figure 3:** Mountains and glaciers surround the emerald-bearing area in the Chitral District, which is situated at approximately 4,500 m above sea level. The mining site and camp are located near the glacier in the centre of the image. Photo by Fawad Ali Awan.



**Figure 4:** (a) A view from the emerald mining site down into the valley shows the narrow access road that traverses rocky terrain in the Hindu Kush Mountains. (b) The campsite that serves the operation lies about 400 m away from and 200 m below the mining site. Photos by Fawad Ali Awan (a) and Imran Khan (b).



**Figure 5:** At the Chitral deposit (far left), miners work in steep terrain in search of emeralds. Photo by Fawad Ali Awan.

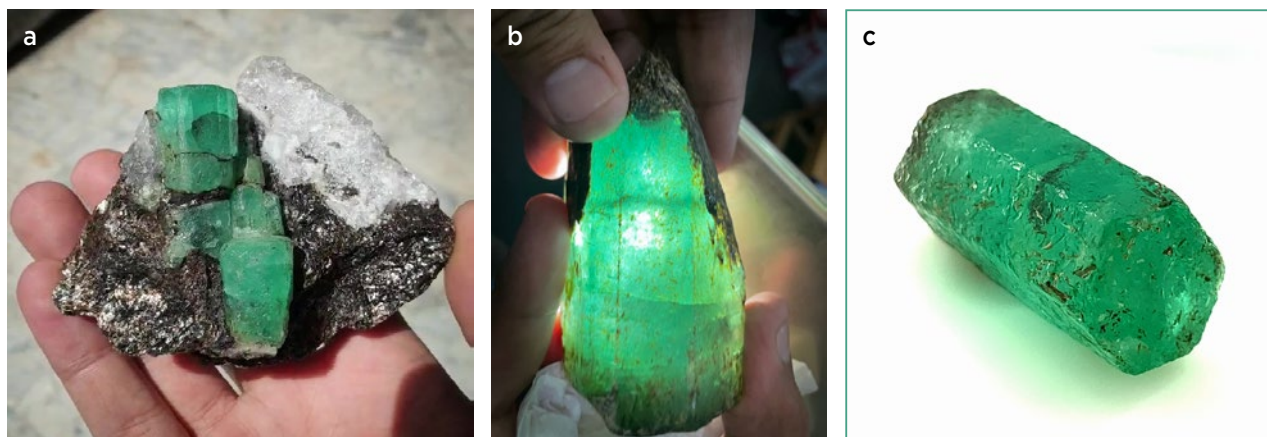


**Figure 6:** Recently, some attractive specimens and large crystals of Chitral emeralds have been recovered. (a) Emeralds occur in a matrix of quartz and brownish mica (see hand for scale); image taken from a video supplied by Dudley Blauwet. (b) An emerald weighing about 300 g is illuminated from behind; photo courtesy of Imran Khan. (c) This well-terminated crystal measures 23.6 × 12.5 mm; photo by Anne Fulton, Dudley Blauwet Gems.

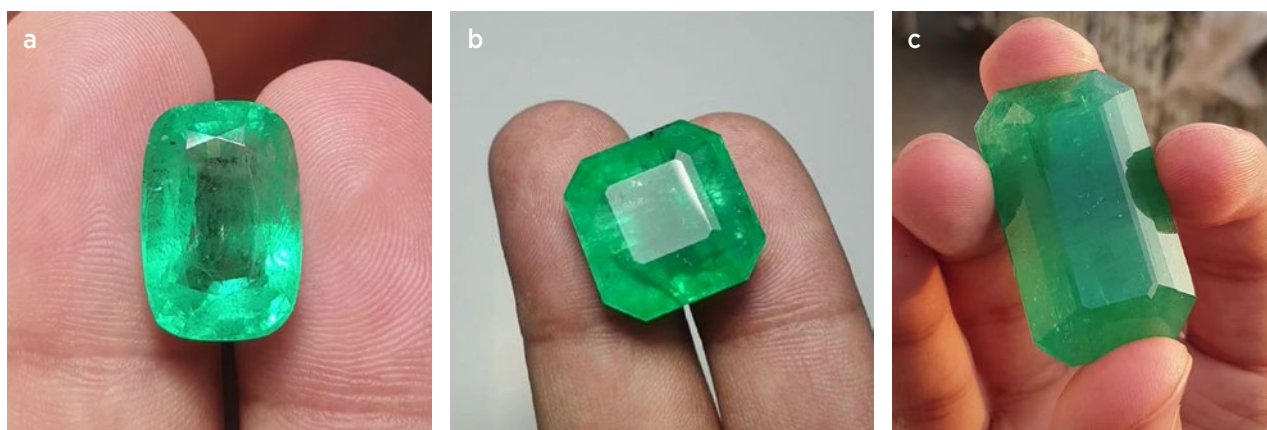


**Figure 7:** These faceted Chitral emeralds, which range from translucent to transparent, weigh (a) 11.4 ct, (b) 25.7 ct and (c) 142.30 ct. Images taken from videos supplied by Dudley Blauwet Gems.

## MATERIALS AND METHODS

Refractive index and density values were obtained for the five faceted emeralds shown in Figure 1. The RI values were measured with a Topcon refractometer, with Anderson liquid (RI = 1.79) as the contact fluid. A Mettler AE163 digital balance with an ME-40290 density measurement unit was used to obtain the samples' densities. The temperature of the water was 23 °C and its density was assumed to be 0.9976 g/cm<sup>3</sup>. Internal features in the emeralds were examined using a Leica microscope with a vertical optical path and an attachable camera unit.

Seven emerald specimens (PK1–PK7; Figure 8a), which were collected in the first days of mining the newly found deposit, were investigated using several analytical techniques at the Johannes Gutenberg-University of Mainz, Germany. For spectroscopic analyses, slices of the emeralds were cut and polished to obtain

plane-parallel faces that were oriented parallel to the *c*-axis (Figure 8b). The same slices were also used for chemical analyses (see below). The colours and dimensions of these prepared samples are given in Table I. Specimen PK3 was the only one for which no slice could be obtained because it was internally fractured (predominately perpendicular to the *c*-axis).

The plane-parallel slices were investigated using polarised ultraviolet-visible-near infrared (UV-Vis-NIR), Fourier-transform infrared (FTIR) and Raman spectroscopy. For all three types of analyses, polarised spectra were acquired in two directions at 90° to each other: one direction with the electric field vector *E* of the incident light parallel to the *c*-axis (*E*||*c*), and the other with *E* being perpendicular to the *c*-axis (*E*⊥*c*). However, for fragment PK3 it was only possible to perform FTIR and Raman spectroscopy in the *E*⊥*c* direction.

UV-Vis-NIR spectra were obtained using a Zeiss Axio

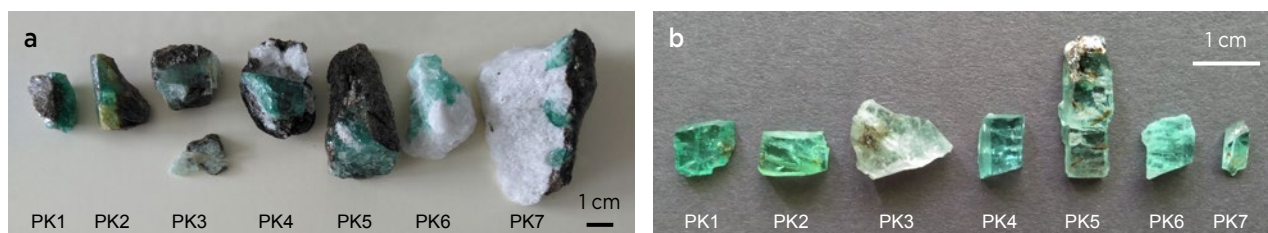


**Figure 8:** (a) The original emerald-bearing samples from Chitral used in this study are shown here in their raw state. (The smaller pieces below sample PK3 broke off during transport.) (b) These beryl samples were sawn from the specimens in Figure 8a and characterised for this report. Photos by C. S. Hanser.

Imager.A2m microscope with an attached Tidas CCD UV-Vis-NIR spectrometer and a Tidas PSS NIR spectrometer. The acquisition time was 160.1 ms in the 300–900 nm range and 231.0 ms for the NIR region (800–1600 nm). An accumulation of 50 runs was used, and no filters were applied.

FTIR spectra were recorded for the NIR and mid-infrared (MIR) regions using a Thermo Scientific Nicolet Continuum infrared microscope. In both cases a total of 100 scans were accumulated with a resolution of  $2\text{ cm}^{-1}$ . An InGaAs detector was used for the  $3900\text{--}10000\text{ cm}^{-1}$  range, while the  $650\text{--}6000\text{ cm}^{-1}$  range was measured with an MCTA detector. The samples were cleaned with ethanol prior to analysis. For both the UV-Vis-NIR and FTIR measurements, the spectra were normalised by relating the absorbance ( $A$ ) to the thickness ( $t$ ) of the samples, and thus obtaining the absorption coefficient ( $\alpha$ ) according to the formula:  $\alpha = (\ln(10) \times A)/t$ .

Raman spectra were recorded with a Horiba Jobin Yvon spectrometer equipped with a CCD detector. A Coherent Sapphire laser unit with a wavelength of 488 nm was used as the excitation source. An acquisition time of 10 s was applied to each wavelength interval, and two runs were accumulated to eliminate artefacts. In addition, the focus was moved slightly into the sample to avoid possible surface effects.

Electron probe micro-analysis (EPMA) was performed with a JEOL JXA-8200 SuperProbe. Calibration was obtained on standards consisting of albite (Na), chromium oxide (Cr), iron oxide (Fe), manganese titanate (Mn and Ti), orthoclase (K), metallic vanadium (V), pollucite (Cs), diopside (Ca and Mg) and synthetic aluminosilicate (Al and Si). The plane-parallel emerald slices were embedded in Technovit 5071 resin and carbon coated prior to analyses. Measurements were performed on five randomly selected spots on each sample, with the exception of the largest sample, PK5, for which six spots were chosen. For PK3, since its surface was uneven as it was not possible to polish it, relatively flat areas were chosen for the analyses.

For the determination of lighter elements and those present at lower concentrations, laser ablation inductively coupled plasma mass spectrometry (LA-ICP-MS) was performed using an Agilent 7500ce quadrupole ICP-MS with an attached ESI New Wave Research ArF excimer 193 nm laser. Calibration and quality control were performed on reference glasses NIST SRM 610 and NIST SRM 612 as external standards for trace elements, and in-house beryl reference material was used to quantify Be concentrations. Silicon ( $^{29}\text{Si}$ ) was used as an internal standard (as determined with EPMA). Five randomly chosen spots were analysed on each sample.

**Table I:** Sample characteristics of the seven beryl samples sawn from the rough specimens.

Sample	Colour	Diaphaneity	Dimensions (mm)	Weight (ct)
PK1	Medium green	Transparent	8.53 × 8.04 × 2.15	1.06
PK2	Light green	Transparent	9.18 × 5.20 × 2.94	1.42
PK3	Pale green	Translucent	12.68 × 9.90 × 3.08	2.28
PK4	Light green	Transparent	8.36 × 5.77 × 3.32	1.40
PK5	Light green	Largely transparent	17.73 × 6.00 × 3.15	3.06
PK6	Light green	Transparent to translucent	6.85 × 6.52 × 2.78	1.18
PK7	Light green	Transparent	7.07 × 3.83 × 1.85	0.33

## RESULTS AND DISCUSSION

### Standard Gemmological Properties

The rough samples were mostly transparent to translucent and light to medium green. Owing partly to blasting being used for the extraction of the material, the crystals were fractured and some had even broken further during transport and later during sample preparation (PK3). Well-developed crystal faces were only present on some of the samples. However, the columnar habit of the crystals and the hexagonal symmetry were recognisable on the majority of them. Areas containing beryl were still embedded in a white quartz-rich host rock and/or encrusted with brownish mica.

The five faceted stones were light to medium green. The RI values were  $n_o = 1.588 \pm 0.002$  and  $n_e = 1.579 \pm 0.002$ , and density values ranged from 2.72 to 2.80 g/cm<sup>3</sup>.

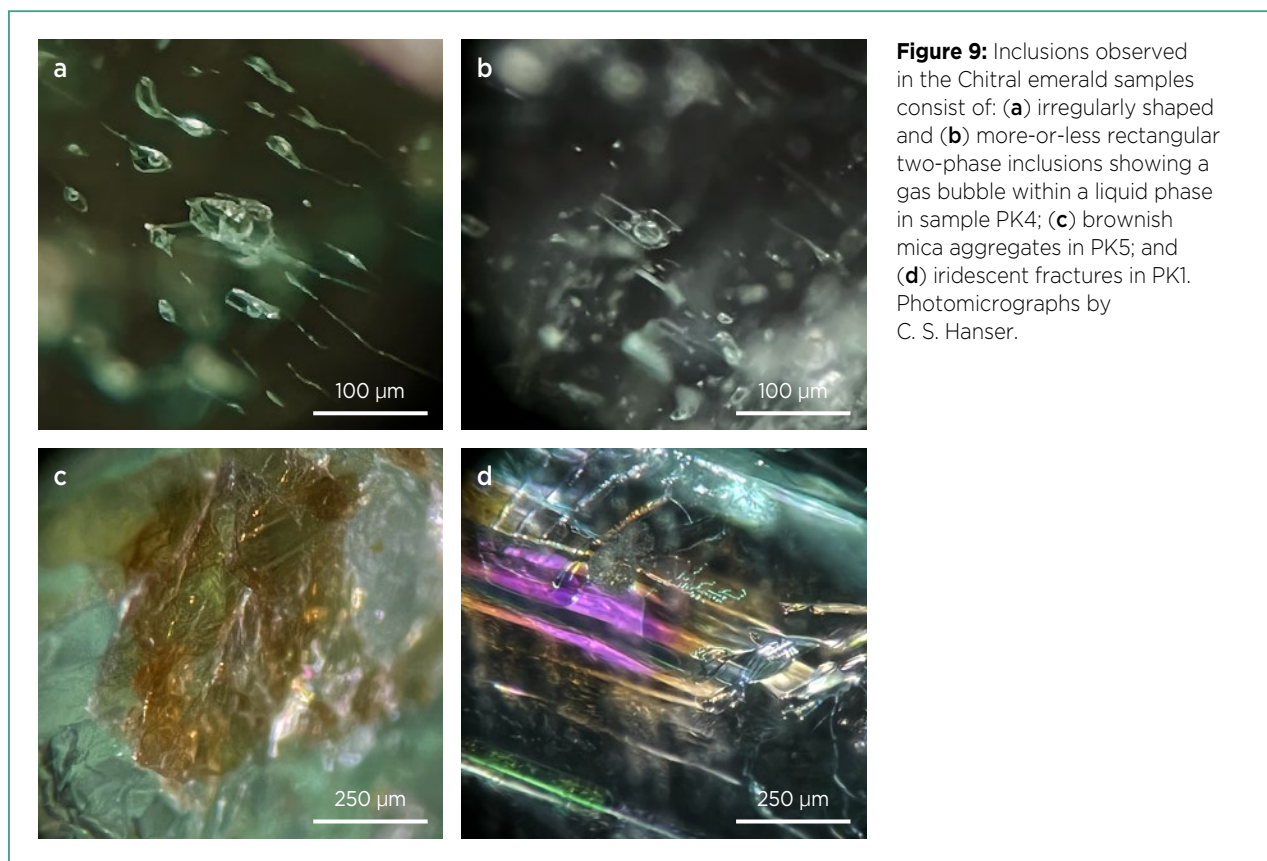
Inclusions in the sample slices consisted of irregularly shaped to rectangular two-phase inclusions containing a gaseous and a liquid phase (Figure 9a, b). Also present were inclusions of quartz and brownish mica (Figure 9c), especially near the rims of the crystals. In addition, many incipient fractures and thin films were found in one sample (Figure 9d). These exhibited strong iridescent colours, which could be seen with the unaided eye and thus partially masked the body colour of this specimen.

The main inclusions present in the faceted stones likewise consisted of mica and two-phase (liquid-gas) inclusions.

### Spectroscopy

**UV-Vis-NIR Spectra.** Figure 10 shows the UV-Vis-NIR spectra of the six emeralds for which plane-parallel slices could be obtained. The Fe<sup>3+</sup> peak between approximately 26882 cm<sup>-1</sup> (372 nm) and 26595 cm<sup>-1</sup> (376 nm) (Goldman *et al.* 1978; Krzemnicki *et al.* 2021) is present in every specimen in the E<sub>Lc</sub> direction (Figure 10a). The broad band near 12048 cm<sup>-1</sup> (830 nm), associated with Fe<sup>2+</sup> (Krzemnicki *et al.* 2021), is also visible in all of the spectra in this direction. This band is weakest in sample PK1 and is also located at a slightly higher wavelength (835 nm) than in the other samples. Fe-related features are common in emeralds from various localities worldwide, except for those found in Colombia (Karampelas *et al.* 2019; Krzemnicki *et al.* 2021).

Also in the E<sub>Lc</sub> direction, the bands near 23256 cm<sup>-1</sup> (430 nm) and 16529 cm<sup>-1</sup> (605 nm)—commonly attributed to Cr<sup>3+</sup>, V<sup>3+</sup>, or both (Wood & Nassau 1968; Gübelin 1989; Krzemnicki *et al.* 2021)—are the most pronounced in PK1, followed by PK2, PK6 and PK7, the three of which are almost identical in this range (Figure 10a). However, the smaller peaks near 15625 cm<sup>-1</sup> (640 nm) and 14577 cm<sup>-1</sup> (686 nm), also associated with Cr<sup>3+</sup> (Wood & Nassau 1968;





Gübelin 1989; Krzemnicki *et al.* 2021), are less clearly visible in all of the samples. On the other hand, the peak at  $7102\text{ cm}^{-1}$  ( $1408\text{ nm}$ ) caused by type II  $\text{H}_2\text{O}$  (Wood & Nassau 1967; Yu *et al.* 2017) is present in all samples.

In the  $E\parallel c$  direction (Figure 10b), samples PK1 and PK2 exhibit almost the same relative intensities for the two  $\text{H}_2\text{O}$  peaks at about  $7151\text{--}7148\text{ cm}^{-1}$  ( $1398\text{--}1399\text{ nm}$ ) and  $7077\text{ cm}^{-1}$  ( $1413\text{ nm}$ ), associated with type I and type II  $\text{H}_2\text{O}$ , respectively (Hu & Lu 2020). For the other four samples, the difference in the relative intensities of their  $\text{H}_2\text{O}$  peaks is greater, with the one at higher wavenumber (shorter wavelength) being stronger. Therefore, the relative amounts of type I and type II  $\text{H}_2\text{O}$  are nearly identical in samples PK1 and PK2, while the other samples contain greater amounts of type I  $\text{H}_2\text{O}$ .

With regard to the features related to  $\text{Cr}^{3+}$ ,  $\text{V}^{3+}$  and  $\text{Fe}^{2+}$ , our samples show similarities to Zambian emeralds (Karampelas *et al.* 2019), which have stronger

absorption related to Fe than from Cr and V. While Afghan Laghman-type emeralds exhibit equally strong  $\text{Fe}^{2+}$ ,  $\text{Cr}^{3+}$  and  $\text{V}^{3+}$  absorption intensities in their spectra, Afghan Panjshir emeralds lack strong  $\text{Fe}^{2+}$  absorption (Krzemnicki *et al.* 2021). Figure 11 compares the  $E\perp c$  spectrum of PK1 to those of two Colombian emeralds from Muzo and Chivor. The Colombian emeralds are missing the strong  $\text{Fe}^{2+}$  absorption band at about  $12048\text{ cm}^{-1}$  ( $830\text{ nm}$ ) present in the spectrum of PK1, while the  $\text{Cr}^{3+}$  and  $\text{V}^{3+}$  bands at  $16529\text{ cm}^{-1}$  ( $605\text{ nm}$ ) and  $23256\text{ cm}^{-1}$  ( $430\text{ nm}$ ) are more pronounced than those in the Chitral emerald. The strong Fe absorption band in the Chitral emeralds can thus serve as an indication of the type of deposit (i.e. schist-hosted; Saeseaw *et al.* 2019).

**Infrared Spectra.** FTIR spectra for the MIR and NIR regions are shown in Figures 12 and 13, respectively. Since no planar slices parallel to the  $c$ -axis could be obtained

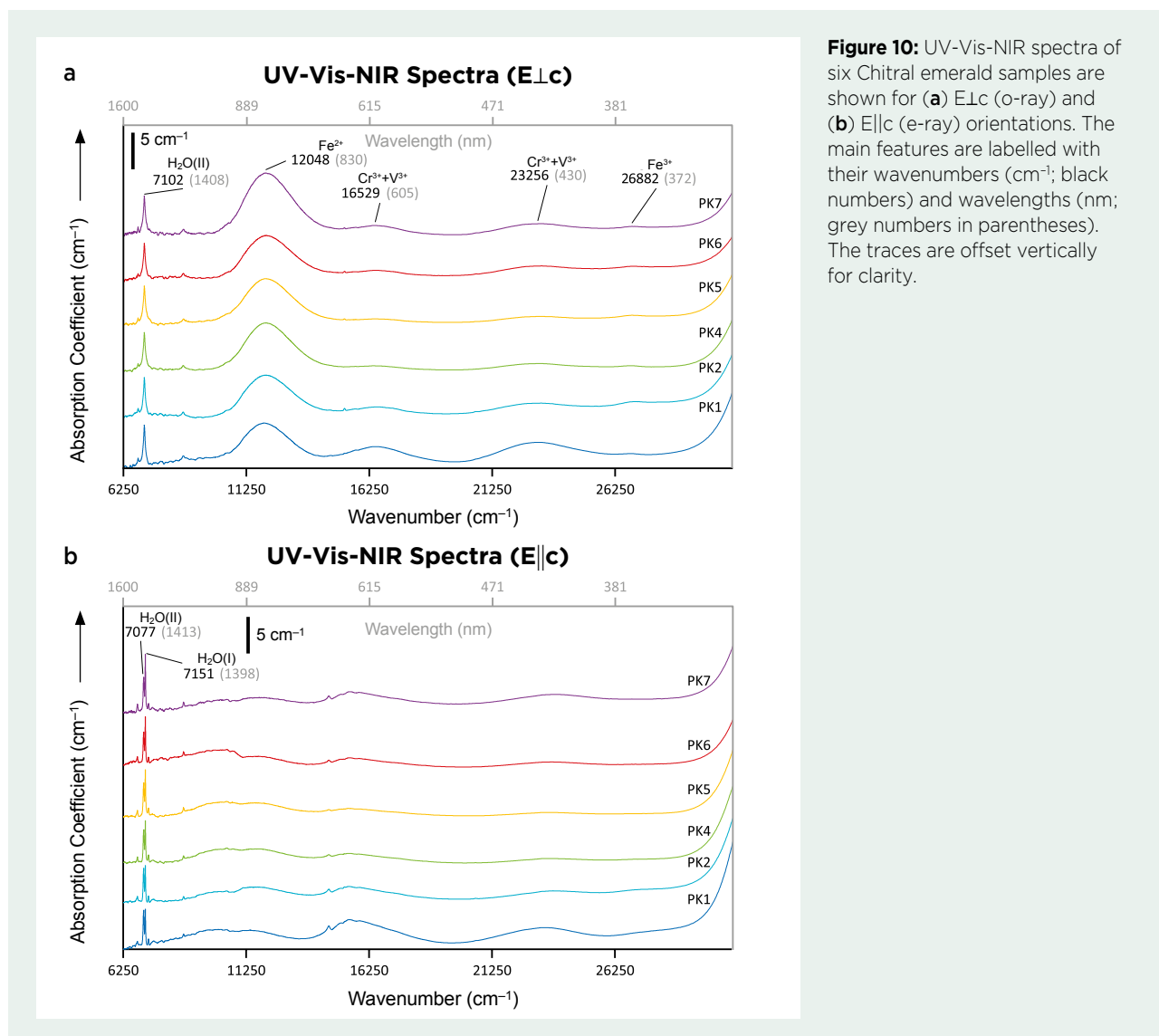


**Figure 10:** UV-Vis-NIR spectra of six Chitral emerald samples are shown for (a)  $E\perp c$  (o-ray) and (b)  $E\parallel c$  (e-ray) orientations. The main features are labelled with their wavenumbers ( $\text{cm}^{-1}$ ; black numbers) and wavelengths (nm; grey numbers in parentheses). The traces are offset vertically for clarity.

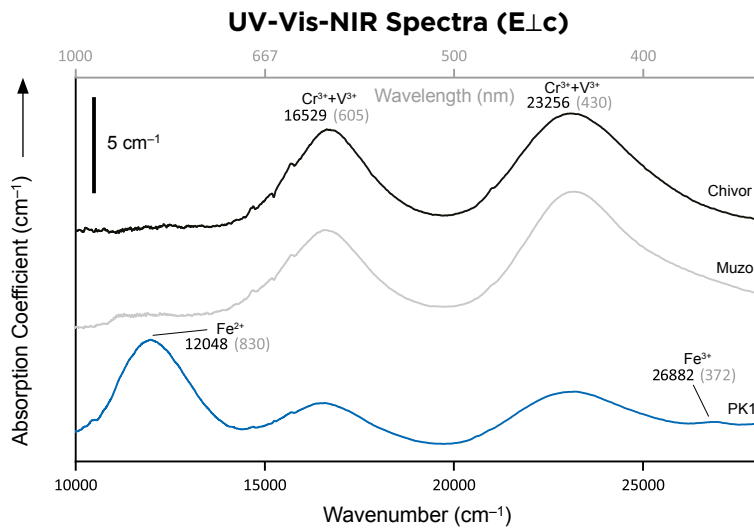


**Figure 11:** The UV-Vis-NIR spectrum for the E||c direction of Chitral sample PK1 is compared to the spectra of Colombian emeralds from Muzo and Chivor. The Colombian stones are missing the strong Fe<sup>2+</sup> absorption band at 12048 cm<sup>-1</sup> (830 nm) present in the spectrum of PK1, while the Cr<sup>3+</sup> and V<sup>3+</sup> bands at 16529 cm<sup>-1</sup> (605 nm) and 23256 cm<sup>-1</sup> (430 nm) are more pronounced than those in the Chitral emerald. The main features are labelled with their wavenumbers (cm<sup>-1</sup>; black numbers) and wavelengths (nm; grey numbers in parentheses). The traces are offset vertically for clarity.

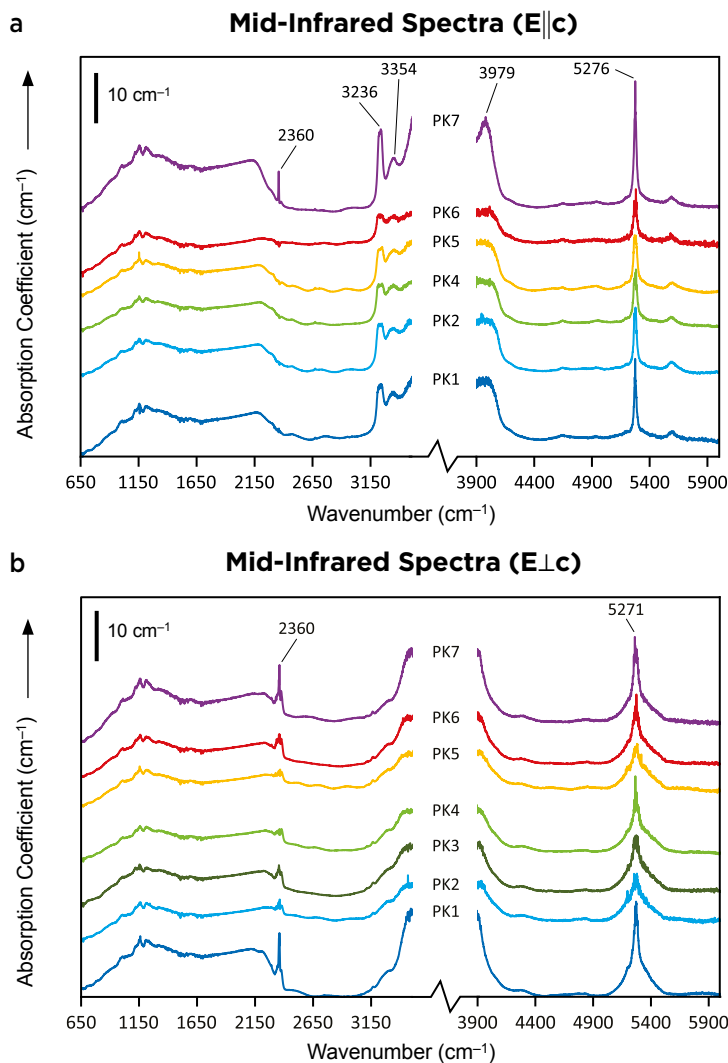


**Figure 12:** Mid-infrared spectra of six Chitral emerald samples are shown for (a) E||c and (b) E⊥c orientations. The 3500–3900 cm<sup>-1</sup> range is not included because strong absorption caused excessive noise, making the spectra unresolvable in that region. The traces are offset vertically for clarity.

for PK3, only one direction (E $\perp$ c) is shown for this sample. Bands in the lower wavenumber range, up to 1250 cm<sup>-1</sup>, represent the vibrational modes of the components constituting the beryl lattice (Wood & Nassau 1968; Krambrock *et al.* 2002; Łodziński *et al.* 2005; Yu *et al.* 2017). Owing to the thickness of the samples, the principal vibrational modes of type I and II H<sub>2</sub>O could not be resolved in the 3500–3700 cm<sup>-1</sup> region (which therefore has been omitted from the spectra in Figure 12).

In the MIR range, the peaks near 3236 and 3979 cm<sup>-1</sup> in the E $\parallel$ c direction (Figure 12a) are caused by type II H<sub>2</sub>O (Mashkovtsev *et al.* 2016; Yu *et al.* 2017). The bands at approximately 5276 cm<sup>-1</sup> (E $\parallel$ c) and 5271 cm<sup>-1</sup> (E $\perp$ c) have been attributed to either type I or type II H<sub>2</sub>O (Wood & Nassau 1967; Mashkovtsev *et al.* 2016; Yu *et al.* 2017; Hu & Lu 2020), and are pronounced in all samples. Contrary to this, features resulting from type I H<sub>2</sub>O at

about 5109 and 5436 cm<sup>-1</sup> (Hu & Lu 2020) are only barely visible. The peak at approximately 2360 cm<sup>-1</sup> is caused by the presence of CO<sub>2</sub> within beryl's structural channels (Łodziński *et al.* 2005; Mashkovtsev *et al.* 2016). It is visible for all samples in the E $\perp$ c direction, and for PK7 it appears in both polarisation directions. The orientation independence of this CO<sub>2</sub> feature is described in the literature (Charoy *et al.* 1996), although it could also be an artefact.

In the NIR range (Figure 13), E $\parallel$ c polarisation shows further H<sub>2</sub>O peaks at 6820, 7074, 7097, 7140 and 7273 cm<sup>-1</sup>, all of which represent overtones of either type I or type II H<sub>2</sub>O (Wood & Nassau 1967; Qiao *et al.* 2019; Hu & Lu 2020). Slight differences in the positions of the H<sub>2</sub>O peaks from those seen in the UV-Vis-NIR spectra (e.g. 7097 cm<sup>-1</sup> in Figure 13 versus 7102 cm<sup>-1</sup> in Figure 10) are due to the lower sensitivity and spectral resolution

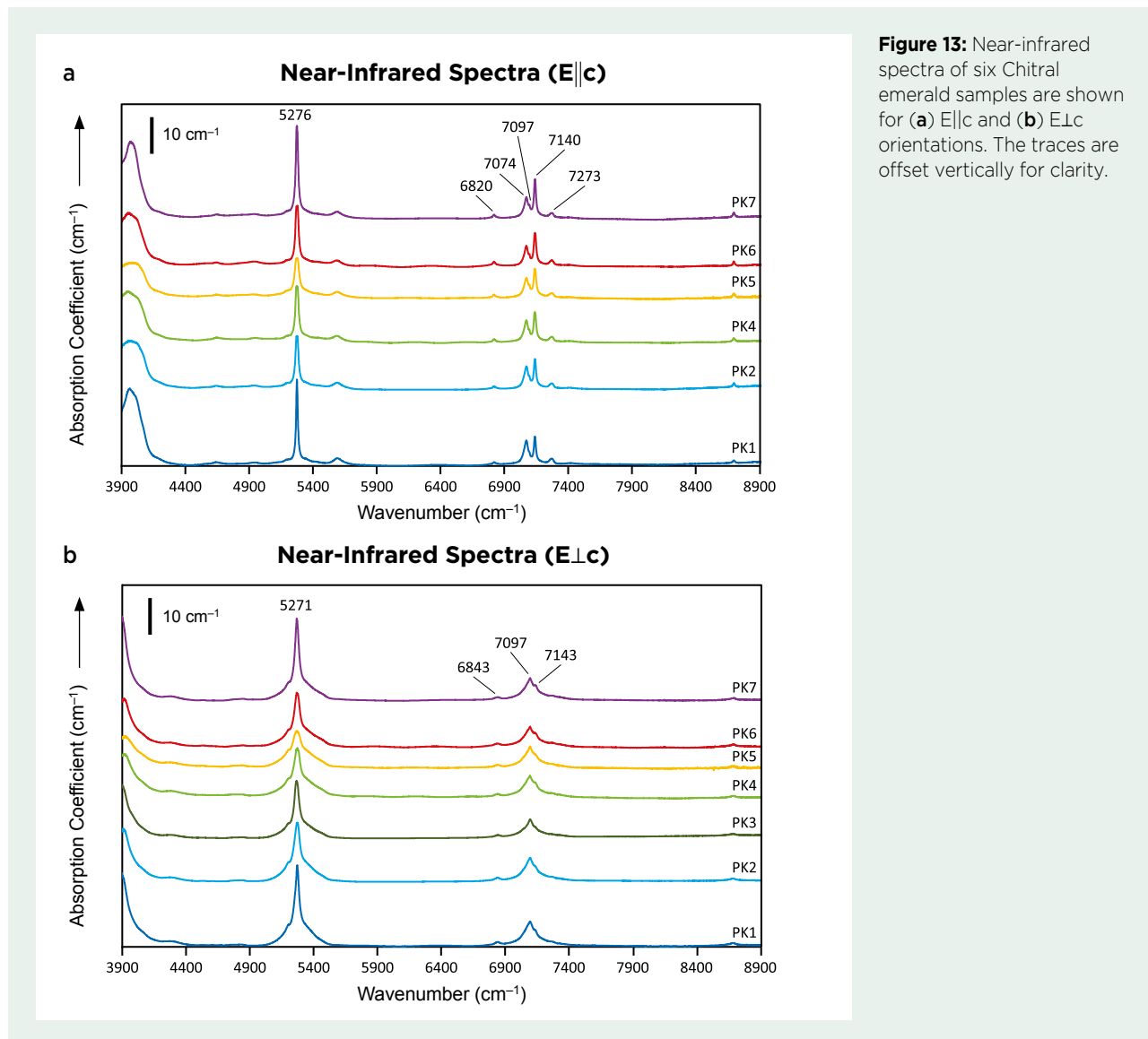


**Figure 13:** Near-infrared spectra of six Chitral emerald samples are shown for (a) E $\parallel$ c and (b) E $\perp$ c orientations. The traces are offset vertically for clarity.

of the UV-VIS-NIR spectrometer in the NIR range than that of the FTIR spectrometer.

**Raman Spectra.** Figure 14 displays Raman spectra of the emeralds. Again, only E<sub>L</sub>c excitation is shown for PK3. Most peaks are present in both sample orientations, but the intensities differ. This is especially true for the peak between 1068 and 1072 cm<sup>-1</sup>, which is stronger in the E<sub>||</sub>c direction. In addition, for E<sub>L</sub>c its neighbouring peaks at approximately 1010–1013 cm<sup>-1</sup> and 1132–1133 cm<sup>-1</sup> are only weakly present or not visible at all, respectively. Likewise, the peaks at 325 and 400 cm<sup>-1</sup> have similar intensities for E<sub>||</sub>c, while the former peak is much weaker or absent for the E<sub>L</sub>c orientation.

The peaks near 3598 cm<sup>-1</sup>, caused by type II H<sub>2</sub>O (Hagemann *et al.* 1990; Karampelas *et al.* 2019), and at

3608 cm<sup>-1</sup>, due to type I H<sub>2</sub>O (Karampelas *et al.* 2019), are present for all samples. The former is stronger for E<sub>L</sub>c and the latter for E<sub>||</sub>c. The only exception is sample PK1, for which the 3598 cm<sup>-1</sup> peak is more intense in both orientations. These results are consistent with what we observed in the UV-Vis-NIR and FTIR spectra. Furthermore, according to Karampelas *et al.* (2019), emeralds from Ethiopia, Madagascar, Zambia and Zimbabwe also show the same relative-intensity ratios as the samples here, with both H<sub>2</sub>O peaks either being of the same intensity or 3598 cm<sup>-1</sup> > 3608 cm<sup>-1</sup> for the E<sub>L</sub>c direction. However, Afghan, Brazilian and Russian emeralds sometimes also show similar intensities for both peaks. Moreover, when the intensities differ, the ratios are reversed compared to those of the beryls from this study. The same is true for Colombian emeralds

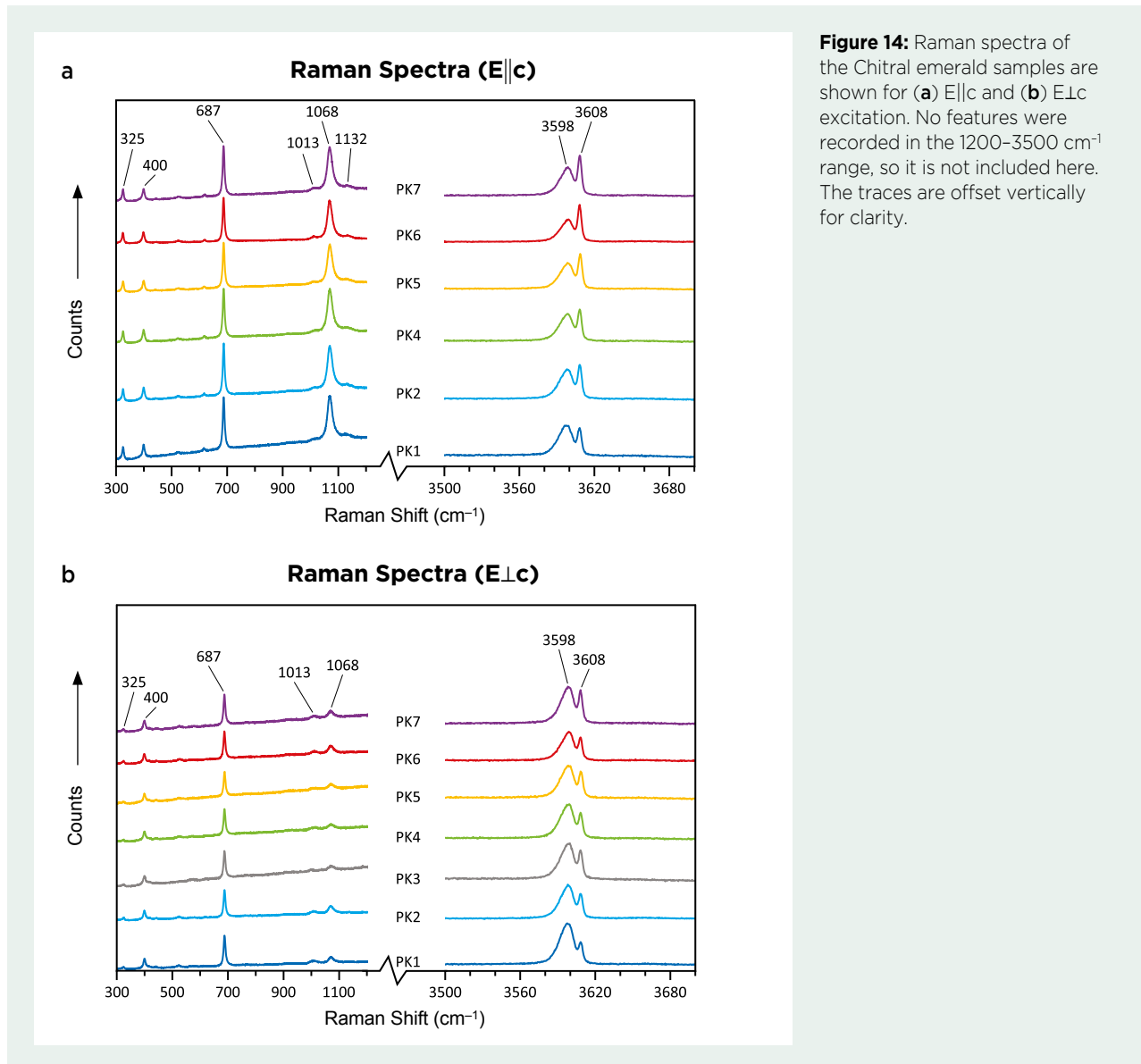


**Figure 14:** Raman spectra of the Chitral emerald samples are shown for (a) E<sub>||</sub>c and (b) E<sub>L</sub>c excitation. No features were recorded in the 1200–3500 cm<sup>-1</sup> range, so it is not included here. The traces are offset vertically for clarity.

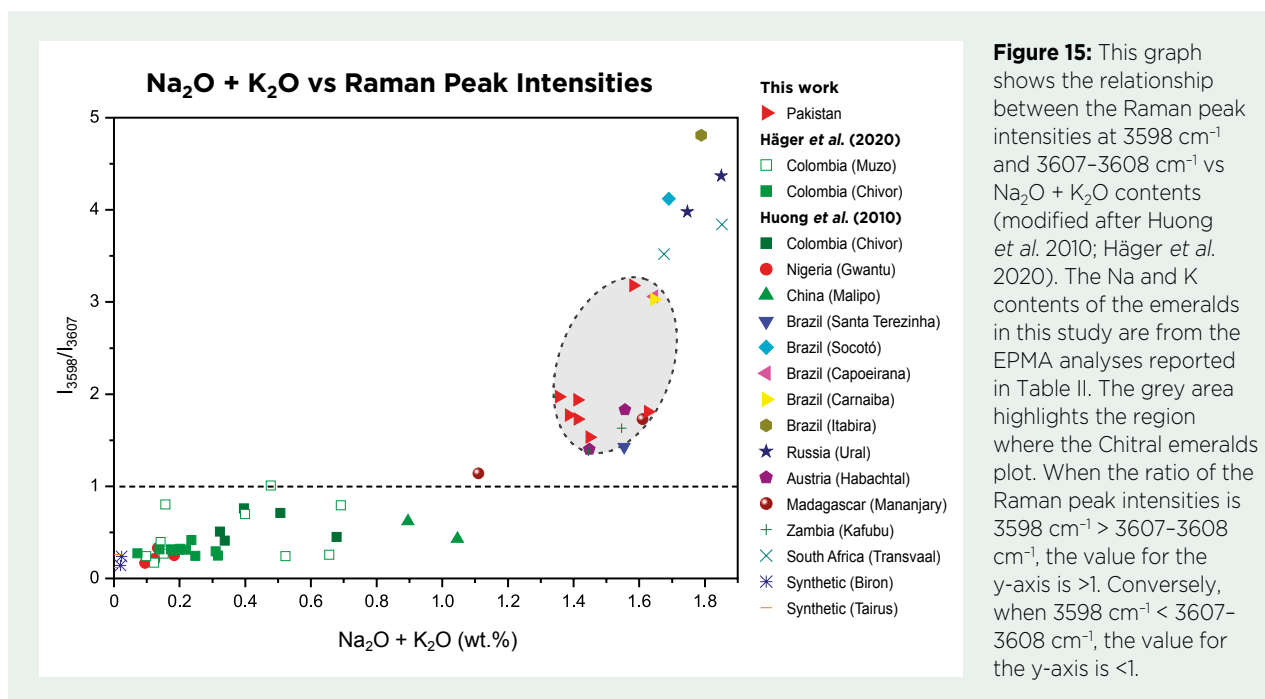


**Figure 15:** This graph shows the relationship between the Raman peak intensities at 3598  $\text{cm}^{-1}$  and 3607–3608  $\text{cm}^{-1}$  vs  $\text{Na}_2\text{O} + \text{K}_2\text{O}$  contents (modified after Huong *et al.* 2010; Häger *et al.* 2020). The Na and K contents of the emeralds in this study are from the EPMA analyses reported in Table II. The grey area highlights the region where the Chitral emeralds plot. When the ratio of the Raman peak intensities is 3598  $\text{cm}^{-1} > 3607\text{--}3608 \text{ cm}^{-1}$ , the value for the y-axis is  $>1$ . Conversely, when 3598  $\text{cm}^{-1} < 3607\text{--}3608 \text{ cm}^{-1}$ , the value for the y-axis is  $<1$ .

(Karampelas *et al.* 2019). A comparison between the intensity ratios for these two Raman peaks and the contents of Na and K in emeralds of different localities is displayed in Figure 15. The Chitral emeralds plot at the higher end with regard to the Na and K contents as well as the Raman peak ratios. For both of these aspects, values are surpassed only by Brazilian, Russian and South African emeralds.

### Chemical Composition

Table II shows the average values for the EPMA analyses of the emeralds. Since it is not possible to measure  $\text{H}_2\text{O}$  with EMPA and the determination of BeO is associated with a large measurement error, the contents of both of these components were fixed to values commonly found in beryls. Including these light elements in the matrix corrections helps to obtain more accurate results in the EPMA data-reduction routine.

The  $\text{SiO}_2$  and  $\text{Al}_2\text{O}_3$  contents of approximately 63–64 wt.% and 15.5–16.5 wt.%, respectively, are lower than what would be expected for a pure, ideal beryl, but they agree with amounts found in the literature for various beryls from other localities worldwide, including emeralds from Swat Valley (Pakistan) and Habachtal (Austria), as well as variously coloured beryls from Brazil, USA, Afghanistan, Russia and India (Aurischio *et al.* 1988; Mathew *et al.* 2000; McMillan *et al.* 2006; Bidny *et al.* 2011). Our samples show  $\text{SiO}_2$  contents that are lower by about 2 wt.% than those reported for Khaltaro emeralds (Laurs *et al.* 1996), but the  $\text{Al}_2\text{O}_3$  contents are similar.

As can be seen from Figure 16a, the Na and Mg contents of the emeralds in this study are higher than those reported for Colombian emeralds (Groat *et al.* 2008; Karampelas *et al.* 2019). All the Chitral samples contain more than 1 wt.% MgO, but the Mg contents are generally lower than those found in emeralds from Madagascar, Zambia and Zimbabwe (Groat *et al.* 2008; Karampelas *et al.* 2019). With regard to the non-framework impurities, Na is the most abundant element in the Chitral emeralds (Figure 16a, c). Only Zimbabwean emeralds are reported to contain more Na (Zwaan 2006; Groat *et al.* 2008).

In contrast to the Na levels, the contents of the other common alkalis (Ca and K) are relatively low. This is also true when comparing these values with those reported in the literature for emeralds from other sources. The low Ca and K contents have little influence on the area in which the Chitral emeralds plot in relation to emeralds from other localities worldwide (Figure 16d, e). Only Colombian and Russian emeralds show notably lower amounts of K, which are sometimes below the detection limit (Karampelas *et al.* 2019).

For the generally less common alkalis, all seven Chitral samples exhibit comparably high values of  $\text{Cs}_2\text{O}$ , surpassing those found in Malagasy and Zambian emeralds (Karampelas *et al.* 2019), while  $\text{Rb}_2\text{O}$  is lower. While this suggests a pegmatitic source, the results obtained for Rb should be considered with caution since Rb was not calibrated on any standard prior to the EPMA analyses (also, see below for LA-ICP-MS results).

**Table II:** Average compositions of the seven beryl samples, analysed by EPMA.<sup>a</sup>

Sample	PK1	PK2	PK3	PK4	PK5	PK6	PK7
<b>Oxide (wt.%)</b>							
SiO <sub>2</sub>	63.38 (0.13)	64.41 (0.13)	63.70 (0.14)	63.68 (0.14)	63.69 (0.38)	63.45 (0.08)	63.94 (0.12)
TiO <sub>2</sub>	nd	nd	nd	nd	nd	nd	0.01 (0.01)
Al <sub>2</sub> O <sub>3</sub>	15.49 (0.2)	15.52 (0.09)	16.03 (0.25)	15.8 (0.18)	15.53 (0.1)	16.36 (0.33)	15.8 (0.29)
Cr <sub>2</sub> O <sub>3</sub>	0.10 (0.03)	0.05 (0.02)	nd	0.04 (0.02)	0.04 (0.02)	0.05 (0.02)	0.09 (0.04)
V <sub>2</sub> O <sub>3</sub>	0.06 (0.01)	0.04 (0.01)	0.03 (0.01)	0.03 (0.01)	0.03 (0.01)	0.04 (0.01)	0.05 (0.004)
Fe <sub>2</sub> O <sub>3</sub> <sup>b</sup>	0.50 (0.01)	0.51 (0.02)	0.54 (0.02)	0.58 (0.02)	0.54 (0.01)	0.38 (0.04)	0.41 (0.02)
BeO <sup>c</sup>	13.60	13.60	13.60	13.60	13.60	13.60	13.60
MnO	0.01 (0.01)	0.01 (0.01)	0.01 (0.01)	0.01 (0.01)	0.01 (0.01)	0.01 (0.004)	0.01 (0.005)
MgO	1.86 (0.09)	1.63 (0.05)	1.74 (0.12)	1.60 (0.13)	1.54 (0.06)	1.29 (0.17)	1.56 (0.20)
CaO	0.05 (0.003)	0.02 (0.01)	0.01 (0.01)	0.04 (0.01)	0.03 (0.01)	0.03 (0.01)	0.03 (0.01)
Na <sub>2</sub> O	1.59 (0.06)	1.43 (0.04)	1.80 (0.07)	1.57 (0.05)	1.47 (0.03)	1.41 (0.08)	1.51 (0.08)
K <sub>2</sub> O	0.04 (0.01)	0.04 (0.01)	0.02 (0.01)	0.04 (0.005)	0.04 (0.01)	0.03 (0.005)	0.03 (0.01)
Cs <sub>2</sub> O	0.30 (0.04)	0.20 (0.02)	0.25 (0.03)	0.44 (0.02)	0.41 (0.02)	0.12 (0.04)	0.17 (0.05)
Rb <sub>2</sub> O	0.02 (0.01)	0.02 (0.01)	0.02 (0.01)	0.02 (0.01)	0.01 (0.01)	0.02 (0.004)	0.02 (0.01)
H <sub>2</sub> O <sup>c</sup>	0.85	0.85	0.85	0.85	0.85	0.85	0.85
Total	97.85 (0.24)	98.34 (0.13)	98.66 (0.15)	98.29 (0.17)	97.78 (0.38)	97.63 (0.11)	98.08 (0.18)

<sup>a</sup> Values represent the average of five to six analysed spots on each sample. Standard deviations are given in parentheses. Abbreviation: nd = not detected.

<sup>b</sup> The standard format for reporting Fe content by our instrument is Fe<sub>2</sub>O<sub>3</sub>; equivalent values are 0.45, 0.46, 0.49, 0.52, 0.48, 0.34 and 0.37 wt.% FeO, respectively, for samples PK1-PK7.

<sup>c</sup> BeO and H<sub>2</sub>O contents are given as fixed values based on typical contents found in beryl.

Regarding the transition metals, Fe is dominant in our samples. Although the binary plots (Figure 16b, d, e) show iron contents as Fe<sup>2+</sup>, it can also be present as Fe<sup>3+</sup>, which does not cause a charge deficiency when substituting for Al in the octahedral position. Furthermore, Fe may also be present in the beryl channel sites, but this is debated in the literature (Goldman *et al.* 1978; Mathew *et al.* 2000; Viana *et al.* 2002; Andersson 2013). While similar Fe contents were reported for Afghan Laghman (Krzemnicki *et al.* 2021) and Russian Ural Mountains (Bidny *et al.* 2011) emeralds, Figures 16 and 17 show that the Chitral emeralds exhibit higher Fe values than Afghan Panjshir and Colombian emeralds, and also overlap with those reported for Zambian emeralds by Groat *et al.*

(2008; see Figure 16b, c). While light-coloured Khaltaro emeralds were reported to also contain FeO contents of about 0.5 wt.%, the darker Khaltaro samples exhibited higher values (by approximately 0.3 wt.%; Laurs *et al.* 1996) compared to the Chitral emeralds in this study.

All of our samples contain greater amounts of Cr<sub>2</sub>O<sub>3</sub> than V<sub>2</sub>O<sub>3</sub> (Figure 16f). This is also true for most emeralds worldwide (Groat *et al.* 2008; Giuliani *et al.* 2019). The only exception in this study is specimen PK3, which does not contain detectable Cr by EPMA and thus owes its pale green colour to V and possibly Fe. Lower Cr than V contents are also found in emeralds from the Mohmand District in Pakistan (Groat *et al.* 2008; Giuliani *et al.* 2019). In our Chitral samples, Cr is at most about twice as high

as V, similar to the ratios reported for Afghan Panjshir type II emeralds (Karampelas *et al.* 2019; Krzemnicki *et al.* 2021). Concerning the remaining trace elements analysed, Mn and Ti are absent or nearly so from all samples.

To determine lighter elements such as Be and Li, LA-ICP-MS analyses were performed on all Chitral samples and the data were compared to those for

emeralds from other localities (e.g. Figure 18; Table III). While the LA-ICP-MS results for Be and Rb are lower than for EPMA (where Be represented an assumed value and Rb was not calibrated), results for the other elements were similar. Furthermore, the Cs contents of our Chitral emeralds are higher than for most important emerald localities, whereas Rb contents are low (again, see Figure 18).

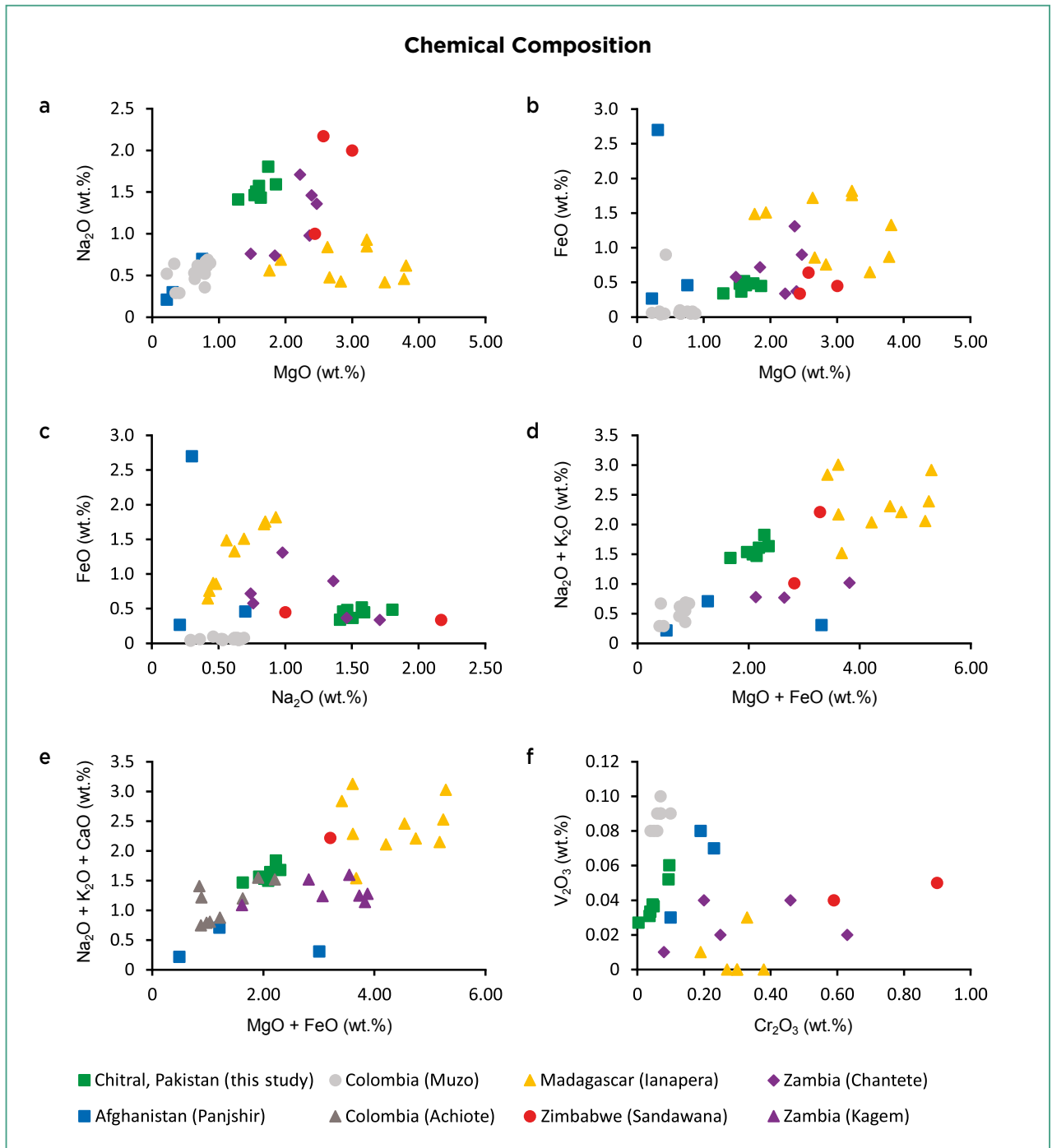


**Figure 16:** Binary plots compare key chemical components of emeralds from various localities to those from Chitral analysed in this study. (FeO was calculated by converting total  $\text{Fe}_2\text{O}_3$  content.) Literature data reported by Groat *et al.* (2008) from Zamboni & Caglioto (1928), Otero Muñoz & Barriga Villalba (1948), Gübelin (1958), Beus & Mineev (1972), Kozłowski *et al.* (1988), Hammarstrom (1989), Ottaway (1991), Vapnik *et al.* (2005), Zwaan *et al.* (2005), Gavrilenko *et al.* (2006) and Zwaan (2006).

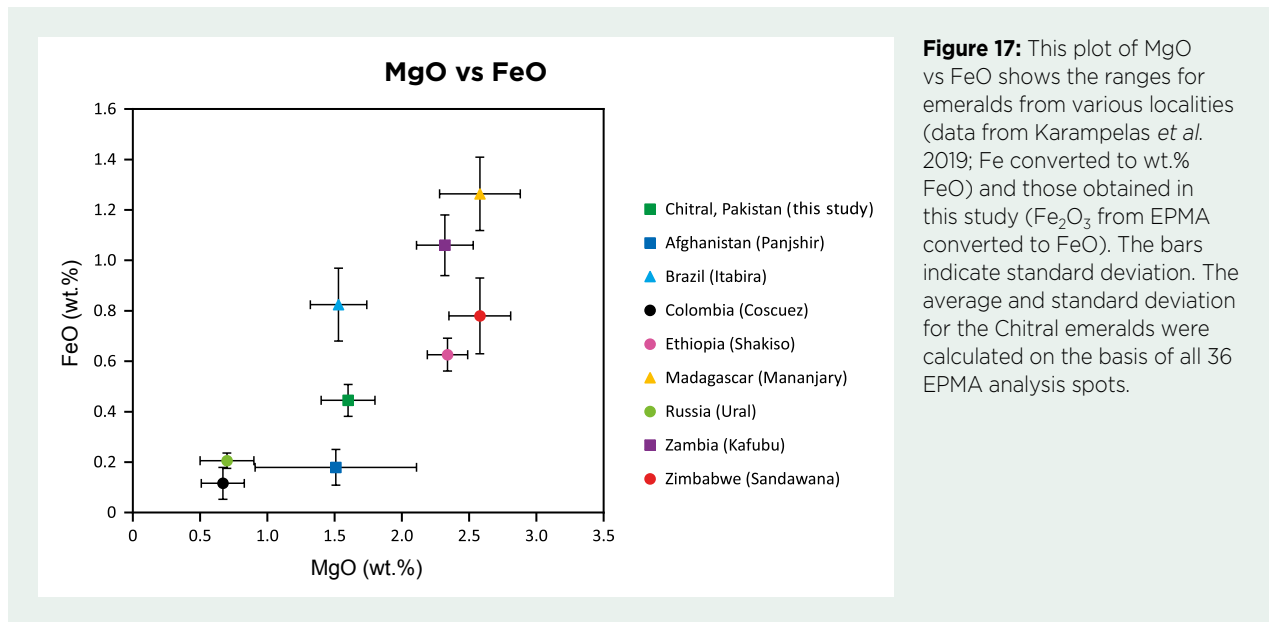


**Figure 17:** This plot of MgO vs FeO shows the ranges for emeralds from various localities (data from Karampelas *et al.* 2019; Fe converted to wt.% FeO) and those obtained in this study ( $\text{Fe}_2\text{O}_3$  from EPMA converted to FeO). The bars indicate standard deviation. The average and standard deviation for the Chitral emeralds were calculated on the basis of all 36 EPMA analysis spots.

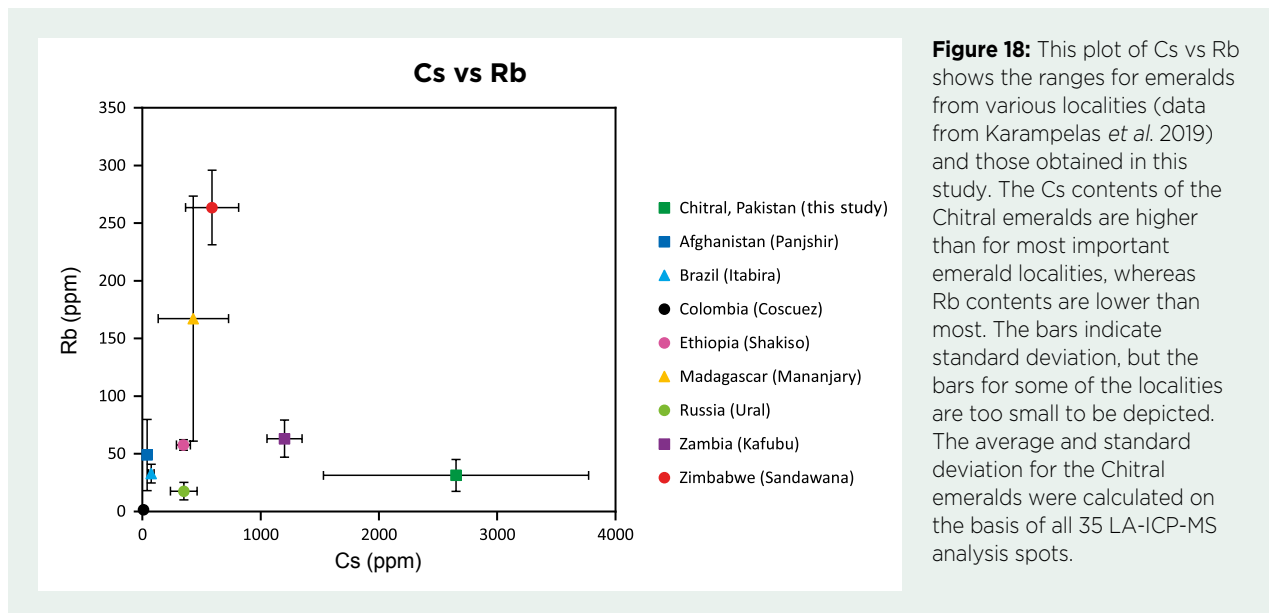


**Figure 18:** This plot of Cs vs Rb shows the ranges for emeralds from various localities (data from Karampelas *et al.* 2019) and those obtained in this study. The Cs contents of the Chitral emeralds are higher than for most important emerald localities, whereas Rb contents are lower than most. The bars indicate standard deviation, but the bars for some of the localities are too small to be depicted. The average and standard deviation for the Chitral emeralds were calculated on the basis of all 35 LA-ICP-MS analysis spots.

This is also true in comparison to Khaltaro emeralds, which showed Cs contents of at most about 2700 ppm, while the Rb values were close to or exceeded 100 ppm (Laurs *et al.* 1996).

All the Chitral specimens contain Li at concentrations around 1000 ppm (except for PK3), suggesting a pegmatitic source. In addition, the average Li contents of these emeralds are higher than those from most other deposits (Figure 19). As with EPMA, LA-ICP-MS analyses showed PK3 to be the emerald with the lowest V and Cr contents. Other elements—such as Ni, Co, Zn and Ga—are, if at all, present only in very small amounts. Rarer elements such as Zr, Y and Nb are mostly below the detection limit or absent.

## CONCLUSION

The Chitral District emeralds investigated in this study show similarities to those from Khaltaro (Pakistan) in that the samples are mostly light to medium green, partly euhedral and can be relatively large. In addition, they occur within quartz- and mica-rich host rocks (Kazmi *et al.* 1989; Laurs *et al.* 1996). Some samples exhibit spectroscopic features similar to those observed in Afghan Laghman emeralds. However, despite the proximity of the Panjshir Valley (only about 200 km away) and the shared tectonic units on both sides of the border, the emeralds in this study show only limited similarities to the various Afghan emeralds with regard to major- and trace-element



**Table III:** Average chemical concentrations of the seven beryl samples, analysed by LA-ICP-MS.\*

Sample	PK1	PK2	PK3	PK4	PK5	PK6	PK7
<b>Element (ppm)</b>							
Li	1203 (57.79)	1315 (76.02)	768.2 (89.30)	1316 (85.60)	1274 (79.68)	996.2 (87.40)	1219 (80.53)
Be	45070 (575.8)	45580 (511.2)	46380 (685.3)	46380 (764.1)	43440 (556.7)	43560 (465.1)	42960 (631.7)
B	4.55 (0.55)	4.71 (0.70)	4.86 (1.36)	5.09 (0.93)	3.74 (0.88)	3.99 (0.92)	4.28 (1.29)
Na	11390 (276.9)	10690 (113.6)	12610 (305.1)	10570 (277.1)	10080 (345.3)	10170 (774.4)	10500 (367.2)
Mg	10940 (507.1)	9833 (272.1)	10120 (571.7)	9332 (652.7)	8709 (488.6)	7713 (1280)	8644 (392.5)
P	nd	4.85 (1.48)	5.87 (2.13)	nd	nd	5.77 (0.43)	nd
K	280.3 (50.56)	199.2 (24.77)	221.0 (15.80)	216.3 (75.02)	217.3 (10.95)	128.8 (23.44)	156.3 (10.17)
Ca	559.2 (13.06)	416.0 (35.99)	414.2 (49.19)	474.9 (18.87)	482.1 (40.41)	494.2 (138.4)	441.4 (37.29)
Sc	83.02 (4.93)	43.37 (2.90)	94.75 (9.61)	98.73 (3.72)	108.6 (8.57)	63.84 (9.53)	43.37 (5.44)
Ti	31.82 (2.42)	31.76 (1.51)	35.29 (1.19)	28.60 (1.17)	27.55 (6.55)	29.18 (3.87)	48.05 (13.02)
V	348.9 (14.80)	181.9 (9.07)	143.1 (9.66)	176.7 (7.98)	160.6 (24.44)	201.8 (18.90)	214.0 (6.67)
Cr	623.3 (235.1)	381.1 (71.98)	321.5 (7.03)	260.0 (42.86)	170.5 (118.1)	278.3 (84.58)	616.9 (145.3)
Mn	18.43 (1.99)	13.87 (2.55)	13.11 (0.91)	18.92 (3.92)	23.04 (1.78)	11.55 (2.45)	10.67 (0.98)
Fe	3525 (119.5)	3505 (178.9)	3727 (237.2)	3918 (318.3)	3626 (133.1)	2635 (475.4)	2440 (76.40)
Co	1.55 (0.10)	2.00 (0.09)	1.73 (0.12)	1.77 (0.11)	2.11 (0.06)	1.51 (0.08)	1.34 (0.09)
Ni	nd	8.31 (4.14)	nd	4.46 (1.22)	4.95 (0.93)	2.87 (0.31)	nd
Zn	10.88 (0.80)	15.85 (0.53)	11.63 (0.72)	12.57 (0.59)	17.08 (1.58)	16.22 (2.41)	13.35 (1.61)
Ga	9.99 (0.29)	10.28 (0.56)	10.42 (2.13)	12.91 (0.62)	15.25 (1.69)	13.87 (0.75)	9.14 (0.45)
Ge	0.43 (0.11)	0.37 (0.03)	0.43 (0.14)	0.53 (0.09)	0.60 (0.14)	0.39 (0.09)	0.48 (0.11)
Rb	53.76 (14.64)	27.67 (6.41)	29.32 (1.58)	31.06 (2.53)	42.42 (7.49)	16.03 (2.57)	18.22 (0.95)
Sr	0.03 (0.01)	0.05 (0.02)	0.04 (0.01)	0.05 (0.02)	0.04 (0.03)	nd	0.12 (0.22)
Zr	nd	nd	nd	nd	0.03 (0.03)	0.03 (0.02)	0.05 (0.01)
Sn	1.50 (0.63)	0.72 (0.55)	1.02 (0.08)	1.06 (0.41)	4.43 (5.09)	0.21 (0.06)	1.41 (0.81)
Cs	3275 (796.5)	2078 (212.4)	2440 (155.7)	3988 (196.6)	4044 (333.6)	1284 (304.7)	1455 (32.39)
Tl	0.17 (0.06)	0.09 (0.04)	0.09 (0.02)	0.11 (0.01)	0.15 (0.03)	0.07 (0.04)	0.05 (0.02)

\* Values represent the average of five analysed spots on each sample. Standard deviations are given in parentheses. Abbreviation: nd = not detected.

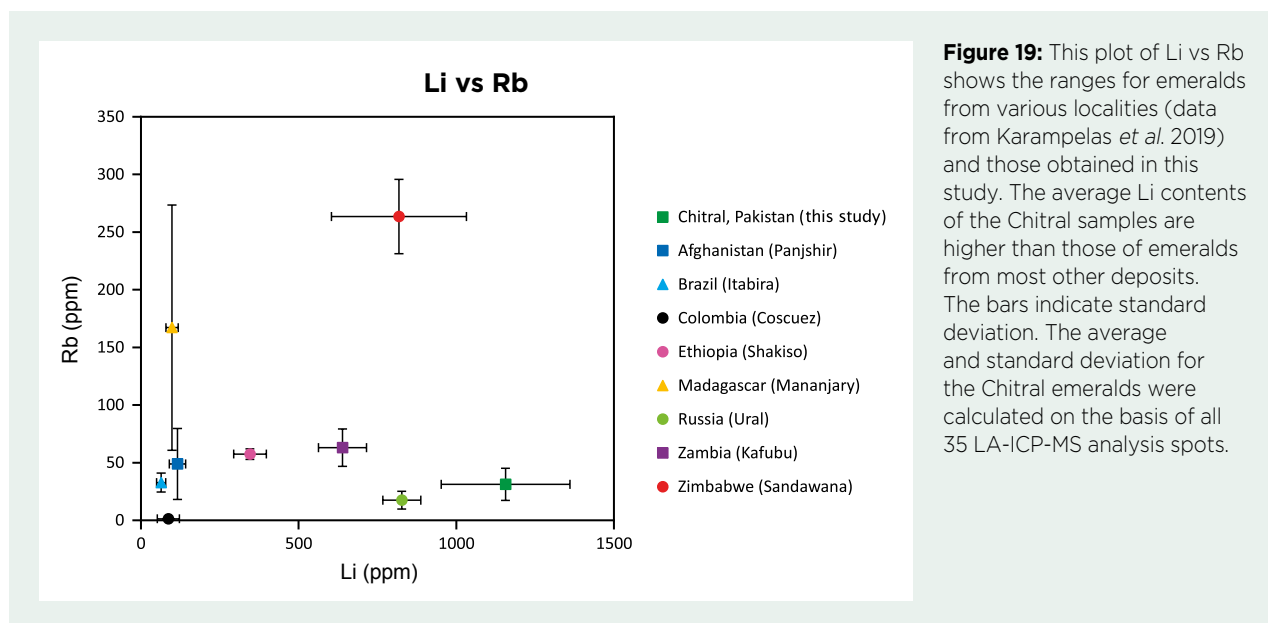


**Figure 19:** This plot of Li vs Rb shows the ranges for emeralds from various localities (data from Karampelas *et al.* 2019) and those obtained in this study. The average Li contents of the Chitral samples are higher than those of emeralds from most other deposits. The bars indicate standard deviation. The average and standard deviation for the Chitral emeralds were calculated on the basis of all 35 LA-ICP-MS analysis spots.

analyses and ratios. The pronounced Fe absorption in the UV-Vis-NIR spectra, the Raman peak ratios and the chemical composition of the Chitral emeralds resemble those reported for Zambian emeralds. However, owing to the different geological environments, there are barely any shared features with Colombian emeralds. The Chitral emeralds of this study exhibit high Cs and Li contents, which indicate a pegmatite-related origin. These values are higher than the ranges reported in the literature for most other important emerald localities. Thus, this trace-element signature can help distinguish Chitral emeralds

from those of many other regions, such as Colombia.

As stated above, the rough emerald samples examined for this study were collected in the very first days of mining. Since then, a few larger gem-quality crystals have been found that show deeper colour saturation (again, see Figure 6). Hence, a follow-up study is in preparation to characterise the more strongly coloured specimens of this deposit. However, owing to the remote location of the mining area and difficulty accessing it, as well as the challenging working conditions at such a high altitude, the annual production will likely be limited.

## REFERENCES

- Andersson, L.O. 2013. The yellow color center and trapped electrons in beryl. *Canadian Mineralogist*, **51**(1), 15–25, <https://doi.org/10.3749/canmin.51.1.15>.
- Aurischio, C., Fioravanti, G., Grubessi, O. & Zanazzi, P.F. 1988. Reappraisal of the crystal chemistry of beryl. *American Mineralogist*, **73**(7–8), 826–837.
- Beus, A.A. & Mineev, D.A. 1972. *Some Geological and Geochemical Features of the Muzo-Coscuéz Emerald Zone, Cordillera Oriental, Colombia*. Empresa Colombiana de Minas (ECOMINAS), Bogotá, Colombia, 58 pp.
- Bidny, A.S., Baksheev, I.A., Popov, M.P. & Anosova, M.O. 2011. Beryl from deposits of the Ural emerald belt, Russia: ICP-MS-LA and infrared spectroscopy study. *Moscow University Geology Bulletin*, **66**(2), 108–115, <https://doi.org/10.3103/s0145875211020037>.
- Charoy, B., de Donato, P., Barres, O. & Pinto-Coelho, C. 1996. Channel occupancy in an alkali-poor beryl from Serra Branca (Goias, Brazil); spectroscopic characterization. *American Mineralogist*, **81**(3–4), 395–403, <https://doi.org/10.2138/am-1996-3-414>.
- Gavrilenko, E.V., Calvo Pérez, B., Castroviejo Bolibar, R. & García del Amo, D. 2006. Emeralds from the Delbegetey deposit (Kazakhstan): Mineralogical characteristics and fluid-inclusion study. *Mineralogical Magazine*, **70**(2), 159–173, <https://doi.org/10.1180/0026461067020321>.
- Giuliani, G., Groat, L.A., Marshall, D., Fallick, A.E. & Branquet, Y. 2019. Emerald deposits: A review and enhanced classification. *Minerals*, **9**(2), article 105 (63 pp.), <https://doi.org/10.3390/min9020105>.
- Goldman, S.D., Rossman, G.R. & Parkin, K.M. 1978. Channel constituents in beryl. *Physics and Chemistry of Minerals*, **3**(3), 225–235, <https://doi.org/10.1007/bf00633572>.
- Groat, L.A., Giuliani, G., Marshall, D.D. & Turner, D. 2008. Emerald deposits and occurrences: A review. *Ore Geology*

- Reviews*, **34**(1–2), 87–112, <https://doi.org/10.1016/j.oregeorev.2007.09.003>.
- Gübelin, E.J. 1958. Emeralds from Sandawana. *Journal of Gemmology*, **6**(8), 340–354, <https://doi.org/10.15506/JoG.1958.6.8.340>.
- Gübelin, E.J. 1989. Gemological characteristics of Pakistani emeralds. In: Kazmi, A.H. & Snee, L.W. (eds) *Emeralds of Pakistan: Geology, Gemology and Genesis*. Springer, New York, New York, USA, 75–92.
- Hagemann, H., Lucken, A., Bill, H., Gysler-Sanz, J. & Stalder, H.A. 1990. Polarized Raman spectra of beryl and bazzite. *Physics and Chemistry of Minerals*, **17**(5), 395–401, <https://doi.org/10.1007/bf00212207>.
- Häger, T., Rojas-Agramonte, Y., Charros-Leal, F., Villalobos-Basler, J.D., Gonzalez-Pinzon, M.A. & Hauzenberger, C. 2020. Smaragde aus Kolumbien. *Gemmologie: Zeitschrift der Deutschen Gemmologischen Gesellschaft*, **69**(1–2), 47–58.
- Hammarstrom, J.M. 1989. Mineral chemistry of emeralds and some associated minerals from Pakistan and Afghanistan: An electron microprobe study. In: Kazmi, A.H. & Snee, L.W. (eds) *Emeralds of Pakistan: Geology, Gemology and Genesis*. Springer, New York, New York, USA, 125–150.
- Hildebrand, P.R., Noble, S.R., Searle, M.P., Waters, D.J. & Parrish, R.R. 2001. Old origin for an active mountain range: Geology and geochronology of the eastern Hindu Kush, Pakistan. *Geological Society of America Bulletin*, **113**(5), 625–639, [https://doi.org/10.1130/0016-7606\(2001\)113%3C0625:oofaam%3E2.0.co;2](https://doi.org/10.1130/0016-7606(2001)113%3C0625:oofaam%3E2.0.co;2).
- Hu, Y. & Lu, R. 2020. Color characteristics of blue to yellow beryl from multiple origins. *Gems & Gemology*, **56**(1), 54–65, <https://doi.org/10.5741/gems.56.1.54>.
- Huong L.T.-T., Häger, T. & Hofmeister, W. 2010. Confocal micro-Raman spectroscopy: A powerful tool to identify natural and synthetic emeralds. *Gems & Gemology*, **46**(1), 36–41, <https://doi.org/10.5741/gems.46.1.36>.
- Jehlička, J., Culka, A., Bersani, D. & Vandenabeele, P. 2017. Comparison of seven portable Raman spectrometers: Beryl as a case study. *Journal of Raman Spectroscopy*, **48**(10), 1289–1299, <https://doi.org/10.1002/jrs.5214>.
- Karampelas, S., Al-Shaybani, B., Mohamed, F., Sangsawong, S. & Al-Alawi, A. 2019. Emeralds from the most important occurrences: Chemical and spectroscopic data. *Minerals*, **9**(9), article 561 (29 pp.), <https://doi.org/10.3390/min9090561>.
- Kazmi, A.H. 1989. A brief overview of the geology and metallogenic provinces of Pakistan. In: Kazmi, A.H. & Snee, L.W. (eds) *Emeralds of Pakistan: Geology, Gemology and Genesis*. Springer, New York, New York, USA, 1–12.
- Kazmi, A.H., Anwar, J., Hussain, S., Khan, T. & Dawood, H. 1989. Emerald deposits of Pakistan. In: Kazmi, A.H. & Snee, L.W. (eds) *Emeralds of Pakistan: Geology, Gemology and Genesis*. Springer, New York, New York, USA, 39–74.
- Khan T.K. 1986. *Geology of the Pegmatite Belt in Chitral, Northwest Frontier Province, Pakistan*. Geological Survey of Pakistan Information Release No. 266, Quetta, Pakistan, 16 pp. + five maps.
- Kozłowski, A., Metz, P. & Estrada Jaramillo, H.A. 1988. Emeralds from Somondoco, Colombia: Chemical composition, fluid inclusions and origin. *Neues Jahrbuch für Mineralogie, Abhandlungen*, **159**(1), 23–49.
- Krambrock, K., Pinheiro, M.V.B., Guedes, K.J., Medeiros, S.M., Schweizer, S., Castañeda, C., Botelho, N.F. & Pedrosa-Soares, A.C. 2002. Radiation-induced centers in Cs-rich beryl studied by magnetic resonance, infrared and optical spectroscopy. *Nuclear Instruments and Methods in Physics Research Section B: Beam Interactions with Materials and Atoms*, **191**(1–4), 285–290, [https://doi.org/10.1016/s0168-583x\(02\)00577-3](https://doi.org/10.1016/s0168-583x(02)00577-3).
- Krzemnicki, M.S., Wang, H.A.O. & Büche, S. 2021. A new type of emerald from Afghanistan's Panjshir Valley. *Journal of Gemmology*, **37**(5), 474–495, <https://doi.org/10.15506/JoG.2021.37.5.474>.
- Laur, B.M., Dilles, J.H. & Snee, L.W. 1996. Emerald mineralization and metasomatism of amphibolite, Khaltaro granitic pegmatite-hydrothermal vein system, Haramosh Mountains, northern Pakistan. *Canadian Mineralogist*, **34**(6), 1253–1286.
- Lawrence, R.D., Kazmi, A.H. & Snee, L.W. 1989. Geological setting of the emerald deposits. In: Kazmi, A.H. & Snee, L.W. (eds) *Emeralds of Pakistan: Geology, Gemology and Genesis*. Springer, New York, New York, USA, 13–38.
- Łodziński, M., Sitarz, M., Stec, K., Kozanecki, M., Fojud, Z. & Jurga, S. 2005. ICP, IR, Raman, NMR investigations of beryls from pegmatites of the Sudety Mts. *Journal of Molecular Structure*, **744–747**, 1005–1015, <https://doi.org/10.1016/j.molstruc.2004.12.042>.
- Mashkovtsev, R.I., Thomas, V.G., Fursenko, D.A., Zhukova, E.S., Uskov, V.V. & Gorshunov, B.P. 2016. FTIR spectroscopy of D<sub>2</sub>O and HDO molecules in the c-axis channels of synthetic beryl. *American Mineralogist*, **101**(1), 175–180, <https://doi.org/10.2138/am-2016-5432>.
- Mathew, G., Karanth, R.V., Rao, T.K.G. & Deshpande, R.S. 2000. Colouration in natural beryls: A spectroscopic investigation. *Journal of Geological Society of India*, **56**(3), 285–303.
- McMillan, N.J., McManus, C.E., Harmon, R.S., De Lucia, F.C. & Miziolek, A.W. 2006. Laser-induced breakdown spectroscopy analysis of complex silicate minerals—Beryl. *Analytical and Bioanalytical Chemistry*, **385**(2), 263–271, <https://doi.org/10.1007/s00216-006-0374-9>.


- Nassau, K. & Wood, D.L. 1968. An examination of red beryl from Utah. *American Mineralogist*, **53**(5–6), 801–806.
- Otero Muñoz, G. & Barriga Villalba, A.M. 1948. *Esmeraldas de Colombia*. Banco de la República, Bogotá, Colombia, 133 pp.
- Ottaway, T.L. 1991. *The geochemistry of the Muzo emerald deposit, Colombia*. MS thesis, University of Toronto, Ontario, Canada, 227 pp., <https://recordcenter.sgc.gov.co/B12/23008010002777/documento/pdf/2105027771103000.pdf>.
- Qiao, X., Zhou, Z., Schwarz, D.T., Qi, L., Gao, J., Nong, P., Lai, M., Guo, K. *et al.* 2019. Study of the differences in infrared spectra of emerald from different mining areas and the controlling factors. *Canadian Mineralogist*, **57**(1), 65–79, <https://doi.org/10.3749/canmin.1800042>.
- Saeseaw, S., Renfro, N.D., Palke, A.C., Sun, Z. & McClure, S.F. 2019. Geographic origin determination of emerald. *Gems & Gemology*, **55**(4), 614–646, <https://doi.org/10.5741/gems.55.4.614>.
- Snee, L.W., Foord, E.E., Hill, B. & Carter, S.J. 1989. Regional chemical differences among emeralds and host rocks of Pakistan and Afghanistan: Implications for the origin of emerald. In: Kazmi, A.H. & Snee, L.W. (eds) *Emeralds of Pakistan: Geology, Gemology and Genesis*. Springer, New York, New York, USA, 93–124.
- Vapnik, Y., Sabot, B. & Moroz, I. 2005. Fluid inclusions in Ianapera emerald, southern Madagascar. *International Geology Review*, **47**(6), 647–662, <https://doi.org/10.2747/0020-6814.47.6.647>.
- Viana, R.R., Jordt-Evangelista, H., da Costa, G.M. & Stern, W.B. 2002. Characterization of beryl (aquamarine variety) from pegmatites of Minas Gerais, Brazil. *Physics and Chemistry of Minerals*, **29**(10), 668–679, <https://doi.org/10.1007/s00269-002-0278-y>.
- Wood, D.L. & Nassau, K. 1967. Infrared spectra of foreign molecules in beryl. *Journal of Chemical Physics*, **47**(7), 2220–2228, <https://doi.org/10.1063/1.1703295>.
- Wood, D.L. & Nassau, K. 1968. The characterization of beryl and emerald by visible and infrared absorption spectroscopy. *American Mineralogist*, **53**(5–6), 777–800.
- Yu, X., Hu, D., Niu, X. & Kang, W. 2017. Infrared spectroscopic characteristics and ionic occupations in crystalline tunneling system of yellow beryl. *JOM*, **69**(4), 704–712, <https://doi.org/10.1007/s11837-017-2266-1>.
- Zahid, M., Jan, M.Q. & Moon, C.J. 2016. Geochemistry of stratabound scheelite mineralisation and associated calc-silicate rocks from Chitral, NE Hindu Kush, Pakistan. *Arabian Journal of Geosciences*, **9**(13), 1–15, <https://doi.org/10.1007/s12517-016-2637-x>.
- Zambonini, F. & Caglioto, V. 1928. Ricerche chimiche sulla roosterite di San Piero in Campo (Isola d'Elba) e sui berilli in generale. *Gazzetta Chimica Italiana*, **58**, 131–152.
- Zanchi, A. & Gaetani, M. 2011. The geology of the Karakoram range, Pakistan: The new 1:100,000 geological map of central-western Karakoram. *Italian Journal of Geosciences*, **13**(2), 161–264, <https://doi.org/10.3301/ijg.2011.09>.
- Zanchi, A., Poli, S., Fumagalli, P. & Gaetani, M. 2000. Mantle exhumation along the Tirich Mir fault zone, NW Pakistan: Pre-mid-Cretaceous accretion of the Karakoram terrane to the Asian margin. *Geological Society, London, Special Publications*, **170**(1), 237–252, <https://doi.org/10.1144/gsl.Sp.2000.170.01.13>.
- Zwaan, J.C. 2006. Gemology, geology and origin of the Sandawana emerald deposits, Zimbabwe. *Scripta Geologica*, **131**, 1–212, <https://repository.naturalis.nl/pub/209632>.
- Zwaan, J.C., Seifert, A.V., Vrána, S., Laurs, B.M., Anckar, B., Simmons, W.B., Falster, A.U., Lustenhouwer, W.J. *et al.* 2005. Emeralds from the Kafubu area, Zambia. *Gems & Gemology*, **41**(2), 116–148, <https://doi.org/10.5741/gems.41.2.116>.

### The Authors

**Carina Silke Hanser FGA DGA\*, Dr Tobias Häger and Prof Dr Roman Botcharnikov**

Institute of Geosciences, Johannes Gutenberg-University Mainz, J.-J.-Becher-Weg 21, 55099 Mainz, Germany, and

Institute of Gemstone Research, Prof.-Schlossmacher-Straße 1, 55743 Idar-Oberstein, Germany  
\*Email: [chanser@uni-mainz.de](mailto:chanser@uni-mainz.de)

 <https://orcid.org/0000-0001-5504-8739>

**Bilal Gul**

Department of Geology, University of Tartu, Ravila 14a, 50411 Tartu, Estonia

### Acknowledgements

This work was partly funded by cooperation between Johannes Gutenberg-University of Mainz, Germany, and Idar-Oberstein, Germany.

The authors thank Imran Khan for supplying the samples used in this study. We also thank Imran Khan and Fawad Ali Awan for providing photos of the mining area. Furthermore, we are grateful for the help of Waqar Ahmad in selecting the samples and Shehzad Hussain for shipping them. We also thank Dudley Blauwet for providing additional images and videos of gem-quality Chitral emeralds. Nora Groschopf, Regina Mertz and Wieland Böhme at Johannes Gutenberg-University assisted with the EPMA and LA-ICP-MS analyses.

# Bid on exceptional gemstones, *selected by* Catawiki experts

Every day, our in-house Experts carefully select a wide range of gemstones from around the world for every collector.



Naomi Howard, FGA, GIA DG, AJP  
Expert Gemstones

Buy and sell on [catawiki.com](https://catawiki.com)



# Gemmological Characteristics of Turquoise from Hami, Xinjiang, China

Yanhan Wu, Quanli Chen, Yan Li, Min Cao, Zuwei Yin, Haitao Wang and Xianyu Liu

**ABSTRACT:** Turquoise from Hami, Xinjiang, China, is an attractive gem material of good quality and nice colour. The deposit shows good potential, although mining is currently forbidden due to the archaeological significance of the area. The turquoise typically forms in veins or as nodules with various associated minerals (i.e. woodhouseite, dawsonite, calcite, alunite, gypsum and quartz, as identified by X-ray diffraction analysis). The main chemical impurities in the turquoise are Si, Sr, Cr and V. Scanning electron microscopy revealed that the turquoise crystallites commonly form compact aggregates with an imbricate arrangement, resulting in low porosity and a dense structure. The relatively high hardness of a brownish yellow variety of Hami turquoise was found to be closely related to the presence of quartz impurities. Some blue-to-green specimens display a distinctive ‘raindrop’ appearance due to the presence of fluorapatite, similar to turquoise from China’s Hubei Province.

*The Journal of Gemmology*, 38(3), 2022, pp. 254–270, <https://doi.org/10.15506/JoG.2022.38.3.254>  
© 2022 Gem-A (The Gemmological Association of Great Britain)

**T**urquoise is a hydrated copper aluminium phosphate ( $\text{CuAl}_6(\text{PO}_4)_4(\text{OH})_8 \cdot 4\text{H}_2\text{O}$ ; Palache *et al.* 1951; Cid-Dresdner 1964, 1965), which is most often light green to greenish blue to light blue (e.g. Figure 1). Turquoise is the fourth-most famous ‘jade’ material recovered in China, following nephrite, ‘Xiuyan jade’ (more than 95% serpentine, from Xiuyan County, Liaoning Province) and ‘Dushan jade’ (containing mainly plagioclase and zoisite, from Dushan, Nanyang, Henan Province). Since Neolithic times, the Chinese people have used turquoise for decorations and adornment (Hao & Hao 2002). Archaeological discoveries in western Iran indicate that turquoise first appeared around 7000 BCE (Hole *et al.* 1969), and its use in ancient Egypt probably dates to within 500–600 years of this time (Close & Minichillo 2010). In its long historical development around the world, turquoise has had both decorative function (Krzemnicki *et al.* 2011) and cultural value (Harbottle & Weigand 1992; Kostov 2019), being endowed with various religious and other symbolic meanings in some regions and countries.

Turquoise is currently sourced mainly from Australia, Chile, China, Egypt, Iran, Mexico, Mongolia, Peru and the United States (Xue *et al.* 2013; Kostov 2019; Shirdam *et al.* 2021; Štubňa & Andrášiová 2021; Štubňa *et al.* 2021). In China, Hubei Province is a significant commercial source of gem-quality turquoise, which has been characterised in detail by various researchers (Guo *et al.* 2010; Zeng *et al.* 2019). Additional deposits in China occur in Anhui, Shaanxi, Henan, Qinghai and other provinces (Yu *et al.* 2021). The origin determination of turquoise using mineralogical and geochemical characteristics has been studied by various researchers (e.g. Yang *et al.* 2003; He *et al.* 2011; Carò *et al.* 2021). The use of Sr, Pb, Cu and H isotopes has also been proposed to distinguish the origin of turquoise (Hull *et al.* 2008; Othmane *et al.* 2015; Thibodeau *et al.* 2015).

In 1981, turquoise was discovered in Xinjiang (officially the Xinjiang Uygur Autonomous Region), a landlocked area in north-western China close to Mongolia (Figure 2a; Ren 1985). The two turquoise localities (Heishanling and Tianhu East) are situated in the Gobi Desert near the

**Figure 1:** Xinjiang turquoise is represented here by two cabochons (13.8 × 10.0 × 4.0 mm and 14.6 × 9.4 × 5.0 mm) and a rough specimen that shows how the turquoise occurs as veins in siliceous rock. Photo by Yanhan Wu.



oasis city of Hami, Xinjiang. (Heishanling is about 200 km south-west of Hami and Tianhu East is about 160 km south-east of Hami.) Hami is positioned near a mountain pass on the famous Silk Road from inland China to the Western Regions, so it is an important location for historical material and cultural exchanges between Asia and Europe. Due to the geographical location of Hami, the study of turquoise in Xinjiang is of great archaeological significance for exploring the cultural exchanges along the Silk Road. Ornaments made of turquoise were found in Tianshanbeilu cemetery (located in the centre of the Hami Oasis) in 1988 (Tong *et al.* 2020), and preliminary archaeological investigations were done in 2018 at the Heishanling and Tianhu East localities by the Xinjiang Cultural Relics Archaeology Institute (Xian *et al.* 2020, 2021). More than 110 pits were excavated at the Heishanling site, which has been divided into several well-defined zones (quarrying, mining-tool processing, ore beneficiation and living areas). Radiocarbon dating of charcoal and animal bones showed that the two sites were developed between 3,300 and 2,400 years ago (Li *et al.* 2019). Most of the turquoise specimens collected from the archaeological sites have been archived in the Hami Museum.

Due to its archaeological significance, the Hami area remains preserved and all exploitation of turquoise has been prohibited by the local government. The potential

output of Xinjiang turquoise is still unknown, but the quality of the material is commercially significant.

Very little systematic study has been done on the gemmological and mineralogical characteristics of Xinjiang turquoise. So far, only one basic report has been published in Chinese (Liu *et al.* 2018). Although it is difficult to obtain samples of Xinjiang turquoise, the present authors were fortunate to procure some pieces from the Heishanling locality from local inhabitants. This article characterises their mineralogical and chemical composition, structural properties and spectral features.

## GEOLOGY

The area belongs to a typical continental extreme-dry climate and is rich in mineral resources such as iron, copper, nickel, gold, phosphorus and vanadium ores (Chen *et al.* 2011).

According to an official report from the Xinjiang Provincial Bureau of Geology and Mineral Resources (Brigade No. 6), the historical turquoise mining area is located on the north side of the Hongliuhe fault (Figure 2b). The deposit is hosted by carbonaceous and siliceous rocks of Early Cambrian age (Tang *et al.* 2005), along the contact between Proterozoic and Cambrian units. The exposed rocks in the mining area are composed of iron-bearing quartzite, carbonaceous shale, muscovite-bearing quartz,

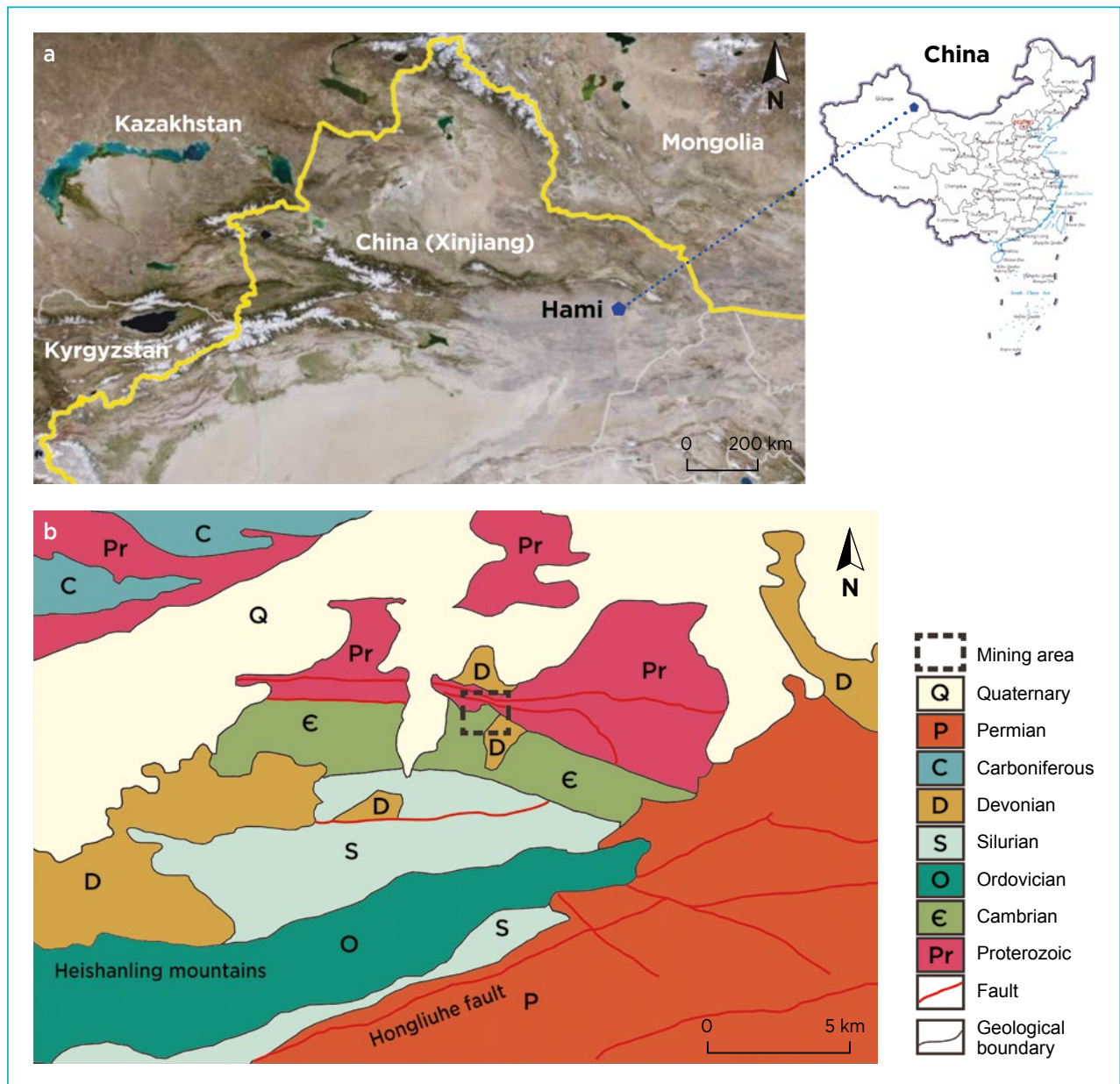


**Figure 2:** (a) Turquoise from Xinjiang, China, is found near the city of Hami (Gaode satellite image from <https://www.amap.com>). (b) A simplified geological map of the Heishanling region (modified from Chen *et al.* 2011) shows the context of the turquoise-mineralised area, which is situated along the contact between Proterozoic and Cambrian rocks.

schist, etc. (Zhang *et al.* 1990). The mineralised zone is 2.5 km long from east to west and ranges from 5 to 40 m wide (Ren 1985). The turquoise formed in an oxidation zone related to a fracture zone associated with the core of a fold structure.

## MATERIALS AND METHODS

The Xinjiang turquoise specimens used for this study (Figure 3) consisted of seven rough samples (W1–W7) and ten polished slabs of various colours and textures (T1–T10). They ranged from light blue to green or

brownish to yellowish green, except for one sample (T10) that was brownish yellow. One brownish yellow turquoise sample from Hubei Province (THB1) was also included for comparison with T10.

Standard gemmological testing of all ten polished samples was carried out at the Gemmological Institute, China University of Geosciences, Wuhan. Refractive indices were measured with an Abbe refractometer, SG was measured by the hydrostatic method, and UV fluorescence was checked with 4W long- and short-wave UV lamps. Microscopy was performed with a Leica M205 A stereo microscope. Four of the rough samples



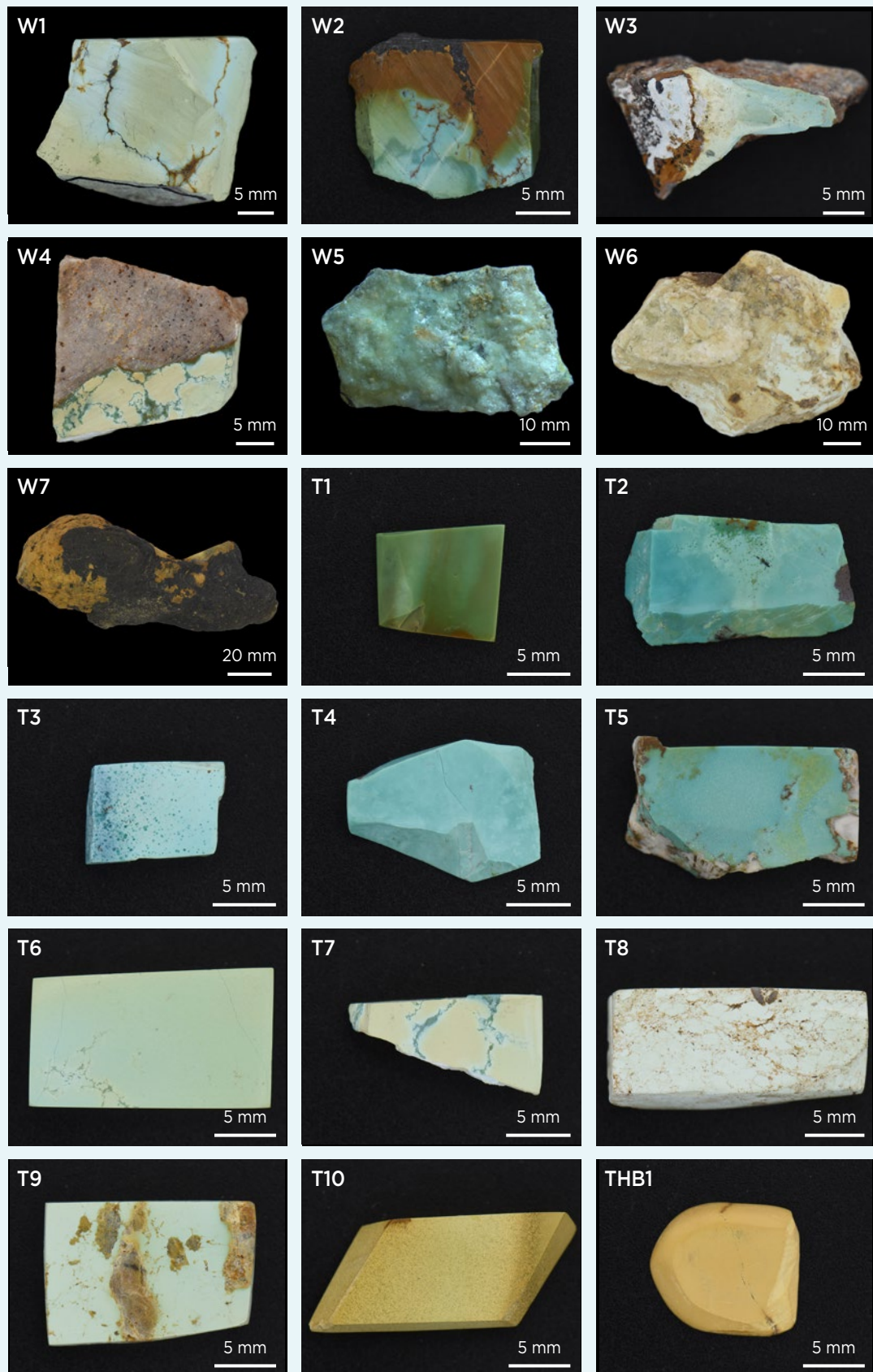


**Figure 3:** The turquoise study samples consist of 17 pieces from Xinjiang (W1-W7 and T1-T10) and, for comparison, one from Hubei (THB1). Photos by Yanhan Wu.

(W1–W4) were selected for slicing in various directions and ground into thin sections (0.03 mm thick) for examination with a petrographic microscope.

To identify the mineral phases present, all of the turquoise specimens were analysed by powder X-ray diffraction (XRD) using a Bruker AXS D8 Focus instrument equipped with a collimator (0.1 mm in diameter) and a Ni filter at the Faculty of Materials Science and Chemistry Institute, China University of Geosciences, Wuhan. The analyses employed  $\text{CuK}\alpha_1$  radiation ( $\lambda = 1.540598 \text{ \AA}$ ) using a voltage of 40 kV, a current of 40 mA, a scanning step of  $0.01^\circ$  and a scan speed of 0.05 s. The XRD data were analysed by MDI Jade 5.0 software and compared with the International Centre for Diffraction Data's PDF-2 database.

The microstructural characteristics of three polished specimens (T4, T6 and T8) were observed with a Thermo Fisher Scientific Apreo S environmental scanning electron microscope (SEM) at the State Key Laboratory of Geological Processes and Mineral Resources, China University of Geosciences, Wuhan. The SEM was operated with an acceleration voltage of 20 kV and a working distance of 10.0 mm.

Major-element analyses of all ten polished samples were carried out with a JEOL JXA-8230 electron probe micro-analyser (EPMA) at Wuhan Sample Solution Analytical Technology Co. Ltd., using an accelerating voltage of 15 kV, a beam current of 10 nA and a spot size of 10  $\mu\text{m}$ . The specimens were carbon coated (20 nm thickness), and the data were processed by ZAF correction. The standards used were jadeite (Na), diopside (Ca and Mg), chromite (Al), olivine (Si), sanidine (K), ferrosferic oxide (Fe), apatite (P), titanium (Ti), johannsenite (Mn), chalcopyrite (Cu), zinc (Zn), topaz (F) and strontium sulphate (S).

Trace-element concentrations were measured on seven polished slabs (T1, T2, T3, T6, T7, T9 and T10) with an Agilent 7700e laser ablation inductively coupled plasma mass spectrometer (LA-ICP-MS) at Wuhan Sample Solution Analytical Technology Co. Ltd. The operating conditions for the LA-ICP-MS instrumentation and data reduction are the same as described by Zong *et al.* (2017).

Laser Raman spectroscopy in the range 100–3700  $\text{cm}^{-1}$  was performed on all ten polished samples with a Bruker Optics Senterra R200 L instrument at the Gemmological Institute, China University of Geosciences, Wuhan. The analyses employed a 532 nm laser, an aperture of 50  $\mu\text{m}$  and a spectral resolution of 3–5  $\text{cm}^{-1}$ . The laser power was 20 mW, and 20 scans were accumulated with a 10 s integration time for each scan.

Fourier-transform infrared (FTIR) spectra were

collected from portions of all ten polished samples in the 400–4000  $\text{cm}^{-1}$  range with a Bruker Vertex 80 infrared spectrometer at the Gemmological Institute, China University of Geosciences, Wuhan. A small amount of specimen powder was mixed with KBr powder in the proportion 1:150 and pressed into pellets. Spectra were acquired from 32 scans using a resolution of 4  $\text{cm}^{-1}$ .

Ultraviolet-visible (UV-Vis) spectroscopy was performed on four polished samples (T3, T6, T7 and T10) at the Gemmological Institute, China University of Geosciences, Wuhan. We used a Lambda 650S spectrophotometer equipped with an integrating sphere attachment and a standard D65 light source. Reflectance spectra were measured from 380 to 780 nm at an interval of 1 nm. The observation angle was  $10^\circ$  and the bandwidth was 2 nm. A standard  $\text{BaSO}_4$  white board was used as the test background.

## RESULTS

### Gemmological Properties

The gemmological properties of the polished specimens are listed in Table I. The samples mostly ranged from blue to green or brownish to yellowish green (with one brownish yellow sample), and displayed light tone and very pale to moderate saturation. They had a waxy to glassy (vitreous) lustre. All samples were inert to long-

**Table I:** Gemmological properties of the polished Xinjiang turquoise specimens.

No.	Colour	Lustre	RI	SG
T1	Brownish yellow and green	Vitreous	1.62	2.76
T2	Bluish green with local dark green spots	Vitreous	1.62	2.90 <sup>a</sup>
T3	Light blue with darker blue spots	Vitreous	1.61	2.59
T4	Light greenish blue	Vitreous	1.62	2.74
T5	Bluish green	Vitreous	1.62	2.74 <sup>b</sup>
T6	Light green	Vitreous	1.61	2.30
T7	Yellowish green	Waxy	— <sup>c</sup>	2.27
T8	Very pale blue	Waxy	—	2.16 <sup>a</sup>
T9	Yellowish green	Waxy	—	2.36 <sup>b</sup>
T10	Brownish yellow	Vitreous	1.61	1.89

<sup>a</sup> Contains iron minerals.

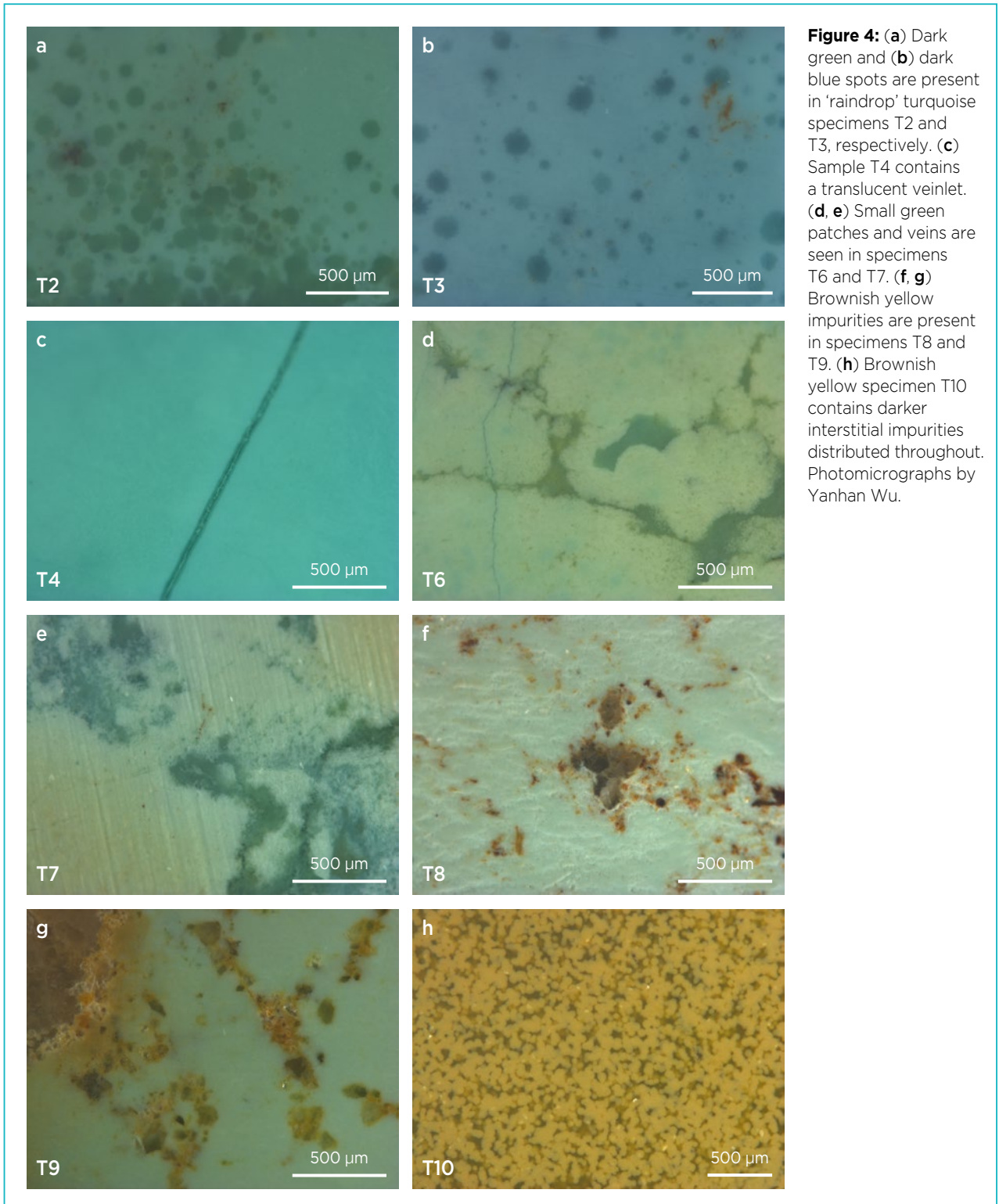
<sup>b</sup> Includes some matrix rock.

<sup>c</sup> The symbol — means the value could not be measured.

wave (365 nm) and short-wave (254 nm) UV radiation.

Specimens T2 and T3 contained areas showing many blue or green spots that were round or near-round when viewed with the microscope (Figure 4a, b), similar to ‘raindrop’ turquoise from Hubei Province (Liu *et al.* 2020). A translucent veinlet was present in specimen T4 (Figure 4c), and veined areas formed by darker green

patches were present in T6 and T7 (Figure 4d, e). Both the raindrops and veins appeared darker and more translucent than the surrounding turquoise. Specimens T8 and T9 contained brownish yellow impurities (Figure 4f, g). Specimen T10 contained interstitial dark brownish yellow areas distributed more-or-less evenly throughout (Figure 4h).



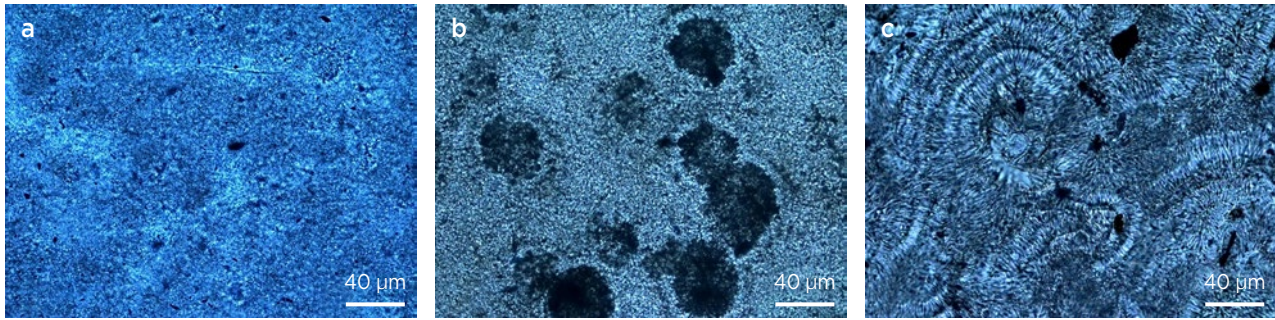


**Figure 5:** Examination of thin sections of Xinjiang turquoise with plane-polarised light shows (a) a micro-crystalline aggregate with a scaly crystallite structure in sample W1, (b) a small number of nodular crystallites in sample W2 and (c) irregular radial granular structures in sample W3. Photomicrographs by Min Cao.

Observations of the thin sections (cut from samples W1–W4) with the petrographic microscope revealed that the turquoise consists mainly of micro-crystalline aggregates, mostly with a scaly crystallite structure (Figure 5a). Locally present were a small number of nodular crystallites (Figure 5b) and irregular radial spherical granular structures (Figure 5c). With cross-polarised light, the highest interference colour seen was low-order grey.

The surrounding rock hosting the turquoise consisted mostly of siliceous slate containing abundant quartz, which formed a sharp contact with the adjacent turquoise (Figure 6a, b). Mica could be seen adjacent to turquoise in one specimen (Figure 6c).

### Associated Minerals

XRD analysis confirmed turquoise as the main phase and identified various associated minerals, including light blue woodhouseite (specimens W3 and T3) and dawsonite (W3), light green calcite and alunite (W5), and white gypsum (W6) and quartz (T3, T6, T7 and T10). Woodhouseite belongs to the alunite group and has the chemical formula  $\text{CaAl}_3(\text{PO}_4)(\text{SO}_4)(\text{OH})_6$ ; the interplanar spacings obtained from the XRD pattern were 5.68, 3.40 and 2.93 Å. Quartz had diffraction peaks

with interplanar spacings of 3.35 Å belonging to the (101) plane, which differs from those of turquoise, with interplanar spacings of 3.44 and 3.27 Å.

### Microstructure

SEM imaging showed that the turquoise crystallites in specimen T4 (SG = 2.74) were closely packed in an imbricate arrangement, with little porosity, dense structure and almost no crystal shape (Figure 7a). The turquoise crystallites in specimen T6 (SG = 2.30) were arranged somewhat closely, in granular and lumpy shapes of variable sizes (Figure 7b). Although their crystal shape was not well defined, a few columnar crystals could be seen. Specimen T8 (SG = 2.16) was less compact, with long, columnar microcrystals (approximately 0.5–5.0 µm) with obvious edges that were randomly oriented (Figure 7c). The microcrystals were not closely connected and the aggregates displayed considerable porosity. In general, the more regular and compact the microcrystals, the higher the density of the turquoise.

### Chemical Composition

Chemical analyses of the turquoise samples by EPMA and LA-ICP-MS are shown in Tables II and III, respectively.

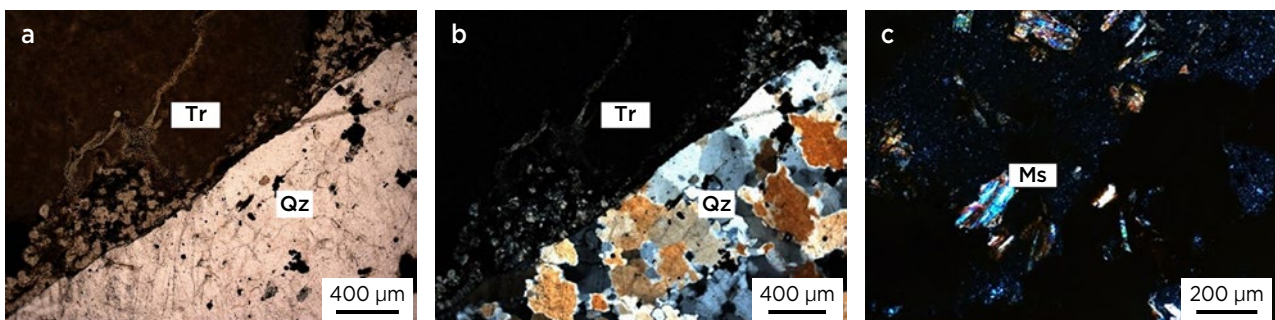


**Figure 6:** Examination of a thin section of Xinjiang turquoise (here, sample W4) with (a) plane-polarised light and (b) cross-polarised light shows a sharp contact between the turquoise and the siliceous host rock. (c) The presence of mica is revealed by its bright interference colours, as seen with cross-polarised light in a thin section of turquoise specimen W-1. Abbreviations: Ms = muscovite, Qz = quartz and Tr = turquoise. Photomicrographs by Min Cao.

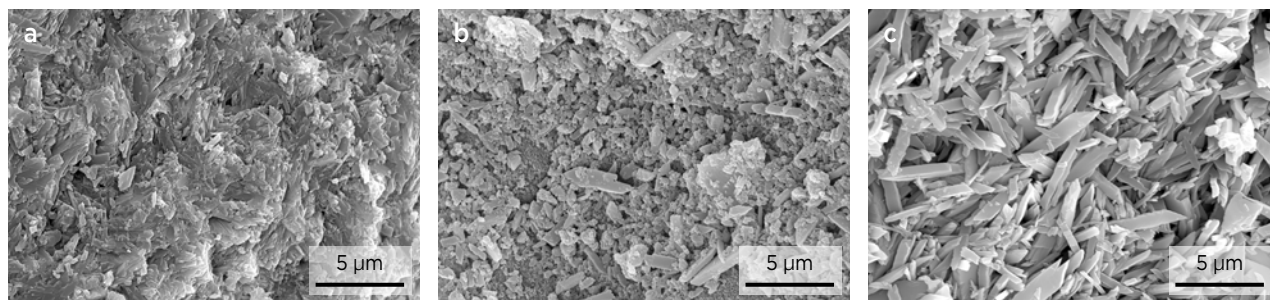


**Figure 7:** SEM imaging reveals the microstructural characteristics of three samples of Xinjiang turquoise. (a) The turquoise crystallites in specimen T4 are closely packed in an imbricate arrangement. (b) Although the shape of most of the crystallites in sample T6 is not well developed, some columnar crystals are present. (c) Long, columnar microcrystals (0.5–5.0 μm) with sharp edges form a less-compact aggregate in specimen T8.

The major-element content determined by EPMA was fairly typical for turquoise for all specimens (except T10; see below). The contents of P<sub>2</sub>O<sub>5</sub> and Al<sub>2</sub>O<sub>3</sub> were 31.85–35.31 wt. % and 31.67–38.39 wt. %, respectively. However, CuO concentrations (6.32–7.74 wt. %) were lower than

the theoretical value (9.78 wt. %). The contents of Fe, Ca and Si were relatively high in some specimens.

The main constituents of the brownish yellow specimen T10—21.61 wt. % P<sub>2</sub>O<sub>5</sub>, 31.20 wt. % Al<sub>2</sub>O<sub>3</sub> and 3.97 wt. % CuO—were lower than the theoretical values.

**Table II:** Average chemical composition of Xinjiang turquoise specimens, measured by EPMA.<sup>a</sup>

Oxides (wt.%)	Ideal (Čejka et al. 2015)	T1	T2		T3		T4		T5	T6	T7		T8	T9	T10	THB1 (Hubei)
			Turquoise substrate	Rain-drop	Turquoise substrate	Rain-drop	Turquoise substrate	Vein			Turquoise substrate	Vein				
SiO <sub>2</sub>	—	1.99	0.50	0.74	0.96	0.17	0.41	0.01	0.10	1.25	3.35	nd	0.19	0.09	10.56	4.67
TiO <sub>2</sub>	—	0.04	0.01	nd	0.01	0.01	0.03	0.03	nd	0.01	0.09	0.08	0.02	0.01	0.02	0.04
Al <sub>2</sub> O <sub>3</sub>	37.60	36.32	35.74	32.50	38.39	31.36	34.92	0.22	33.76	34.95	35.46	10.61	36.90	31.67	31.20	27.98
MgO	—	0.02	0.01	0.04	0.02	nd	0.02	0.10	0.02	0.28	0.31	0.04	0.03	0.01	0.24	0.11
CaO	—	0.25	0.19	4.24	0.29	8.10	0.24	48.83	0.07	3.65	1.18	35.23	0.30	0.12	7.78	0.38
MnO	—	0.02	nd	0.02	nd	0.01	0.01	0.02	0.01	0.01	0.02	nd	0.01	nd	nd	0.01
FeO <sub>tot</sub> <sup>b</sup>	—	1.69	1.67	2.19	0.78	0.65	2.04	0.24	3.08	1.70	2.11	1.28	2.72	7.63	4.28	9.64
CuO	9.78	6.42	7.34	7.35	7.59	6.25	7.16	0.71	7.38	6.32	7.74	2.31	7.25	6.47	3.97	7.02
ZnO	—	0.31	0.27	0.02	0.14	0.01	0.14	nd	0.06	0.19	0.11	nd	0.31	0.19	0.13	0.20
Na <sub>2</sub> O	—	0.19	0.15	0.27	0.16	0.25	0.36	0.92	0.13	0.17	0.46	0.75	0.08	0.08	0.18	0.04
K <sub>2</sub> O	—	0.06	0.04	0.08	0.07	0.09	0.09	0.05	0.09	0.06	0.13	nd	0.11	0.08	0.08	0.06
P <sub>2</sub> O <sub>5</sub>	34.90	33.44	34.14	34.03	35.31	34.05	34.25	32.28	34.71	33.28	31.85	34.53	34.81	34.78	21.61	30.40
F	—	nd	nd	0.16	0.04	0.64	nd	2.89	0.01	nd	0.01	2.71	nd	nd	nd	nd
SO <sub>3</sub>	—	0.15	0.18	0.44	0.27	0.80	0.35	2.67	0.31	0.29	0.44	2.42	0.52	0.38	0.21	0.29
Total <sup>c</sup>	82.18	80.90	80.24	82.08	84.03	82.39	80.02	88.97	79.73	82.16	83.26	89.96	83.28	81.51	80.26	80.84
FeO <sub>tot</sub> /CuO	—	0.26	0.23	0.30	0.10	0.10	0.29	0.34	0.42	0.27	0.27	0.55	0.38	1.18	1.08	1.38

<sup>a</sup> Average of 2 point analyses. Abbreviation: nd = not detected.

<sup>b</sup> Includes FeO and Fe<sub>2</sub>O<sub>3</sub>.

<sup>c</sup> Does not include H<sub>2</sub>O; the theoretical value of H<sub>2</sub>O in turquoise is 17.72 wt. %.

**Table III:** Trace-element concentrations (in ppm) of turquoise from Xinjiang and elsewhere in China, measured by LA-ICP-MS.<sup>a</sup>

Sample (and spot no.)	Li	V	Cr	Co	Ni <sup>b</sup>	Ga	Sr	Mo	Ba	U
T1-1	716.5	656.9	2486	5.420	9.253	454.2	291.1	39.98	109.9	50.48
T1-2	727.4	750.1	2552	6.231	19.37	423.1	329.0	37.57	102.8	49.19
T2-1	433.0	452.9	2664	0.652	1.526	22.44	227.6	11.82	215.8	70.04
T2-2	462.7	590.2	2600	0.769	nd	19.92	188.2	15.54	228.5	47.44
T3-1	163.4	489.5	1983	0.609	nd	11.03	31530	26.23	732.0	82.55
T3-2	228.1	525.8	1981	1.016	1.685	11.21	7833	14.28	526.7	95.89
T6-1	474.6	401.7	4101	1.909	2.306	771.3	247.7	64.80	403.2	21.24
T6-2	467.4	384.5	4010	2.181	12.37	326.6	342.3	64.17	411.1	21.70
T7-1	590.3	348.5	4529	3.774	10.13	140.4	214.8	62.60	406.1	18.22
T7-2	578.4	336.3	4291	4.322	14.20	126.8	1710	66.54	416.2	20.26
T9-1	0.825	753.1	2531	2.541	nd	535.3	88.86	28.66	254.6	28.49
T9-2	1.526	755.2	2573	3.672	3.620	508.7	93.81	29.57	240.4	26.79
T10-1	4.551	413.2	2370	6.945	6.305	209.1	62.35	32.57	100.4	17.48
T10-2	6.604	374.5	2238	8.355	10.45	210.5	59.77	29.86	87.91	15.63
Average	346.8	516.6	2922	3.457	6.515	269.3	3087	37.44	302.5	40.39
Bijiashan, Anhui	—	31.30	—	77.20	0.83	—	—	—	—	0.47
Ma'anshan, Anhui	0.139	25.24	5.927	27.83	0.857	10.37	3.431	0.018	—	0.984
Yun, Hubei	2.37	—	—	6.37	—	5.37	—	66.97	1279	66.36
Zhushan, Hubei	0.115	310.5	325.9	1.313	0.768	19.48	19.25	147.2	1598	67.27
Ankang, Shaanxi	22.48	—	—	3.976	—	3.728	13.95	27.50	770.6	8.084
Luonan, Shaanxi	13.45	—	—	3.20	—	16.78	175.8	2.35	1112	2.16

<sup>a</sup> Sources of data for turquoise from Anhui, Hubei and Shaanxi provinces: He *et al.* 2011 (Ma'anshan and Zhushan); Luo 2017 (Luonan and Yun); Liu *et al.* 2018 (Ankang); Shen & Zhao 2019 (Bijiashan). The symbol — means not reported.

<sup>b</sup> The detection limit for Ni ranged from 1.80 to 2.86 ppm.

The contents of FeO<sub>tot</sub> (4.28 wt. %), CaO (7.78 wt. %) and SiO<sub>2</sub> (10.56 wt. %) were significantly higher than the theoretical values, and SiO<sub>2</sub> was also much higher than for other turquoise specimens.

In the raindrop turquoise (specimens T2 and T3; see Figure 4a, b), the composition of the turquoise substrate was significantly different from that of the dark spots. The contents of P<sub>2</sub>O<sub>5</sub>, Al<sub>2</sub>O<sub>3</sub> and CuO in the turquoise substrate were close to the ideal values, indicating that specimens T2 and T3 were relatively pure turquoise. However, elevated amounts of CaO were measured in the dark spots in both samples (4.24 and 8.10 wt. %); these values are much higher than those in the turquoise substrate (0.19 and 0.29 wt. %), indicating the presence of a Ca-containing phase in the raindrops.

Compositional differences were also found between the turquoise and veins in specimens T4 and T7 (Figure 4c, e), with the veins containing much lower Al<sub>2</sub>O<sub>3</sub> and CuO, and significantly more CaO. Again, this suggests the presence of a Ca-containing phase in the veins. In addition, the turquoise substrate in T7 contained anomalously high SiO<sub>2</sub> (3.35 wt. %).

As seen in Table II, the EPMA analyses showing enriched Ca also have elevated F and SO<sub>3</sub> values (i.e. in the raindrops or veins of samples T2, T3, T4 and T7).

Differences in the colouration of Xinjiang specimens were compared with variations in their Fe and Cu contents. The more yellow the hue of the turquoise, the greater the FeO<sub>tot</sub> content (which increased from 0.78 to 7.63 wt. %; Table II), and also the greater the FeO<sub>tot</sub>/CuO

ratio (0.10–1.18). Thus, we suggest that the colouration of Xinjiang turquoise is closely related to Fe and Cu content.

Regarding the trace-element analyses obtained by LA-ICP-MS, the compositions of our Xinjiang samples were somewhat different than those of turquoise from elsewhere in China (Table III). Overall, our Xinjiang samples contained higher Sr and Cr, somewhat higher V, and lower Ba. The Li contents of samples T9 and T10 (0.825–6.604 ppm) were similar to those of turquoise from elsewhere in China, while the other Xinjiang specimens contained much higher Li values (163.4–727.4 ppm).

### Raman and FTIR Spectroscopy

The Raman spectra of the Xinjiang turquoise specimens were basically consistent with that of typical turquoise. The strongest peak, near  $1040\text{ cm}^{-1}$ , belongs to the stretching vibration of  $\nu_3(\text{PO}_4^{3-})$ , while the next-strongest peak, near  $3472\text{ cm}^{-1}$ , is generated by the stretching vibration of  $\nu(\text{OH})$  (Figure 8a; Čejka *et al.* 2015). Additional peaks (visible, but not labelled, in Figure 8a) also occurred near  $647$ ,  $595$ ,  $552$ ,  $477$  and  $424\text{ cm}^{-1}$ , and weak peaks were present at  $3294$  and  $3094\text{ cm}^{-1}$ .

In addition to the Raman features of typical turquoise, one or two weak peaks were present at  $987$ – $1004\text{ cm}^{-1}$

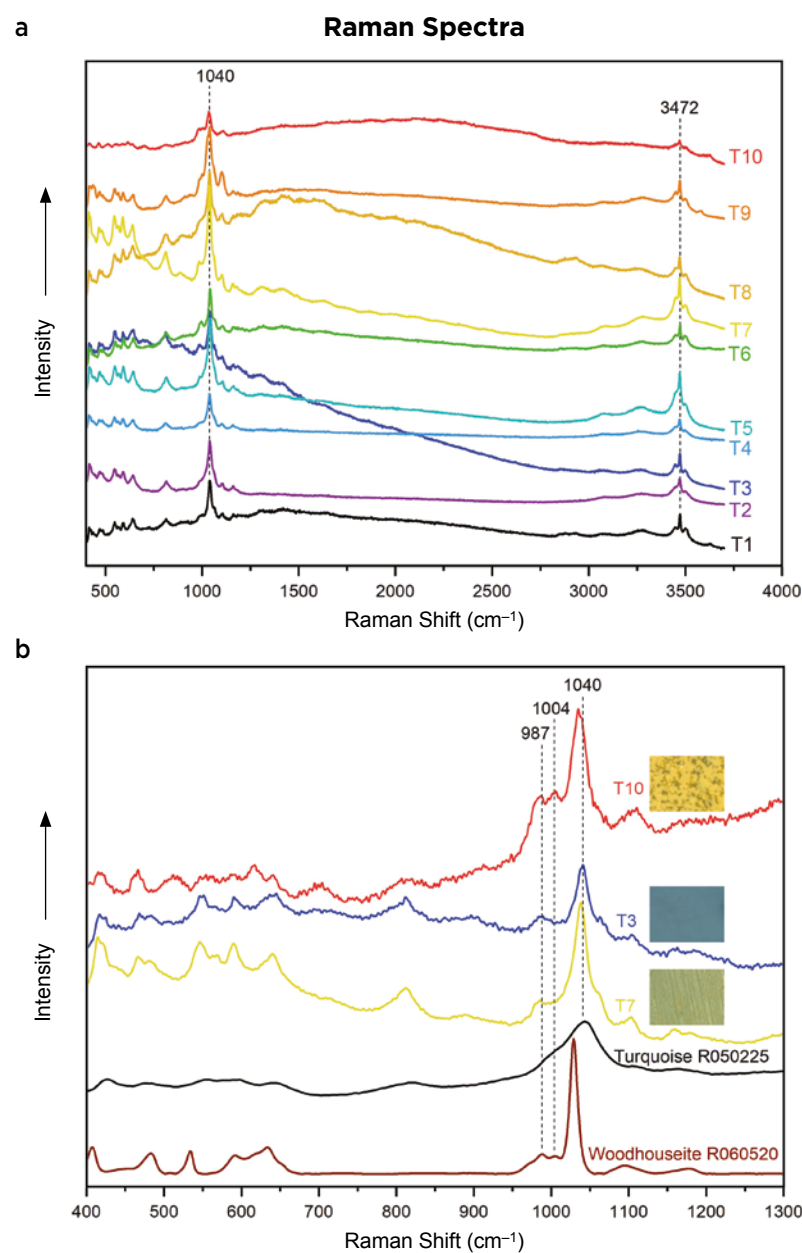


**Figure 8:** (a) Raman spectra of our Xinjiang specimens are generally consistent with the peaks seen in typical turquoise. (b) Additional small peaks at  $987$ – $1004\text{ cm}^{-1}$  belonging to woodhouseite are present in the Raman spectra of specimens T3, T7 and T10. (The main woodhouseite peak at  $1029\text{ cm}^{-1}$  is obscured by the dominant peak for turquoise at  $1040\text{ cm}^{-1}$ .) Reference spectra for turquoise (<https://rruff.info/R050225>) and woodhouseite (<https://rruff.info/R060520>) are provided for comparison. The spectra are offset vertically for clarity.

in, for example, specimens T3, T7 and 10 (Figure 8b). These peaks are consistent with those of woodhouseite, and given the growth environment of turquoise—and the XRD results for our samples—we conclude that some of them contain a small amount of woodhouseite.

Raman analyses were obtained for the dark spots in the raindrop turquoise (T2 and T3) and the veins in specimens T4 and T7 (Figure 9). In T7, the 1040  $\text{cm}^{-1}$  peak was present in the Raman spectrum of the vein material, but it was no longer the strongest peak. Instead, the most intense peak was at 966  $\text{cm}^{-1}$ , which is characteristic of fluorapatite. We therefore identified the vein material as a mixture of turquoise and fluorapatite. A similar Raman peak at 966  $\text{cm}^{-1}$  was present in the Raman spectra of the vein cutting T4 and in the spectra of the dark spots in specimens T2 and T3, indicating that they likewise contained fluorapatite. The content of fluorapatite varied, as shown by differences in the intensity of the 966  $\text{cm}^{-1}$  peak. Overall, we consider fluorapatite to be the main impurity in the raindrops and veins.

The FTIR spectra of our Xinjiang turquoise samples were basically similar regardless of the colour and texture variations shown by the samples, except that the intensities of the bands shifted slightly (Figure 10). Five groups of characteristic bands were observed in the ‘fingerprint’ area of the spectra (1300–400  $\text{cm}^{-1}$ ; Reddy *et al.* 2006; Čejka *et al.* 2015): (1) at 1200–1000  $\text{cm}^{-1}$ , assigned to

the asymmetric stretching vibration of  $\nu_3(\text{PO}_4^{3-})$ ; (2) at 905  $\text{cm}^{-1}$ , related to the symmetric stretching vibration of  $\nu_1(\text{PO}_4^{3-})$ ; (3) at 780  $\text{cm}^{-1}$ , due to the bending vibration of  $\nu(\text{OH})$ ; (4) at 650–480  $\text{cm}^{-1}$ , from the asymmetric bending vibration of  $\nu_4(\text{PO}_4^{3-})$ ; and (5) at 432  $\text{cm}^{-1}$ , assigned to the symmetric bending vibration of  $\nu_2(\text{PO}_4^{3-})$ .

In addition, three groups of characteristic peaks were present in the ‘functional group’ area of the spectra (4000–1300  $\text{cm}^{-1}$ ; Reddy *et al.* 2006; Chen *et al.* 2012; Čejka *et al.* 2015): (1) at about 3509 and 3465  $\text{cm}^{-1}$ , due to the stretching vibration of  $\nu(\text{OH})$ ; (2) at about 3286 and 3074  $\text{cm}^{-1}$ , assigned to the stretching vibration of  $\nu(\text{H}_2\text{O})$ ; and (3) at about 1637  $\text{cm}^{-1}$ , related to the bending vibration of  $\nu(\text{H}_2\text{O})$ .

The shapes and band positions recorded in the infrared spectra of our Xinjiang turquoise specimens were roughly the same as those of typical turquoise, including samples from Hubei (Zeng *et al.* 2019), Anhui (Chen & Qi 2007) and Shaanxi (Shi & Cai 2008) provinces.

### UV-Vis Spectroscopy

In the visible range, the reflectance spectra of the various-coloured Xinjiang turquoise samples had somewhat similar shapes, formed essentially by two main regions of absorption: one between 380 and 500 nm and the other above 580 nm (Figure 11). However, the positions of the peaks varied somewhat according to the

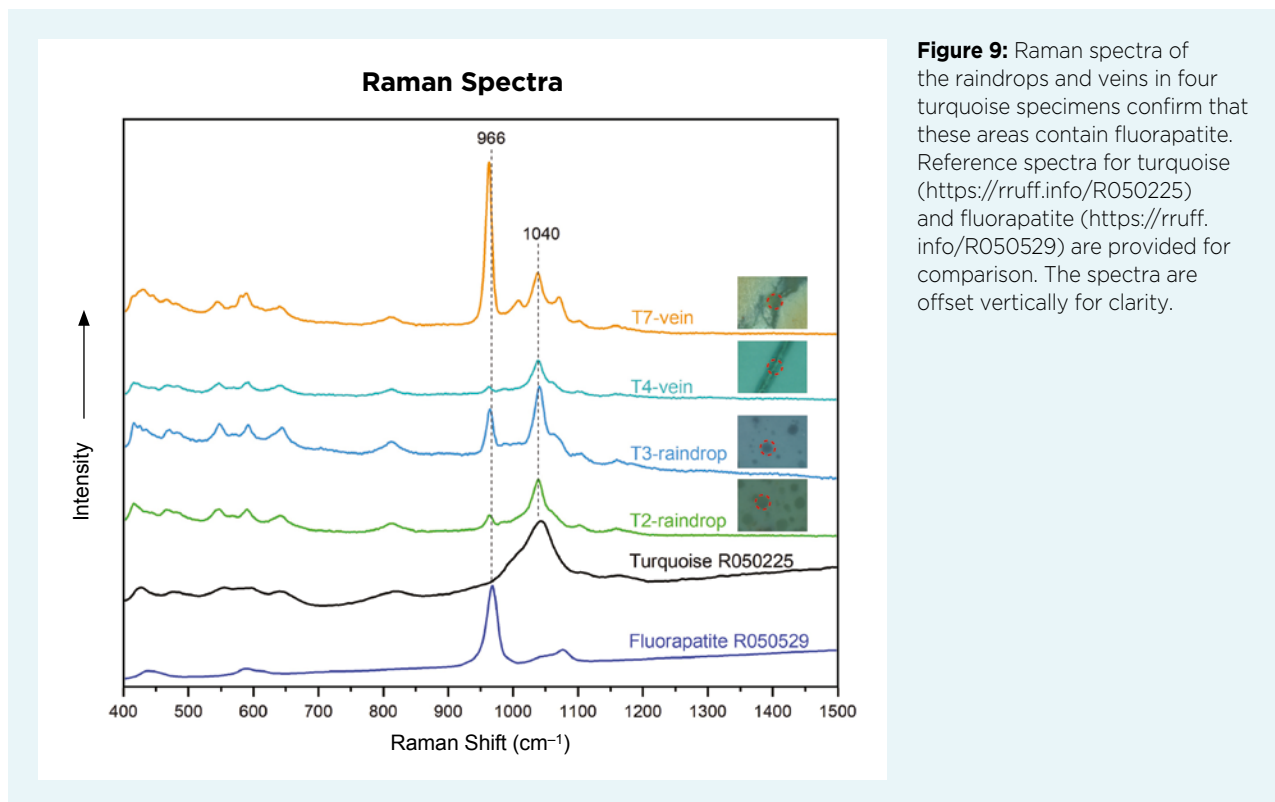


**Figure 9:** Raman spectra of the raindrops and veins in four turquoise specimens confirm that these areas contain fluorapatite. Reference spectra for turquoise (<https://rruff.info/R050225>) and fluorapatite (<https://rruff.info/R050529>) are provided for comparison. The spectra are offset vertically for clarity.



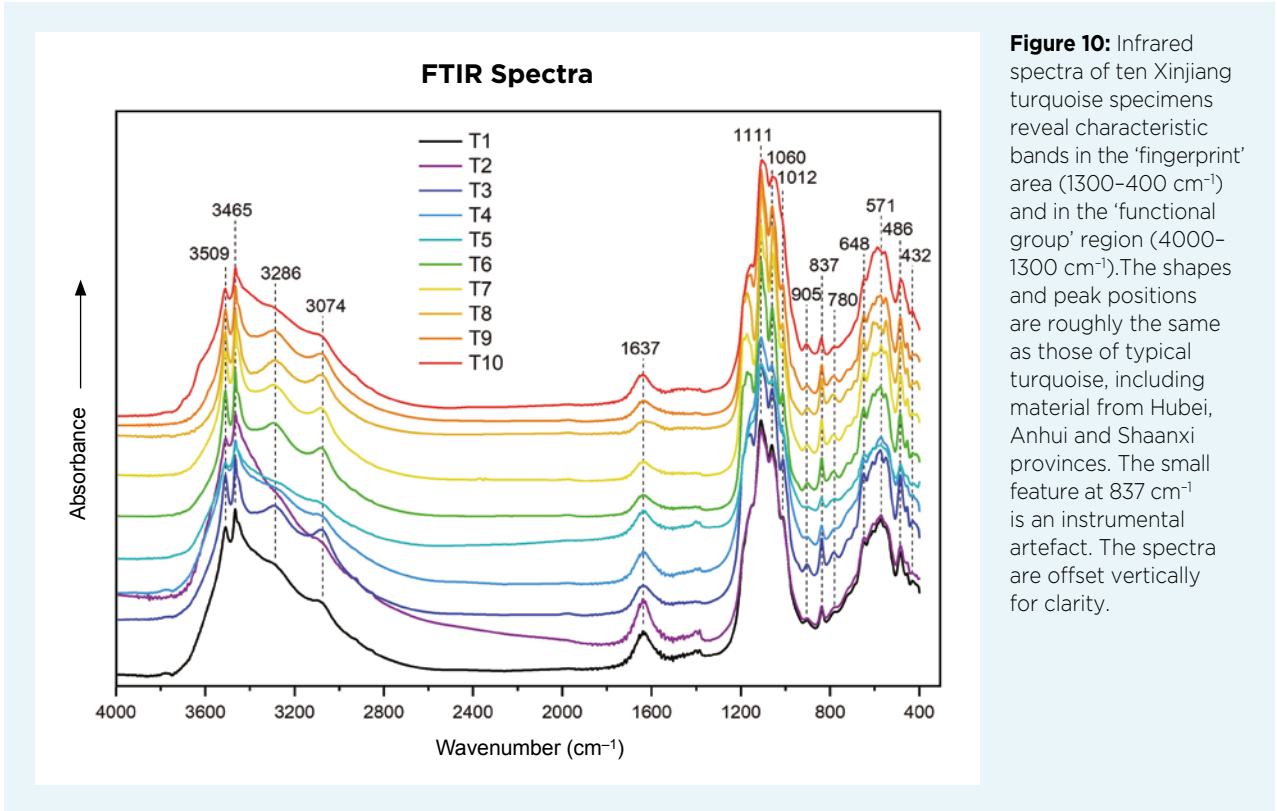


**Figure 10:** Infrared spectra of ten Xinjiang turquoise specimens reveal characteristic bands in the ‘fingerprint’ area (1300–400  $\text{cm}^{-1}$ ) and in the ‘functional group’ region (4000–1300  $\text{cm}^{-1}$ ). The shapes and peak positions are roughly the same as those of typical turquoise, including material from Hubei, Anhui and Shaanxi provinces. The small feature at 837  $\text{cm}^{-1}$  is an instrumental artefact. The spectra are offset vertically for clarity.

different colours of the samples, as would be expected. For blue turquoise, the relative absorption intensity was strongest in the red region, with no obvious absorption

peak in the blue range and a weak, broad absorption in the violet region at around 415 nm. For the brownish yellow turquoise, the absorption intensity was strongest

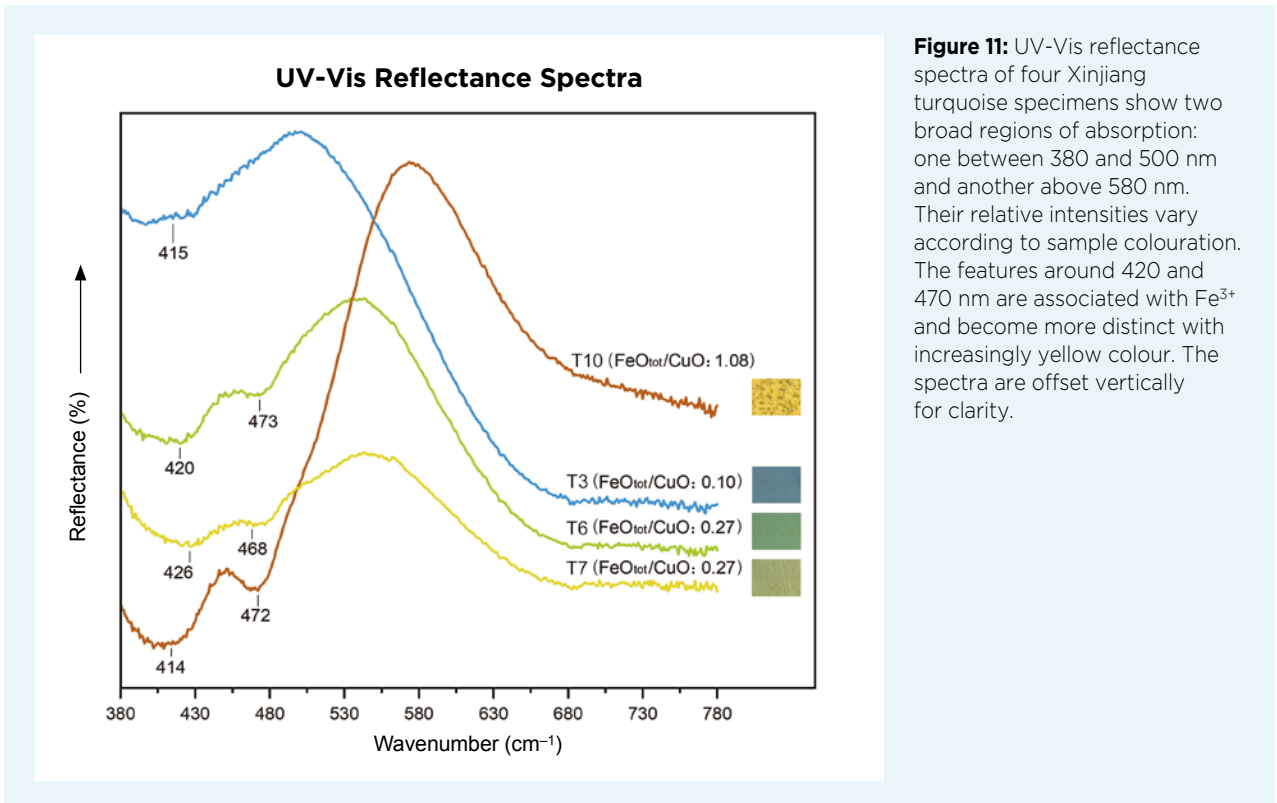


**Figure 11:** UV-Vis reflectance spectra of four Xinjiang turquoise specimens show two broad regions of absorption: one between 380 and 500 nm and another above 580 nm. Their relative intensities vary according to sample colouration. The features around 420 and 470 nm are associated with  $\text{Fe}^{3+}$  and become more distinct with increasingly yellow colour. The spectra are offset vertically for clarity.

in the violet-to-blue range, while absorption in the red region was weak, consistent with the sample's colour. Absorption peaks around 420 and 470 nm in turquoise have been associated with  $\text{Fe}^{3+}$  instead of  $\text{Al}^{3+}$  (Wang & Guo 2021), and these became more distinct with an increase in the yellow hue of our specimens. The broad absorption centred around 683 nm belongs to the crystal-field band of  $\text{Cu}^{2+}$  (Zhang *et al.* 1982).

## DISCUSSION

### Silica Content

Some of our Xinjiang turquoise samples contained significant amounts of Si. The contents of  $\text{SiO}_2$  in samples T1 and T3 averaged 1.99 and 0.96 wt.%, respectively, while light green specimen T6 contained 1.25 wt.%  $\text{SiO}_2$  and yellowish green sample T7 had 3.35 wt.%  $\text{SiO}_2$ . The  $\text{SiO}_2$  content of brownish yellow specimen T10 averaged 10.56 wt.%, with a maximum value of 11.81 wt.%.

In general, brownish yellow turquoise is weathered and shows porous texture, so it displays poor lustre and is difficult to polish. However, specimen T10 displayed glassy lustre. It also contained the highest  $\text{SiO}_2$  recorded in this study, and the inferred relatively high quartz content is evident in T10's higher hardness, thus improving its lustre. By comparison, brownish yellow sample THB1 from Hubei contained much less  $\text{SiO}_2$  (4.67 wt.%), and it was softer and showed a lower lustre. We performed a scratch test on each sample using a piece of fluorite (Mohs hardness = 4), and as expected it was easier to scratch THB1 than T10 (Figure 12). In addition, XRD analysis of T10 confirmed that its  $\text{SiO}_2$  content was due to the presence of quartz (peak at 3.35 Å). Thus, quartz crystallites in turquoise can improve its hardness, as well as its lustre.

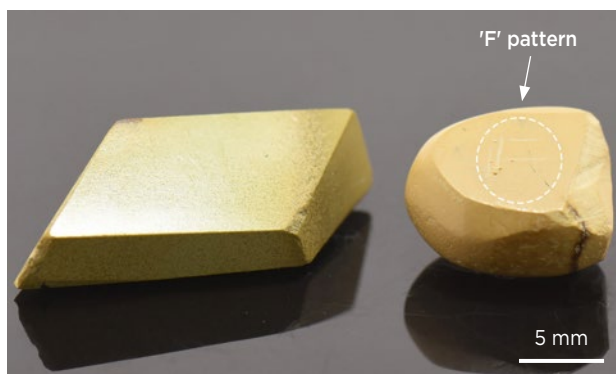


**Figure 12:** Brownish yellow turquoise from Xinjiang (left, sample T10) and Hubei (right, specimen THB1) are shown for comparison. Scratch testing with a piece of fluorite was successful at inscribing the letter 'F' on the Hubei sample, but not on the harder Xinjiang sample. Photo by Yanhan Wu.

### Turquoise Formation and Impurity Content

A typical turquoise deposit begins with the deposition of copper sulphides, which takes place when hydrothermal fluids leach copper from the surrounding rock, typically associated with the intrusion of a calc-alkaline magma with moderate to high silica content that is relatively oxidised. The Cu is redeposited in more concentrated form as a porphyry copper deposit, in which veins of copper sulphide fill joints and fractures in the rock. Copper deposition takes place mostly in the potassic alteration zone, which is characterised by conversion of existing feldspar to K-feldspar, together with the deposition of quartz and micas, at around 400–600°C (Watanabe *et al.* 2018).

Turquoise is a secondary or supergene mineral (Anthony *et al.* 2001) that forms when meteoric water (e.g. rain or snowmelt) circulates through the porphyry Cu deposit. Dissolved oxygen in the water oxidises the copper sulphides to soluble sulphates, and the acidic, copper-laden solution then reacts with Al- and K-bearing minerals in the host rock to precipitate turquoise (King 2002). The turquoise typically forms veins that are hosted by volcanic rock or phosphate-rich sediments. Deposition usually takes place at a relatively low temperature (90–195°C) and seems to occur more readily in arid environments (King 2002).

In addition to turquoise, a small amount of woodhouseite was found in the Xinjiang turquoise specimens. Woodhouseite can form during weathering of phosphorus and sulphur-bearing strata (Qi *et al.* 1998). A large iron-ore deposit is known near Hami, and is accompanied by chalcopyrite, sphalerite and other sulphides (Mi *et al.* 2014). When a sulphur-containing Fe deposit exists in the vicinity of turquoise, the sulphur can oxidise to form  $\text{SO}_3$  (Shi & Cai 2007). After hydration, water that contains  $\text{SO}_4^{2-}$  can then penetrate into the turquoise deposit where  $\text{PO}_4^{3-}$  is metasomatised by  $\text{SO}_4^{2-}$  to form woodhouseite. A previous study described several examples of woodhouseite associated with turquoise from Zhushan County, Hubei Province (Shi & Cai 2008). The light blue colour of the woodhouseite is reportedly due to small amounts of Cu (Shi 2008).

The 'raindrop' variety of turquoise is very rare and has been reported only from Hubei Province. The current article provides the first report of a new source of raindrop turquoise in Xinjiang (Figure 13). The EPMA chemical data (showing enriched Ca, F and S) and Raman spectroscopy (peak at 966  $\text{cm}^{-1}$ ) confirmed the presence of fluorapatite in the dark spots in specimens T2 and T3 (Figure 4a, b), and in the veins in specimens T4 and T7 (Figure 4c, e).



**Figure 13:** Raindrop turquoise is relatively rare, but a small amount of this material has been produced from Xinjiang (left, sample T3), which is similar to that from Hubei (right), the only other source known previously for this turquoise variety. Photo by Yanhan Wu.

The chemical formula of fluorapatite is  $\text{Ca}_5(\text{PO}_4)_3\text{F}$ , but P can be replaced by small, highly charged cations such as S. Fluorapatite is by far the most abundant apatite-group mineral in rocks (Chang *et al.* 1998). Liu *et al.*

(2020) first speculated that the raindrops and veins in Hubei turquoise could be by-products of weathering and leaching. When phosphate minerals undergo weathering, some of their components are dissolved in meteoric water and can then migrate in the form of colloidal or molecular solutions. Phosphate solutions carrying Ca and F can precipitate secondary phosphate minerals (fluorapatite) under appropriate physical and chemical conditions. If such crystallisation occurs in the pores within turquoise, then it can precipitate as distinct spots (raindrops). If fluorapatite crystallises in cracks, it appears as veins. For example, the vein in specimen T4 (Figure 4c) obviously formed by precipitation from a later solution entering the turquoise along a crack. The geological environments of Xinjiang and Hubei turquoise are quite similar, and the raindrops and veins are most likely by-products of weathering and leaching (Liu *et al.* 2020).

## CONCLUSIONS

Xinjiang hosts turquoise of archaeological significance that also has commercial potential because of the material's attractive colouration and good quality. The turquoise mostly occurs as veins or nodules (e.g. Figure 14), and its colour ranges from blue to green, brownish



**Figure 14:** Turquoise from Xinjiang occurs as veins or nodules. Although Xinjiang is a source of good-quality turquoise, mining is currently forbidden due to ongoing archaeological studies in the area. Photo by Yanhan Wu.

to yellowish green, or brownish yellow. The greater the ratio of  $\text{FeO}_{\text{tot}}/\text{CuO}$ , the stronger the yellow hue. The turquoise is associated with woodhouseite, dawsonite, calcite, alunite, gypsum and quartz. Compared with material from elsewhere in China, Xinjiang turquoise contains relatively high contents of Si, Sr, Cr and V. The hardness of the brownish yellow turquoise samples was found to be closely related to the concentration of quartz crystallites. ‘Raindrop’ turquoise, previously known only from Hubei, is documented here for the first time in material from Xinjiang. Its distinctive spotted

appearance is due to the presence of fluorapatite, which is also present in cross-cutting veins in some samples.

Since 2016, archaeological research on Xinjiang turquoise has been an important part of the study of cultural exchanges in ancient north-west China. Here we have introduced the gemmological characteristics of Xinjiang turquoise, which helps provide information about its origin. The future availability of Xinjiang turquoise will depend on whether mining is permitted by the local government after the ongoing archaeological studies of the area have been completed.

## REFERENCES

- Anthony, J.W., Bideaux, R.A., Bladh, K.W. & Nichols, M.C. (eds) 2001. *Handbook of Mineralogy*, Vol. 4. Mineralogical Society of America, Chantilly, Virginia, USA, <http://www.handbookofmineralogy.org/pdfs/turquoise.pdf>.
- Carò, F., Schorsch, D., Smieska, L. & Santarelli, B. 2021. Non-invasive XRF analysis of ancient Egyptian and Near Eastern turquoise: A pilot study. *Journal of Archaeological Science: Reports*, **36**, article 102893 (14 pp.), <https://doi.org/10.1016/j.jasrep.2021.102893>.
- Čejka, J., Sejkora, J., Macek, I., Malíková, R., Wang, L., Scholz, R., Xi, Y. & Frost, R.L. 2015. Raman and infrared spectroscopic study of turquoise minerals. *Spectrochimica Acta Part A: Molecular and Biomolecular Spectroscopy*, **149**, 173–182, <https://doi.org/10.1016/j.saa.2015.04.029>.
- Chang, L.L.Y., Howie, R.A. & Zussman, J. 1998. *Rock-Forming Minerals—Non-silicates: Sulphates, Carbonates, Phosphates, Halides*, Vol. 5B, 2nd edn. The Geological Society, London, viii + 392 pp.
- Chen, Q. & Qi, L. 2007. Study on the vibrational spectra characters of water in turquoise from Ma’anshan. *Journal of Mineralogy and Petrology*, **27**(1), 30–35, <https://doi.org/10.19719/j.cnki.1001-6872.2007.01.006> (in Chinese).
- Chen, J., Zheng, Y., Gao, J.B. & Xiao, Z. 2011. Prospecting target optimization in Heishanling region of Beishan area, Xinjiang. *Xinjiang Geology*, **29**(4), 438–441 (in Chinese).
- Chen, Q., Yin, Z., Qi, L. & Xiong, Y. 2012. Turquoise from Zhushan County, Hubei Province, China. *Gems & Gemology*, **48**(3), 198–204, <https://doi.org/10.5741/gems.48.3.198>.
- Cid-Dresdner, H. 1964. The crystal structure of turquois [sic]. *Die Naturwissenschaften*, **51**(16), 380–381, <https://doi.org/10.1007/bf00637241>.
- Cid-Dresdner, H. 1965. Determination and refinement of the crystal structure of turquois [sic],  $\text{CuAl}_6(\text{PO}_4)_4(\text{OH})_8 \cdot 4\text{H}_2\text{O}$ . *Zeitschrift für Kristallographie*, **121**, 87–113, <https://doi.org/10.1524/zkri.1965.121.2-4.87>.
- Close, A.E. & Minichillo, T. 2010. Neolithic tombs in southwestern Sinai. *Journal of Arid Environments*, **74**(7), 829–841, <https://doi.org/10.1016/j.jaridenv.2009.03.005>.
- Guo, Y., Zhang, J. & Jin, L. 2010. Effect of water adsorption on bluish-green chromaticity and hue of turquoise in Zhushan, Hubei Province. *Acta Mineralogica Sinica*, **30**(S1), 39–40, <https://doi.org/10.16461/j.cnki.1000-4734.2010.s1.013> (in Chinese).
- Hao, Y. & Hao, F. 2002. Chinese turquoise culture of the New Stone Age. *Acta Petrologica et Mineralogica*, **21**(z1), 147–150 (in Chinese).
- Harbottle, G. & Weigand, P.C. 1992. Turquoise in pre-Columbian America. *Scientific American*, **266**(2), 78–85, <https://doi.org/10.1038/scientificamerican0292-78>.
- He, X., Chen, L., Li, Q., Gu, D., Gan, F., Li, F. & Li, Z. 2011. Trace elements and rare earth elements characteristics of turquoise from Zhushan and Ma’anshan area. *Rock and Mineral Analysis*, **30**(6), 709–713, <https://doi.org/10.15898/j.cnki.11-2131/td.2011.06.007> (in Chinese).
- Hole, F., Flannery, K.V. & Neely, J.A. 1969. *Prehistory and Human Ecology of the Deh Luran Plain: An Early Village Sequence from Khuzistan, Iran*. University of Michigan Museum of Anthropological Archaeology, Ann Arbor, Michigan, USA, 482 pp. (see pp. 189–204), <https://doi.org/10.3998/mpub.11395036>.
- Hull, S., Fayek, M., Mathien, F.J., Shelley, P. & Durand, K.R. 2008. A new approach to determining the geological provenance of turquoise artifacts using hydrogen and copper stable isotopes. *Journal of Archaeological Science*, **35**(5), 1355–1369, <https://doi.org/10.1016/j.jas.2007.10.001>.

- King, R.J. 2002. Turquoise. *Geology Today*, **18**(3), 110–114, <https://doi.org/10.1046/j.1365-2451.2002.00345.x>.
- Kostov, R.I. 2019. Archaeomineralogy of turquoise in Eurasia. In: Querré, G., Cassen, S. & Vigier, E. (eds.) *La Parure en Callaïs du Néolithique Européen*. Archaeopress Publishing Ltd, Oxford, 387–396, <https://doi.org/10.32028/9781789692808>.
- Krzemnicki, M.S., Herzog, F. & Zhou, W. 2011. A historic turquoise jewelry set containing fossilized dentine (odontolite) and glass. *Gems & Gemology*, **47**(4), 296–301, <https://doi.org/10.5741/gems.47.4.296>.
- Li, Y., Tan, Y. & Jia, Q. 2019. Preliminary investigation of two ancient turquoise ore sites in Hami, Xinjiang. *Archaeology and Cultural Relics*, No. 6, 22–27, <https://doi.org/10.3969/j.issn.1000-7830.2019.06.004> (in Chinese).
- Liu, L., Yang, M. & Li, Y. 2020. Unique raindrop pattern of turquoise from Hubei, China. *Gems & Gemology*, **56**(3), 380–400, <https://doi.org/10.5741/gems.56.3.380>.
- Liu, X., Lin, C., Li, D., Zhu, L., Song, S., Liu, Y. & Shen, C. 2018. Study on mineralogy and spectroscopy of turquoises from Hami, Xinjiang. *Spectroscopy and Spectral Analysis*, **38**(4), 1231–1239 (in Chinese).
- Luo, Y.F. 2017. *The gemological and mineralogical characteristics of turquoise from Luonan, Shaanxi*. MS thesis, China University of Geosciences, Beijing, China.
- Mi, D., Zhou, C., Zhang, J. & Tang, X. 2014. Geological characteristics and genetic analysis of Tianhu iron deposit in Hami area, Xinjiang. *Contributions to Geology and Mineral Resources Research*, **29**(2), 223–229 (in Chinese).
- Othmane, G., Hull, S., Fayek, M., Rouxel, O., Geagea, M.L. & Kyser, T.K. 2015. Hydrogen and copper isotope analysis of turquoise by SIMS: Calibration and matrix effects. *Chemical Geology*, **395**, 41–49, <https://doi.org/10.1016/j.chemgeo.2014.11.024>.
- Palache, C., Berman, H. & Frondel, C. 1951. *The System of Mineralogy of James Dwight Dana and Edward Salisbury Dana*, Vol. 2, 7th edn. John Wiley and Sons Inc., New York, New York, USA, 1,124 pp.
- Qi, L., Yan, W. & Yang, M. 1998. Turquoise from Hubei Province, China. *Journal of Gemmology*, **26**(1), 1–12, <https://doi.org/10.15506/JoG.1998.26.1.1>.
- Reddy, B.J., Frost, R.L., Weier, M.L. & Martens, W.N. 2006. Ultraviolet-visible, near infrared and mid infrared reflectance spectroscopy of turquoise. *Journal of Near Infrared Spectroscopy*, **14**(4), 241–250, <https://doi.org/10.1255/jnirs.641>.
- Ren, J.W. 1985. Hexi Dianzi and Hami turquoise. *Earth*, **1**, 30 (in Chinese).
- Shen, C. & Zhao, E. 2019. Mineralogical characteristics and genetic mechanism of turquoise deposit in Bijiaoshan area in Anhui Province. *Journal of Jilin University (Earth Science Edition)*, No. 6, 1591–1606, <https://doi.org/10.13278/j.cnki.jjuese.20190125> (in Chinese).
- Shi, Z. 2008. Diagenetic origin of Al-phosphate-sulfate minerals in Cambrian Period carbon-silicon slate, Zhushan, Hubei. *Journal of Geology*, **32**(2), 109–112 (in Chinese).
- Shi, Z. & Cai, K. 2007. Study on the turquoise and residual-minerals from Yue'ertan of Shanxi. *Superhard Material Engineering*, **19**(4), 56–60 (in Chinese).
- Shi, Z. & Cai, K. 2008. A study of turquoise and secondary woodhouseite from Yuertan, Baihe County, Shaanxi Province. *Acta Petrologica et Mineralogica*, **27**(2), 164–170 (in Chinese).
- Shirdam, B., Shen, A., Yang, M., Mokhtari, Z. & Fazliani, H. 2021. Persian turquoise: The ancient treasure of Neyshabur. *Gems & Gemology*, **57**(3), 240–257, <https://doi.org/10.5741/gems.57.3.240>.
- Štubňa, J. & Andrášiová, A. 2021. Gem Notes: Turquoise from Armenia. *Journal of Gemmology*, **37**(5), 454–456, <https://doi.org/10.15506/JoG.2021.37.5.454>.
- Štubňa, J., Bačík, P., Fridrichová, J. & Hanus, R. 2021. Gem Notes: Turquoise from Mongolia. *Journal of Gemmology*, **37**(5), 456–458, <https://doi.org/10.15506/JoG.2021.37.5.456>.
- Tang, Y., Mei, H., Pan, K., Liu, D., Zhou, N. & Xin, H. 2005. *Non-metallic Deposits of Xinjiang, China*. Geological Publishing House, Beijing, China, 239 pp. (in Chinese).
- Thibodeau, A.M., Killick, D.J., Hedquist, S.L., Chesley, J.T. & Ruiz, J. 2015. Isotopic evidence for the provenance of turquoise in the southwestern United States. *Geological Society of America Bulletin*, **127**(11–12), 1617–1631, <https://doi.org/10.1130/b31135.1>.
- Tong, J., Ma, J., Li, W., Chang, X., Yu, J., Wang, J., Ma, Y., Tian, Y. et al. 2020. Chronology of the Tianshanbeilu cemetery in Xinjiang, northwestern China. *Radiocarbon*, **63**(1), 343–356, <https://doi.org/10.1017/rdc.2020.96>.
- Wang, X. & Guo, Y. 2021. The impact of trace metal cations and absorbed water on colour transition of turquoise. *Royal Society Open Science*, **8**(2), article 201110 (20 pp.), <https://doi.org/10.1098/rsos.201110>.
- Watanabe, Y., Sato, R. & Sulaksono, A. 2018. Role of potassic alteration for porphyry Cu mineralization: Implication for the absence of porphyry Cu deposits in Japan. *Resource Geology*, **68**(2), 195–207, <https://doi.org/10.1111/rge.12165>.

- Xian, Y., Li, Y. & Yu, C. 2020. A survey of the ancient turquoise mining site at Heishanling in Ruoqiang, Xinjiang. *Cultural Relics*, No. 8, 4–13, <https://doi.org/10.13619/j.cnki.cn11-1532/k.2020.08.001> (in Chinese).
- Xian, Y., Fan, J., Li, Y. & Yu, C. 2021. Where did the treasure come from? Discovery and recognition of two ancient turquoise mining sites in Xinjiang. *Cultural Relics World*, No. 7, 59–62 (in Chinese).
- Xue, Y., Deng, W.H., He, X.M. & Li, D.D. 2013. Gemological features of turquoise from Hubei and Shaanxi provinces. *Gemology & Technology: 2013 China Gems & Jewelry Academic Conference*, China Gems Magazine, Beijing, 218–224 (in Chinese).
- Yang, X.Y., Yong-Fei, Z., Yang, X.M., Liu, X. & Wang, K. 2003. Mineralogical and geochemical studies on the different types of turquoise from Maanshan area, east China. *Neues Jahrbuch für Mineralogie, Monatshefte*, **2003**(3), 97–112, <https://doi.org/10.1127/0028-3649/2003/2002-0097>.
- Yu, X.-Y., Long, Z.-Y., Zhang, Y., Qin, L.-J., Zhang, C., Xie, Z.-R., Wu, Y.-R., Yan, Y. *et al.* 2021. Overview of gemstone resources in China. *Crystals*, **11**(10), article 1189 (22 pp.), <https://doi.org/10.3390/cryst11101189>.
- Zeng, X., Yang, Z., Li, X., Lei, X., Huang, S. & Chen, Y. 2019. Study on the vibration spectra of turquoise imitation and natural turquoise from Zhushan County, Hubei Province. *Spectroscopy and Spectral Analysis*, **39**(3), 834–839 (in Chinese).
- Zhang, H., Lin, C., Ma, Z. & Yang, Z. 1982. Magnetic properties, characteristic spectra and colour of turquoise. *Acta Mineralogica Sinica*, **4**, 254–261, <https://doi.org/10.16461/j.cnki.1000-4734.1982.04.004> (in Chinese).
- Zhang, L.C., Liu, D.G. & Tang, Y.L. 1990. *Mineral Resources in Xinjiang*. Hong Kong Educational and Cultural Press Ltd, Hong Kong, 328 pp. (in Chinese).
- Zong, K., Klemd, R., Yuan, Y., He, Z., Guo, J., Shi, X., Liu, Y., Hu, Z. *et al.* 2017. The assembly of Rodinia: The correlation of early Neoproterozoic (ca. 900 Ma) high-grade metamorphism and continental arc formation in the southern Beishan Orogen, southern Central Asian Orogenic Belt (CAOB). *Precambrian Research*, **290**, 32–48, <https://doi.org/10.1016/j.precamres.2016.12.010>.

### The Authors

**Yanhan Wu** FGA<sup>1</sup>, **Dr Quanli Chen**\*<sup>1,2</sup>,  
**Dr Yan Li** FGA<sup>1</sup>, **Min Cao** FGA<sup>3</sup>,  
**Prof. Zuowei Yin** FGA DGA<sup>1</sup>, **Haitao Wang**<sup>4</sup>  
**and Dr Xianyu Liu**<sup>5</sup>

<sup>1</sup> Gemmological Institute, China University of Geosciences, No. 388 Lumo Rd., 430074 Wuhan, China  
\*Email: chenquanli@cug.edu.cn

<sup>2</sup> School of Jewelry, West Yunnan University of Applied Sciences, No. 1 Ruixing Rd., 679100 Tengchong, China

<sup>3</sup> National Gemstone Testing Center's Shenzhen laboratory, No. 4 Beilinan Rd., 518020 Shenzhen, China

<sup>4</sup> College of Creative Design, Shenzhen Technology University, No. 3002 Lantian Rd., 518118 Shenzhen, China



<sup>5</sup> College of Jewelry, Shanghai Jian Qiao University, No. 1111 Huchenghuan Rd., 201306 Shanghai, China

### Acknowledgements

This research was supported financially by the National Key R&D Program of China (no. 2018YFF0215400). In addition, this work was partially supported by the Gemmological Institute, China University of Geosciences (Wuhan) with grant no. CIGTXM-201703. The publication of this article in the year 2022 marks the 30th anniversary of the Gemmological Institute (Wuhan) and the 70th anniversary of the China University of Geosciences (Wuhan).

Join us on social media to keep up-to-date with the latest news, events and offers from Gem-A

 facebook.com/GemAofGB  
 @GemAofGB  
 linkd.in/1GisBTP

 Instagram: @gemaofgb  
 WeChat: Scan the QR code to add us on WeChat



# An innovator in gemstone reporting

- Identification of colored gemstones • Country of origin determination • Full quality and color grading analysis



AMERICAN GEMOLOGICAL LABORATORIES



580 5th Ave • Suite 706 • New York, NY 10036, USA  
www.agilgemlab.com • +1 (212) 704 - 0727

# Origin of Emeralds in a Late-Eighteenth-Century Pectoral Cross and Ring from St Peter's Archabbey, Salzburg, Austria

Karl Schmetzer and H. Albert Gilg

**ABSTRACT:** A pectoral cross with nine emeralds and a ring containing one emerald were donated in 1786 to newly elected Abbot Dominikus Hagenauer of St Peter's Abbey, Salzburg, Austria. Both jewels were examined by microscopy and with a portable X-ray fluorescence unit. The emeralds' inclusion patterns and chemical properties indicate they are of Colombian origin, although oral tradition has assumed they came from Austria's Habachtal deposit. The faceting style of the accompanying diamonds indicates that the ring might be somewhat older than the pectoral cross.

*The Journal of Gemmology*, 38(3), 2022, pp. 272–283, <https://doi.org/10.15506/JoG.2022.38.3.272>  
© 2022 Gem-A (The Gemmological Association of Great Britain)

The examination of ancient and medieval jewellery gives insight into historical events, trade routes and technical developments such as cutting methods, etc. over the course of time. Of special interest is determining the origin of the gemstones set in these historical objects. If the jewel has a known history—including information about manufacture, ownership in various periods of time, and possible repairs or replacements of lost stones—the insights obtained from research into the gems may be extremely valuable. For example, we might find chronological and geographical parallels for other ornaments for which less documentation has survived. Such research also expands our understanding of which gem mines were worked and when, the historical trade networks for gems and, potentially, relative gem values at the time.

This article reports on an examination of two late-eighteenth-century jewels that contribute to this body of knowledge with regard to emeralds (Figure 1).

## *Habachtal, Austria, as a Historical Source of Emerald*

The sources of emeralds used in jewelled pieces dating

from antiquity to the nineteenth century is an ongoing matter of controversy. It has been speculated that the emerald deposit in the Habachtal valley—located in the Pinzgau region of Salzburg federal state, Austria—might have been known to the Celts and Romans, with some authors (e.g., Sinkankas 1981; Giuliani *et al.* 2000) even going so far as to suggest that the deposit had been exploited and mined by the Romans. However, written documentation or clear archaeological evidence is lacking to verify a link to this deposit in antiquity.

Remaining from the Middle Ages, we know of the Saint Louis emerald of the French King Louis IX (1214–1270), a highly included and fractured stone weighing about 51.60 ct (Figure 2). It was originally mounted in a crown dating to the thirteenth century, and it has been assigned to the Habachtal occurrence on the basis of its oxygen isotopic composition (Giuliani *et al.* 2000; Stehrer 2000; for details on the technique, see Giuliani *et al.* 1998). Similar results were provided for an emerald from a piece of Roman jewellery (Giuliani *et al.* 2001).

For the Renaissance and Baroque eras, oral tradition links the emeralds in monstrances (e.g. Figure 3) and other liturgical insignia in churches of the Pinzgau and





**Figure 1:** The emerald-bearing pectoral cross and emerald ring examined for this study were donated to Dominikus Hagenauer in 1786. The pectoral cross measures 12.5 × 5.8 cm and the size of the upper emerald is 8.5 × 7 mm. Courtesy of St Peter's Archabbey, Salzburg; photo by N. Urban.



**Figure 2:** The 51.60 ct Saint Louis emerald, now at the Muséum National d'Histoire Naturelle in Paris (MIN000-5298), has been assigned to originate from the Habachtal deposit in Austria. The thirteenth-century crown associated with the emerald no longer exists. Photo by H. A. Gilg.

Salzburg areas to Habachtal (Hanke 1958; Hagn 2019, 2021). Such oral tradition also exists in the monastery of St Peter's Abbey in Salzburg (elevated to an archabbey since 1927) for the emeralds in the two objects studied in the present article—a pectoral cross and an emerald ring (again, see Figure 1) of Abbot Dominikus Hagenauer, which have a known history since the end of the eighteenth century. However, no scientific examination—such as inclusion study, trace-element analyses, etc.—exists that offers any conclusive link between the emeralds set in these religious objects and the Habachtal deposit,



**Figure 3:** (a) The monstrance in the Salzburg Cathedral Museum (Pretiosenmonstranz) was manufactured in 1697 by goldsmith Ferdinand Sigmund Amende (see Rudolph 2021). (b) The upper part was designed as a crown and contains 24 emeralds which have been assigned, by oral tradition, to the Habachtal deposit. Photos by H. A. Gilg.

which could provide evidence of emerald mining there in the eighteenth century.

The first known mention of the emerald location in Habachtal in a scientific journal is by K. M. Schroll in 1797. Initial mining operations were performed for a few years in the early 1860s by Viennese jeweller Samuel Goldschmidt, followed by the English company 'Emerald Mines Limited' in 1895 (Schmetzer 2021, 2022). Prior to the late eighteenth century, single stones might have been found on occasion, especially in the secondary part of the deposit, but there is no verifiable evidence of formal emerald mining activities. Several publications describing regular mining operations at Habachtal before 1800 have been found to be erroneous (Schmetzer 2021, 2022).

A few larger emerald crystals of high quality were mined in Habachtal in the nineteenth and twentieth centuries (Figure 4), but the majority of them were smaller and heavily included (Figure 5), and a high percentage were not of facetable quality. This makes any assignment to the Habachtal deposit of high-quality emeralds in historical pieces of jewellery suspicious or, at least, questionable. Therefore, the authors were grateful to obtain permission to be the first investigators



**Figure 4:** This 16.4 g (3.3 cm long) emerald crystal from Habachtal was sold by the Bergman company in 1883 to the British Museum in London. It is one of the largest samples found at Habachtal in the nineteenth century. The Bergman company, located in Innsbruck, Tyrol, Austria, was involved in emerald recovery at Habachtal in the 1870s and early 1880s. Photo courtesy of the Natural History Museum, London, © The Trustees of the Natural History Museum, London.



**Figure 5:** A high percentage of the emeralds mined in Habachtal between 1860 and 1940 were heavily included small stones of non-facetable quality. These emerald crystals in matrix from Habachtal, with the largest crystal measuring 7 mm long, were purchased for the collection of St Peter's Abbey, Salzburg, in the first decades of the twentieth century. Photo by K. Schmetzer.

to examine the late-eighteenth-century pectoral cross and emerald ring of Abbot Hagenauer of St Peter's Archabbey.

## HISTORY

St Peter's Abbey (Figure 6), now designated an archabbey, is located in the historical centre of Salzburg. It is considered one of the oldest (or even the oldest) monasteries in the German-speaking area, with a continuous history since its foundation in 696 CE. Dominikus Hagenauer (1746–1811), born Kajetan Rupert Hagenauer, was elected abbot of St Peter's Abbey in January 1786. The only contemporary written information about the emerald-bearing pectoral cross and emerald ring is in Hagenauer's diary, which various authors cite with the same wording (e.g. Dopsch & Juffinger 1982; Angermüller 2006). No further information is available in the archive of St Peter's Archabbey dating to the eighteenth century (G. Hirtner, pers. comm. 2020). Hagenauer's diary entry, dated 23 March 1786, reads (translated from German):

Today my old father [Johann Lorenz Hagenauer] visited me together with Mr Franz Weiser, my confirmation godfather. The first one donated to me an emerald pectoral cross, decorated with diamonds, valued 580 fl [gulden] and the latter one gave me a similar ring, valued 120 fl.

Johann Lorenz Hagenauer (1712–1792) descended from a dynasty of merchants. He and his family were close friends of the Mozart family, who lived for several

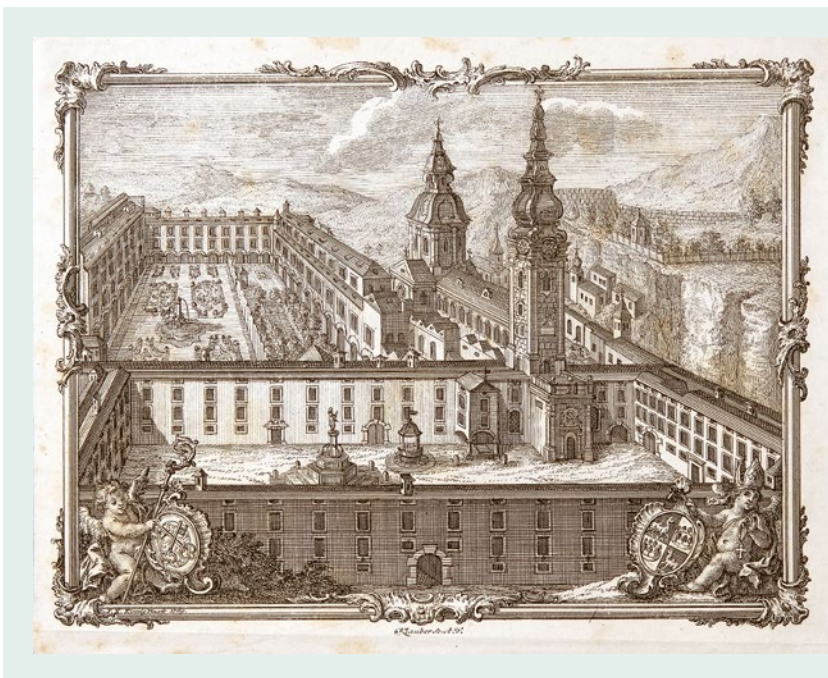


**Figure 6:** St Peter's Archabbey is considered one of the oldest monasteries in the German-speaking area, founded in 696 CE during the early Middle Ages. Copper engraving by F. X. Kinnig, 1769; courtesy of St Peter's Archabbey, Salzburg.

decades in Hagenauer's house in Salzburg. Franz Andreas Weiser (1739–1817) was a merchant and member of the city council of Salzburg. His father, Ignatz Anton Weiser (1701–1785), also a merchant, was mayor of Salzburg and the lyricist for one of Wolfgang Amadeus Mozart's operas (*Singspiel*). Both men were members of the patrician families of Salzburg.



**Figure 7:** This portrait of Abbot Dominikus Hagenauer shows him wearing the emerald pectoral cross and emerald ring examined for this study. Unknown artist, ca. 1786; courtesy of St Peter's Archabbey, Salzburg.

The portrait of Abbot Dominikus Hagenauer in Figure 7 shows him wearing both the emerald pectoral cross and ring. The abbot brought out the objects for special events, as did his successors on occasion. No repair or replacement of the stones in either object is documented.

An 1876 inventory of St Peter's Abbey describes the gemstones as Brazilian emeralds (G. Hirtner, pers. comm. 2022). However, the origin of this information is not clear, and according to the literature Brazilian emeralds were not available in the trade before 1914 (Bauer & Schloßmacher 1932).

## MATERIALS AND METHODS

Both objects—the pectoral cross and the ring—were examined on the premises of the mineral collection of St Peter's Archabbey. Following our initial visual inspection of the objects (noting particularly the gem cutting styles), the inclusion pattern in the emeralds was documented (Figure 8) using a Leitz Ortholux microscope equipped with three long-working-distance objectives (UM 10/0.22, UT 40/0.35 and UT 50/0.62) and a Fujifilm X-T100 camera.

The emeralds were then chemically analysed (Figure 9) with a portable Bruker Tracer III-SD energy-dispersive X-ray fluorescence (EDXRF) analyser equipped with a rhodium anode, a silicon drift detector with a resolution of 147 eV at 10,000 cps, and a portable vacuum pump system. The spot size of the primary beam was about  $2 \times 3$  mm. We used two analytical conditions for the measurements. The first set-up, with an accelerating voltage of 15 kV and a beam current of 25  $\mu$ A under vacuum, was



**Figure 8:** The emerald pectoral cross (shown here) and ring were examined in 2020 by optical microscopy. Photo by H. A. Gilg.

used to analyse the elements of interest in the emeralds (Mg, Al, Si, V, Cr and Fe). There was no interference between the fluorescence lines from these elements and those present in the mountings of the gemstones (Au, Ag, Cu, Pb and Ni). However, some minor Bragg peaks related to X-ray diffraction of Bremsstrahlung (mainly the continuous part of the primary X-ray radiation) interfered with the elements K, Ca, Ti and Mn. Therefore, we deployed a second set-up with 40 kV and 30  $\mu$ A using a yellow filter (0.001 mil Ti and 0.012 mil Al) that eliminated the weak Bragg peaks in the spectra. Artax 7.4.8.2 software and a series of ten natural- and synthetic-emerald standards with a wide compositional range ( $\leq 2.4$  wt.% MgO,  $\leq 0.87$  wt.% FeO,  $\leq 0.96$  wt.% Cr<sub>2</sub>O<sub>3</sub> and  $\leq 0.48$  wt.% V<sub>2</sub>O<sub>3</sub>) were used in the calibration process for element quantification. The emerald standards had been previously analysed or were chemically analysed in the course of our study by electron probe micro-analysis (EPMA) and, in part, by laser ablation inductively coupled plasma mass spectrometry (LA-ICP-MS).

Some major components in emerald, such as BeO, Na<sub>2</sub>O and H<sub>2</sub>O, cannot be detected with our portable XRF device. Therefore, we used the measured element-to-silicon ratios at 15 kV and 25  $\mu$ A and an assumed full occupancy of the Si position in the beryl structure with six atoms per formula unit (apfu) in concert with the respective values of the emerald standards to calculate the element concentrations for Mg, Al, V, Cr and Fe per formula unit and as weight-percent (wt.%) oxides. As such, we employed a specially developed calibration process that used the analysed emeralds as external standards and the Si contents of the samples as an internal standard.

In order to verify our approach, and because numerous analyses of Habachtal emeralds in the literature lack vanadium values, we analysed several reference emerald



**Figure 9:** In 2020, the emerald pectoral cross (shown here) and ring were also analysed with a portable X-ray fluorescence unit. Photo by H. A. Gilg.

samples from Habachtal (collection of C. Weise, Munich, Germany) and from Colombia (collections of Dr T. Häger, Mainz, Germany, and Dr D. Schwarz, Bangkok, Thailand) using our portable EDXRF analyser. We performed 15 analyses of the Habachtal emeralds and six analyses of the Colombian samples, and compared the results with previously published chemical data, mostly based on EPMA and partly on LA-ICP-MS analyses.

## RESULTS AND DISCUSSION

The pectoral cross measures 12.5  $\times$  5.8 cm, with a vertical row of seven emeralds and two placed horizontally on either side of the centre emerald, all mounted with prongs (see Figure 1). Numerous diamonds, together with their metal mountings, form floral motifs.

The central emerald of the ring measures about 9 mm in diameter (again, see Figure 1). The stone is set with prongs and surrounded by two rows of small diamonds.

### *Visual Examination: Gemstone Cutting Styles*

**Pectoral Cross.** The emeralds in the pectoral cross were intense green and were square or rectangular in shape, in sizes of 8.5  $\times$  7, 7.5  $\times$  7, 7  $\times$  7, 7  $\times$  6 and 5  $\times$  5 mm (Figure 10). All were step cuts, with two rows of facets on the crown, each row with four larger and four smaller faces (Figure 11). All the diamonds were rose cuts of different shapes: round (up to 3 mm diameter), oval, triangular, pear and navette (up to 4.5  $\times$  3.5 mm).

**Ring.** The somewhat lighter green emerald in the ring consisted of a round brilliant-style cut, with a diameter of 9 mm (Figure 12). It had a table size that was approximately 50–55% of the stone's diameter (Figure 13).



**Figure 10:** Detailed views of the pectoral cross show that the emeralds are step cuts and the diamonds are all rose cuts. The emerald in the centre of the cross measures 7 × 7 mm. Photos by K. Schmetzer.

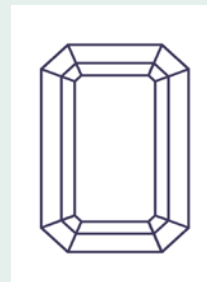


**Figure 11:** Schematic representation of the cutting style of the emeralds in the pectoral cross.

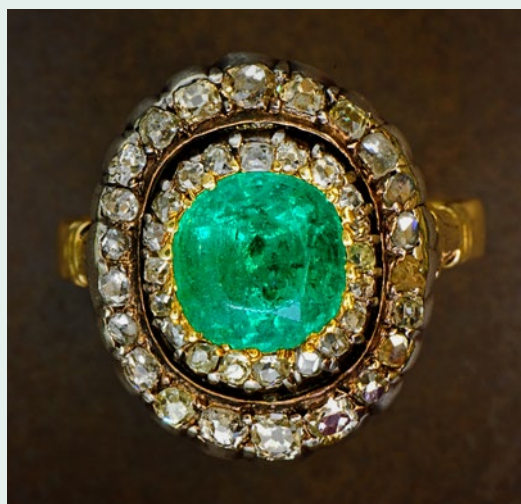


**Figure 12:** The ring features a brilliant-cut emerald surrounded by diamonds that are arranged in two rows and faceted into table and rose cuts. The emerald is approximately 9 mm in diameter. Courtesy of St Peter's Archabbey, Salzburg; photo by N. Urban.

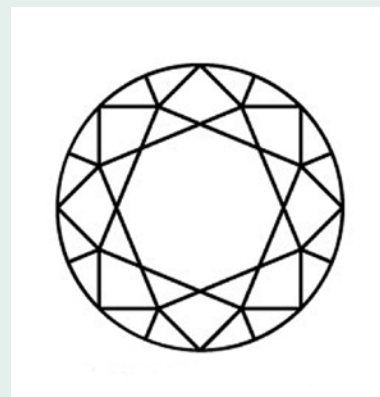


**Figure 13:** Schematic representation of the faceted emerald in the ring.

The diamonds, set in two rows around the emerald, consisted of rose cuts and table cuts. The diameter of the diamonds in the inner row was about 1 mm and in the outer row about 2 mm. The table-cut diamonds were square or rectangular, with four crown facets each, or octagonal, with eight crown facets. Such simple table cuts, especially with only four crown facets, represent older cuts than the brilliant type normally performed at the end of the eighteenth century, but this style was still used for smaller stones in the eighteenth century and even later in the nineteenth century (see, e.g. Tillander 1995; Ogden 2018).

### **Microscopic Examination: Inclusions**

Most of the emeralds in the pectoral cross were extremely clean, especially compared to the emerald in the ring (again, see Figures 10 and 12). Occasionally, the former

contained fluid inclusions and partially healed feathers, similar to the pattern described below in more detail for the ring.

The emerald in the ring was heavily included and, by visual means, dissimilar to those in the pectoral cross. It contained numerous fluid inclusions, mainly two-phase (liquid and gas) and three-phase (liquid, gas and cubic crystals; Figure 14). These fluid inclusions were often elongate and occasionally displayed necking-down features. They ranged from less than 5 µm to 100 µm long. They generally contained a dark-appearing vapour bubble, a colourless cubic solid inclusion (halite?) and a dominant aqueous (liquid) phase (Figure 14a). One inclusion had a second cubic crystal (possibly sylvite) and a third unknown solid phase (Figure 14b).

None of the emeralds in the pectoral cross and ring displayed the pattern of internal features typically seen

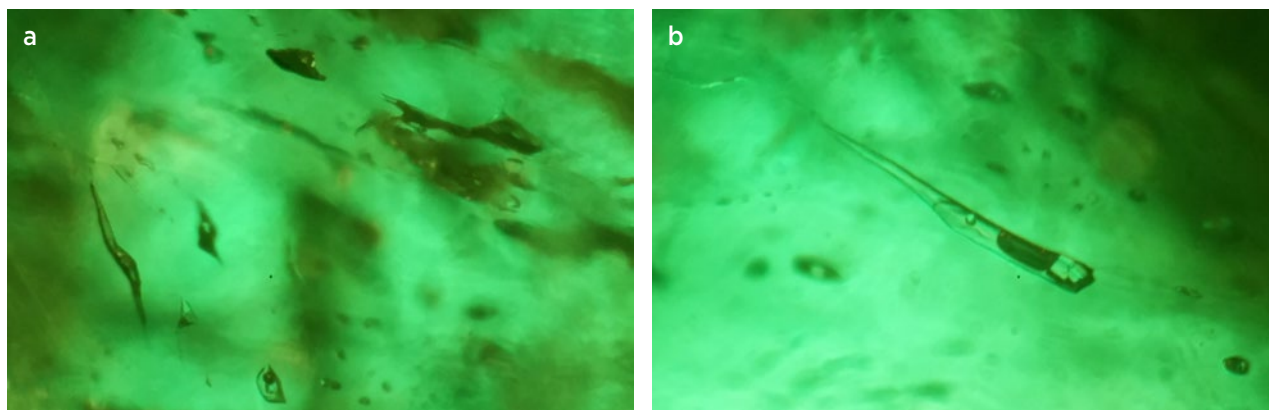


**Figure 14:** (a) Multiphase inclusions are common in the emerald of the ring. Most contain a dark vapour bubble, a colourless cubic solid inclusion (possibly halite) and an aqueous phase. (b) One inclusion in this emerald also contains a second cubic crystal (possibly sylvite) and a third (unknown) solid phase. Photomicrographs by H. A. Gilg; field of view 0.75 × 0.56 mm each.

in Habachtal emeralds, consisting of numerous mineral inclusions and growth zoning (see, e.g., Gübelin 1956; Grundmann 1981, 1984, 1991; Gübelin & Koivula 1986, 2008; Thomas *et al.* 2020). The most common inclusions in Habachtal emeralds consist of mineral phases including biotite, muscovite, chlorite, amphiboles (tremolite-actinolite), tourmaline, epidote, graphite and apatite. Fluid inclusions in Habachtal emeralds frequently consist of aqueous liquid-rich two-phase and aqueous-carbonic three-phase inclusions.

By contrast, the inclusion pattern we observed is typical of Colombian emeralds (see, e.g., Gübelin 1940; Gübelin & Koivula 1986, 2008; Kozłowski *et al.* 1988; Bosshart

1991; Giuliani *et al.* 1995). These are characterised by two-phase (liquid-gas), halite-bearing three-phase and aqueous-carbonic multiphase inclusions. In addition to halite, solid daughter phases within the fluid-filled cavities include sylvite, calcite, dolomite and sphalerite. The most frequent solid inclusions reported in Colombian emeralds are pyrite, albite, quartz, white mica and carbonates including parisite-(Ce).

### Chemical Composition

The chemical composition of the emeralds in the pectoral cross and ring is presented in Table I. In addition, representative EDXRF spectra of emeralds in the ring and

**Table I:** Chemical composition of emeralds in the pectoral cross and the ring of Abbot Dominikus Hagenauer.<sup>a</sup>

Analysis point <sup>b</sup>	P1	P2	P3a	P3b	P4	P5	P6	P7	P8	P9	R1a	R1b
<b>Oxides (wt.%)</b>												
SiO <sub>2</sub>	64.9	64.8	63.6	64.1	65.3	64.3	64.4	64.4	64.5	63.8	65.5	65.7
Al <sub>2</sub> O <sub>3</sub>	16.0	15.9	14.5	15.1	16.6	15.4	15.4	15.4	15.5	14.7	16.8	17.0
Cr <sub>2</sub> O <sub>3</sub>	0.41	0.26	0.53	0.49	0.41	0.64	0.59	0.61	0.37	0.57	0.23	0.17
V <sub>2</sub> O <sub>3</sub>	0.51	0.41	0.73	0.75	0.81	0.54	0.74	0.60	0.48	0.81	0.38	0.22
FeO	0.14	0.11	0.16	0.13	0.12	0.18	0.14	0.13	0.17	0.20	0.24	0.14
MgO	1.50	0.89	0.91	0.89	1.26	1.62	1.66	1.41	0.89	1.39	0.97	0.92
Sum Cr <sub>2</sub> O <sub>3</sub> + V <sub>2</sub> O <sub>3</sub>	0.92	0.67	1.26	1.24	1.22	1.18	1.31	1.21	0.85	1.38	0.61	0.39
<b>Cations</b>												
Si	6.00	6.00	6.00	6.00	6.00	6.00	6.00	6.00	6.00	6.00	6.00	6.00
Al	1.74	1.74	1.61	1.67	1.80	1.69	1.69	1.69	1.70	1.63	1.81	1.83
Cr	0.03	0.02	0.04	0.04	0.03	0.05	0.04	0.05	0.03	0.04	0.02	0.01
V	0.04	0.03	0.06	0.06	0.06	0.04	0.06	0.05	0.04	0.06	0.03	0.02
Fe	0.01	0.01	0.01	0.01	0.01	0.01	0.01	0.01	0.01	0.02	0.02	0.01
Mg	0.21	0.12	0.13	0.12	0.17	0.23	0.23	0.20	0.12	0.20	0.13	0.13
Sum Al position	2.03	1.92	1.85	1.90	2.07	2.02	2.03	2.00	1.90	1.95	2.01	2.00

<sup>a</sup> Total iron as FeO; cations calculated to Si = 6.

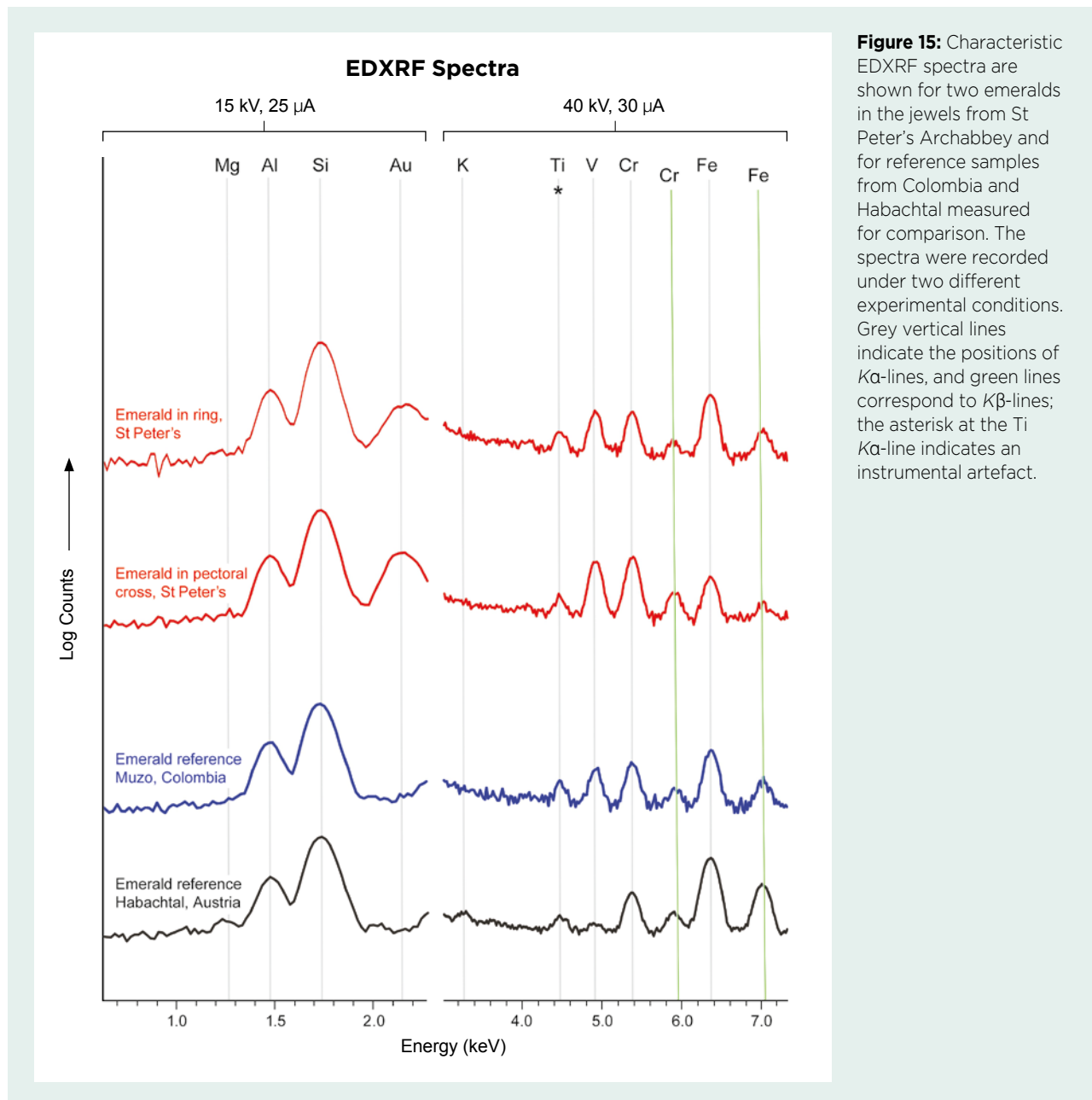
<sup>b</sup> P = pectoral and R = ring; the letters 'a' and 'b' indicate analyses of different spots on the same stone.

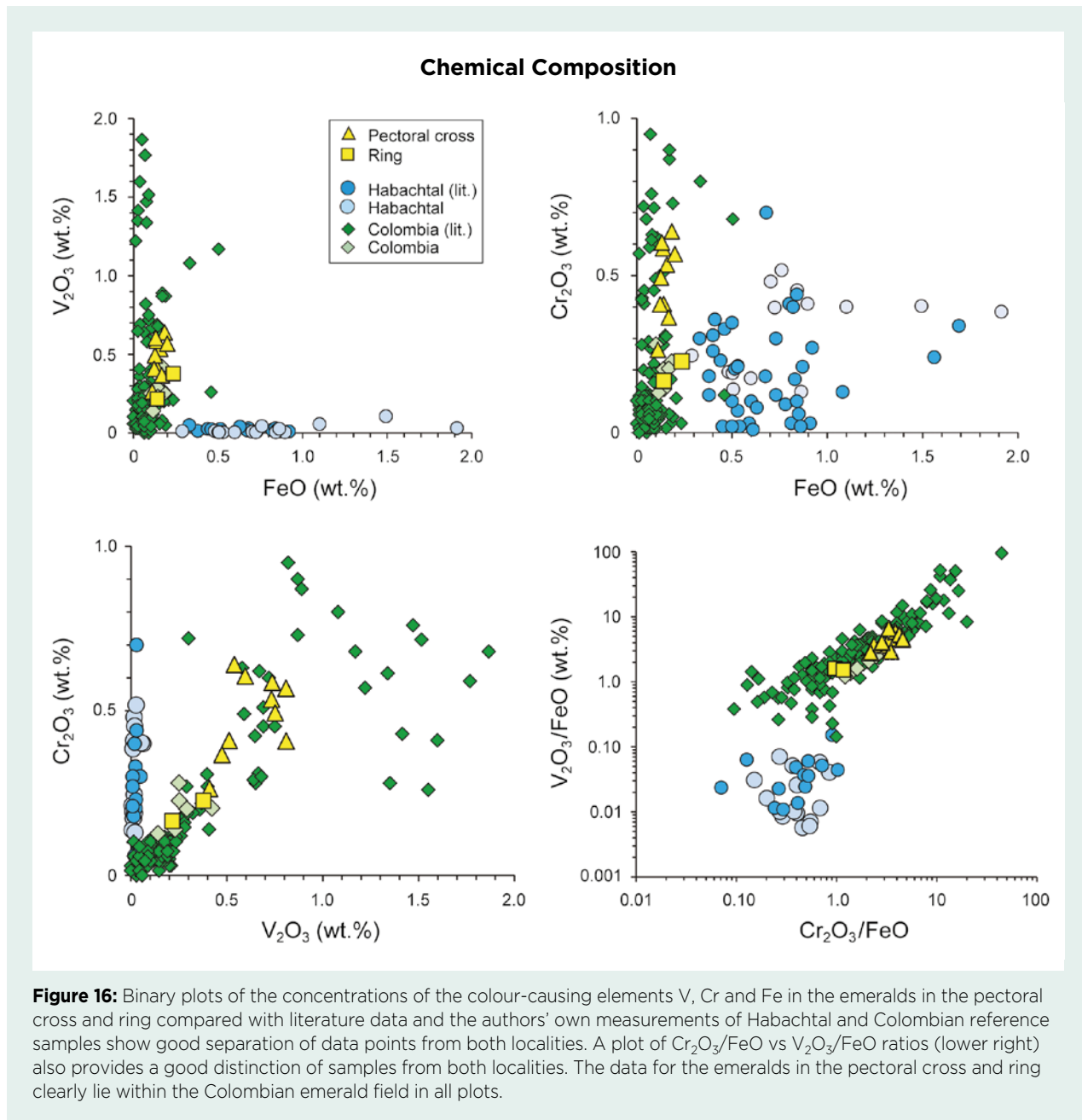
pectoral cross are shown in Figure 15 and compared to spectra of typical emeralds from Colombia and Habachtal. The spectra consist of two parts for each emerald according to the two different measurement conditions under vacuum (mainly for lighter elements) and in air. The intensities of the different peaks represent the chemical composition of the samples. The most significant variation in the EDXRF spectra is seen in the intensity of the V peak: emeralds in the pectoral cross and ring show similarities to the reference spectrum from Colombia, while the reference spectrum from Habachtal contains much less V.

The emeralds showed relatively low MgO contents (<1.7 wt.%), in some cases close to or at the detection

limit of our portable EDXRF unit. Due to the low energy of the characteristic Mg  $K\alpha$ -line, the Mg signal is very sensitive to absorption by air and thus is easily influenced by a non-ideal measurement geometry and by the vacuum level obtained with the portable pump system. This also applies somewhat to the Al signal, but plotting the  $Al_2O_3/SiO_2$  vs  $MgO/Al_2O_3$  ratios at least partly improves the situation and minimises the experimental errors (see below).

The concentrations of colour-causing trace elements in the emeralds of the pectoral cross and the ring (i.e. 0.11–0.24 wt.% FeO, 0.17–0.64 wt.%  $Cr_2O_3$  and 0.22–0.81 wt.%  $V_2O_3$ ) are in the range known for Colombian emeralds. The somewhat lighter green emerald in the ring had the lowest concentrations of Cr and V (see Table I).





The elements K, Rb, Ca and Sr were not detected—indicating the absence of inclusion minerals such as micas and Ca-bearing phases of carbonate-, apatite-, amphibole- or epidote-group minerals expected for Habachtal emeralds—and is consistent with our microscopic examination of the samples.

Various binary or ternary chemical plots have been applied in the literature to help differentiate the origin of emeralds (e.g. Giuliani *et al.* 2015, 2019; Aurisicchio *et al.* 2018; Karampelas *et al.* 2019). In Figure 16, the concentrations of the chromophore elements (V, Cr and Fe) in the emeralds of the pectoral cross and ring are plotted together with literature data for stones from Habachtal

(Bakakin *et al.* 1970; Hänni 1980; Grundmann 1983; Franz *et al.* 1986, 2020; Fillmann 1987; Schrader 1987; Aurisicchio *et al.* 1988, 2006, 2018; Schwarz 1991; Calligaro *et al.* 2000) and Colombia (Sinkankas 1981; Kozłowski *et al.* 1988; Schwarz 1992; Calligaro *et al.* 2000; Fritsch *et al.* 2002; Pignatelli *et al.* 2015; Svadlenak 2015; Aurisicchio *et al.* 2018; Häger *et al.* 2020). The diagrams also include data points for the reference emeralds from Habachtal and Colombia that we analysed with our portable EDXRF device; our data for these reference samples overlap with the literature, confirming the validity of our approach.

All of the data points for the emeralds from the pectoral cross and ring are consistent with a Colombian



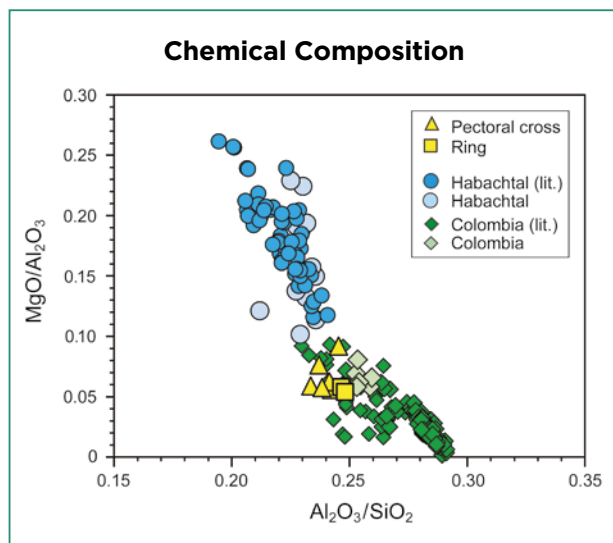


**Figure 17:** A plot of  $\text{Al}_2\text{O}_3/\text{SiO}_2$  vs  $\text{MgO}/\text{Al}_2\text{O}_3$  ratios also provides a good separation of Habachtal from Colombian emeralds. Again, the samples from the pectoral cross and ring plot within the compositional range of Colombian emeralds.

origin. According to the time frame of the pectoral cross and ring, there are no other known and relevant historical emerald deposits to consider with the exception of those in Egypt. Data for Egyptian emeralds overlap those from Habachtal for the trace elements considered here (H. A. Gilg, unpublished), and thus Egypt is also excluded as a possible origin of these emeralds.

A plot of  $\text{Al}_2\text{O}_3/\text{SiO}_2$  vs  $\text{MgO}/\text{Al}_2\text{O}_3$  ratios (Figure 17) also shows different population fields for Habachtal and Colombian emeralds and, again, that the stones from the pectoral cross and ring have compositions consistent with those of Colombian emeralds. Using this type of diagram reduces, at least partly, the influence of the measurement geometry on the Mg, Al and Si peaks and the low energy of the Mg signal. The chemical difference between the two groups of emeralds shown in this plot is mainly due to the lower Mg and higher Al contents of Colombian emeralds compared to those from Habachtal.

### Historical Inferences

The pectoral cross and ring were donated to Abbot Hagenauer in March 1786, about two months after his election. Differences in the cutting styles of the emeralds,

and particularly the diamonds, as well as the characteristics of the complete design of the Abbot's insignia, indicate that the two pieces of jewellery were probably made by different goldsmiths, most likely in different workshops. The table-cut diamonds in the ring show cutting styles used in previous centuries before the donation of the jewels, and even later, in the nineteenth century (see, e.g. Tillander 1995; Ogden 2018). The rose cuts of the diamonds in both pieces are later styles (typical for the seventeenth and eighteenth centuries) than the simple table cuts prepared in the centuries before. In both cases, we assume that the goldsmiths simply used the diamonds available to them in their workshops, either as recently faceted gems or diamonds salvaged from older jewels. A different time period for the manufacture of the two objects is possible, but not certain.

Given the presence of some table-cut diamonds in the ring, and the general use of this type of jewellery object, it seems possible that the ring might have been older than the other jewel, having been owned by the Weiser family for some time—years or even decades—before 1786. The pectoral cross, a special piece of jewellery used more exclusively by abbots and bishops, was most likely ordered by the Hagenauer family shortly after the Abbot's election and would have been prepared by a different goldsmith with the gemstones available to his workshop in 1786.

## CONCLUSIONS

A pectoral cross and ring donated in 1786 to Abbot Dominikus Hagenauer of St Peter's Abbey in Salzburg contain a total of ten emeralds. Although oral tradition dictates that these emeralds are from the Habachtal deposit in Austria, their inclusion pattern points to a Colombian origin. This is confirmed by chemical data, in which plots of the main and trace elements overlap the population fields of Colombian emeralds, and the data points are clearly separated from those of Habachtal. The overall visual appearance of the emeralds—particularly those in the pectoral cross which contain few inclusions—is also much more consistent with a Colombian origin compared to Habachtal.

## REFERENCES

- Angermüller, R. 2006. Leopold Mozart und Dominicus Hagenauer 1786/87. In: Fuchs, I. (ed) *Festschrift Otto Biba zum 60. Geburtstag*. Hans Schneider Verlag, Tutzing, Germany, 151–186.
- Auriscchio, C., Fioravanti, G., Grubessi, O. & Zanazzi, P.F. 1988. Reappraisal of the crystal chemistry of beryl. *American Mineralogist*, **73**(7–8), 826–837.

- Auriscchio, C., Corami, A., Ehrman, S., Graziani, G. & Cesaro, S.N. 2006. The emerald and gold necklace from Oplontis, Vesuvian area, Naples, Italy. *Journal of Archaeological Science*, **33**(5), 725–734, <https://doi.org/10.1016/j.jas.2005.10.011>.
- Auriscchio, C., Conte, A.M., Medeghini, L., Ottolini, L. & De Vito, C. 2018. Major and trace element geochemistry of emerald from several deposits: Implications for genetic models and classification schemes. *Ore Geology Reviews*, **94**, 351–366, <https://doi.org/10.1016/j.oregeorev.2018.02.001>.
- Bakakin, V.V., Rylov, G.M. & Belov, N.V. 1970. X-ray diffraction data for identification of beryl isomorphs. *Geochemistry International*, **7**(6), 924–933.
- Bauer, M. & Schloßmacher, K. 1932. *Edelsteinkunde*, 3rd edn. Bernhard Tauchnitz, Leipzig, Germany, 871 pp. (see p. 536).
- Bosshart, G. 1991. Emeralds from Colombia (part 2). *Journal of Gemmology*, **22**(7), 409–425, <https://doi.org/10.15506/JoG.1991.22.7.409>.
- Calligaro, T., Dran, J.C., Poirot, J.P., Querré, G., Salomon, J. & Zwaan, J.C. 2000. PIXE/PIGE characterisation of emeralds using an external micro-beam. *Nuclear Instruments and Methods in Physics Research Section B: Beam Interactions with Materials and Atoms*, **161–163**, 769–774, [https://doi.org/10.1016/S0168-583X\(99\)00974-X](https://doi.org/10.1016/S0168-583X(99)00974-X).
- Dopsch, H. & Juffinger, R. 1982. *Das älteste Kloster im deutschen Sprachraum: St. Peter in Salzburg*. Salzburger Landesregierung, Kulturabteilung, Salzburg, Germany, 431 pp. (see pp. 399–400), <http://opac.regesta-imperii.de/id/189366>.
- Fillmann, K. 1987. *Gefügekundliche und genetische Aspekte von Einschlüssen in Smaragden ausgewählter Lagerstätten*. Diplomarbeit, University of Mainz, Germany.
- Franz, C., Grundmann, G. & Ackermann, D. 1986. Rock forming beryl from a regional metamorphic terrain (Tauern Window, Austria): Parageneses and crystal chemistry. *Tschermaks Mineralogische und Petrographische Mitteilungen*, **35**(3), 167–192, <https://doi.org/10.1007/bf01082084>.
- Franz, G., Vyshnevskiy, O., Taran, M., Khomenko, V., Wiedenbeck, M., Schiperski, F. & Nissen, J. 2020. A new emerald occurrence from Kruta Balka, western Peri-Azovian region, Ukraine: Implications for understanding the crystal chemistry of emerald. *American Mineralogist*, **105**(2), 162–181, <https://doi.org/10.2138/am-2020-7010>.
- Fritsch, E., Rondeau, B., Notari, F., Michelou, J.-C., Devouard, B., Peucat, J.-J., Chalain, J.-P., Lulzac, Y. et al. 2002. Les nouvelles mines d'émeraude de La Pita (Colombie) 2<sup>e</sup> partie. *Revue de Gemmologie A.F.G.*, No. 144, 13–21.
- Giuliani, G., Cheilletz, A., Arboleda, C., Carrillo, V., Rueda, F. & Baker, J.H. 1995. An evaporitic origin of the parent brines of Colombian emeralds: Fluid inclusion and sulphur isotope evidence. *European Journal of Mineralogy*, **7**(1), 151–166, <https://doi.org/10.1127/ejm/7/1/0151>.
- Giuliani, G., France-Lanord, C., Coget, P., Schwarz, D., Cheilletz, A., Branquet, Y., Giard, D., Martin-Izard, A. et al. 1998. Oxygen isotope systematics of emerald: Relevance for its origin and geological significance. *Mineralium Deposita*, **33**(5), 513–519, <https://doi.org/10.1007/s001260050166>.
- Giuliani, G., Chaussidon, M., Schubnel, H.-J., Piat, D.H., Rollion-Bard, C., France-Lanord, C., Giard, D., de Narvaez, D. et al. 2000. Oxygen isotopes and emerald trade routes since antiquity. *Science*, **287**(5453), 631–633, <https://doi.org/10.1126/science.287.5453.631>.
- Giuliani, G., Chaussidon, M., France-Lanord, C., Savay-Guerraz, H., Chiappero, P.-J., Schubnel, H.-J., Gavrilenko, E. & Schwarz, D. 2001. L'exploitation des mines d'émeraudes d'Autriche et de la Haute-Egypte à l'époque gallo-romaine : Mythe ou réalité? *Revue de Gemmologie A.F.G.*, No. 143, 20–24.
- Giuliani, G., Branquet, Y., Fallick, A.E., Groat, L.A. & Marshall, D. 2015. Emerald deposits around the world, their similarities and differences. *InColor*, Special Issue, December, 56–69.
- Giuliani, G., Groat, L.A., Marshall, D., Fallick, A.E. & Branquet, Y. 2019. Emerald deposits: A review and enhanced classification. *Minerals*, **9**(2), article 105 (63 pp.), <https://doi.org/10.3390/min9020105>.
- Grundmann, G. 1981. Die Einschlüsse der Berylle und Phenakite des Smaragdorkommens im Habachtal (Land Salzburg, Österreich). *Der Karinthin*, No. 84, 227–237.
- Grundmann, G. 1983. *Die Genese der regionalmetamorphen, metasomatisch-horizontgebunden Beryll-Mineralisationen des Habachtals, Land Salzburg, Österreich*. Dissertation, Technical University of Berlin, Germany, 207 pp.
- Grundmann, G. 1984. Die Einschlußwelt der Habachtaler Smaragde. *Mineralientage München '84 "Schätze der Alpen"*, Munich, Germany, 26–28 October, 48–53.
- Grundmann, G. 1991. *Smaragd*. extraLapis No. 1, Christian Weise Verlag, Munich, Germany, 93 pp.
- Gübelin, E. 1940. Differentiation between Russian and Colombian emeralds. *Gems & Gemology*, **3**(6), 89–92.
- Gübelin, E.J. 1956. Emerald from Habachtal. *Journal of Gemmology*, **5**(7), 342–361, <https://doi.org/10.15506/JoG.1956.5.7.342>.
- Gübelin, E.J. & Koivula, J.I. 1986. *Photoatlas of Inclusions in Gemstones*. ABC Edition, Zurich, Switzerland, 532 pp.

- Gübelin, E.J. & Koivula, J.I. 2008. *Photoatlas of Inclusions in Gemstones*, Vol. 3. Opinio Publishers, Basel, Switzerland, 672 pp.
- Häger, T., Rojas-Agramonte, Y., Charris-Leal, F., Villalobos-Basler, J.D., Gonzalez-Pinzon, M.A. & Hauzenberger, C. 2020. Smaragde aus Kolumbien. *Gemmologie: Zeitschrift der Deutschen Gemmologischen Gesellschaft*, **69**(1/2), 47–57.
- Hagn, K. 2019. Das “grüne Gold” aus den Tauern. *Salzburger Nachrichten, Juwelen & Uhren Weihnachtsjournal 2019*, 40–43.
- Hagn, K. 2021. Das grüne Gold. *Salzburger Nachrichten, Treffpunkt Salzburg*, September, 18.
- Hanke, H. 1958. Smaragde aus dem Habachtal. *Kosmos*, **54**(8), 320–324.
- Hänni, H.A. 1980. *Mineralogische und mineralchemische Untersuchungen an Beryll aus alpinen Zerrklüften*. Dissertation, University of Basel, Switzerland, 107 pp.
- Karampelas, S., Al-Shaybani, B., Mohamed, F., Sangsawong, S. & Al-Alawi, A. 2019. Emeralds from the most important occurrences: Chemical and spectroscopic data. *Minerals*, **9**(9), article 561 (29 pp.), <https://doi.org/10.3390/min9090561>.
- Kozłowski, A., Metz, P. & Estrada Jaramillo, H.A. 1988. Emeralds from Somondoco, Colombia: Chemical composition, fluid inclusions and origin. *Neues Jahrbuch für Mineralogie, Abhandlungen*, **159**(1), 23–49.
- Ogden, J. 2018. *Diamonds: An Early History of the King of Gems*. Yale University Press, New Haven, Connecticut, USA and London, 408 pp.
- Pignatelli, I., Giuliani, G., Ohnenstetter, D., Agrosi, G., Mathieu, S., Morlot, C. & Branquet, Y. 2015. Colombian trapiche emeralds: Recent advances in understanding their formation. *Gems & Gemology*, **51**(3), 222–259, <https://doi.org/10.5741/gems.51.3.222>.
- Rudolph, S. 2021. Zwei Monstranzen aus dem Salzburger Domschatz. In: Witting, T. & Weinhold, U. (eds) *Farbfassungen auf Gold und Silber*. Sandstein Kommunikation GmbH, Dresden, Germany, 172–181, <https://doi.org/10.11588/arthistoricum.864.C11240>.
- Schmetzer, K. 2021. History of emerald mining in the Habachtal deposit of Austria, part I. *Gems & Gemology*, **57**(4), 338–371, <https://doi.org/10.5741/gems.57.4.338>.
- Schmetzer, K. 2022. History of emerald mining in the Habachtal deposit of Austria, part II. *Gems & Gemology*, **58**(1), 18–46, <https://doi.org/10.5741/gems.58.1.18>.
- Schrader, H.W. 1987. *Natürliche und synthetische Smaragde. Ein Beitrag zur Kristallchemie der Berylle*. Dissertation, University of Mainz, Germany, 204 pp.
- Schroll, K.M. 1797. Grundriss einer Salzburgerischen Mineralogie. *Jahrbücher der Berg- und Hüttenkunde*, **1**, 95–196.
- Schwarz, D. 1991. Die chemischen Eigenschaften der Smaragde III. Habachtal/Österreich und Uralgebirge/UdSSR. *Zeitschrift der Deutschen Gemmologischen Gesellschaft*, **40**(2/3), 103–143.
- Schwarz, D. 1992. The chemical properties of Colombian emeralds. *Journal of Gemmology*, **23**(4), 225–233, <https://doi.org/10.15506/JoG.1992.23.4.225>.
- Sinkankas, J. 1981. *Emerald and Other Beryls*. Chilton Book Company, Radnor, Pennsylvania, USA, 665 pp.
- Stehrer, S. 2000. Rätsel um Smaragd geklärt. *Salzburger Nachrichten, Juwelen & Uhren Weihnachtsjournal*, **56**, 11 April, 11.
- Svadlenak, E. 2015. *<sup>40</sup>Ar/<sup>39</sup>Ar ages and trace element variations in Colombian emeralds*. BS (Hons) thesis, Oregon State University, Corvallis, Oregon, USA, 59 pp., [https://ir.library.oregonstate.edu/concern/honors\\_college\\_theses/9c67ws368](https://ir.library.oregonstate.edu/concern/honors_college_theses/9c67ws368).
- Thomas, R., Davidson, P. & Rericha, A. 2020. Emerald from the Habachtal: New observations. *Mineralogy and Petrology*, **114**(3), 161–173, <https://doi.org/10.1007/s00710-020-00700-4>.
- Tillander, H. 1995. *Diamond Cuts in Historic Jewellery: 1381–1910*. Art Books International, London, 248 pp.

### The Authors

#### Dr Karl Schmetzer

Taubenweg 16, 85238 Petershausen, Germany  
Email: SchmetzerKarl@hotmail.com

#### Prof. Dr H. Albert Gilg

Chair of Engineering Geology, School of Engineering and Design, Technical University of Munich, Arcisstr. 21, 80333 Munich, Germany  
Email: agilg@tum.de

### Acknowledgements

The authors are grateful to Dr Korbinian Birnbacher, archabbot of St Peter's Archabbey in Salzburg, for permission to examine the pectoral cross and ring of Dominikus Hagenauer, and to Norbert E. Urban, our host at the premises of the mineral collection of St Peter's during the examination. We also thank Dr Dietmar Schwarz (Bangkok, Thailand) and Dr Tobias Häger (Mainz, Germany) for providing the Colombian emerald standards, as well as Christian Weise (Munich, Germany), who provided the reference emeralds from Habachtal.

# Conferences

## AGA LAS VEGAS CONFERENCE

The 2022 Accredited Gemologists Association (AGA) conference took place on 9 June during the JCK Show in Las Vegas, Nevada, USA. It was the first time AGA held an in-person conference since the COVID-19 pandemic began. The event was attended by 62 people and featured three speakers focusing on diamonds. The conference was opened by AGA president **Teri Brossmer**, who also introduced the speakers.

**Martin Rapaport** (Rapaport Group, New York, New York, USA) discussed the state of the global diamond industry (Figure 1). First he examined the interactions between the lingering effects of the COVID-19 pandemic and current economic and social transformations. China's restrictive response to COVID-19 has stalled diamond demand in that country, while sanctions over Russia's war with Ukraine also threaten the diamond supply chain since 30% of global rough production comes from Alrosa. Changing social values are reflected by growing universal concerns over climate change and social responsibility, and are coming at a time when millennials are getting older (and potentially buying engagement rings). Rapaport then emphasised the importance of creating an ethical diamond market, including a fully audited certification process in which mines and manufacturers must provide full and honest

disclosure of their sources. He closed by stressing that the essence of our business is about the symbolic emotional value of diamonds—and how they make people feel—rather than being about the diamonds themselves.

**Michael Goren** (Sarine Technologies, Sofia, Bulgaria) covered technology-driven innovations and their impact on diamond traceability and grading. He described how a diamond can be traced at each step—from producer to manufacturer to grading laboratory to retailer—using blockchain technology. A high level of integrity and trustworthiness can be attained by using automated systems that independently create and collate verifiable data collected at various stages (i.e. from the rough stone through various stages of planning, cutting and polishing, and finally the finished stone), and this can be augmented by additional pertinent information about the diamond, as found in Sarine's 'Diamond Journey' reports. Goren then described newly developed automated diamond grading technology that uses artificial intelligence. The system utilises precision technology with self-monitoring capabilities, and grading is done in the cloud using algorithms and a 'crowd wisdom' approach which includes data on diamonds pre-graded by multiple gemmologists and the use of a machine-learning system to perform certain predictions.



**Figure 1:** Martin Rapaport delivers his presentation on the state of the diamond industry at the AGA Conference in Las Vegas. Photo by B. M. Laurs.

**Dr Yun Luo** and **Thomas M. Moses** (Gemological Institute of America, New York) discussed the impact of blue fluorescence on diamond appearance, referring to an article published in the Summer 2021 issue of *Gems & Gemology* (Vol. 57, No. 2, pp. 102–123). They explained that a diamond's colour is only occasionally impacted in stones which have strong to very strong blue fluorescence, and this impact also depends on the amount of UV component in the viewing environment. The hazy

appearance sometimes observed in diamonds with strong fluorescence is not produced by the fluorescence itself—which instead causes minor contrast loss—but rather is primarily due to atomic-scale light-scattering defects or nano-inclusions.

The next AGA conference will take place during the February 2023 gem and mineral shows in Tucson, Arizona, USA.

*Brendan M. Laurs FGA*

## 23RD GENERAL MEETING OF THE INTERNATIONAL MINERALOGICAL ASSOCIATION

On 18–22 July 2022, the quadrennial meeting of the International Mineralogical Association (IMA) took place at the Cité Centre de Congrès in Lyon, France. The conference featured a series of plenary lectures and several parallel sessions of oral presentations on a variety of mineralogical topics. A 653-page abstracts volume can be downloaded at [https://www.ima2022.fr/medias/content/files/interventions\\_abstracts\\_v4.pdf](https://www.ima2022.fr/medias/content/files/interventions_abstracts_v4.pdf). The conference featured three sessions on gems: (1) Gemstones from the Deep: A Celebration of the Career of George E. Harlow; (2) Haiyi 200 Years On: What News [*sic*] in Gem Research? (honouring the career of Dr Gaston Giuliani); and (3) Mineralogy and Gemology in Cultural Heritage. In addition, various presentations of interest to gemmologists were given in other sessions. Oral presentations attended by this author are summarised below.

In light of the session in his honour, **Dr George Harlow** (American Museum of Natural History, New York, USA) chronicled the history of his career, in which he built collections, organised exhibitions and performed geological fieldwork around the world while researching jade, ruby, etc. He also described the power of collections for research, education and exhibitions, as well as for providing an archive of our planet and universe. In another presentation in this session, **Dr Emmanuel Fritsch** (IMN-CNRS and University of Nantes, France) and colleagues reviewed blue short-wave UV luminescence in minerals and gems (i.e. blue sapphire, tourmaline, synthetic spinel and dumortierite). Proving the origin of the blue fluorescence is difficult, but it is likely related to titanate ( $\text{TiO}_6$ ) groups with a relatively short Ti–O distance of less than 2 Å.

Emerald was the subject of three presentations. **Dr Gaston Giuliani** (IRD and CRPG, University of Lorraine, Nancy, France) announced the publication of his new book titled *Émeraudes, Tout un Monde !* (Figure 2), which was released in July 2022. The book, which is

entirely in French, was edited by Dr Giuliani and consists of 65 articles by 86 authors on the geological, geochemical, gemmological, historical and societal aspects of emeralds. Dr Giuliani then reviewed his classification for the genetic types of emerald deposits, giving examples of each type and explaining their origins. **Dr Isabella Pignatelli** (University of Lorraine, Nancy, France) and co-authors used X-ray computed tomography to investigate unusual specimens of Colombian emerald (see their article in *The Journal*, Vol. 38, No. 1, 2022, pp. 26–43).

**Dr Stefanos Karampelas** (Laboratoire Français de Gemmologie, Paris, France) and co-authors performed a gemmological study of a 3.19 ct faceted emerald, reportedly from Egypt, in the collection of the Paris School of Mines museum. The stone was probably acquired by the museum in the mid- to late-19th century. The gemmological properties all indicated a Colombian source, thus invalidating its reported Egyptian origin.

Several presentations covered gem corundum. **Dr Pornsawat Wathanakul** (Kasetsart University, Bangkok, Thailand) proposed a revised cause of blue colouration in sapphire:  $\text{Fe}^{3+}$ – $\text{Ti}^{4+}$  electron-acceptor pairs. XANES spectroscopy of various blue sapphire samples (natural, heated, diffusion-treated and synthetic) confirmed that Ti is present as  $\text{Ti}^{4+}$ , but also that Fe exists only as  $\text{Fe}^{3+}$ , thus negating the long-held concept of intervalence charge transfer between  $\text{Fe}^{2+}$  and  $\text{Ti}^{4+}$  causing blue colouration. **Dr Wei Zhou** and colleagues (Swiss Gemmological Institute SSEF, Basel, Switzerland) discussed the geographic origin determination of blue sapphires from Kashmir and Madagascar (Andranondambo) using trace-element contents. Natural chemical zoning resulted in variations in the elements that were measured (i.e. Zr, Nb, Sn, La, Ce, Hf, Ta and W in Madagascar samples, and Nb, Sn, Ta and W in Kashmir sapphires). **Dr Elena Sorokina** (Johannes Gutenberg-Universität Mainz, Germany) and co-authors investigated

the age and formation conditions of ruby mineralisation in the eastern Pamir Mountains. Rb-Sr dating yielded an age of  $23 \pm 1.6$  million years, similar to ruby deposits in Myanmar and Afghanistan. Pamir rubies formed at unusually low pressures (minimum of 1–1.2 kbar) and a temperature of approximately 760°C. **Wim Vertrieet** (Gemological Institute of America [GIA], Bangkok, Thailand) and co-authors reviewed the identification of low-temperature heat treatment of gem corundum (i.e. up to about 1200°C, which starts causing damage to rutile ‘silk’ inclusions). This treatment is commonly applied to optimise the colour of pink sapphire from Ilakaka (Madagascar) and ruby from Mozambique, and also to lighten blue sapphire. The treatment may have subtle but unpredictable effects on the visual appearance of inclusions. FTIR spectroscopy can show changes in the  $3309\text{ cm}^{-1}$  OH-related band, which may develop new features at  $3232$  and  $3185\text{ cm}^{-1}$  if the band is strong enough to begin with. **Dr Michael Jollands** (GIA, New York, New York, USA) and **Dr Etienne Balan** (Sorbonne University, Paris, France) studied how Be is incorporated into corundum. They used ‘density functional theory’ to suggest that in the Be-Al-O system, Be is likely in triangular coordination in corundum (i.e. bonded to three oxygens on the basal plane of a normally occupied octahedral site). When H is present, OH groups form at the opposite face of the octahedron, and Be-H defects are also possible (in which Be is bonded to three O and one H).

Several presentations covered tourmaline. **Drs Barbara Dutrow** and **Darrell J. Henry** (Louisiana State University, Baton Rouge, Louisiana, USA) reported on green Mg-rich gem tourmalines (mainly dravite and uvite) from

Tanzania coloured by V, Cr and Ti. The tourmalines formed in two different geological environments (calcitic marbles or gneisses), and showed attractive green colouration only when their chromophores were present in appropriate amounts (not too high or low). Otherwise, the stones appeared over-dark or had undesirable yellow or brown colour modifiers. In another presentation, **Dr Dutrow** and co-authors investigated the origin determination of Cu-bearing tourmaline using statistical analyses of LIBS and electron microprobe data. The three localities—Brazil, Mozambique and Nigeria—were correctly identified with over 95% accuracy. **Dr Henry** then reviewed tourmaline nomenclature and the classification of tourmaline group minerals in separate presentations. **Dr Vanni Moggi Cecchi** (Natural History Museum, University of Florence, Italy) and colleagues described the process of cleaning and restoring two exceptional historic matrix specimens of tourmaline from Elba Island in Italy. They were mined in 1881 and sold to the museum in 1882. After many decades they were in need of special attention to remove dust and old glue, and to repair several broken crystals. The cleaning and restoration process was completed at the Mineralogical Collection Professionals laboratory in Italy. **Alessandra Altieri** (Sapienza University of Rome, Italy) and co-authors correlated the colouration and composition of gem tourmaline crystals from Elba Island. Specifically, dark-coloured caps at the terminations of the crystals show enrichments in Fe and Mn that are due to late-stage opening of the geochemical system via the rupture of the gem-bearing cavities. **Floriana Rizzo** (University of Bari Aldo Moro, Italy) and co-authors performed chemical analysis and single-crystal X-ray

**Figure 2:** Dr Gaston Giuliani highlights his new book on emerald during an IMA session honouring his career, while co-chair Dr Isabella Pignatelli looks on. Photo by B. M. Laurs.



diffraction on a slice of oscillatory-zoned polychrome tourmaline from the Anjanabonoina pegmatite in Madagascar. Most of the zones consisted of fluor-liddicoatite, whereas the brownish yellow core was Mn-rich fluor-elbaite containing a small amount of Ti.

Jade was the subject of several presentations, and three of them were of interest to a gemmological audience. **Dr Samuel Angiboust** (Ecole Normale Supérieure de Lyon, France) and co-authors studied deformed jadeitites from Myanmar, the Polar Urals (Russia) and Guatemala, and found that white jadeite formed first and was then followed (at a lower temperature) by domains of green jadeite, marking a tectonic overprint associated with repeated deep earthquakes in the mantle wedge. **Dr Hans-Peter Schertl** and **Dr Walter V. Maresch** (Institute of Geology, Mineralogy and Geophysics, Ruhr-University Bochum, Germany) documented the geological origin of omphacite jade from the Dominican Republic, which formed due to a combination of fluid-driven mass transport and the metamorphism of plagiogranite. **Jean-Claude Vannay** (Musée Cantonal de Géologie, Lausanne, Switzerland) and co-authors investigated jade pebbles from rivers draining the Swiss Plateau. Three types were distinguished: (1) jadeitites with 75–89 vol.% jadeite, (2) omphacitites with 77–94 vol.% omphacite and (3) omphacite-kyanite-clinozoisite rocks with 56–73 vol.% omphacite. The last type is the most common, and is the first-known kyanite-bearing jade.

In other presentations on coloured stones, **Dr Jean-Emmanuel Martelat** (Université Claude Bernard Lyon 1, Lyon, France) and co-authors reviewed the geology of tsavorite deposits in southern Kenya, which are hosted along a north-south-trending corridor for more than 100 km. They are inferred to have formed at pressures ranging from 4 to 10 kbar and at high temperatures (granulite-facies conditions). The low Fe content of the tsavorite shows parallels with Colombian emerald (i.e. likely due to an evaporite-related origin and the removal of Fe from the system via pyrite crystallisation). **Dr Stefanos Karampelas** and co-authors studied garnet inclusions in five gem-quality sapphires from Tanzania (e.g. Figure 3). SEM-EDS chemical analysis of surface-reaching inclusions in some of the samples yielded a pyrope-rich composition (about 45%) along with some almandine (about 35%) and grossular (about 20%) components. Raman analyses suggested that all the garnet inclusions had similar compositions and that most likely they are mantle derived. **Dr Vladimir Khomenko** (National Academy of Sciences of Ukraine, Kyiv, Ukraine) and **Dr Gerhard Franz** (Technische Universität Berlin, Germany)

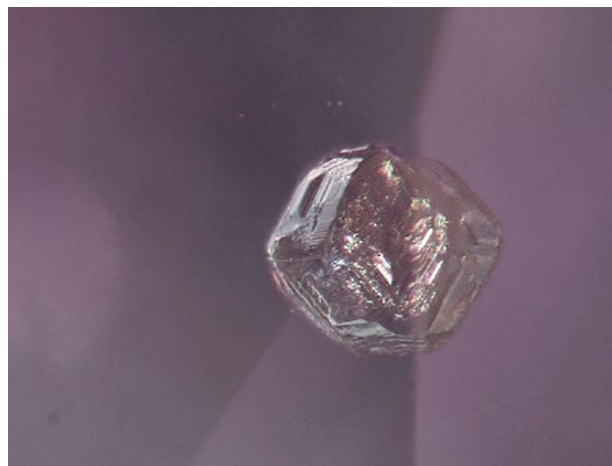


**Figure 3:** A euhedral garnet inclusion is present in a 1.44 ct colour-change sapphire (greenish blue to purple) from Tanzania. Photomicrograph by Ugo Hennebois/LFG; image width 0.8 mm.

investigated gem-quality heliodor from Ukraine, and found that low contents of both type I and type II H<sub>2</sub>O, and the presence of H<sub>2</sub>S and CO (indicating reducing conditions), are diagnostic of heliodor from this locality. **Dr Féodor Blumentritt** (IMN-CNRS and University of Nantes, France; and GGTL Laboratories Switzerland, Genève, Switzerland) and co-authors examined the central role of the Cl vacancy in the photochromism of hackmanite and scapolite. The authors correlated the size of the vacancy with variations in the photogenerated colouration, providing strong evidence for the Cl vacancy causing the purple colour of hackmanite and the blue colour of marialite. **Dr Lutz Nasdala** (University of Vienna, Austria) and co-authors explained the unusual embayed surface texture on gem-quality pebbles of metamict ekanite from Sri Lankan gem placers as being due to alteration that presumably occurred during a late metamorphic stage or hydrothermal overprint. The softer altered material later was removed during weathering and alluvial transport, leaving concave surface patterns on the ekanite pebbles.

Various poster presentations at the IMA conference covered topics of interest to gemmologists, including: hydrogen in natural diamond; nitrogen-vacancy photochromic effects on the colour of pink diamond; rapid screening for photochromism in sapphire using absorption spectroscopy; portable Raman spectroscopy for mineral identification; fluorescence spectroscopy for pearl identification; Raman spectroscopy of Pb-rich tourmaline from Minh Tien, Vietnam; the occurrence and origin of gems and minerals from northern Pakistan; and the crystal chemistry of tourmaline from Minas Gerais, Brazil.

*Brendan M. Laurs FGA*

# Gem-A Notices

## MESSAGE FROM GEM-A CEO ALAN HART



I hope you enjoy this issue of *The Journal of Gemmology*. We continue living in challenging times as we grapple with global uncertainties due to the current geopolitical landscape, cost of living crisis, economic downturn and impending recession. It is in times of

difficulty that we call on the collective strength and resilience of our staff, Membership, students and partners as we navigate through these complexities to continue providing much-needed gemmology education and Membership services to support the gem and jewellery trade. To that end, Gem-A now has a hybrid working policy. We are proud to offer this flexibility to our staff, allowing them to work both in-office and at home.

This is not unlike the choice our students have in pursuing their coursework online or at an Accredited Teaching Centre. And in that regard, we have again shifted gears: while we continue to offer online courses to our ODL students, we were thrilled to welcome our in-person students back to Ely Place for the term starting this autumn.

Looking further ahead, I am delighted to announce that the Gem-A Conference will make an in-person return this autumn on Sunday 6 November. Registration for the conference and gala dinner are now open, and I encourage you to sign up soon. I personally look forward to offering a warm welcome to many of our Members and associates whom we have not had the opportunity to see for some time.

I would like to extend my sincerest thanks once again for your ongoing support and I look forward to seeing many of you again soon.

## GEMINTRO IS NOW TAKING REGISTRATIONS



*GemIntro* is the first entry-level course offered by Gem-A, and is available entirely online. Students can go at their own pace and discover the basics of gemmology from home. Participants will work towards an accredited Ofqual Level 2 qualification, accompanied by a formal Gem-A certificate. This interactive and informative course is designed for those who are already working in the gem and jewellery trade and want to develop their knowledge further, and also for gem enthusiasts who are curious about delving deeper into gemmology. Those wishing to explore the many career opportunities associated with the study and application of gemmology may

also find the course useful. Registrations are now being accepted (priced at £220), and students will have access to course materials for six months from the registration date. No previous qualifications or experience are required. More information can be found at <https://gemintro.gem-a.com>. To discuss becoming a *GemIntro* reseller or bulk licencing packages, email [education@gem-a.com](mailto:education@gem-a.com).



Join us on social media to keep up-to-date with the latest news, events and offers from Gem-A

 [facebook.com/GemAofGB](https://www.facebook.com/GemAofGB)  
 [@GemAofGB](https://twitter.com/GemAofGB)  
 [linkd.in/1GisBTP](https://www.linkedin.com/company/1GisBTP)

 Instagram: @gemaofgb  
 WeChat: Scan the QR code to add us on WeChat







## GEM-A CONFERENCE IS NOW TAKING REGISTRATIONS

The Gem-A Conference will make an in-person return on Sunday 6 November at etc.venues County Hall, which overlooks the River Thames and the Houses of Parliament. This year's event will feature seven expert speakers and will conclude with a much-anticipated gala dinner (also at etc.venues County Hall), which will provide a fantastic opportunity to network with other gemmologists and jewellery professionals in an informal setting. Registration for the conference and gala dinner are now open, and more information can be found at <https://gem-a.com/event/conference-2022>. On Monday 7 November, attendees will have the option to attend a series of workshops and field trips to make the absolute most of their visit to London.

## GEM-A GRADUATION AND PRESENTATION OF AWARDS

The Gem-A Graduation and Presentation of Awards ceremony will be held at the Royal Institution of Great Britain on Monday 7 November. The Graduation Ceremony celebrates the achievements of our most recent graduating class, including special awards and prize winners. The Royal Institution of Great Britain is a Grade I-listed building in the Mayfair district of central London, and was founded in March 1799 with the aim of introducing new technology and teaching science to the general public. On graduation night, attendees will have access to the Library and Georgian Room (traditional book-lined rooms with graceful Georgian architecture), and to the Faraday Museum situated on the ground floor.



## 2022 ANNUAL GENERAL MEETING

This year the Gem-A Annual General Meeting (AGM) will be held on Wednesday 26 October at 17:00. The AGM will be held at Gem-A's headquarters on Ely Place. To encourage participation from our global Membership base, voting on the resolutions will take place prior to the AGM via Civica Election Services. More information on the voting platform and access to the AGM documentation will be provided in due course.



## GIFTS TO THE ASSOCIATION

Gem-A is most grateful to the following for their generous donations that will support continued research and teaching:

**Elaine Gregson**, United Kingdom, for donating three pieces of ivory jewellery.

**Gabriel Kleinberg**, Gemmology Diploma student, United Kingdom, for donating a bracelet set with sapphires and garnet-topped doublets.

# Learning Opportunities

## CONFERENCES AND SEMINARS

### **Jewellery & Gem World Hong Kong**

16–19 September 2022

Hong Kong

<https://jgw.exhibitions.jewellerynet.com/specialevent>

*Note:* Includes a seminar programme

### **International Colored Gemstone Association (ICA) Congress**

23–25 September 2022

Shenzhen, China, and online

[www.gemstone.org/ica-congresses](http://www.gemstone.org/ica-congresses)

### **Jewellery & Gem World Singapore**

27–30 September 2022

Singapore

<https://jgws.g.exhibitions.jewellerynet.com/why-visit>

*Note:* Includes a seminar programme

### **The Munich Show**

30 September–2 October 2022

Munich, Germany

<https://munichshow.de/en/highlights-en>

*Note:* Includes a seminar programme

### **Geological Society of America Annual Meeting (GSA Connects 2022)**

9–12 October 2022

Denver, Colorado, USA, and online

<https://community.geosociety.org/gsa2022/home>

*Session of interest:* Gemological Research in the 21st Century—Gem Minerals and Localities

### **Canadian Gemmological Association (CGA) Conference**

21–23 October 2022

Vancouver, British Columbia, Canada

<https://canadiangemmological.com/2022-cga-conference-2>

### **GemGenève**

3–6 November 2022

Geneva, Switzerland

<https://gemgeneve.com>

*Note:* Includes a seminar programme

### **Gem-A Conference**

6 November 2022

London

<https://gem-a.com/event/conference-2022>

### **NAJA 59th Winter Education Conference**

29–30 January 2023

Tucson, Arizona, USA

<https://najaappraisers.com/event/59th-winter-education-conference>

### **AGTA GemFair Tucson**

31 January–5 February 2023

Tucson, Arizona, USA

<https://agta.org/agta-gem-fair-tucson/seminars>

*Note:* Includes a seminar programme

### **Tucson Gem and Mineral Show**

9–12 February 2023

Tucson, Arizona, USA

[www.tgms.org/show](http://www.tgms.org/show)

*Note:* Includes a seminar programme

### **Inhorgenta Munich**

24–27 February 2023

Munich, Germany

<https://www.inhorgenta.com/en>

*Note:* Includes a seminar programme

### **MJSA Expo**

5–7 March 2023

New York, New York, USA

[https://mjsa.org/eventsprograms/mjsa\\_expo](https://mjsa.org/eventsprograms/mjsa_expo)

### **Scottish Gemmological Association Conference**

28 April–1 May 2023

Location TBA

<https://www.scottishgemmology.org>

### **American Gem Society Conclave**

1–3 May 2023

Louisville, Kentucky, USA

<https://www.americangemsociety.org/conclave-2023>

**37th International Gemmological Conference (IGC 2023)**

22–26 May 2023

Tokyo, Japan

<https://www.igc-gemmology.org/igc-2023>*Note:* Includes pre- and post-conference field trips to jadeite deposits and a pearl farm.**JCK Las Vegas**

2–5 June 2023

Las Vegas, Nevada, USA

<https://lasvegas.jckonline.com/en-us.html>*Note:* Includes a seminar programme**Sainte-Marie-aux-Mines Mineral & Gem Show**

21–25 June 2023

Sainte-Marie-aux-Mines, France

[www.sainte-marie-mineral.com](http://www.sainte-marie-mineral.com)*Note:* Includes a seminar programme**Jewellery & Gem Asia Hong Kong**

22–25 June 2023

Hong Kong

<https://jga.exhibitions.jewellerynet.com/visiting-whyvisit>*Note:* Includes a seminar programme**OTHER EDUCATIONAL OPPORTUNITIES****Gem-A Workshops and Courses**

Gem-A, London

<https://gem-a.com/education>**GemIntro Course**

Gem-A, online

<https://gemintro.gem-a.com>**L'École Masterclass: From Prague to Dresden: Precious Gemstones, Jewels and Savoir-Faire of Saxony and Bohemia**

Germany and Czech Republic

29 September–2 October 2022

<https://www.lecolevancliefarpels.com/fr/en/masterclass-prague-dresden>**A History of Gemstones: Antiquity to the 19th Century**

Online

4–13 October 2022

<https://ruigalopim.com/events>**Travel with the Met: Uncover the Treasures of London**

London

6–12 October 2022

[https://www.metmuseum.org/-/media/files/join-and-give/travel-with-the-met/2021/jn-met-jewelry\\_1006\\_brochure.pdf](https://www.metmuseum.org/-/media/files/join-and-give/travel-with-the-met/2021/jn-met-jewelry_1006_brochure.pdf)**Gemstone Safari to Tanzania**

11–28 January 2023

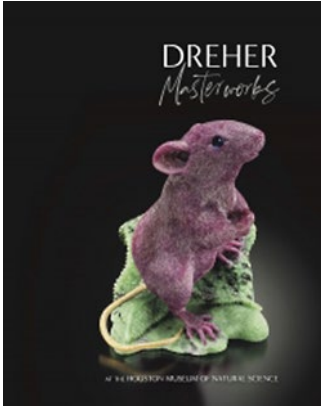
<https://www.free-form.ch/tanzania/gemstonesafari.html>**Lectures with The Society of Jewellery Historians**

Society of Antiquaries of London, Burlington House

[www.societyofjewelleryhistorians.ac.uk/current\\_lectures](http://www.societyofjewelleryhistorians.ac.uk/current_lectures)

- Maria Filomena Guerra—Fresh Scientific Insights in Ancient Egyptian Gold Technology  
27 September 2022
- Saltanat Amir—Gold Saka Microbeads: Early Iron Age Luxury in the Great Steppe and  
Abidemi Babalola—Not Just Jewellery: Glass Bead Technology, Economy, and Artistic Expression in Ile-Ife, Nigeria  
25 October 2022
- Usha Balakrishnan—Minakari: Where Flowers Bloom. The History & Art of Enamelling in India  
22 November 2022
- Natasha Awais-Dean—Jewels Captured in Perpetuity: The Jewellery Book of Anne of Bavaria  
24 January 2023
- Richard Edgecumbe—TBA  
28 February 2023
- Vivian Watson—History of Hatton Gardens  
28 March 2023
- Estelle Ottenwelter—Insight into Early Medieval Elite Jewellery from Bohemia  
23 May 2023
- Patrick Davison—Contemporary Maker Talking About His Own Work  
27 June 2023

# New Media



## Dreher Masterworks at the Houston Museum of Natural Science

By Gloria A. Staebler and Terry C. Wallace Jr, 2022.

Houston Museum of Natural Science, Houston, Texas, USA, and Lithographie, Denver, Colorado, USA, [https://www.lithographie.org/bookshop/dreher\\_masterworks.htm](https://www.lithographie.org/bookshop/dreher_masterworks.htm), 368 pages, illus., ISBN 978-1734131093. USD160.00 hardcover.

The book's forward by Joel A. Bartsch is a wonderfully written tribute describing his first experience seeing a carving by Gerd Dreher. Until then, he had never seen 'carvings that possessed the imagination and creativity that animated Gerd's wondrous works'. Joel's statement is embodied by this book, which showcases the many wondrous Dreher carvings that are on display at the Houston Museum of Natural Science (Texas, USA) through 29 May 2023.

Photos by Jeff Scovil (one of the great photographers of the gem and mineral world) are used throughout the book, mostly as full-page images and often showing an animal carving from more than one angle. The printing is done on paper of thick and luxurious quality using a seven-colour process so the carvings almost look real.

The main part of the book starts after introducing its various contributors, an amazing group of well-known experts. Chapter 1, titled 'In Continuum: Idar-Oberstein's Lapidary Heritage', covers the general history of the Hunsrück upland of Germany, where Idar-Oberstein is located—an enclave known for producing fine lapidary arts for over five centuries. I particularly like the authors' use on page 2 of a 1776 lithograph from Cosimo Collini, the director of the Mannheim Cabinet of Natural History.

His visit to the area depicts a 'remarkably sophisticated agate mining and cutting center'. Idar-Oberstein's lapidary industry was reluctant to adopt new tools, methods and materials, but that change came when German emigrants to Brazil began sending large quantities of agate and jasper to Idar-Oberstein. Italian methods of dyeing agate were introduced in 1819, and in ensuing decades the treatment techniques were improved—and kept secret. In the mid-nineteenth century, German carvers travelled to Paris to gain skills in cameo, intaglio and sculpture cutting, some working with Cartier or Fabergé. Later, Idar-Oberstein benefitted as this generation of carvers returned home.

Chapter 2, 'Intelligent Design: Animal Carvings from the House of Fabergé', is a synopsis of Fabergé, from Carl Fabergé's birth in St Petersburg, Russia, in 1846, to the House of Fabergé earning the coveted 'Goldsmith to the Imperial Crown' title in 1885. From 1890 until it closed in 1917, the company delivered 7,800 pieces annually. Carl was said to have once asked, 'Where shall I find enough craftsmen?' The first Fabergé carving commissions arrived in Idar-Oberstein around 1885, and the connection between Fabergé and Idar-Oberstein developed when dealer-broker Maritza Stern received orders and worked with local artisans to exceed the standards for craftsmanship demanded by Fabergé. The chapter makes the case that some of the works attributed to Fabergé might not have been done in Russia.

The founding of the Dreher legacy begins with Chapter 3, 'The World at War: The Winds of Change...' at the onset of World War I, with a well-written history of the Dreher family during those turbulent years. A wonderful photo on page 30 depicts three generations of Dreher's circa 1918. A sub-chapter titled 'The Golden Twenties' follows Paul Dreher, the first of the three Dreher's featured in this book. This chapter also revisits the Stern family, who were very active in Idar-Oberstein from the middle of the nineteenth century into the 1930s, and concludes when, following World War II, Paul Dreher returned home in 1948.

Chapter 4, titled 'Integrity: The Art of Paul Dreher', continues the story as Idar-Oberstein provided ample opportunities for the entrepreneurial artist. A subchapter covers Werner Stern, whose work brought him to Idar-Oberstein twice a year, sometimes accompanied by his daughter Marion. Werner met Paul Dreher and began acquiring the pieces that are now in the Marion Stern collection. Some of these are featured in this chapter in beautiful colour, starting with a carving of a penguin family on an ice floe.

Chapter 5, 'Innovation: The Torch Is Passed', chronicles the next phase in the Dreher family of carvers. Gerd

Dreher formally began his apprenticeship in 1955 when he was 16 years old. He was one of a post-war group of young lapidarists who became Idar-Oberstein legends, including Erwin Pauly, Dieter Jerusalem, and Bernd Munsteiner. Paul Dreher passed away in 1968, leaving the business to Gerd. One personal friend of this reviewer, David P. Wilber, is credited with recognising the Dreher talent and demanding that Gerd sign his work. Wilber's prominence within the gem and mineral world helped spread the Dreher name, and many core clients came from this community, myself included. Gerd took the mosaic concept of lapidary art to the next level and developed a more elaborate natural pose for his objects. By 1985 Gerd was established as an 'artist in his own right'. Four beautiful colour pages include a two-page spread of a peacock 'composed of upward of 350 individual pieces'.

Chapter 6 is titled 'Ingenuity: Gerd Dreher, Carving Artist'. The 1980s brought change with the invention of diamond-sintered tools, which allowed minute details and intricate carving of harder materials such as ruby. The new tools were expensive and the learning curve steep. Gerd studied the family's drawings and sketches for inspiration. He said, 'As a fourth generation of this family legacy I am determined to keep raising the standard of our carvings'. Through keen observation and research, Gerd developed an extraordinary ability to read stones and visualise the creature he could see residing in them. The text brilliantly describes Gerd's vision and multistep process.

Gerd and his wife Brigitte wanted their only son, Patrick, to carry on the legacy. After graduating from business school, Patrick signed up as an apprentice to his father in 1988. Following a break to complete his military service, he went to work with Gerd in 1994. Patrick developed a niche skillset that complemented his father's expertise. Both worked independently on

some carvings and collaborated on others.

Among the many collectors Wilber introduced to Gerd were Herb and Monika Obodda, whose collection comprises 42 pieces, all of which are included in the Houston exhibition. The chapter is rounded out with 95 full-colour pages.

Chapter 7 is titled 'Intention: Robert Meyers, Collector'. Robert became interested in Dreher carvings through a friend and, in 1981, he and his wife Lisette visited Idar-Oberstein and purchased a small elephant included in this exhibit and illustrated in the book. Meyers is today the longest-standing customer, having collected Dreher carvings for four decades. Nineteen pages of colour photos represent Meyers' collection.

Chapter 8 is titled 'Inheritance: Patrick Dreher Carries on the Tradition'. Patrick is an accomplished craftsman, but his ideas differ from those of his Dreher predecessors. He still retains the discipline of Gerd, but he has diversified into often working with gem materials of greater transparency. He has managed to capture their natural lustre and ability to take a high polish, expanding the Dreher repertoire of carvings. Nine pages of Patrick's carvings are included in this chapter.

Chapter 9 concludes the book with three pages of bibliography, interspersed with two more magnificent full-page photos of Gerd Dreher's carvings.

I personally love Dreher carvings and have been fortunate to provide the family with some wonderful rough material for carving. I got to know Gerd, Brigitte and Patrick well, and this helped me obtain some great Dreher pieces. This book is beautifully done by all those involved, and anyone who likes gemstones or carvings should own a copy.

**Bill Larson FGA**

Pala International, Fallbrook, California, USA



## Sapphire: A Celebration of Colour

By Joanna Hardy, 2021.  
Thames & Hudson,  
London, [https://  
thamesandhudson.com/  
sapphire-a-celebration-of-  
colour-9780500024775](https://thamesandhudson.com/sapphire-a-celebration-of-colour-9780500024775),  
328 pages, illus., ISBN  
978-0500024775.  
GBP85.00 hardcover.

Joanna Hardy's *Sapphire: A Celebration of Colour* rounds out her series of books on 'The Big Three', following *Emerald: Twenty-One Centuries of Jeweled Opulence* (2014) and *Ruby: The King of Gems* (2017). This homage to sapphire doesn't fail to deliver. It initially presents as a big, luxurious coffee-table-style book, but it is so much more: sweeping in content and liberally illustrated with magnificent photographs of inclusions, loose sapphires of all colours and jewellery.

Lauded in many cultures around the world for millennia, the hardness of sapphire combined with its

occurrence in sizeable crystals has helped secure it as one of the most beloved of precious stones. Hardy begins with a chapter on early trade in sapphires, including trade routes and a section on early cuts and cutting styles. Interest in sapphire was piqued by the campaigns of Alexander the Great, travel along the Silk Road and early trader Marco Polo, all of which helped expose different parts of the world to sapphires early on. Before ruby and spinel, sapphire began to appear in European jewellery from the first century BCE. Illustrations of ancient sapphire jewellery in this section include images of two of the oldest sapphire rings known to exist.

Medicinal and talismanic properties of sapphire through the ages are covered, including a detailed description of the famous Talisman of Charlemagne, reputedly a sapphire receptacle for splinters of the True Cross. Metaphysical jewels, medieval goldsmiths, bishops' rings and mourning rings of early Europe are featured, along with a discussion of the negative connotations attributed to sapphire in Hindu astrology. A page titled 'Treasure Trove Logistics' describes British legal protocol in regards to someone finding and claiming found treasure.

The chapter 'Profiles and Portraits' delves into intaglios, reverse intaglios, cameos and carved sapphires, offering insight into their talismanic properties and influence on human cultural history. Considering the hardness of sapphire, the jewels showcased are true wonders of glyptic artistry. A spectacular example shown is a 10-cm-tall sapphire carved figure of Venus standing upon a 116 ct red spinel intaglio depicting Medusa.

It is somewhat predictable that blue sapphire would be the star of royal crowns, both ancient and more recent, due to the colour's association with heaven and the celestial powers, and the size of sapphires available. Famous crowns and some that are not so well known, studded with sapphires, are pictured in colour and described in detail, providing valuable information to jewellery historians who haven't had easy access to these regalia in the past.

The importance of jewels has always been included in court etiquette to indicate status, wealth and power. The popularity of sapphire was not confined to European court jewels. The courts of India and the island today called Sri Lanka, with access to relatively plentiful sapphire mines, also understood the importance of spectacular regalia and made liberal use of it to indicate rank or authority. When the cultures of both the East and West began to interact and trade, the wearing of court jewels became even more important as a way of communicating status. Quite a variety of court jewels

are described, from specific collections such as the Romanov jewels to important single sapphire creations such as the 478.68 ct pendant made by Cartier for Queen Marie of Romania.

Sapphires are so prevalent in the jewels of the British royal family they are given a chapter of their own. From the sapphire brooch given to Queen Victoria by Prince Albert the day before their wedding in 1840 to the iconic sapphire-and-diamond engagement ring given to Diana by Prince Charles in 1981, blue sapphires have been symbols of love and honour.

Throughout the book, the use of sapphire during specific decorative periods such as Arts & Crafts and Art Deco are considered. Factors affecting society as a whole tended to drift down to decorative trends. In this regard, the rejection of the machine age is displayed in the meticulous handcraftsmanship of the Arts & Crafts period of the 1880s through the early 1900s. Conversely, the advent of the modern machine age was embraced during the Art Deco period, roughly 1920–1940. In addition, certain noted makers produced memorable sapphire jewels. Consider, for example, the Iris brooch made by Paulding Farnham for Tiffany & Co. (featuring Montana sapphires) and the Collier Hindou necklace designed by Cartier for French socialite Daisy Fellowes. Liberal use of sapphires helps make these jewels truly unforgettable.

The singular allure of star sapphires was brought to the fore in the 1930s and 1940s, in part due to the clever use of the stone by jewellers such as Paul Flato, Raymond Yard and Mauboussin who catered heavily to movie stars of the era. Mary Pickford, Carole Lombard, Jean Harlow, Myrna Loy and Joan Crawford all had jewellery featuring star sapphires, perhaps hoping that the stone's glamour would reflect back on to them. Similarly, members of 'high society' and the 'jet set' used both star sapphires and non-phenomenal sapphires to connote star status. An excellent example of this is the Duchess of Windsor's Cartier panther jewel, featuring a deep blue 152.35 ct sapphire cabochon. Other sapphire collections of the rich and famous are mentioned, including Elizabeth Taylor's Bulgari sautoir and a spectacular sapphire necklace owned by American businesswoman and philanthopist Marjorie Merriweather Post.

Noteworthy sapphire jewellery collections are profiled, together with tips on the art of collecting drawn from the author's experience with some of the most significant collections in existence. A chapter titled '21st Century' includes brief sketches of many of the most important jewellers on the world stage today, who have used sapphire in all its varied hues as the central focus of their works. Artists mentioned include well-known houses

such as Cartier and Van Cleef & Arpels, but also the lesser-known ateliers of Silvia Furmanovich and Mark Nuell.

The book wraps up with a chapter on ‘Sapphire Discoveries’, describing different sapphire localities throughout the world, their geology and the people who inhabit the regions. The author actually visited many of the sites under discussion and witnessed firsthand the mining and sorting techniques used there.

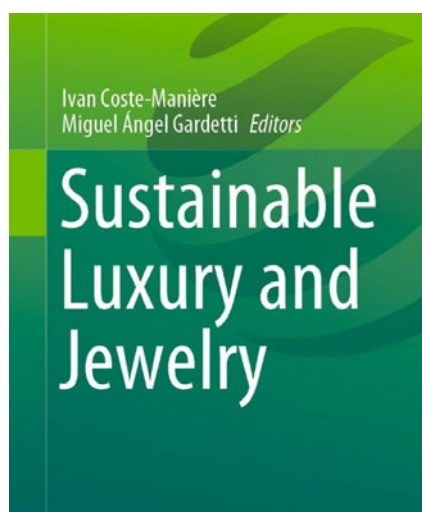
I most heartily recommend this lavishly illustrated

book to gemmologists, appraisers, jewellery historians and anyone interested in sapphire or contemplating a major sapphire purchase. It is a compelling book certain to inspire further study of what is one of the world’s most popular and beloved gems.

**Jo Ellen Cole**

Cole Appraisal Services

Los Angeles, California, USA



## Sustainable Luxury and Jewelry

Ed. by Ivan Coste-Manière and Miguel Ángel Gardetti, 2021. Springer Nature Singapore Pte Ltd, Singapore, xi + 253 pages, illus., ISBN 978-9811624537 (hardcover), ISBN 978-9811624568 (softcover) or e-ISBN 978-9811624544, <https://doi.org/10.1007/978-981-16-2454-4>. EUR139.09 hardcover, EUR96.29 softcover or EUR74.89 eBook.

**T**his book consists of 11 articles and is part of the series ‘Environmental Footprints and Eco-design of Products and Processes’. The book’s strengths—and its fascination—lie in the broad sweep of the doors it opens to learning about the craftsmanship of jewellers, and the scarcity and beauty of natural resources. Its topics traverse the globe from Italian ethical fashion to Indian luxury jewellery manufacture, Australian cultured pearls and the well-known Tanzanian gem tanzanite. It also includes carefully elaborated ethnographic-like accounts of the work of those who craft conventional materials but also push the boundaries of traditional practice. The book also attempts to deal with some of the deeply troubling areas of the supply chain, referring repeatedly to the 2006

film ‘Blood Diamond’ and highlighting the ineffectiveness of the Kimberley Process as the industry’s response to such illicit flows and unethical practices. Some of the articles draw on scholarly research to build the book’s arguments, providing a welcome balance to more sensational writing that can be found in various reports by media outlets and non-governmental organisations.

The book’s first article provides an ethnographic study of Gioielleria Belloni, Italy’s first ethical jewellery store, and its use of Canadian diamonds and fair-mined gold. The authors found that Italian customers believed that their purchases contributed to saving the planet and protecting miners. This provided a commercial advantage for marketers of luxury products through territorialisation and the useful cachet ‘fair and ethically made in Italy’.

The next article, ‘Disrupting the Chain: The Luxury of Craftsmanship’, is a thoughtful and well-written piece that champions the work of three expert craftsmen and their understanding of fair-trade gold, ethically sourced diamonds and environmental awareness. It is argued that luxury cannot exist without superb craftsmanship and that this is what makes jewellery a luxury item, beyond a brand. A pointed critique is made of large-scale, so-called luxury manufacturing jewellers that bypass the need for craftsmanship and hand design, producing finished pieces that do not embody meaning and legacy.

Another article explores Indian jewellery and its celebration of true handmade luxury, epitomised by the Sabayasachi jewellery store. The authors argue strongly for local craftsmanship and identify a key aspect of luxury as being concerned with *why* one should buy rather than *what* one should buy.

The following article provides rare insight into the world of Australian natural and cultured pearls, and pearl jewellers such as Kailis and Paspaley. The author explores the notions of these gems as ‘underwater luxury goods’ whose luxury lies not only in their uniqueness and scarcity but also in their meaning and long history.

The latter is revealed by the use of pearls and pearl shell by Australian indigenous peoples dating back 30,000 years. A separate article then looks at Polynesian and Japanese pearl history and the cultural and spiritual nature of pearls. A critique of the book is that neither chapter refers to important progress that has been made in ensuring the sustainability of pearling, such as the work of Dr Laurent Cartier and others.

Next is an article that covers ‘Traceability, Sustainability, and Circularity as Mechanism [*sic*] in the Luxury Jewelry Industry Creating Emotional Added Value’. Based on industry interviews, the author argues for sustainable luxury jewellery production while taking a critical stance regarding the Kimberley Process, the fair-trade and fair-mined gold standards, and some questionable actions by the Responsible Jewellery Council. She provides useful insight into defining features of luxury and its role in promoting traceability, sustainability and circularity. The jewellery industry, she argues, could be at the forefront of recycling but is lagging behind other fashion industries in terms of sustainability and transparency. In response to this call for creativity, she proposes ‘circular strategies’ for luxury jewellery production, with steps that include incentives for jewellers to collect, save and recycle metals and minerals. She also designed a ‘see-through methodology’ to capture key sustainability details about the design and manufacture of a piece of jewellery, simplifying the complex task jewellers face in understanding the twists and turns of their various supply chains.

The unique gem material tanzanite, its origin, its certification and traceability are discussed very thoroughly in a piece which recognises that it is the Maasai people who must control the sustainable development of this violet-blue stone found only in Tanzania. Of particular interest is a detailed account of the gem’s turbulent history.

An article titled ‘Jewelry Design in the Luxury Sector: Artistry, Craft, Technology and Sustainability’ covers the design and manufacture of jewellery through interviews with four designers involved to varying degrees with the manufacture of their creations, thus exploring the ‘boundaries of craft and luxury’. For example, Mark Bloomfield of sustainable luxury brand Electrobloom champions craftsmanship and the use of recycled materials, but is ‘not willing to sacrifice creativity and innovation in the interest of making more product, faster’ (p. 157). Queenie Cao, an assistant designer with Marc Jacobs, describes a team-oriented process where the design ‘will represent the work of the company and not yourself’ and there is ‘no actual piece making in the company’ (p. 167). The chapter also describes the

experiences of a small online survey of ten employees at Tiffany and Co.’s manufacturing sites, which provides a disappointing critique of workplace health, safety and employee management.

Two of the articles in the book cover diamond—including how a stone’s origin impacts the luxury of a piece of jewellery, and prospects for laboratory-grown diamonds in jewellery. The first one weighs the pros and cons of whether a synthetic diamond can be a luxury stone, and it is concluded ‘synthetics are not rare or given at life’s great moments nor should they be’ (p. 186). As in other parts of the book, the themes of blood diamonds and the inadequacy of the Kimberley Process are mentioned repeatedly. The contribution of small-scale diamond mining to local communities does not rate a mention. Instead, the small-scale diamond miner is demonised, and the work of the Diamond Development Initiative and De Beers’ GemFair projects with small-scale miners is ignored. The article on laboratory-grown diamond unfortunately lacks objectivity and is misleading on a number of counts. For example, a 2010 disaster in Chile concerned a copper-gold mine, not a diamond mine, and conflict diamonds are conflated with all small-scale-mined stones.

An article titled ‘Tackling Modern Slavery in Africa’ provides a rather academic survey of this complex topic based on a review of the literature. However, its lack of qualitative accounts and primary research constrain its scope, as does the focus only on Africa, thus leaving out important parts of the modern slavery ‘supply chain’ (e.g. domestic labour in the Gulf States).

*Sustainable Luxury and Jewelry* brings together a variety of authors who generally provide well-researched perspectives on the nature of luxury and craftsmanship in the twenty-first century, at a time when issues of ethical sourcing and sustainability are growing in importance in the public eye. A weakness is its failure to understand the vital livelihood that the small-scale mining of metals and gem materials provides for many millions of the world’s poorest citizens. Enjoyment of the book is also hampered by weak editing of some chapters, the lack of an index and illegible reproduction of some figures.

As Pandora announces it will launch its laboratory-grown diamond pieces in the USA and jewellers boycott Russian diamonds following its invasion of Ukraine, those who are concerned with sustainable luxury will find much to ponder in this monograph.

**Dr Lynda Lawson**

The University of Queensland  
Queensland, Australia



# Other Book Titles

## COLOURED STONES

### **Eighteenth Annual Sinkankas Symposium: Alexandrite and Other Color-Change Gemstones**

Ed. by Stuart Overlin, 2022. Pala International Inc., Fallbrook, California, USA, 100 pp., ISBN 978-0991532063. USD39.00 softcover (no longer available) or free PDF.

### **Émeraudes, Tout un Monde !**

Ed. by Gaston Giuliani, 2022. Les Éditions du Piat, Saint-Julien-du-Pinet, France, 448 pages, ISBN 978-2917198513 (in French). EUR55.00 hardcover.

## CULTURAL HERITAGE

### **Liangzhu Jade Artifacts: Legal Instrument and Royalty**

By Bin Liu, 2022. Zhejiang University Press, Hangzhou, China, and Springer Nature Singapore, 168 pages, ISBN 978-9811902918 or e-ISBN 978-9811902925, <https://doi.org/10.1007/978-981-19-0292-5>. USD119.00 hardcover or USD89.00 eBook.

## DIAMOND

### **Alluvial Diamond from the Cuango-Angola Region**

By Zola Mayimona, 2021. Self-published via Scientia Scripts, Chişinău, Moldova, 52 pages, ISBN 978-6203997903. EUR43.90 softcover.

### **Diamond: Genesis, Mineralogy and Geochemistry**

Ed. by Karen Smit, Steve Shirey, Graham Pearson, Thomas Stachel, Fabrizio Nestola and Thomas Moses, 2022. *Reviews in Mineralogy and Geochemistry*, Vol. 88, Mineralogical Society of America, Chantilly, Virginia, USA, xvi + 876 pages, ISBN 978-1946850102, <https://doi.org/10.2138/rmg.2022.88.00>. USD65.00 softcover or free PDF.

### **Diamonds: The Queen's Collection**

By Caroline de Guitaut, 2022. Royal Collection Trust, London, 120 pages, ISBN 978-1909741843. GBP14.95 hardcover.

## GEM LOCALITIES

### **Minerals and Gemstones of Southern Africa**

By Bruce Cairncross, 2022. Struik Nature, Cape Town,

South Africa, 296 pages, ISBN 978-1775847533 or e-ISBN 978-1775847540. ZAR450.00 softcover or ZAR382.00 eBook.

## GENERAL REFERENCE

### **Fleischer's Glossary of Mineral Species 2022, 13th Edition**

By Malcolm E. Back, 2022. Mineralogical Association of Canada, Québec, 488 pages, ISBN 978-0921294641. CDN45.00 softcover.

## INSTRUMENTATION

### **Microscopic Techniques for the Non-Expert**

Ed. by Sathish-Kumar Kamaraj, Arun Thirumurugan, Shanmuga Sundar Dhanabalan and Samuel A. Hevia, 2022. Springer Nature, Cham, Switzerland, xii + 247 pages, ISBN 978-3030995416 or e-ISBN 978-3030995423, <https://doi.org/10.1007/978-3-030-99542-3>. EUR139.09 hardcover or EUR106.99 PDF.

## JEWELLERY HISTORY

### **Making It Mine: Sir Arthur Russell and His Mineral Collection**

By Roy E. Starkey, 2022. Self-published via British Mineralogy in association with the Natural History Museum, London, 432 pages, ISBN 978-0993018244. GBP50.00 (UK), GBP60.00 (rest of Europe), GBP75.00 (rest of world) or GBP80.00 (Australia and New Zealand) hardcover, including postage.

## JEWELLERY AND OBJETS D'ART

### **350 Words for Jewellery/350 Worte für Schmuck**

By Barbara Schmidt, 2022. Self-published, 280 pages, ISBN 978-3982051246 (in English and German). EUR35.00 hardcover.

### **Engraved Gems: Cameos, Intaglios and Rings from the Guy Ladrière Collection/Pierres Gravées: Camées, Intailles et Bagues de la Collection Guy Ladrière**

By Philippe Malgouyres, 2022. Mare & Martin and L'École School of Jewelry Arts, Paris, France, 304 pages, ISBN 978-2362220647 (English) or ISBN 978-2362220579 (French). EUR49.00 softcover.

**Jewelry + Image/Schmuck + Image**

Ed. by Olaf Thormann and Sabine Epple, 2022. Arnoldsche Art Publishers, Stuttgart, Germany, 368 pages, ISBN 978-3897906624 (in English and German). USD44.00 hardcover.

**A Mind of Their Own: Jewellery from Austria. Focusing on Women Artists**

Ed. by Ursula Guttmann, Susanne Hammer and Gabriele Kutschera, 2022. Arnoldsche Art Publishers, Stuttgart, Germany, 144 pages, ISBN 978-3897906594. USD28.00 softcover.

**Women Jewellery Designers, 2nd edn.**

By Juliet Weir-de La Rochefoucauld, 2022. ACC Art Books, Woodbridge, Suffolk, 360 pages, ISBN 978-1788841856. GBP45.00 hardcover.

**Eureka! Self-Collected Minerals**

Ed. by Wendell Wilson, 2022. Mineralogical Record, Tucson, Arizona, USA, 412 pages, no ISBN. USD40.00 softcover.

**How Did Our Garden Grow? The History of Hatton Garden**

By Vivian Watson, 2022. The History Press, London, 424 pages, ISBN 978-1803990415 or e-ISBN 978-1803991436. GBP32.00 softcover or GBP12.99 eBook.

**Illumination: Born of Light**

By Stuart Wilensky, Troy Wilensky and Evan D'Arpino, 2022. Wilensky Exquisite Minerals, New York, New York, USA, 65 pages, no ISBN. USD25.00 softcover.

**MISCELLANEOUS**

**Candy**

By Stuart Wilensky, Troy Wilensky and Evan D'Arpino, 2022. Wilensky Exquisite Minerals, New York, New York, USA, 65 pages, no ISBN. USD25.00 softcover.

**ORGANIC/BIOGENIC GEMS**

**Flowers in Amber**

By George Poinar, 2022. Springer, Cham, Switzerland, xv + 215 pages, ISBN 978-3031090431 or e-ISBN 978-3031090448, <https://doi.org/10.1007/978-3-031-09044-8>. EUR69.54 hardcover or EUR53.49 eBook.

**Gem-A INSTRUMENTS**

**OVER 100 PRODUCTS AVAILABLE**

**Buy Gem-A Instruments online!**

**View the full collection at: [shop.gem-a.com](http://shop.gem-a.com)**

**GEM-A MEMBERS!**

Log in to the Gem-A Instruments website and gain instant access to discounted rates.

**Username** is your Gem-A membership number.

**Password** your surname with a capitalised first letter.

You must log in before adding products to your basket.

We recommend changing your password in the account settings.



# REGISTER NOW!



# GemINTRO

*GemIntro* is a Level 2, online, entry-level course which will introduce you to the fascinating world of gemmology and the enormous variety of beautiful gems available. You can discover the basics of gemmology at your own pace - perfect for anyone looking to start or grow their career in the gems and jewellery trade, or for those completely new to gemmology and with an interest in gems.

Register now at [gem-a.com/gemintro](http://gem-a.com/gemintro)



## Gem-A

THE GEMMOLOGICAL ASSOCIATION  
OF GREAT BRITAIN



# Literature of Interest

## COLOURED STONES

**Atomic and microstructural origin of banded colours in purple-blue variety of agate from Yozgat Province, Turkey.** R. Lorenzi, A. Zullino, V. Gagliardi, L. Prosperi, A. Paleari and I. Adamo, *Physics and Chemistry of Minerals*, **49**, 2022, article 33 (8 pp.), <https://doi.org/10.1007/s00269-022-01208-3>.\*

**Based on color calculation and in-situ element analyze to study the color origin of purple chalcedony.** H. Luo and A.H. Shen, *Spectroscopy and Spectral Analysis*, **42**(6), 2022, 1891–1898, <http://www.gpxygpfx.com/EN/Y2022/V42/I06/1891> (in Chinese with English abstract).\*

**Caractéristiques des émeraudes de Musakashi, Zambie [Characteristics of emeralds from Musakashi, Zambia].** U. Hennebois, S. Karampelas and A. Delaunay, *Revue de Gemmologie A.F.G.*, No. 216, 2022, 15–17 (in French with English abstract).

**Characteristics of channel-water in blue-green beryl and its influence on colour.** H. Wang, T. Shu, J. Chen and Y. Guo, *Crystals*, **12**(3), 2022, article 435 (13 pp.), <https://doi.org/10.3390/cryst12030435>.\*

**The chemical composition of trapiche-like quartz from Huanggangliang area, Inner Mongolia, China.** L. Jiang, Z. Chen and Y. Liu, *Crystals*, **12**(1), 2022, article 122 (13 pp.), <https://doi.org/10.3390/cryst12010122>.\*

**Chemical constituents and spectra characterization of gem-grade triplite.** Y. Lü, J. Pei, Y. Gao and B. Chen, *Spectroscopy and Spectral Analysis*, **42**(4), 2022, 1204–1208, <http://www.gpxygpfx.com/EN/abstract/abstract12606.shtml> (in Chinese with English abstract).\*

**Color genesis and compositional characteristics of color-change sapphire from Fuping, China.** H. Wang, X.Y. Yu, F. Liu, M. Alam and G.C. Wu, *Crystals*, **12**(4), 2022, article 463 (13 pp.), <https://doi.org/10.3390/cryst12040463>.\*

**A comparative study of the gemological characteristics and inclusions in spinels from Myanmar and Tajikistan.** Y. Zhang, J.R. Zhu and

X.Y. Yu, *Crystals*, **12**(5), 2022, article 617 (14 pp.), <https://doi.org/10.3390/cryst12050617>.\*

**Comparative study on the origin and characteristics of Chinese (Manas) and Russian (East Sayan) green nephrites.** J. Wang and G. Shi, *Minerals*, **11**(12), 2021, article 1434 (18 pp.), <https://doi.org/10.3390/min11121434>.\*

**Correlations between garnet species and vibration spectroscopy: Isomorphous substitution implications.** W. Li, J. Zheng, J. Pei, X. Xu and T. Chen, *Crystals*, **12**(1), 2022, article 104 (16 pp.), <https://doi.org/10.3390/cryst12010104>.\*

**The effect of Munsell neutral value scale on the color of yellow jadeite and comparison between AP and K-means clustering color grading schemes.** Z. Liu and Y. Guo, *Crystals*, **12**(2), 2022, article 241 (13 pp.), <https://doi.org/10.3390/cryst12020241>.\*

**Effects of transition metal ions on the colour of blue-green beryl.** H. Wang, Q. Guan, Y. Liu and Y. Guo, *Minerals*, **12**(1), 2022, article 86 (15 pp.), <https://doi.org/10.3390/min12010086>.\*

**An evolutionary model and classification scheme for nephrite jade based on veining, fabric development, and the role of dissolution-precipitation.** M.S. Tarling, S.A.F. Smith, M. Negrini, L.W. Kuo, W.H. Wu and A.F. Cooper, *Scientific Reports*, **12**(1), 2022, article 7823 (12 pp.), <https://doi.org/10.1038/s41598-022-11560-7>.\*

**Fluid inclusion and chemical composition characteristics of emeralds from Rajasthan area, India.** L.J. Qin, X.Y. Yu and H.S. Guo, *Minerals*, **12**(5), 2022, article 641 (20 pp.), <https://doi.org/10.3390/min12050641>.\*

**Gemmological characteristic of brown sapphire from Guinea, Africa.** L. Yu and S. Pan, *Journal of Gems & Gemmology*, **24**(3), 2022, 10–19, <https://tinyurl.com/3jddp7ka> (in Chinese with English abstract).\*

**Gemological and mineralogical studies of greenish blue apatite in Madagascar.** Z.-Y. Zhang, B. Xu, P.-Y. Yuan and Z.-X. Wang, *Crystals*, **12**(8), 2022, article 1067 (19 pp.), <https://doi.org/10.3390/cryst12081067>.\*

**Gemology, mineralogy, and coloration mechanism of pinkish-purple cobaltoan dolomite from the Democratic Republic of Congo.** Y. Yan and X.Y. Yu, *Crystals*, **12**(5), 2022, article 639 (14 pp.), <https://doi.org/10.3390/cryst12050639>.\*

**Genesis of color zonation and chemical composition of Penglai sapphire in Hainan Province, China.** G.Y. Wang, X.Y. Yu and F. Liu, *Minerals*, **12**(7), 2022, article 832 (15 pp.), <https://doi.org/10.3390/min12070832>.\*

**Geochemistry of beryl varieties: Comparative analysis and visualization of analytical data by principal component analysis (PCA) and t-distributed stochastic neighbor embedding (t-SNE).** S. Skublov, A. Gavrilchik and A. Berezin, *Journal of Mining Institute*, **255**, 2022, 455–469, <https://doi.org/10.31897/pmi.2022.40>.\*

**Hematite exsolutions in corundum from Cenozoic basalts in Changle, Shandong Province, China: Crystallographic orientation relationships and interface characters.** Q. Zhao, S. Zhao and C. Xu, *Crystals*, **12**(7), 2022, article 905 (12 pp.), <https://doi.org/10.3390/cryst12070905>.\*

**Luminescence verte du corindon sous rayonnement UV [Green luminescence of corundum under UV radiation].** M. Vigier and E. Fritsch, *Revue de Gemmologie A.F.G.*, No. 216, 2022, 18–25 (in French with English abstract).

**Mineralogical and geochemical characteristics of banded agates from placer deposits: Implications for agate genesis.** M. Shen, Z. Lu and X. He, *ACS Omega*, **7**(27), 2022, 23858–23864, <https://doi.org/10.1021/acsomega.2c02538>.\*

**Mineralogy characteristics and coloration mechanism of green tourmaline in Tanzania.** L. Tao, C. Jin, Z. Zhang and X. Han, *Rock and Mineral Analysis*, **41**(2), 2022, 324–331 (in Chinese with English abstract).

**Mineralogy and geochemistry of “Laoshan jade” from Shandong Province, China: Implications for petrogenesis.** X. Yu, Y. Liu and C. Cao, *Crystals*, **12**(2), 2022, article 243 (20 pp.), <https://doi.org/10.3390/cryst12020243>.\*

**Minor elements and color causing role in spinel: Multi-analytical approaches.** T. Pluthametwisute, B. Wanthanachaisaeng, C. Saiyasombat and C. Sutthirat,

*Minerals*, **12**(8), 2022, article 928 (19 pp.), <https://doi.org/10.3390/min12080928>.\*

**Natural radioactivity in select serpentinite-related nephrite samples: A comparison with dolomite-related nephrite.** D. Malczewski, M. Sachanbiński and M. Dziurawicz, *Gems & Gemology*, **58**(2), 2022, 196–213, <https://doi.org/10.5741/gems.58.2.196>.\*

**New insights into coloration mechanism in violet-red pyrope-almandine.** P. Yang and Y. Guo, *Crystals*, **12**(3), 2022, article 379 (11 pp.), <https://doi.org/10.3390/cryst12030379>.\*

**Quantitative definition of strength of chromophores in gemstones and the impact on color change in pyralpspite garnets.** Z. Sun, A.C. Palke, N.D. Renfro, J.M. Rizzo, D.B. Hand and D. Sanchez, *Color Research and Application*, **47**(5), 2022, 1134–1154, <https://doi.org/10.1002/col.22789>.

**Research of geographical origin of sapphire based on three-dimensional fluorescence spectroscopy: A case study in Sri Lanka and Laos sapphires.** Y. Zhang, M. Chen, S. Ye and J. Zheng, *Spectroscopy and Spectral Analysis*, **42**(5), 2022, 1508–1513, <http://www.gpxygpfx.com/EN/Y2022/V42/I05/1508> (in Chinese with English abstract).\*

**Research on spectral characteristics and coloration of natural cobalt spinel.** L. Tao, M. Shi, L. Xu, X. Han and Z. Liu, *Spectroscopy and Spectral Analysis*, **42**(7), 2022, 2130–2134, <http://www.gpxygpfx.com/EN/Y2022/V42/I07/2130> (in Chinese with English abstract).\*

**The shape of ekanite.** L. Nasdala, K.A. Geeth Sameera, G.W.A. Rohan Fernando, M. Wildner, C. Chanmuang N., G. Habler, A. Erlacher and R. Škoda, *Gems & Gemology*, **58**(2), 2022, 156–167, <https://doi.org/10.5741/gems.58.2.156>.\*

**Spectroscopy and chromaticity characterization of yellow to light-blue iron-containing beryl.** Y. Shang, Y. Guo and J. Tang, *Scientific Reports*, **12**(1), 2022, article 10765 (10 pp.), <https://doi.org/10.1038/s41598-022-11916-z>.\*

**Spice of life: Emeralds from Africa.** L. Langeslag, *Gemmology Today*, June 2022, 98–104, <https://tinyurl.com/ypxht9v6>.\*

**Staurolite and its role as an ornamental.** S. Stocklmayer, *Australian Gemmologist*, **28**(1), 2022, 8–17.

**A study on apatite from Mesozoic alkaline intrusive complexes, central High Atlas, Morocco.** P. Yuan, B. Xu, Z. Wang and D. Liu, *Crystals*, **12**(4), 2022, article 461 (21 pp.), <https://doi.org/10.3390/cryst12040461>.\*

**Study on the experimental conditions of quantitative analysis of turquoise by electron probe.** R. Liu, F. Wang, F. Li, L. Guo, S. Cao and L. Yu, *Journal of Gems & Gemmology*, **24**(3), 2022, 44–51, <https://tinyurl.com/55c86hn9> (in Chinese with English abstract).\*

**Study on gemological characteristics of blue sapphires from Baw-Mar mine, Mogok, Myanmar.** S. Chen, H. Tan, C. Zhang, Y. Teng and E. Zu, *Crystals*, **11**(11), 2021, article 1275 (11 pp.), <https://doi.org/10.3390/cryst11111275>.\*

**Study on the spectral characteristics of scapolite from Madagascar.** W. Ding, Q. Chen, S. Ai and Z. Yin, *Spectroscopy and Spectral Analysis*, **42**(7), 2022, 2194–2199, <http://www.gpxygpfx.com/EN/Y2022/V42/I07/2194> (in Chinese with English abstract).\*

**Types and genetic mechanism of chrysoberyl deposits.** Z. Ma, T. Hong, S. Liu, H. Li, H. Ma, W. Wang and X. Xu, *Acta Petrologica Sinica*, **38**(4), 2022, 943–962, <https://tinyurl.com/3ey833xv> (in Chinese with English abstract).\*

**Water molecules in channels of natural emeralds from Dayakou (China) and Colombia: Spectroscopic, chemical and crystal structural investigations.** Y.Y. Zheng, X.Y. Yu, B. Xu, T.Y. Zhang, M.K. Wu, J.X. Wan, H.S. Guo, Z.Y. Long *et al.*, *Crystals*, **12**(3), 2022, article 331 (17 pp.), <https://doi.org/10.3390/cryst12030331>.\*

## CULTURAL HERITAGE

**A gemological and spectroscopic study with mobile instruments of “emeralds” from the coronation crown of Napoleon III.** S. Karampelas, E. Gaillou, A. Herreweghe, F. Maouche, U. Hennebois, S. Leblan, B.M. Sainte Beuve, M. Lechartier *et al.*, *Gems & Gemology*, **58**(2), 2022, 168–183, <https://doi.org/10.5741/gems.58.2.168>.\*

**The lost emerald mines of Ecuador: Contrasting patterns of emerald use in native South America.** W. Bray, *Andean Past*, **13**, 2022, article 8 (35 pp.), <https://tinyurl.com/mwfajrsd>.\*

**A Sui-Tang dynasty woman’s crown: Analyzing form, glass and class.** J. Du, T. Eckfeld, J. Yang, F. Jiang, Q. Zhang and Y. Shao, *Heritage Science*, **10**(1), 2022, article 45 (26 pp.), <https://doi.org/10.1186/s40494-022-00679-5>.\*

## DIAMONDS

**Analysis of abnormal birefringence and graphite inclusions in Zimbabwean diamonds.** C. Sun, T. Lu, Z. Song, M. He and Z. Deng, *Rock and Mineral Analysis*, **41**(2), 2022, 199–210 (in Chinese with English abstract).

**Black diamonds and carbonados: A reflective overview.** R.F. Hansen and L.J. Rennie, *Australian Gemmologist*, **28**(1), 2022, 26–36.

**Chameleon diamond.** J. Chapman, *Australian Gemmologist*, **28**(1), 2022, 46–47.

**Diamond-destructive mantle metasomatism: Evidence from the internal and external textures of diamonds and their nitrogen defects.** Y. Fedortchouk, I.L. Chinn, S.H. Perritt, Z. Zhang, R.A. Stern and Z. Li, *Lithos*, **414–415**, 2022, article 106616 (19 pp.), <https://doi.org/10.1016/j.lithos.2022.106616>.

**A look at diamonds and diamond mining in Guyana.** R. Bassoo and K. Befus, *Gems & Gemology*, **58**(2), 2022, 138–155, <https://doi.org/10.5741/gems.58.2.138>.\*

**Multispectral identification characteristics of the natural pink diamond.** Z. Kong, D. Yu, J. Liu, Z. Wang, Q. Peng and X. Yan, *Superhard Material Engineering*, **34**(1), 2022, 52–56 (in Chinese with English abstract).

**Summary of gemmological and spectroscopic characteristics of a blue-white phosphorescent diamond.** L. Shi and H. Zhu, *Superhard Material Engineering*, **34**(1), 2022, 62–66 (in Chinese with English abstract).

**Using luminescence for diamond identification.** J. Chapman, *Australian Gemmologist*, **28**(1), 2022, 40–45.

## FAIR TRADE

**Diamond mind: The Liberian project.** B. West, *Gemmology Today*, June 2022, 82–88, <https://tinyurl.com/3bpbvcvfk>.\*

**Gemstones: Strategies from mine to market.**

O. Quiniquini, *JNA*, No. 434, 2022, 14–20, <https://news.jewellerynet.com/uploads/ebook/jna/2022/July2022/14> (in English and Chinese).\*

**Global initiative: A rough cut trade – Madagascar.**

M. Hunter and L. Lawson, *Gemmology Today*, June 2022, 74–81, <https://tinyurl.com/bdftkcm>.\*

**Sanctions on Russia—Short-term shortages:****Long-term opportunity for lab-grown diamonds.**

R. Shor, *Gems&Jewellery*, **31**(2), 2022, 18–20.

**GEM LOCALITIES**

**Beryllium minerals in New Hampshire.** D. Dallaire, *Rocks & Minerals*, **97**(3), 2022, 208–235, <https://doi.org/10.1080/00357529.2022.2028096>.

**Focus Ethiopia: Opals from Wegel Tena & Shewa.**

G. Dominy, *Gemmology Today*, June 2022, 6–9, <https://tinyurl.com/38rmb4r3>.\*

**Gemstone deposits of eastern Kenya and Tanzania controlled by ancient meteorite impacts and continental collision – An exploration model.** J.M. Saul, *Australian Gemmologist*, **28**(1), 2022, 18–25.**Metallogenic age, formation process and prospecting direction of marble-related nephrite deposit in China.** Y. Jing, Y. Liu, Y. Zhang and M. Abuduwayiti, *Acta Petrologica et Mineralogica*, **41**(3), 2022, 651–667, <https://bit.ly/3dZ9BqG> (in English with Chinese abstract).\***Mineralogy and geochemistry of JingFenCui (rhodonite jade) deposit from Beijing, China.**

Z.J. Kang, G. Shi, W. Lei, C. An, L. Liu, S. Liu, F. Lu and L. Xu, *Crystals*, **12**(4), 2022, article 483 (13 pp.), <https://doi.org/10.3390/cryst12040483>.\*

**Origin of gem-quality megacrysts in the Cenozoic alkali basalts from the Muling area, northeastern China.** L. Hu, S. Pan, R. Lu, J. Zheng, H. Dai,

A. Guo, L. Yu and H. Sun, *Lithos*, **422–423**, 2022, article 106720 (12 pp.), <https://doi.org/10.1016/j.lithos.2022.106720>.

**Out in the field: My El Dorado [Ethiopia].** H. Sisay,

*Gemmology Today*, June 2022, 90–97, <https://tinyurl.com/72h4xwnn>.\*

**A preliminary investigation of gemstones, mines, miners and problems in Gilgit-Baltistan, Pakistan.**

M. Alam, Y. Bano, A. Rasheed, S. Ali and A. Lateef, *Journal of Mountain Area Research*, **7**, 2022, 37–43, <https://journal.kiu.edu.pk/index.php/JMAR/article/view/93>.\*

**Primary source of alluvial diamonds from the Santo Antônio do Bonito, Santo Inácio, and Douradinho rivers, Coromandel region, Minas Gerais, Brazil.**

R.S. Pereira, L.D.V.d. Carvalho and R.A. Fuck, *Journal of South American Earth Sciences*, **111**, 2021, article 103461 (15 pp.), <https://doi.org/10.1016/j.jsames.2021.103461>.

**Sedimentology, geomorphology, structural controls, and detrital zircon ages of the Itiquira River****diamond placer deposits, Mato Grosso, western Brazil.** P.M. de Paula Garcia, R.K. Weska and E.L.

Dantas, *Journal of South American Earth Sciences*, **114**, 2022, article 103712 (20 pp.), <https://doi.org/10.1016/j.jsames.2022.103712>.

**The tremolites of St. Lawrence County, New York.**

M.R. Walter, *Rocks & Minerals*, **97**(2), 2022, 142–151, <https://doi.org/10.1080/00357529.2022.2004513>.

**INSTRUMENTATION AND TECHNOLOGY****Analysis of the development of detection technology in gemstone identification from the perspective of patents.** Q. Zhou and A.H. Shen, *Journal of Gems & Gemmology*, **24**(3), 2022, 71–78, <https://tinyurl.com/yckv686z> (in Chinese with English abstract).\*
**An application of charge-coupled device (CCD) tomography system for gemological industry—A****review.** F.M. Rahalim, J. Jamaludin, S.N. Raisin, W.Z.W. Ismail, I. Ismail, R.A. Rahim and Y.A. Wahab, in I. M.

Khairuddin *et al.* Eds., *Enabling Industry 4.0 through Advances in Mechatronics*. Springer, Singapore, 2022, 31–41, [https://doi.org/10.1007/978-981-19-2095-0\\_4](https://doi.org/10.1007/978-981-19-2095-0_4).

**Critical evaluation of portable Raman spectrometers: From rock outcrops and planetary analogs to cultural heritage – A review.** J. Jehlička and A. Culka,

*Analytica Chimica Acta*, **1209**, 2022, article 339027 (44 pp.), <https://doi.org/10.1016/j.aca.2021.339027>.

**Identifying the origins of Tianhuang stones based on Raman spectroscopy and pattern recognition****algorithms.** T. Liu, L. Kong, L. Lin, H. Xu, Z. Zhou and M. Huang, *Laser Physics*, **32**(4), 2022, article 045702

(5 pp.), <https://doi.org/10.1088/1555-6611/ac5b77>.

**A quantitative approach to gemstone identification using Raman spectroscopy combined with machine learning.** W.I.W.Y. Boteju, M.K.A.S. Gunarathna, T.L.M.D. Fonseka, H.N.S. Peiris, L.A.R. Silva, N.N.S.S. Jayathilaka, L.A.G.D. Jayasekara, P.N. Perera *et al.*, *Sri Lankan Journal of Physics*, **23**(1), 2022, 1–15, <https://doi.org/10.4038/sljp.v23i1.8110>.\*

## JEWELLERY HISTORY

**American beauties: Nineteenth century jewellery in Currier and Ives prints.** A.V. Sandecki, *Jewellery Studies — The Journal of The Society of Jewellery Historians*, No. 3, 2021, 3–12, [https://www.societyofjewelleryhistorians.ac.uk/JSO\\_2021\\_3.pdf](https://www.societyofjewelleryhistorians.ac.uk/JSO_2021_3.pdf).\*

**L'harmonie dans les bijoux Art Nouveau de René Lalique [Harmony in René Lalique's Art Nouveau jewellery].** U. Allanic, *Revue de Gemmologie A.F.G.*, No. 216, 2022, 6–9 (in French).

**Jewellery and precious objects in the formation of Habsburg family relationships.** J. Hausenblasová and B. Kubíková, *Journal of the History of Collections*, 2022, article fhac016 (15 pp.), <https://doi.org/10.1093/jhc/fhac016>.

**Unveiling the long history of the massive diamond-set badge of the Order of the Golden Fleece of King D. João VI of Portugal.** J.J. Rumsey Teixeira, *Jewellery Studies — The Journal of The Society of Jewellery Historians*, No. 1, 2022, 3–16, [https://www.societyofjewelleryhistorians.ac.uk/JSO\\_2022\\_1.pdf](https://www.societyofjewelleryhistorians.ac.uk/JSO_2022_1.pdf).\*

## MISCELLANEOUS

**Colored Stones Unearthed: Inclusions in gemstones.** J.E. Shigley, A.C. Palke, J.I. Koivula and N.D. Renfro, *Gems & Gemology*, **58**(2), 2022, 234–242, <https://www.gia.edu/gems-gemology/summer-2022-colored-stones-unearthed>.\*

**Grade school: The color of gemstones – Simply about complex.** N. Zolotukhina, *Gemmology Today*, June 2022, 66–72, <https://tinyurl.com/2p8zfn9k>.\*

**It is hard to be a gem in a rhinestone world: A diamond museum collection between history and science.** G. Pratesi, A. Franza, E. Lascialfari, L. Fantoni, F. Malesani and A. Hirata, *Geoheritage*, **13**(4), 2021, article 103 (15 pp.), <https://doi.org/10.1007/s12371-021-00624-1>.

**Minerals, magic, and science: IMA designates 2022 as the Year of Mineralogy.** P.J. Heaney, *Rocks & Minerals*, **97**(2), 2022, 130–133, <https://doi.org/10.1080/00357529.2022.2004511>.

**Photomicrography on gemstone inclusions from the artistic aspects.** M.Z. Daud, M. Ibrahim, N.H.M. Yaakob, N.S.M. Anuar and M. Omar, *New Design Ideas*, **6**(1), 2022, 31–39, <https://tinyurl.com/3zh876h7>.\*

**Touching history: The king of diamonds.** South African History Online, *Gemmology Today*, June 2022, 54–64, <https://tinyurl.com/2p9mvxe6>.\*

## NEWS PRESS

**After 350 years, sea gives up lost jewels of Spanish shipwreck.** D. Alberge, *The Guardian*, 31 July 2022, <https://tinyurl.com/2nxxsbey>.\*

**The bluest stone [Dominican Republic larimar].** J. Conaway, *New York Times*, 27 May 2022, <https://www.nytimes.com/2022/05/27/fashion/jewelry-larimar-dominican-republic.html>.\*

**Now you can own a fraction of a fancy colored diamond.** K. Shirley, *Bloomberg*, 12 May 2022, <https://tinyurl.com/5haax4hs>.\*

**Russia fights efforts to declare it an exporter of 'blood diamonds'.** D. Searcey, *New York Times*, 16 August 2022, <https://www.nytimes.com/2022/08/16/climate/russia-conflict-diamonds-kimberley-process.html>.\*

**Saxon pendant with Roman jewel found in Kingsey field.** BBC News, 19 June 2022, <https://www.bbc.co.uk/news/uk-england-beds-bucks-herts-61764960.amp>.\*

**Unraveling the mystery of macle jewelry.** K. Beckett, *New York Times*, 4 July 2022, <https://www.nytimes.com/2022/07/04/style/unraveling-the-mystery-of-macle-jewelry.html>.\*

## ORGANIC/BIOGENIC GEMS

**Changes to the ivory law leads to new testing considerations.** M. Campbell Pedersen, *Gems&Jewellery*, **31**(2), 2022, 24–26.

**Characteristics of newly discovered amber from Phu Quoc, Vietnam.** Le Ngoc Nang, Pham Trung



Hieu, Lam Vinh Phat, Pham Minh Tien, Ho Nguyen Tri Man and Ha Thuy Hang, *Gems & Gemology*, **58**(2), 2022, 184–194, <https://doi.org/10.5741/gems.58.2.184>.

**Characteristics of photoluminescence and Raman spectra, and the occurrence of trace elements of blue amber from Dominican Republic and Mexico.**

J. Liu, J. Zhang, X. Yan, X. Huang, J. Xu, X. Jiang and J. Yan, *Rock and Mineral Analysis*, **41**(2), 2022, 272–280 (in Chinese with English abstract).

**Identification of treated Baltic amber by FTIR and FT-Raman—A feasibility study.**

D. Karolina, M.S. Maja, D.S. Magdalena and Ż. Grażyna, *Spectrochimica Acta Part A: Molecular and Biomolecular Spectroscopy*, **279**, 2022, article 121404 (11 pp.), <https://doi.org/10.1016/j.saa.2022.121404>.

**Method of price formation of amber samples on the basis of gemmological-consumer indicators.**

R.S. Kirin, P.M. Baranov, S.V. Shevchenko and V.M. Korotayev, *Journal of Geology, Geography and Geoecology*, **31**(2), 2022, 321–332, <https://doi.org/10.15421/112230>.\*

## PEARLS

**Study on freshwater cultured white pearls from Anhui Province based on chromaticity and Raman spectra.**

M. Li, Y. Teng, H. Tan and E. Zu, *Spectroscopy and Spectral Analysis*, **42**(5), 2022, 1504–1507, <http://www.gpxygpfx.com/EN/Y2022/V42/105/1504> (in Chinese with English abstract).\*

**Unique spectral characteristics of natural-color Edison pearls cultured in *Hyriopsis cumingii*, and its formation mechanisms.**

X. Yan, Y. Jiang, H. Jin, T. Chen, Y. Zhou, J. Liu and J. Yan, *Micron*, **160**, 2022, article 103324, <https://doi.org/10.1016/j.micron.2022.103324>.

## SIMULANTS

**Gemmological characteristics and chemical composition of a new type of black jadeite and three imitations.**

B. Zheng, K. Li and Y. Zhang, *Crystals*, **12**(5), 2022, article 658 (12 pp.), <https://doi.org/10.3390/cryst12050658>.\*

**The study of five jade imitations from Bangkok's Yaowarat Road.**

M. Seneewong-Na-Ayuthaya, *Gems&Jewellery*, **31**(2), 2022, 32–35.

## SOCIAL STUDIES

**Frictions and opacities in the Myanmar-China jade trade.**

H. Kloppenborg Møller, in G. Cederlöf and W. V. Schende, Eds., *Flows and Frictions in Trans-Himalayan Spaces*. Amsterdam University Press, Amsterdam, The Netherlands, 2022, 203–229, <https://doi.org/10.2307/j.ctv2jsh08c.11>.\*

**Women in Thailand's gem and jewellery industry and the sustainable development goals (SDGs): Empowerment or continued inequity?**

L. Lawson and A.R. Chowdhury, *Environmental Science & Policy*, **136**, 2022, 675–684, <https://doi.org/10.1016/j.envsci.2022.07.018>.

## SYNTHETICS

**Chemical vapor deposited diamond with versatile grades: From gemstone to quantum electronics.**

Y. Zheng, C. Li, J. Liu, J. Wei, X. Zhang, H. Ye and X. Ouyang, *Frontiers of Materials Science*, **16**(1), 2022, article 220590 (38 pp.), <https://doi.org/10.1007/s11706-022-0590-z>.

**Discussion on gem-quality lab-grown diamond.**

Z. Cai, J. Zhang, X. Chen, Y. Liu and W. Huang, *Superhard Material Engineering*, **34**(1), 2022, 37–42 (in Chinese with English abstract).

**The influence of light path length on the color of synthetic ruby.**

B. Yuan, Y. Guo and Z. Liu, *Scientific Reports*, **12**(1), 2022, article 5943 (15 pp.), <https://doi.org/10.1038/s41598-022-08811-y>.\*

**Progress of chemical vapor deposition (CVD) diamond.**

C. Li, F. Ren, S. Shao, L. Mou, Q. Zhang, J. He, Y. Zheng, J. Liu *et al.*, *Journal of Synthetic Crystals*, **51**(5), 2022, 759–780 (in Chinese with English abstract).

**Spectroscopy characterization study on quality and defects of pure diamond [film].**

Y. Zhang, K. Wang, J. Li, Z. Qin and Y. Tian, *Journal of Synthetic Crystals*, **51**(5), 2022, 926–932 (in Chinese with English abstract).

**UV-Vis-NIR spectroscopic characteristics of vanadium-rich hydrothermal synthetic emeralds from Russia.**

Y. Yang, A.H. Shen, Y. Fan, W. Huang and J. Pei, *Spectroscopy and Spectral Analysis*, **42**(4), 2022, 1199–1203, <http://www.gpxygpfx.com/EN/abstract/abstract12605.shtml> (in Chinese with English abstract).\*

## TREATMENTS

**Chemical and spectral variations between untreated and heat-treated rubies from Mozambique and Madagascar.** Q. Lu, X. Li, L. Sun and B. Qin, *Minerals*, **12**(7), 2022, article 894 (12 pp.), <https://doi.org/10.3390/min12070894>.\*

**Comparison of natural and dyed fire opal.** J. Wu, H. Ma, Y. Ma, P. Ning, N. Tang and H. Li, *Crystals*, **12**(3), 2022, article 322 (15 pp.), <https://doi.org/10.3390/cryst12030322>.\*

**The different inclusions' characteristics between natural and heat-treated tanzanite: Evidence from Raman spectroscopy.** S. Yang, H. Ye and Y. Liu, *Crystals*, **11**(11), 2021, article 1302 (14 pp.), <https://doi.org/10.3390/cryst11111302>.\*

**The effects of thermal treatment and irradiation on the chemical properties of natural diamonds.** I. Litvak, A. Cahana, Y. Anker, S. Ruthstein and H. Cohen, *Physical Chemistry Chemical Physics*, **24**(19), 2022, 11696–11703, <https://doi.org/10.1039/d2cp00764a>.

**Identification of heat-treated sapphires from Sri Lanka: Evidence from three-dimensional fluorescence spectroscopy.** Y. Zhang and M. Chen, *Crystals*, **12**(2), 2022, article 293 (13 pp.), <https://doi.org/10.3390/cryst12020293>.\*

**Identification of jadeite filled with inorganic materials using UV fluorescence, infrared spectroscopy and LIBS techniques.** C. Yang, Z. Huang, J. Zuo, Z. Lu, T. Lu and Z. Tang, *Rock and Mineral Analysis*, **41**(2), 2022, 281–290 (in Chinese with English abstract).

**Spectroscopic features of electron-irradiated diamond crystals from the Mir kimberlite pipe, Yakutia.** M.I. Rakhmanova, A.Y. Komarovskikh, A.L. Ragozin, O.P. Yuryeva and V.A. Nadolnny, *Diamond and Related Materials*, **126**, 2022, article 109057 (6 pp.), <https://doi.org/10.1016/j.diamond.2022.109057>.

**Study on heat treatment and spectroscopy of sapphire from Baw-mar mine, Mogok, Myanmar.**

S. Chen, H. Tan, E. Zu and N. Shen, *Acta Petrologica et Mineralogica*, **41**(4), 2022, 857–864, <https://bit.ly/3pNpzGR> (in Chinese with English abstract).\*

**Treatments applied to garnet and spinel.** A. Palke, *GemGuide*, **41**(4), 2022, 4–9.

## COMPILATIONS

**G&G Micro-World.** Colourless apatite in emerald • Blue apatite in garnet • Diamond in diamond • Etch channels in diamond • 'Eye' pattern in rock • Filler textures in fracture-filled emerald • Flux-grown beryl on an aquamarine seed crystal • Boomerang-shaped tantalite-(Mn) in topaz • Cinnabar in fluorite. *Gems & Gemology*, **58**(2), 2022, <https://tinyurl.com/2wbvdfy8>.\*

**Gem News International.** Aquamarine crystal with unusual etch features • Topaz in red beryl • Cat's-eye omphacite jade • Three-rayed asterism in quartz • Zircon with strong photochromism • Sourcing Pakistan emeralds by Myne London • Glass-and-quartz triplet imitating emerald • Heated Mozambique ruby • Yellow sapphires with unstable color • Auction highlights • Maine (USA) tourmaline exhibition • *Brilliance* exhibit at the Natural History Museum of Los Angeles County, California, USA • American diamonds exhibit at the Smithsonian Institution • GIA's alumni association. *Gems & Gemology*, **58**(2), 2022, <https://tinyurl.com/3tx5e5kt>.\*

**Lab Notes.** Orange benitoite • Natural, synthetic and simulated blue sapphire 'rough' • De Beers Cullinan Blue diamond • Green diamond with unusual radiation stains • 10 ct HPHT-treated CVD-grown diamond • Reported *Cassia* pearl from Florida, USA • RFID devices in South Sea bead-cultured pearl necklaces • A star and cat's-eye color-change sapphire • Bicoloured Cu-bearing tourmaline. *Gems & Gemology*, **58**(2), 2022, <https://tinyurl.com/yknma5mu>.\*

## CONFERENCE PROCEEDINGS

**23rd General Meeting of the International Mineralogical Association.** Lyon, France, 18–22 July 2022, 653 pp., [https://www.ima2022.fr/medias/content/files/interventions\\_abstracts\\_v4.pdf](https://www.ima2022.fr/medias/content/files/interventions_abstracts_v4.pdf).\*

\*Article freely available for download or reading online, as of press time



# Gem-A

THE GEMMOLOGICAL ASSOCIATION  
OF GREAT BRITAIN



# BOOK NOW!

## Gem-A Conference 2022

# November 6

etc.venues County Hall, London

**Bringing together  
the greatest minds  
in gemmology**



This year's Conference boasts an incredible line-up of seven expert speakers and is a must-attend event for anyone interested in gemmology. The Conference will be held at etc.venues County Hall, which overlooks the River Thames and the Houses of Parliament.

### REASONS TO ATTEND

- Amazing line-up of seven experts in their respective fields.
- Enjoy a rare opportunity to network with fellow gemmologists and industry professionals in a relaxed environment.
- Enhance your knowledge and stay up-to-date with developments in our evolving sectors.
- Exclusive workshops and tours including private viewings.
- Add to the Conference experience by joining us for the Gem-A Conference dinner on the evening of November 6.

► **To register and buy tickets visit:**  
**[gem-a.com/event/conference-2022](https://gem-a.com/event/conference-2022)**



